

Periodic and Aperiodic Variability in the Molecular Cloud ρ Ophiuchus

J. Robert Parks^{1,2}, Peter Plavchan¹, Russel J. White², & Alan H. Gee¹

ABSTRACT

Presented are the results of a near-IR photometric survey on 1678 stars in the direction of the ρ Ophiuchus (ρ Oph) star forming region using data from the 2MASS Calibration Database. For each target in this sample, up to 1584 individual J , H and K_s band photometric measurements with a cadence of ~ 1 day are obtained over 3 observing seasons spanning ~ 2.5 years; it is the most intensive survey of stars in this region to date. This survey identifies 101 variable stars with ΔK_s band amplitudes from 0.044 to 2.31 mag and $\Delta(J-K_s)$ color amplitudes ranging from 0.053 to 1.47 mag. Of the 72 young ρ Oph star cluster members included in this survey, 79% are variable; in addition, 22 variable stars are identified as candidate members. Based on the temporal behavior of the K_s time-series, the variability is distinguished as either periodic, long time-scale or irregular. This temporal behavior coupled with the behavior of stellar colors is used to assign a dominant variability mechanism. A new period-searching algorithm finds periodic signals in 32 variable stars with periods between 0.49 to 92 days. The chief mechanism driving periodic variability for 18 stars is rotational modulation of cool starspots while 3 periodically vary due to accretion-induced hot spots. The time-series for 6 variable stars contain discrete periodic “eclipse-like” features with periods ranging from 3 to 8 days.. These features may be asymmetries in the circumstellar disk, potentially sustained or driven by a proto-planet at or near the co-rotation radius. Aperiodic, long time-scale variations in stellar flux are identified in the time-series for 31 variable stars with time-scales ranging from 64 to 790 days. The chief mechanism driving long time-scale variability are variable extinction or mass accretion rates. The majority of the variable stars (40) exhibit sporadic, aperiodic variability over no discernable time-scale. No chief variability mechanism could be identified for these variable stars.

¹Infrared Processing and Analysis Center, California Institute of Technology, Contact: parksj@chara.gsu.edu

²Georgia State University, Department of Physics and Astronomy

Subject headings: infrared radiation, methods: statistical, stars: individual, stars: pre-main sequence, stars: variables, constellation name: ρ Ophiuchus

1. INTRODUCTION

Photometric variability in young stars is an ubiquitous phenomenon. Physical mechanisms causing this variability include, but are not limited to, rotational modulation of starspots, evolution of the circumstellar environment, interstellar extinction, transit events and stellar pulsation. Large sample variability studies such as by Herbst et al. (1994) indicate these mechanisms often operate concurrently resulting in very complex photometric time-series in T Tauri stars. Interpretations are primarily limited because broad band photometry acquired by seeing-limited telescopes are unable to spatially resolve the inner regions around young stars, which are on the order of milliarcseconds for low mass stars in nearby star-forming regions.

High cadence, long temporal baseline photometric surveys, however, can temporally resolve the variations and help identify the dominant mechanism responsible for the variability. This type of survey work has the prospect of identifying peculiar observational phenomenon that may hold clues to unsolved problems in star and planet formation. One example is the physical interpretation of AA Tau-like variability (Bouvier et al. 2003). This variability presents as discrete drops in flux from a nearly constant “continuum” flux level. The phenomenon is not unique to this star; Morales-Calderón et al. (2011) identified 38 stars exhibiting similar variability during an intensive photometric monitoring campaign of young stellar objects (YSOs) in the Orion Nebula Cluster. They find these dips have durations of 1 to a few days decreasing the flux by several tenths of magnitude in the IRAC bands and as much as 1.5 mag in the J band. These dips either appeared only once in 40 days (the survey’s temporal baseline) or were periodic with periods between 2 to 14 days. The current physical interpretation for these observations is periodic obscuration of the star by a high latitude “warp” in the circumstellar disk (Bertout 2000; Bouvier et al. 2003). Longer temporal baseline photometric monitoring of additional YSOs will place better constraints on the periodic nature of these events which in turn will confirm/constrain the current physical interpretation.

Intensive photometric monitoring is most useful when it is conducted at a range of wavelengths. Near-IR observations probe the very inner regions from ~ 0.01 to 1 AU for low mass stars (Dullemond & Monnier 2010). As young stars are typically rapidly rotating,

this region includes both the co-rotation radius and dust sublimation radius. For a median disk lifetime of 5 Myr, this corresponds to millions of dynamical times at these orbital radii (Haisch et al. 2001). Therefore any indication of asymmetries in the circumstellar disk must be driven by some phenomenon (i.e. inclined magnetic dipole, planetary formation). Understanding the physics in this region is of particular interest to protoplanetary formation and migration, as well as how mass accretes onto the star.

ρ Ophiuchus (ρ Oph) makes an excellent laboratory to test the ability of high cadence, long temporal near-IR observations to distinguish between variability mechanisms in young stars. ρ Oph is a dense star-forming region containing a few hundred known young stellar objects (YSOs) with ages ranging from 0.3 to 3 Myr. The region is rich with variable stars; previous surveys having identified more than 100 photometrically variable stars (Greene & Young 1992; Barsony et al. 1997, 2005; Bontemps et al. 2001; Wilking et al. 2005; Alves de Oliveira & Casali 2008). Photometric surveys are limited to the near- to far-IR due to large amounts of visual extinction ranging from 5 to 25 A_V in the cloud core (Cambr esy 1999). This complex interstellar environment could itself be responsible for detected photometric variability.

Plavchan et al. (2008, hereafter P08) carried out a pilot study of 57 stars in the ρ Oph field using photometry collected by the Two Micron All-Sky Survey Calibration Point Source Working Database (2MASS Cal-PSWDB). That study identified periodic variability in two YSOs given a sample of candidate M stars. The study presented here expands on the initial pilot study performed in P08 and will include the full ρ Oph field data set from the 2MASS Cal-PSWDB to better understand the variability of young stars in this cloud.

In §2, the details concerning the observations and source selection for this survey are discussed. The variability analysis, along with a discussion on advantages to high cadence observations, is presented in §3. The methods used to find both periodic and long time-scale variability are found in §4. In §5, the characteristics of the variability catalog, as well as a discussion of variability mechanisms is presented. This section also discusses 6 stars where two variability mechanisms are estimated to operate concurrently. Finally §6 contains a summary of the findings reported by this work.

2. OBSERVATIONS AND SAMPLE SELECTION

2.1. Observations

The Two Micron All-Sky Survey (Skrutskie et al. 2006, 2MASS) imaged nearly the entire sky via simultaneous drift scanning in three near-infrared bands (JHK_s) between

1997 and 2001. Observations were taken at the northern Mt. Hopkins Observatory and the southern CTIO facility. Photometric calibration for 2MASS required hourly observations of 35 calibration fields split evenly between the northern and southern hemispheres. Each calibration field is 1° in length and $8.5'$ wide. One calibration field lies in the direction of the Ophiuchus constellation. This field is centered at $\alpha = 16^h 27^m 15.6^s$ and $\delta = -24^\circ 41' 23''$ (J2000) and covers part of the ρ Oph L1688 cloud core (Bok 1956). These data have an observing cadence of ~ 1 epoch per day. A complete observation is comprised of six consecutive 1.3 second scans in declination with a nearly constant right ascension. Each scan is offset by $5''$ in right ascension to minimize errors from pixel effects. The six scans, or "scan group", are finally co-added to minimize short time-scale and systematic variations. A complete scan group is obtained in approximately 8 minutes (Cutri et al. 2006, §III.2b). The maximum number of scans for a single star is 1584 divided by 6 or 264 scan groups.

Photometry is extracted from the calibration field via the 2MASS Point Source Catalog (2MASS PSC) automated processing system. Details of the system's implementation are described in Cutri et al. (2006); here a brief summary is given. Photometry for sources fainter than $J = 9$, $H = 8.5$ and $K_s = 8$ mag, are extracted by profile-fitting. Profile-fitting compares the source flux to a pre-generated point spread function (PSF) via χ^2 minimization. The PSFs are selected from a look-up table with respect to a dimensionless seeing index that is updated regularly during each scan. The seeing index characterizes the atmospheric seeing during specific observations. The library of PSFs is generated by empirically fitting the 50 brightest stars in a single 2MASS calibration scan with a specific average seeing index. This scan is not necessarily of the ρ Oph field, but a calibration field containing a different slice of the sky. An error at the few-percent level may be present in the resulting photometry due to mismatched PSFs arising from rapid seeing variations.

For the few sources brighter than the above cut off magnitudes, photometry are extracted using a $4''$ fixed aperture corrected using a curve-of-growth. Atmospheric seeing conditions can place as much as 15% of the flux from a point source outside this fixed aperture. A curve-of-growth correction is a constant factor added to measured photometry to simulate measurements taken using an "infinite" aperture. The benefit of this method is avoiding decreased signal-to-noise and potential source confusion arising from large aperture photometry. However, curve-of-growth corrections assume the sources are unresolved single stars that can be approximated by a PSF. Therefore photometry for extended sources (i.e. stars embedded in bright nebular emission) or multiple systems are not properly characterized with this method. All the data scans are compiled in the 2MASS Cal-PSWDB.

2.2. Source Identification

The source selection in the ρ Oph field is similar to that described in P08, which is summarized here. A *parent sample* catalog of 7815 sources is constructed from a co-added deep image of the field (Cutri et al. 2006). For each target in the parent sample, the 2MASS Cal-PSWDB is searched for detections within a $2''$ matching radius. This radius is several σ larger than the 2MASS Point Source Catalog (PSC) astrometric precision and astrometric bias between the PSWDB and PSC (Zacharias et al. 2005; Skrutskie et al. 2006). This ensures confidence all Cal-PSWDB detections for the parent 7815 sources are found within the PSC astrometric precision.

Of the 7815 stars identified in the parent sample, 1678 stars have a sufficient number of detections for variability and periodic analysis. This sample of 1678 stars is henceforth referred to as the *target sample*. A 'sufficient number' is defined as stars detected in $\geq 10\%$ of the observations in either J , H or K_s and ≥ 50 detections in the J band. The first constraint ensures a sufficient number of data points for a robust periodogram computation. The 10% limit is an *ad hoc* limit chosen to reduce the noise present in the variability statistics. The second constraint removes sources near the FOV edges that are not present in most scans.

Finally, despite the success of the 2MASS prescription to produce high-quality photometric measurements, occasionally photometry affected by latent image artifacts, spurious detections and poor quality detections still persist in the database. The reader is referred to P08 for a full treatment on how sources with poor photometry are characterized and excluded. Cutri et al. (2006) describes the different varieties of latent image artifacts arising from a number of phenomenon associated with the optical system. These artifacts are identified and removed via visual inspection. Multiple simultaneous detections found within the $2''$ search radius of a target, which are typically spurious byproducts of the source extraction pipeline, are eliminated. Simultaneous detections are when two (or more) detected sources are identified with a single source in the 2MASS Cal-PSWDB. Secondary detections are typically $\sim 0.5 - 1.5$ magnitudes fainter than the primary detection. In addition, they are typically detected in only one passband and only in one of the six scans. Unaccounted for spurious detections can give the appearance of variability and introduce systematic noise into any underlying periodic signals. Photometric measurements with poor spatial fits to the model PSF are also excluded from our analysis. A poor spatial fit occurs when the χ^2 value between the observed stellar profile and a model PSF is > 10 . This is flagged as 'E' quality photometry within the Cal-PSWDB. Image saturation, cosmic rays, hot pixels, extended emission or partially resolved doubles could account for this poor quality fit to the photometry (Cutri et al. 2006). Photometry with poor spatial fits are systematically brighter by a few tenths of a magnitude, and this can falsely trigger the identification of variability.

Table 1, available only on-line, lists the 1678 stars analyzed for variability. The magnitudes and errors listed are extracted from a co-added image of all calibration scans in that particular band.

Table 1. Catalog of 2MASS stars in ρ Oph

RA (degrees)	Dec (degrees)	N_{Jobs}	N_{Hobs}	N_{Kobs}	J^a (mag)	H^a (mag)	K_s^a (mag)
246.730759	-25.067987	262	261	244	16.972±0.011	16.174±0.012	15.659±0.028
246.731262	-25.062096	258	258	258	17.048±0.016	16.163±0.014	15.631±0.029
246.731293	-24.955822	6	70	72	16.508±0.005	15.796±0.006	15.431±0.009
246.731308	-25.015520	263	263	262	13.980±0.001	13.048±0.001	12.747±0.001
246.731323	-24.472427	6	41	32	17.272±0.000	16.440±0.043	15.327±0.014
246.731323	-25.130241	198	174	67	16.973±0.010	16.211±0.012	15.720±0.026
246.731750	-25.146633	187	139	47	16.987±0.010	16.227±0.013	15.726±0.028
246.731796	-24.863796	102	105	36	15.868±0.003	15.030±0.003	14.694±0.004
246.731934	-25.135702	16	4	11	16.107±0.014	15.431±0.017	15.150±0.013
246.732269	-25.137508	262	260	246	12.371±0.001	11.786±0.001	11.552±0.001
246.732315	-24.272905	257	257	237	17.171±0.019	15.971±0.008	15.216±0.007
246.732391	-24.678473	148	164	96	17.358±0.157	16.277±0.012	14.943±0.005
246.732437	-24.812038	246	244	176	17.242±0.034	16.113±0.009	15.321±0.008
246.732620	-25.045347	263	263	263	16.925±0.008	16.195±0.010	15.661±0.022
246.732666	-25.075741	32	20	4	15.975±0.003	14.987±0.003	14.544±0.003
246.732986	-25.150526	91	58	19	16.773±0.006	16.096±0.007	15.669±0.016
246.733047	-25.007963	263	262	253	17.125±0.015	16.276±0.016	15.758±0.033
246.733154	-25.170332	257	228	87	14.916±0.001	14.325±0.002	14.124±0.002
246.733368	-24.918989	263	263	263	16.820±0.006	16.046±0.006	15.593±0.012
246.733490	-24.929148	262	262	258	17.131±0.039	16.297±0.030	15.753±0.080
246.733704	-24.689774	263	263	263	17.213±0.149	16.351±0.032	15.380±0.016
246.733826	-25.157961	263	263	263	16.861±0.006	16.165±0.007	15.694±0.016
246.733902	-24.257549	242	234	156	17.175±0.014	15.680±0.004	14.829±0.004
246.734070	-24.857338	86	55	16	17.091±0.023	16.318±0.028	15.678±0.051
246.734085	-24.727442	6	2	3	15.841±0.002	14.145±0.001	13.384±0.001
246.734161	-24.221361	254	233	124	17.196±0.098	16.369±0.027	15.475±0.023
246.734222	-25.056364	170	154	51	17.075±0.015	16.312±0.020	15.782±0.043
246.734268	-24.857550	263	262	262	17.100±0.021	16.319±0.025	15.672±0.050
246.734329	-24.927412	263	263	263	14.781±0.001	14.082±0.001	13.833±0.002
246.734375	-24.211395	199	231	157	16.856±0.006	15.258±0.003	14.515±0.003
246.734375	-24.271996	217	216	109	14.333±0.001	12.413±0.001	11.585±0.001
246.734406	-24.894926	14	11	3	15.990±0.003	15.097±0.002	14.804±0.003
246.734497	-24.770220	78	66	16	16.025±0.003	14.657±0.002	14.107±0.002
246.734558	-24.823215	262	262	262	17.239±0.029	16.206±0.009	15.499±0.011
246.734695	-24.710396	148	104	22	17.211±0.017	16.290±0.011	15.539±0.011
246.734711	-25.002422	6	13	10	16.785±0.005	16.082±0.006	15.607±0.012
246.734741	-24.777399	166	142	48	17.245±0.025	16.249±0.011	15.601±0.016
246.734772	-24.688976	42	258	262	17.197±0.068	16.183±0.008	14.934±0.004
246.735107	-24.550400	33	16	5	17.356±0.174	16.614±0.000	15.277±0.009
246.735260	-24.766090	37	31	7	15.162±0.001	13.864±0.001	13.272±0.001
246.735352	-25.007532	76	90	31	17.071±0.025	16.276±0.041	15.759±0.000
246.735458	-25.010090	227	225	137	15.048±0.001	14.098±0.001	13.790±0.001
246.735535	-24.761787	263	262	263	16.428±0.004	14.975±0.002	14.370±0.002
246.735870	-24.889076	13	12	1	16.761±0.005	15.990±0.005	15.537±0.008
246.736069	-25.007456	3	8	10	17.044±0.032	16.202±0.053	15.441±0.000

Table 1—Continued

RA (degrees)	Dec (degrees)	N_{Jobs}	N_{Hobs}	N_{Kobs}	J^a (mag)	H^a (mag)	K_s^a (mag)
246.736221	-25.152752	12	13	4	15.615±0.002	15.191±0.002	14.989±0.004
246.736221	-24.943670	239	247	213	17.064±0.020	16.376±0.039	15.760±0.063
246.736557	-24.230934	32	19	7	12.352±0.001	10.378±0.001	9.298±0.001
246.736740	-24.211903	263	262	252	16.948±0.006	15.362±0.003	14.628±0.003
246.736938	-25.108862	263	263	263	17.090±0.031	16.346±0.057	15.661±99.000
246.737045	-25.064198	4	58	263	14.671±0.001	13.943±0.001	13.687±0.001
246.737091	-24.476904	11	3	4	17.326±0.033	14.665±0.002	12.776±0.001
246.737152	-24.779715	21	18	6	17.262±0.027	16.251±0.011	15.586±0.014
246.737381	-24.685369	257	255	215	17.250±0.031	15.527±0.003	14.109±0.002
246.737396	-24.922001	255	257	250	14.749±0.001	13.892±0.001	13.612±0.001
246.737427	-24.931984	9	95	181	17.118±0.020	16.326±0.019	15.653±0.029
246.737503	-25.179195	41	44	19	16.049±0.002	15.397±0.003	15.173±0.004
246.737595	-24.900654	263	263	263	16.946±0.006	16.031±0.005	15.558±0.009
246.737747	-24.294201	135	141	63	16.949±0.000	16.371±0.044	15.482±0.031
246.737762	-25.095303	263	262	251	16.807±0.008	15.917±0.006	15.357±0.009
246.737808	-25.067343	10	5	10	16.461±0.004	15.642±0.004	15.324±0.005
246.738007	-24.344467	163	152	154	17.134±0.000	16.492±0.039	15.431±0.020
246.738068	-24.938709	219	256	257	16.743±0.005	15.836±0.004	15.349±0.005
246.738190	-25.051514	5	7	3	16.762±0.005	15.936±0.005	15.491±0.007
246.738266	-25.109398	25	13	3	16.978±0.007	16.171±0.007	15.678±0.015
246.738266	-25.094763	263	263	263	16.175±0.004	15.352±0.003	15.036±0.005
246.738281	-24.744131	256	256	262	17.267±0.080	16.339±0.020	15.618±0.022
246.738297	-25.168690	163	94	22	16.693±0.005	16.018±0.005	15.596±0.011
246.738342	-24.247541	6	3	9	17.129±0.010	15.555±0.003	14.617±0.003
246.738403	-24.353350	263	262	259	17.321±0.095	16.285±0.008	15.099±0.004
246.738480	-24.740463	258	258	258	17.041±0.007	15.632±0.004	14.927±0.003
246.738495	-24.983459	262	259	223	17.037±0.010	16.307±0.013	15.700±0.029
246.738525	-25.167128	263	263	263	16.469±0.004	15.822±0.004	15.485±0.007
246.738541	-24.996620	48	174	176	17.088±0.032	16.408±0.061	15.891±0.121
246.738541	-25.125563	262	262	261	17.130±0.037	16.358±0.036	15.796±0.072
246.738678	-24.742460	263	263	263	17.189±0.045	16.334±0.018	15.655±0.022
246.738693	-25.159550	9	19	10	17.073±0.017	16.380±0.031	15.794±0.089
246.738800	-24.594057	263	263	263	17.332±0.073	15.095±0.002	12.766±0.001
246.738953	-24.705124	263	263	263	17.227±0.084	16.456±0.036	15.548±0.029
246.738983	-25.154888	263	263	263	16.555±0.004	15.565±0.003	15.161±0.004
246.739105	-24.931013	257	258	249	15.133±0.001	14.428±0.001	14.159±0.002
246.739182	-25.053665	263	263	263	16.761±0.005	15.981±0.005	15.538±0.008
246.739212	-25.100748	73	87	36	16.706±0.004	15.740±0.004	15.366±0.005
246.739273	-24.883030	263	263	263	14.135±0.001	13.396±0.001	13.109±0.001
246.739288	-24.830378	216	221	160	12.508±0.001	10.870±0.001	10.181±0.001
246.739334	-25.152531	254	237	126	17.091±0.029	16.262±0.045	15.847±0.119
246.739410	-24.880718	263	263	261	16.972±0.007	16.213±0.008	15.630±0.018
246.739456	-24.240559	240	248	210	17.434±0.143	16.346±0.043	15.477±0.029
246.739670	-24.768280	133	92	24	10.724±0.001	10.073±0.001	9.899±0.001
246.739944	-24.780933	163	149	56	17.220±0.055	16.338±0.031	15.704±0.051

Table 1—Continued

RA (degrees)	Dec (degrees)	N_{Jobs}	N_{Hobs}	N_{Kobs}	J^a (mag)	H^a (mag)	K_s^a (mag)
246.740067	-24.689837	134	83	17	17.345±0.083	16.400±0.013	15.356±0.007
246.740067	-25.013088	175	203	182	14.559±0.001	13.941±0.001	13.692±0.001
246.740128	-25.127583	79	131	263	17.073±0.011	16.318±0.014	15.754±0.035
246.740295	-24.899952	10	3	7	17.056±0.010	16.309±0.012	15.734±0.027
246.740402	-24.967394	31	18	4	17.170±0.032	16.396±0.029	15.733±0.042
246.740417	-24.275091	123	117	37	17.180±0.074	16.439±0.036	15.689±0.041
246.740433	-25.047426	7	66	68	17.048±0.009	16.149±0.007	15.617±0.013
246.740463	-24.927614	263	263	263	17.077±0.032	16.442±0.055	15.790±0.121
246.740540	-25.117210	228	196	88	15.894±0.002	15.060±0.002	14.792±0.003
246.740570	-24.837749	263	263	263	17.147±0.020	16.312±0.019	15.729±0.032
246.740601	-25.140648	19	100	91	16.442±0.003	15.793±0.004	15.435±0.006
246.740616	-25.037638	78	120	165	16.085±0.002	15.297±0.003	15.031±0.004
246.740646	-25.078651	263	263	263	17.066±0.015	16.305±0.021	15.731±0.053
246.740829	-24.938803	17	4	8	17.141±0.022	16.368±0.024	15.808±0.062
246.740952	-24.356203	225	238	154	17.399±0.191	16.446±0.018	15.209±0.005
246.740997	-25.109524	39	19	4	16.969±0.009	16.193±0.012	15.652±0.033
246.741150	-24.876930	253	252	252	15.711±0.002	14.861±0.002	14.562±0.002
246.741165	-24.964417	21	13	5	14.260±0.001	13.447±0.001	13.182±0.001
246.741241	-24.308483	255	253	199	17.109±0.009	14.669±0.002	13.392±0.001
246.741257	-24.268812	151	140	143	17.320±0.075	16.313±0.020	15.577±0.021
246.741364	-25.065683	87	136	54	17.049±0.010	16.256±0.010	15.725±0.021
246.741898	-25.108734	95	53	4	16.162±0.003	15.416±0.003	15.140±0.004
246.742050	-25.048517	198	216	116	17.042±0.008	16.224±0.008	15.684±0.017
246.742126	-24.992636	243	222	110	17.044±0.034	16.236±0.030	15.565±0.085
246.742142	-25.080198	20	10	4	17.159±0.032	16.327±0.028	15.788±0.059
246.742203	-24.980259	11	71	64	15.059±0.001	14.300±0.001	14.007±0.002
246.742340	-25.097437	8	12	13	15.576±0.002	14.700±0.002	14.396±0.002
246.742432	-24.281530	77	71	24	17.244±0.084	16.377±0.037	15.628±0.040
246.742477	-25.127331	218	171	66	16.146±0.003	15.170±0.002	14.861±0.003
246.742538	-24.993433	186	207	115	16.789±0.005	15.860±0.004	15.440±0.007
246.742599	-24.882959	9	8	3	17.135±0.015	16.366±0.018	15.694±0.046
246.742783	-24.267208	101	93	30	17.278±0.035	16.180±0.007	15.327±0.006
246.742813	-24.841093	258	252	200	16.352±0.003	15.232±0.002	14.763±0.003
246.742844	-24.627962	6	7	7	17.321±0.113	16.643±0.058	14.363±0.002
246.742874	-25.129557	263	263	263	16.885±0.006	16.125±0.006	15.668±0.014
246.743011	-25.178873	263	263	263	12.367±0.001	11.669±0.001	11.415±0.001
246.743088	-25.103554	8	6	3	17.058±0.030	16.316±0.059	15.982±99.000
246.743134	-24.774351	5	18	136	15.084±0.001	13.680±0.001	13.056±0.001
246.743301	-24.358301	9	4	3	16.218±0.003	13.164±0.001	11.488±0.001
246.743378	-24.858831	263	263	263	17.054±0.008	16.170±0.007	15.659±0.013
246.743439	-25.113102	105	75	20	16.866±0.005	16.130±0.006	15.668±0.012
246.743484	-24.758816	76	39	8	10.850±0.001	8.841±0.002	7.703±0.002
246.743484	-25.010162	239	259	262	16.680±0.004	15.912±0.004	15.518±0.007
246.743484	-25.120901	263	263	263	16.260±0.003	15.555±0.003	15.288±0.005
246.743576	-24.872126	249	256	219	14.146±0.001	13.212±0.001	12.866±0.001

Table 1—Continued

RA (degrees)	Dec (degrees)	N_{Jobs}	N_{Hobs}	N_{Kobs}	J^a (mag)	H^a (mag)	K_s^a (mag)
246.743576	-25.069925	257	262	262	16.530±0.004	15.693±0.004	15.365±0.005
246.743591	-25.041874	243	253	247	17.107±0.009	16.135±0.006	15.640±0.011
246.743713	-24.454042	65	28	7	17.598±0.000	16.612±0.082	15.349±0.015
246.743774	-24.995674	258	258	258	16.929±0.006	16.026±0.005	15.563±0.009
246.743774	-24.760160	263	263	263	9.841±0.001	8.204±0.002	7.125±0.001
246.743958	-25.138395	263	263	263	17.083±0.016	16.311±0.021	15.798±0.046
246.744019	-24.242891	263	263	263	17.264±0.025	16.208±0.007	15.432±0.007
246.744202	-24.767410	263	263	263	15.392±0.001	14.000±0.001	13.364±0.001
246.744217	-24.728842	262	263	263	16.858±0.005	15.256±0.002	14.461±0.002
246.744232	-24.838827	65	28	6	17.185±0.039	16.300±0.019	15.695±0.031
246.744247	-24.955593	250	246	158	15.539±0.002	15.009±0.002	14.767±0.003
246.744324	-24.309591	133	140	63	15.520±0.002	12.994±0.001	11.547±0.001
246.744461	-24.936634	238	232	136	17.145±0.015	16.319±0.014	15.686±0.025
246.744476	-24.415384	217	190	74	17.449±0.133	16.439±0.018	14.652±0.003
246.744644	-25.115198	263	262	254	16.481±0.004	15.791±0.004	15.378±0.006
246.744858	-25.058491	260	252	192	16.941±0.006	16.170±0.007	15.665±0.015
246.744858	-25.027151	263	260	238	17.291±0.051	16.384±0.034	15.743±0.058
246.745010	-24.994553	210	218	154	17.088±0.021	16.269±0.022	15.595±0.040
246.745392	-24.827406	261	254	185	17.163±0.043	16.374±0.035	15.769±0.060
246.745499	-25.011797	9	11	3	16.750±0.005	15.924±0.005	15.513±0.007
246.745560	-25.004211	13	2	6	15.670±0.002	14.926±0.002	14.651±0.003
246.745605	-25.125343	71	68	23	13.767±0.001	13.183±0.001	12.960±0.001
246.745789	-24.858589	136	257	262	17.104±0.010	16.236±0.009	15.693±0.016
246.745850	-24.936262	145	148	55	17.087±0.030	16.422±0.050	15.688±0.108
246.745926	-25.148781	122	159	72	16.974±0.007	16.304±0.010	15.726±0.025
246.746017	-24.599096	134	137	66	16.407±0.003	13.460±0.001	11.866±0.001
246.746048	-25.166656	263	255	259	17.069±0.016	16.325±0.029	15.640±0.071
246.746063	-24.743559	210	201	200	17.145±0.010	15.893±0.004	15.204±0.004
246.746155	-24.787884	260	251	171	16.935±0.032	16.255±0.011	15.567±0.012
246.746216	-24.225351	263	263	263	17.131±0.009	15.637±0.003	14.883±0.003
246.746353	-25.043615	255	255	255	16.755±0.005	15.793±0.004	15.400±0.005
246.746475	-25.102919	240	195	63	17.153±0.020	16.311±0.016	15.767±0.029
246.746490	-24.582909	262	263	251	17.391±0.172	16.872±0.244	15.103±0.004
246.746552	-24.942129	31	34	11	17.134±0.022	16.388±0.035	15.863±0.070
246.746582	-24.904682	11	3	7	16.936±0.006	16.140±0.006	15.669±0.012
246.746597	-25.115286	3	3	15	14.325±0.001	13.591±0.001	13.328±0.001
246.746857	-24.803207	257	256	256	17.008±0.007	15.722±0.004	15.055±0.004
246.747269	-25.038698	258	257	257	17.147±0.038	16.332±0.047	15.904±0.106
246.747314	-24.943592	205	227	211	17.111±0.038	16.406±0.044	15.797±0.085
246.747498	-25.045210	165	97	22	17.141±0.028	16.288±0.029	15.790±0.073
246.747513	-24.817213	263	263	263	16.362±0.003	14.848±0.002	14.204±0.002
246.747620	-25.111332	155	121	33	16.157±0.003	15.400±0.003	15.141±0.004
246.747681	-25.105272	9	25	3	17.186±0.042	16.410±0.038	15.810±0.072
246.747726	-24.823729	7	3	7	16.651±0.004	15.482±0.003	14.946±0.003
246.747925	-24.217596	13	5	5	17.214±0.013	16.003±0.005	15.297±0.005

Table 1—Continued

RA (degrees)	Dec (degrees)	N_{Jobs}	N_{Hobs}	N_{Kobs}	J^a (mag)	H^a (mag)	K_s^a (mag)
246.747940	-25.165606	263	263	263	16.648±0.004	15.983±0.005	15.585±0.009
246.747955	-24.330738	262	262	262	17.280±0.022	15.548±0.003	14.236±0.002
246.748398	-24.909201	263	263	263	17.163±0.023	16.291±0.024	15.776±0.057
246.748444	-24.814663	86	47	11	17.253±0.059	16.382±0.024	15.681±0.029
246.748459	-25.062992	40	16	3	16.930±0.006	16.133±0.007	15.621±0.013
246.748520	-25.046345	142	134	44	16.929±0.006	16.120±0.007	15.597±0.013
246.748520	-25.123934	263	263	263	16.521±0.004	15.747±0.004	15.410±0.006
246.748596	-25.026711	34	150	147	16.975±0.018	16.203±0.025	15.602±0.046
246.748657	-24.261997	263	263	263	14.229±0.001	12.404±0.001	11.642±0.001
246.748962	-24.968887	8	3	6	16.209±0.003	15.372±0.003	15.092±0.004
246.748993	-25.093334	263	263	263	17.097±0.028	16.417±0.046	15.657±0.149
246.749191	-24.986050	263	263	262	17.076±0.010	16.284±0.011	15.731±0.025
246.749359	-25.133659	256	260	258	17.105±0.032	16.290±0.070	15.975±0.134
246.749466	-25.038149	262	259	203	15.599±0.002	14.877±0.002	14.616±0.003
246.749527	-24.198206	48	51	20	17.169±0.045	16.185±0.019	15.445±0.023
246.749649	-25.139311	263	263	263	16.244±0.003	15.421±0.003	15.125±0.004
246.749680	-24.198650	248	242	154	17.210±0.029	16.183±0.011	15.489±0.014
246.749771	-24.272959	35	20	4	17.041±0.007	15.632±0.004	14.893±0.003
246.749771	-24.966293	38	13	3	16.339±0.003	15.465±0.003	15.174±0.004
246.749817	-25.047056	12	20	8	17.127±0.034	16.234±0.033	15.625±0.053
246.749893	-24.326603	26	27	8	17.200±0.070	16.239±0.007	14.975±0.003
246.749908	-24.925961	260	259	234	16.739±0.004	15.725±0.004	15.340±0.005
246.749939	-25.075859	263	263	262	17.119±0.026	16.408±0.041	15.674±0.084
246.749985	-25.157314	263	263	263	16.215±0.003	15.349±0.003	14.899±0.003
246.750031	-25.018356	5	8	3	17.110±0.033	16.367±0.049	15.756±0.106
246.750031	-24.292454	250	226	106	17.326±0.104	16.424±0.037	15.617±0.034
246.750092	-25.124519	18	7	2	17.205±0.042	16.332±0.026	15.503±0.025
246.750198	-24.284424	261	260	256	17.293±0.048	16.207±0.007	15.319±0.005
246.750275	-24.939075	201	171	59	16.238±0.003	15.389±0.003	15.114±0.004
246.750275	-25.028532	259	251	176	11.207±0.001	10.612±0.001	10.361±0.001
246.750320	-25.108772	165	181	86	16.778±0.005	16.012±0.005	15.578±0.009
246.750504	-24.860676	263	263	263	16.198±0.003	15.265±0.002	14.940±0.003
246.750519	-24.951561	30	41	14	15.783±0.002	14.729±0.002	14.360±0.002
246.750534	-24.998018	7	11	4	17.106±0.020	16.363±0.030	15.770±0.065
246.750549	-25.036093	262	262	258	17.126±0.026	16.340±0.026	15.702±0.050
246.750687	-25.114477	263	263	263	16.987±0.019	16.234±0.048	15.533±0.060
246.750732	-25.114920	100	83	27	16.992±0.021	16.285±0.060	15.549±0.054
246.750931	-24.294949	240	223	109	17.365±0.119	16.430±0.032	15.636±0.029
246.751144	-24.908239	249	227	119	16.664±0.004	15.668±0.004	15.286±0.005
246.751144	-24.956137	263	263	263	15.796±0.002	14.915±0.002	14.643±0.002
246.751190	-24.713514	259	258	224	17.250±0.090	16.422±0.022	15.529±0.017
246.751266	-25.080460	5	12	11	16.977±0.007	16.190±0.007	15.647±0.014
246.751389	-25.012247	262	262	263	16.551±0.004	15.870±0.004	15.513±0.007
246.751450	-24.921116	258	258	258	16.979±0.007	16.171±0.007	15.676±0.013
246.751511	-25.161835	14	12	3	16.711±0.004	15.933±0.005	15.543±0.008

Table 1—Continued

RA (degrees)	Dec (degrees)	N_{Jobs}	N_{Hobs}	N_{Kobs}	J^a (mag)	H^a (mag)	K_s^a (mag)
246.751541	-25.097633	263	263	259	16.842±0.005	15.917±0.005	15.506±0.007
246.751938	-24.976969	189	183	79	15.646±0.002	14.884±0.002	14.587±0.002
246.752243	-24.360102	9	3	5	17.274±0.124	15.803±0.005	14.355±0.002
246.752274	-24.778955	100	84	28	16.514±0.004	14.828±0.002	14.013±0.002
246.752335	-24.273695	53	25	5	13.432±0.001	11.840±0.001	10.997±0.001
246.752609	-24.425325	48	13	2	17.160±0.000	16.499±0.033	15.284±0.007
246.752701	-24.417547	12	6	5	17.349±0.050	16.259±0.007	15.100±0.004
246.752716	-25.000906	13	4	3	16.614±0.004	15.829±0.004	15.466±0.006
246.752914	-25.140646	263	263	263	17.186±0.025	16.372±0.026	15.757±0.039
246.752960	-24.917158	258	258	258	15.194±0.001	14.444±0.001	14.162±0.002
246.752975	-24.774199	40	30	8	13.670±0.001	12.002±0.001	11.233±0.001
246.752991	-24.889130	8	5	3	17.089±0.009	16.266±0.009	15.701±0.022
246.752991	-25.144203	146	99	25	17.110±0.011	16.206±0.009	15.673±0.020
246.753006	-24.897182	263	263	262	16.598±0.004	15.858±0.004	15.488±0.006
246.753159	-24.359386	25	21	5	17.366±0.102	16.095±0.007	14.841±0.003
246.753159	-25.053015	262	262	262	17.345±0.060	16.368±0.032	15.530±0.027
246.753174	-24.855795	10	4	7	16.985±0.006	16.142±0.006	15.638±0.011
246.753250	-25.124668	6	5	8	16.521±0.004	15.752±0.004	15.417±0.006
246.753311	-24.947714	248	240	145	16.871±0.005	16.129±0.006	15.649±0.011
246.753403	-24.818514	163	105	25	17.236±0.044	16.345±0.034	15.773±0.046
246.753510	-25.147215	248	202	69	16.828±0.005	15.957±0.005	15.547±0.008
246.753525	-24.766174	6	4	10	16.871±0.005	15.423±0.003	14.684±0.003
246.753586	-25.103720	262	263	263	17.142±0.016	16.249±0.012	15.671±0.023
246.753723	-24.995443	241	250	207	16.165±0.003	15.082±0.002	14.721±0.003
246.753876	-24.271313	263	263	263	17.291±0.028	16.224±0.009	15.485±0.009
246.753983	-25.182510	14	28	33	16.800±0.007	16.100±0.010	15.616±0.019
246.754059	-25.125971	10	10	5	17.111±0.016	16.258±0.014	15.698±0.023
246.754074	-24.814829	263	259	214	17.235±0.052	16.383±0.035	15.807±0.059
246.754272	-25.095930	54	39	6	16.304±0.003	15.519±0.003	15.225±0.004
246.754288	-24.952431	3	130	263	16.941±0.006	16.214±0.007	15.711±0.015
246.754425	-24.796709	263	263	263	16.603±0.004	15.020±0.002	14.214±0.002
246.754440	-25.068176	238	249	240	16.354±0.003	15.637±0.003	15.342±0.005
246.754578	-24.847099	250	247	235	16.736±0.004	15.563±0.003	15.114±0.004
246.754639	-24.228893	44	52	17	17.123±0.009	15.832±0.004	15.124±0.004
246.754715	-24.982483	10	3	8	13.432±0.001	12.724±0.001	12.448±0.001
246.755035	-24.957472	16	19	7	17.179±0.041	16.313±0.038	15.708±0.088
246.755035	-25.098391	30	35	12	15.956±0.002	15.105±0.002	14.834±0.003
246.755264	-25.062794	255	251	183	16.696±0.004	15.888±0.004	15.508±0.007
246.755295	-24.798414	256	249	181	17.354±0.041	16.298±0.013	15.635±0.016
246.755493	-25.168692	263	263	263	17.223±0.083	16.348±0.035	15.534±0.030
246.755524	-24.876833	263	263	263	17.082±0.008	16.140±0.006	15.619±0.011
246.755539	-24.380417	257	248	161	17.412±0.180	16.450±0.142	15.368±0.018
246.755615	-24.871017	103	113	46	17.121±0.012	16.349±0.015	15.734±0.032
246.755814	-25.139650	13	7	4	17.183±0.016	16.319±0.014	15.756±0.026
246.755875	-24.976624	67	111	135	17.047±0.023	16.315±0.037	15.975±0.143

Table 1—Continued

RA (degrees)	Dec (degrees)	N_{Jobs}	N_{Hobs}	N_{Kobs}	J^a (mag)	H^a (mag)	K_s^a (mag)
246.756195	-25.167433	112	125	67	16.994±0.008	16.285±0.012	15.700±0.032
246.756302	-24.910250	263	263	263	17.169±0.029	16.317±0.027	15.733±0.052
246.756317	-25.143431	184	189	93	16.608±0.004	15.928±0.005	15.549±0.008
246.756638	-25.017836	191	143	48	17.101±0.009	16.187±0.007	15.672±0.014
246.756714	-25.056927	39	27	7	17.099±0.024	16.341±0.035	15.693±0.090
246.756729	-24.851709	12	4	2	17.149±0.017	16.193±0.010	15.636±0.019
246.756760	-24.976877	8	2	1	16.931±0.006	16.155±0.007	15.615±0.016
246.756760	-24.360228	210	182	74	14.272±0.001	11.051±0.001	9.384±0.001
246.756836	-25.165745	255	255	255	16.936±0.006	16.227±0.008	15.686±0.019
246.756927	-24.942846	12	5	2	14.002±0.001	13.315±0.001	13.065±0.001
246.757324	-24.932966	263	263	263	17.121±0.027	16.398±0.048	15.810±0.099
246.757370	-24.908503	11	9	2	16.696±0.004	15.937±0.005	15.544±0.007
246.757401	-25.010666	29	35	16	17.050±0.008	16.243±0.008	15.713±0.017
246.757416	-25.129646	48	175	175	17.125±0.022	16.383±0.040	15.867±99.000
246.757492	-25.172138	263	263	263	17.088±0.023	16.392±0.054	15.689±0.067
246.757507	-25.068356	19	13	4	16.992±0.007	16.246±0.009	15.708±0.020
246.757751	-25.135826	255	256	229	16.829±0.005	16.061±0.005	15.589±0.009
246.757797	-24.946932	235	262	262	16.215±0.003	15.397±0.003	15.133±0.004
246.757843	-25.097927	262	260	229	17.099±0.015	16.386±0.022	15.780±0.051
246.758118	-24.368259	262	262	262	17.534±0.105	15.504±0.003	13.181±0.001
246.758148	-24.245800	176	132	37	17.353±0.036	16.334±0.013	15.587±0.013
246.758270	-24.261374	55	62	30	17.253±0.014	16.096±0.006	15.382±0.005
246.758453	-24.781078	7	5	94	17.449±0.079	16.391±0.019	15.552±0.015
246.758484	-24.912212	42	13	2	16.133±0.003	15.392±0.003	15.084±0.004
246.758560	-24.237148	41	35	8	17.047±0.007	15.529±0.003	14.795±0.003
246.758728	-25.006041	43	20	4	17.123±0.030	16.465±0.057	15.824±0.096
246.758987	-24.877764	17	6	2	17.159±0.021	16.371±0.025	15.798±0.060
246.759338	-24.863434	263	263	260	17.176±0.018	16.375±0.019	15.794±0.042
246.759506	-24.197283	263	263	263	17.272±0.043	16.239±0.011	15.395±0.010
246.759537	-25.091494	8	10	5	17.096±0.011	16.271±0.011	15.726±0.024
246.759552	-25.173203	250	257	252	17.105±0.029	16.496±0.077	16.044±99.000
246.759720	-24.624172	89	41	5	14.173±0.001	10.438±0.001	8.030±0.001
246.759827	-25.176250	196	216	152	16.222±0.003	15.279±0.003	14.968±0.003
246.759842	-24.929228	263	263	263	16.704±0.004	15.821±0.004	15.470±0.006
246.759857	-25.161737	14	7	7	16.934±0.006	16.009±0.005	15.588±0.009
246.760147	-24.901754	169	185	186	17.111±0.016	16.355±0.021	15.676±0.045
246.760178	-25.106197	6	9	9	14.383±0.001	13.411±0.001	13.110±0.001
246.760239	-25.094362	263	263	263	16.870±0.005	16.123±0.006	15.649±0.011
246.760406	-24.731108	262	261	233	15.495±0.002	13.617±0.001	12.757±0.001
246.760483	-24.896351	213	252	244	14.799±0.001	13.878±0.001	13.575±0.001
246.760513	-24.943216	61	35	9	17.142±0.025	16.454±0.037	15.795±0.108
246.760681	-25.129038	235	209	103	16.917±0.006	16.143±0.006	15.646±0.013
246.760818	-24.835270	15	7	11	15.855±0.002	14.652±0.002	14.164±0.002
246.760880	-24.799465	2	21	19	16.660±0.004	15.348±0.003	14.657±0.003
246.760910	-24.734659	263	263	263	17.345±0.047	16.291±0.012	15.498±0.011

Table 1—Continued

RA (degrees)	Dec (degrees)	N_{Jobs}	N_{Hobs}	N_{Kobs}	J^a (mag)	H^a (mag)	K_s^a (mag)
246.760941	-25.079725	8	6	9	16.768±0.005	16.066±0.005	15.618±0.011
246.761093	-24.776232	231	226	124	13.348±0.001	11.596±0.001	10.665±0.001
246.761215	-25.184999	6	81	118	16.655±0.016	15.935±0.028	15.466±0.062
246.761292	-25.066795	263	263	263	16.995±0.010	16.313±0.017	15.727±0.038
246.761490	-25.045506	154	122	40	11.449±0.001	10.387±0.001	10.019±0.001
246.761520	-24.215494	210	210	211	17.251±0.015	16.080±0.006	15.412±0.006
246.761765	-25.141516	263	263	263	12.786±0.001	12.123±0.001	11.899±0.001
246.761826	-24.952679	37	20	5	15.817±0.002	15.105±0.002	14.850±0.003
246.761856	-24.419268	257	256	256	17.350±0.155	16.444±0.046	15.335±0.010
246.761902	-24.315140	253	252	194	13.090±0.001	11.049±0.001	10.096±0.001
246.761963	-24.907104	13	15	5	16.891±0.005	16.072±0.005	15.632±0.010
246.762054	-24.889269	20	3	2	17.079±0.008	16.160±0.007	15.653±0.013
246.762100	-24.752535	31	49	17	16.780±0.005	15.057±0.002	14.259±0.002
246.762115	-24.343933	136	211	160	16.832±0.005	14.413±0.001	13.180±0.001
246.762344	-25.139839	184	122	32	17.041±0.022	16.225±0.023	15.604±0.037
246.762512	-24.437368	38	75	51	17.375±0.100	15.621±0.003	12.544±0.001
246.762589	-25.082260	243	228	124	16.514±0.004	15.789±0.004	15.453±0.006
246.762695	-24.835979	28	43	50	17.223±0.019	16.306±0.015	15.729±0.028
246.762726	-25.086535	4	17	13	15.997±0.002	15.282±0.002	15.011±0.003
246.762802	-24.886368	250	263	263	16.023±0.002	15.260±0.003	14.962±0.003
246.762833	-24.298433	15	42	20	16.264±0.003	13.775±0.001	12.575±0.001
246.762848	-24.245068	8	22	3	17.044±0.006	15.762±0.004	15.122±0.004
246.762863	-24.940948	116	122	42	17.099±0.016	16.353±0.023	15.813±0.048
246.762878	-24.764877	52	28	5	17.312±0.036	16.272±0.009	15.444±0.008
246.762878	-24.884378	108	42	8	15.445±0.002	14.559±0.002	14.233±0.002
246.762894	-24.943659	258	258	258	16.442±0.003	15.628±0.003	15.333±0.005
246.762924	-24.318180	7	2	5	17.360±0.048	16.323±0.010	15.487±0.009
246.762970	-24.733807	18	16	6	14.720±0.001	12.879±0.001	12.052±0.001
246.763016	-25.075115	36	18	4	16.579±0.004	15.751±0.004	15.418±0.006
246.763031	-24.276827	2	187	192	13.200±0.001	11.633±0.001	10.774±0.001
246.763062	-25.165901	263	263	263	16.322±0.003	15.492±0.003	15.170±0.004
246.763092	-25.061146	8	3	6	17.128±0.017	16.226±0.012	15.692±0.024
246.763107	-24.401106	261	260	260	17.336±0.087	16.334±0.010	15.117±0.004
246.763199	-24.947929	9	20	25	17.076±0.010	16.309±0.011	15.768±0.026
246.763672	-25.171967	255	259	254	16.997±0.008	16.146±0.007	15.638±0.013
246.763718	-24.201227	117	262	262	17.239±0.023	16.234±0.009	15.532±0.010
246.763824	-25.021496	258	258	257	16.551±0.004	15.676±0.004	15.345±0.005
246.763824	-24.840492	263	263	262	17.177±0.011	16.219±0.008	15.672±0.012
246.763931	-24.908590	30	17	5	16.713±0.004	15.829±0.004	15.455±0.006
246.764084	-24.893082	263	263	262	15.429±0.001	14.750±0.002	14.493±0.002
246.764130	-24.208923	20	38	18	17.198±0.011	15.948±0.005	15.285±0.005
246.764236	-24.369820	39	16	2	17.442±0.131	16.567±0.063	15.289±0.007
246.764328	-24.993689	263	262	258	14.318±0.001	13.527±0.001	13.257±0.001
246.764374	-24.913891	238	227	130	16.313±0.003	15.579±0.003	15.273±0.005
246.764694	-24.733583	7	45	35	16.905±0.006	15.406±0.003	14.636±0.003

Table 1—Continued

RA (degrees)	Dec (degrees)	N_{Jobs}	N_{Hobs}	N_{Kobs}	J^a (mag)	H^a (mag)	K_s^a (mag)
246.764725	-25.172762	239	262	262	16.386±0.003	15.725±0.004	15.439±0.006
246.764786	-24.977114	263	263	263	17.145±0.023	16.308±0.021	15.748±0.045
246.764908	-24.276812	214	236	221	17.157±0.019	15.700±0.004	14.838±0.003
246.764984	-24.971508	12	12	4	17.035±0.008	16.218±0.008	15.684±0.016
246.764984	-24.334810	15	29	13	16.944±0.006	14.768±0.002	13.464±0.001
246.765121	-25.126707	109	70	19	16.366±0.003	15.616±0.003	15.342±0.005
246.765198	-24.948490	263	262	262	17.114±0.016	16.420±0.025	15.779±0.050
246.765259	-25.152760	10	115	231	17.109±0.021	16.353±0.033	15.819±0.101
246.765411	-24.920961	254	254	231	17.051±0.008	16.238±0.009	15.714±0.019
246.765640	-25.111982	262	262	262	14.382±0.001	13.731±0.001	13.494±0.001
246.765671	-25.069242	64	40	9	17.128±0.014	16.273±0.011	15.692±0.019
246.765808	-25.025282	262	262	245	14.924±0.001	14.270±0.001	14.027±0.002
246.765945	-25.071283	216	234	176	15.900±0.002	15.059±0.002	14.784±0.003
246.766083	-25.098223	17	2	2	17.081±0.009	16.233±0.009	15.716±0.019
246.766098	-25.059322	10	5	2	16.940±0.006	15.964±0.005	15.529±0.007
246.766129	-24.905785	263	263	263	16.325±0.003	15.599±0.003	15.317±0.005
246.766281	-24.951754	263	263	263	17.026±0.008	16.199±0.008	15.694±0.017
246.766434	-24.230253	263	263	263	17.240±0.014	16.012±0.005	15.292±0.005
246.766663	-24.308201	261	260	258	15.890±0.002	13.855±0.001	12.944±0.001
246.766815	-24.673220	246	227	121	17.461±0.133	16.544±0.045	15.123±0.004
246.767075	-25.143785	88	136	153	16.781±0.005	15.952±0.005	15.550±0.008
246.767090	-24.962513	253	238	134	17.064±0.012	16.288±0.015	15.751±0.042
246.767090	-24.474903	262	260	236	16.550±0.004	13.027±0.001	10.870±0.001
246.767120	-24.902493	201	155	46	16.453±0.003	15.644±0.003	15.325±0.005
246.767349	-25.009157	89	48	9	16.320±0.003	15.670±0.004	15.373±0.005
246.767395	-25.124893	8	2	5	15.753±0.002	15.092±0.002	14.850±0.003
246.767670	-25.176456	49	22	4	17.148±0.029	16.413±0.041	15.779±0.070
246.767792	-24.898878	230	221	221	15.679±0.002	14.744±0.002	14.438±0.002
246.767883	-24.804842	8	3	6	16.684±0.004	15.419±0.003	14.822±0.003
246.768036	-24.197735	263	263	263	17.385±0.055	16.344±0.022	15.634±0.026
246.768082	-24.866238	35	12	2	15.877±0.002	14.955±0.002	14.631±0.002
246.768112	-24.978901	142	93	24	17.077±0.029	16.356±0.045	15.804±0.110
246.768234	-24.961782	263	263	262	17.077±0.009	16.173±0.007	15.623±0.012
246.768280	-24.209644	19	14	3	15.927±0.002	14.328±0.001	13.638±0.001
246.768295	-25.172762	213	191	77	16.433±0.003	15.659±0.004	15.391±0.005
246.768311	-24.872257	263	263	263	15.767±0.002	15.034±0.002	14.733±0.003
246.768402	-24.857536	17	2	6	16.638±0.004	15.744±0.004	15.359±0.005
246.768417	-25.158325	224	230	225	15.928±0.002	15.217±0.002	14.992±0.003
246.768433	-25.006374	263	263	263	13.792±0.001	13.096±0.001	12.850±0.001
246.768463	-25.023140	193	158	59	16.816±0.005	15.850±0.004	15.450±0.006
246.768677	-24.707766	170	205	131	17.352±0.062	16.338±0.011	15.319±0.006
246.768814	-24.716524	31	36	15	12.000±0.001	10.478±0.001	9.821±0.001
246.768906	-25.042665	33	38	18	15.058±0.001	14.325±0.001	14.063±0.002
246.768997	-24.703840	11	10	4	12.271±0.001	10.580±0.001	9.831±0.001
246.769058	-24.454285	249	222	102	16.454±0.003	13.070±0.001	11.175±0.001

Table 1—Continued

RA (degrees)	Dec (degrees)	N_{Jobs}	N_{Hobs}	N_{Kobs}	J^a (mag)	H^a (mag)	K_s^a (mag)
246.769089	-25.162308	165	122	48	16.243±0.003	15.590±0.003	15.340±0.005
246.769104	-24.995356	85	52	13	17.164±0.011	16.275±0.009	15.743±0.016
246.769333	-24.924337	257	259	249	16.992±0.014	16.220±0.022	15.681±0.061
246.769440	-24.924677	179	136	37	17.003±0.011	16.221±0.016	15.680±0.050
246.769577	-25.150167	121	106	34	17.150±0.025	16.267±0.017	15.502±0.015
246.769608	-24.761732	15	10	3	17.301±0.039	16.217±0.010	15.513±0.010
246.769730	-25.179161	257	257	247	16.787±0.005	16.127±0.006	15.654±0.013
246.769791	-24.847944	244	245	229	16.962±0.006	15.783±0.004	15.275±0.005
246.769897	-24.863289	263	263	263	17.175±0.042	16.328±0.036	15.772±0.078
246.769943	-24.868364	16	7	3	17.121±0.010	16.118±0.006	15.584±0.010
246.769958	-24.932888	193	148	43	16.657±0.004	15.992±0.005	15.594±0.008
246.770096	-24.788397	258	258	258	17.250±0.049	16.421±0.022	15.653±0.021
246.770218	-24.914377	255	255	255	17.135±0.039	16.359±0.040	15.780±0.091
246.770264	-24.854544	222	173	72	16.933±0.006	15.960±0.005	15.505±0.006
246.770309	-25.003698	14	5	11	15.923±0.002	15.246±0.003	14.986±0.003
246.770462	-25.054527	57	35	9	14.569±0.001	13.840±0.001	13.577±0.001
246.770645	-25.140514	6	4	2	15.280±0.002	14.323±0.002	13.978±0.002
246.770706	-25.031477	77	54	20	16.456±0.003	15.782±0.004	15.456±0.006
246.770874	-25.146795	105	104	42	12.014±0.001	11.509±0.001	11.310±0.001
246.770950	-24.739624	138	115	37	15.783±0.002	14.107±0.001	13.308±0.001
246.770996	-24.925669	92	83	21	17.161±0.032	16.340±0.026	15.744±0.057
246.771057	-24.795004	4	18	30	17.444±99.000	16.383±0.040	15.480±0.027
246.771103	-25.167370	255	257	257	16.922±0.006	16.189±0.007	15.702±0.016
246.771133	-24.957487	254	259	256	17.113±0.031	16.410±0.052	15.757±0.118
246.771286	-24.279083	128	114	34	17.027±0.007	15.487±0.003	14.739±0.003
246.771439	-24.980293	263	263	263	14.153±0.002	13.303±0.002	12.984±0.001
246.771484	-25.129562	252	237	151	16.926±0.006	16.052±0.005	15.558±0.008
246.771545	-24.335421	8	18	5	12.700±0.001	10.440±0.001	9.341±0.001
246.771637	-25.041271	7	2	2	17.195±0.045	16.307±0.035	15.846±0.080
246.771667	-24.248150	6	6	2	17.264±0.020	16.269±0.009	15.616±0.010
246.771683	-24.194397	227	203	90	15.783±0.012	14.211±0.006	13.544±0.007
246.771698	-24.891954	256	247	163	17.185±0.020	16.373±0.020	15.752±0.055
246.771805	-24.992462	263	263	263	16.073±0.003	15.167±0.003	14.852±0.003
246.771851	-24.608212	259	256	231	17.266±0.149	16.437±0.114	14.455±0.003
246.771942	-24.878325	257	257	257	16.812±0.005	16.025±0.005	15.611±0.008
246.771988	-24.914228	263	263	263	17.093±0.015	16.317±0.019	15.756±0.041
246.772079	-24.289640	255	242	154	17.293±0.036	16.221±0.011	15.451±0.009
246.772186	-25.161106	263	263	263	15.361±0.001	14.591±0.001	14.364±0.002
246.772232	-24.825331	237	227	122	17.276±0.039	16.385±0.024	15.700±0.030
246.772293	-25.034142	12	4	6	17.082±0.016	16.306±0.022	15.803±0.051
246.772385	-24.862595	8	3	5	17.168±0.015	16.169±0.008	15.588±0.012
246.772659	-24.342674	3	8	14	17.057±0.007	14.416±0.001	12.980±0.001
246.772659	-24.955385	263	263	263	16.618±0.004	15.606±0.003	15.234±0.004
246.772690	-24.754148	262	263	262	17.282±0.028	16.210±0.008	15.460±0.007
246.772720	-24.912580	3	6	9	15.290±0.001	14.521±0.001	14.214±0.002

Table 1—Continued

RA (degrees)	Dec (degrees)	N_{Jobs}	N_{Hobs}	N_{Kobs}	J^a (mag)	H^a (mag)	K_s^a (mag)
246.772736	-24.873913	263	263	263	16.067±0.003	15.153±0.002	14.823±0.003
246.772766	-24.408319	261	261	255	17.372±0.089	16.536±0.046	15.527±0.025
246.772781	-24.801346	253	236	131	17.061±0.008	15.711±0.004	14.944±0.003
246.772827	-25.003105	121	128	54	15.960±0.002	15.232±0.002	14.933±0.003
246.772842	-25.061348	22	6	11	17.058±0.033	16.317±0.058	15.991±0.160
246.773071	-24.873737	84	67	21	16.067±0.003	15.153±0.002	14.823±0.003
246.773300	-24.225620	255	259	257	14.243±0.001	12.934±0.001	12.316±0.001
246.773346	-24.850622	111	90	27	17.192±0.030	16.365±0.027	15.829±0.046
246.773422	-25.168964	34	30	9	14.244±0.001	13.497±0.001	13.274±0.001
246.773483	-24.937523	14	3	6	16.929±0.007	16.065±0.006	15.594±0.012
246.773514	-24.938366	262	262	262	17.012±0.014	16.200±0.019	15.608±0.047
246.773575	-25.149471	36	134	109	17.207±0.027	16.409±0.026	15.844±0.048
246.773605	-24.670246	5	5	8	17.455±0.093	16.343±0.010	13.898±0.001
246.773682	-24.326866	263	263	263	17.267±0.016	15.767±0.004	14.729±0.003
246.773758	-24.874182	215	236	222	14.290±0.001	13.716±0.001	13.451±0.001
246.773788	-25.179443	252	238	148	17.066±0.012	16.351±0.020	15.814±0.051
246.773804	-24.948997	261	250	157	16.442±0.003	15.760±0.004	15.445±0.006
246.773834	-24.989147	263	262	253	16.900±0.006	16.153±0.006	15.666±0.011
246.774048	-24.789062	21	49	69	17.272±0.024	16.268±0.009	15.559±0.009
246.774063	-25.107588	258	256	223	17.098±0.016	16.376±0.029	15.824±0.055
246.774094	-24.862440	263	263	263	17.217±0.036	16.245±0.020	15.666±0.041
246.774231	-25.024239	93	63	19	17.069±0.029	16.317±0.051	15.695±0.157
246.774338	-24.619061	13	13	13	17.394±0.127	16.458±0.099	15.278±0.008
246.774429	-24.901575	137	206	189	16.170±0.003	15.179±0.002	14.747±0.003
246.774475	-25.027214	249	225	106	17.014±0.008	16.230±0.009	15.701±0.018
246.774628	-24.993830	75	48	8	11.515±0.001	10.429±0.001	10.067±0.001
246.774689	-25.000607	232	218	113	16.713±0.004	15.780±0.004	15.416±0.005
246.774719	-25.131950	20	7	6	16.067±0.002	15.384±0.003	15.125±0.004
246.774750	-24.311090	3	263	263	17.115±0.008	15.769±0.004	14.806±0.003
246.774796	-24.270737	261	260	260	17.339±0.088	16.405±0.035	15.579±0.028
246.774796	-24.870644	263	263	263	17.173±0.015	16.394±0.020	15.846±0.043
246.774872	-24.438417	173	164	58	17.147±0.009	13.361±0.001	11.024±0.001
246.774902	-24.476698	109	60	19	16.905±0.005	14.467±0.001	13.029±0.001
246.774918	-24.957367	151	149	59	16.979±0.008	16.127±0.008	15.597±0.018
246.775208	-24.636698	70	44	9	15.804±0.002	15.123±0.002	14.672±0.003
246.775269	-24.768789	258	258	258	17.399±0.071	16.392±0.032	15.808±0.054
246.775299	-24.954842	223	155	39	14.282±0.001	13.624±0.001	13.367±0.001
246.775375	-24.427608	263	263	263	17.558±0.000	16.524±0.063	15.394±0.018
246.775375	-24.409691	263	263	263	17.437±0.070	16.394±0.013	15.370±0.007
246.775436	-25.147890	68	68	21	17.256±0.040	16.457±0.050	15.753±0.066
246.775513	-24.876211	108	130	59	17.109±0.011	16.289±0.012	15.761±0.027
246.775650	-24.896963	11	8	2	13.167±0.001	12.049±0.001	11.698±0.001
246.775726	-24.957190	229	246	211	17.013±0.017	16.174±0.018	15.576±0.038
246.775894	-24.966921	226	222	151	17.180±0.026	16.290±0.023	15.810±0.045
246.776016	-25.050467	6	4	19	16.596±0.004	15.661±0.004	15.201±0.004

Table 1—Continued

RA (degrees)	Dec (degrees)	N_{Jobs}	N_{Hobs}	N_{Kobs}	J^a (mag)	H^a (mag)	K_s^a (mag)
246.776016	-24.909048	253	251	222	16.450±0.003	15.455±0.003	15.052±0.004
246.776245	-24.223505	263	263	263	16.634±0.004	14.986±0.002	14.278±0.002
246.776428	-25.095751	123	109	50	17.105±0.023	16.352±0.038	15.711±0.088
246.776443	-24.975151	195	164	55	17.182±0.033	16.327±0.025	15.579±0.022
246.776489	-24.874088	31	80	38	17.163±0.025	16.337±0.028	15.755±0.054
246.776489	-24.290480	34	40	15	16.178±0.003	14.577±0.001	13.886±0.001
246.776520	-24.260263	236	202	82	17.365±0.043	16.341±0.016	15.652±0.018
246.776550	-24.275373	237	220	150	17.354±0.064	16.372±0.025	15.691±0.028
246.776672	-25.052975	258	258	231	17.136±0.015	16.290±0.013	15.720±0.022
246.776718	-24.848455	8	6	2	15.727±0.002	14.795±0.002	14.426±0.002
246.776810	-25.055901	15	11	3	16.488±0.003	15.746±0.004	15.445±0.006
246.777084	-25.103775	11	5	7	17.101±0.011	16.305±0.012	15.763±0.028
246.777115	-24.322542	263	262	263	17.074±0.007	14.919±0.002	13.793±0.001
246.777206	-24.972616	47	17	4	16.615±0.004	15.712±0.004	15.374±0.005
246.777206	-25.114538	263	263	263	17.047±0.021	16.304±0.046	15.749±0.101
246.777405	-24.706207	5	5	2	17.384±0.072	16.443±0.022	15.488±0.013
246.777435	-24.356531	173	122	28	17.331±0.118	16.461±0.024	15.261±0.006
246.777481	-24.696856	65	59	18	12.386±0.001	11.331±0.001	10.705±0.001
246.777512	-25.117121	261	261	258	14.949±0.001	14.122±0.001	13.863±0.001
246.777557	-24.810177	221	207	113	17.277±0.044	16.408±0.039	15.809±0.051
246.777679	-24.864716	263	263	263	15.669±0.002	14.669±0.001	14.282±0.002
246.777817	-25.168514	35	32	10	15.369±0.001	14.497±0.001	14.098±0.002
246.777908	-25.089340	8	2	8	15.318±0.001	14.484±0.001	14.221±0.002
246.777939	-24.834885	200	188	130	16.918±0.005	16.055±0.005	15.558±0.007
246.778000	-25.144464	9	53	47	13.852±0.007	13.087±0.010	12.899±0.002
246.778076	-24.295286	10	3	5	17.257±0.021	16.315±0.011	15.639±0.013
246.778244	-24.637451	228	212	99	17.433±0.073	14.096±0.001	10.767±0.001
246.778595	-25.159046	159	259	262	15.295±0.001	14.428±0.001	14.047±0.002
246.778656	-24.713120	263	260	221	17.376±0.048	16.342±0.010	15.407±0.007
246.778671	-25.008490	11	4	2	15.039±0.001	14.072±0.001	13.700±0.001
246.779190	-24.262583	8	5	2	16.678±0.004	14.967±0.002	14.228±0.002
246.779205	-25.050922	244	206	87	16.438±0.003	15.637±0.003	15.317±0.005
246.779297	-24.727425	262	261	242	17.104±0.008	15.476±0.003	14.599±0.002
246.779373	-24.889729	262	263	263	17.171±0.031	16.499±0.049	15.853±0.086
246.779404	-25.017406	109	60	11	17.158±0.015	16.287±0.013	15.691±0.023
246.779419	-25.135309	257	256	255	16.600±0.004	16.030±0.005	15.626±0.010
246.779495	-24.279657	41	45	17	17.213±0.011	15.771±0.004	15.045±0.004
246.780106	-25.170446	15	10	5	14.629±0.001	13.888±0.001	13.667±0.001
246.780243	-25.141754	14	8	2	17.107±0.014	16.362±0.021	15.810±0.051
246.780365	-25.161192	67	68	27	14.217±0.001	13.697±0.001	13.490±0.001
246.780548	-24.202360	263	263	263	17.236±0.048	16.358±0.024	15.748±0.032
246.780655	-25.148659	251	229	114	16.939±0.006	16.251±0.008	15.708±0.018
246.780777	-24.904802	237	194	70	16.833±0.005	16.134±0.006	15.587±0.012
246.781143	-24.845217	256	261	248	16.940±0.006	15.879±0.004	15.403±0.005
246.781143	-24.986485	263	263	263	16.769±0.006	15.775±0.005	15.360±0.008

Table 1—Continued

RA (degrees)	Dec (degrees)	N_{Jobs}	N_{Hobs}	N_{Kobs}	J^a (mag)	H^a (mag)	K_s^a (mag)
246.781158	-24.985958	85	73	25	16.914±0.009	15.934±0.006	15.470±0.011
246.781174	-24.881758	248	240	153	13.726±0.001	13.128±0.001	12.872±0.001
246.781281	-24.684441	142	129	121	17.439±0.096	16.409±0.013	14.502±0.002
246.781296	-24.776003	49	30	5	13.462±0.001	12.029±0.001	11.322±0.001
246.781311	-25.069157	18	4	8	16.663±0.004	15.833±0.004	15.482±0.006
246.781479	-25.082346	262	262	263	13.656±0.001	12.954±0.001	12.713±0.001
246.781647	-24.212475	10	241	262	17.361±0.043	16.343±0.017	15.674±0.018
246.781723	-24.283131	254	238	132	16.460±0.003	14.848±0.002	14.073±0.002
246.781738	-25.172329	263	260	230	17.048±0.011	16.353±0.019	15.811±0.048
246.781754	-24.304850	28	9	9	17.022±0.006	15.641±0.003	14.969±0.003
246.781784	-25.073893	195	202	111	16.291±0.003	15.527±0.003	15.250±0.004
246.781952	-24.977417	262	262	253	17.166±0.024	16.362±0.032	15.825±0.091
246.782013	-24.847694	258	258	258	17.221±0.031	16.324±0.021	15.764±0.036
246.782043	-25.055359	258	258	257	16.772±0.005	15.946±0.005	15.494±0.010
246.782318	-24.225819	37	44	13	16.947±0.006	15.491±0.003	14.853±0.003
246.782639	-25.121321	262	262	262	17.113±0.016	16.375±0.022	15.868±0.060
246.782883	-24.769037	199	188	84	17.208±0.049	16.328±0.027	15.645±0.032
246.782990	-24.937738	12	5	8	15.412±0.002	14.737±0.002	14.473±0.002
246.783112	-24.674715	11	7	8	17.547±0.155	16.337±0.010	13.712±0.001
246.783188	-24.217194	31	33	8	17.298±0.026	16.294±0.013	15.608±0.016
246.783249	-24.972828	263	263	263	16.942±0.008	16.040±0.007	15.512±0.011
246.783279	-24.972294	263	263	263	16.941±0.006	16.035±0.006	15.508±0.009
246.783386	-25.021955	263	263	262	17.137±0.021	16.411±0.031	15.786±0.093
246.783417	-24.970465	28	12	2	16.133±0.003	15.400±0.003	15.143±0.004
246.783539	-24.335281	2	151	263	17.243±0.013	14.821±0.002	13.377±0.001
246.783615	-25.117081	230	197	148	16.334±0.003	15.584±0.003	15.310±0.005
246.783630	-24.892876	9	263	263	17.164±0.012	16.362±0.013	15.769±0.025
246.783676	-24.938990	263	263	263	16.822±0.005	16.072±0.006	15.606±0.012
246.783783	-25.096460	124	142	52	16.910±0.006	16.184±0.007	15.695±0.014
246.783859	-24.812227	198	126	33	17.297±0.037	16.332±0.020	15.698±0.027
246.784058	-25.171352	263	263	263	16.994±0.007	16.256±0.009	15.751±0.020
246.784149	-24.773638	35	110	84	17.246±0.013	16.145±0.006	15.474±0.006
246.784149	-24.707903	72	52	13	15.365±0.001	12.252±0.001	10.723±0.001
246.784149	-24.777971	190	129	39	16.701±0.004	15.058±0.002	14.327±0.002
246.784225	-25.060514	169	159	69	17.156±0.032	16.343±0.035	15.872±0.071
246.784286	-24.839815	2	5	37	17.130±0.009	16.187±0.007	15.654±0.010
246.784332	-25.135077	13	15	5	17.093±0.009	16.229±0.009	15.686±0.018
246.784393	-25.169378	102	64	20	15.765±0.002	15.028±0.002	14.792±0.003
246.784409	-24.776373	263	263	263	16.063±0.003	14.574±0.002	13.863±0.002
246.784531	-24.293964	232	204	73	17.310±0.046	16.362±0.020	15.717±0.025
246.784576	-24.808014	50	14	9	17.054±0.007	15.585±0.003	14.796±0.003
246.784775	-25.150612	33	54	47	16.805±0.005	16.106±0.006	15.671±0.013
246.784775	-25.046839	260	258	254	17.092±0.023	16.491±0.044	15.766±0.089
246.784805	-24.244259	29	95	81	17.271±0.039	16.372±0.026	15.729±0.038
246.784836	-24.242016	13	5	7	15.215±0.001	13.896±0.001	13.300±0.001

Table 1—Continued

RA (degrees)	Dec (degrees)	N_{Jobs}	N_{Hobs}	N_{Kobs}	J^a (mag)	H^a (mag)	K_s^a (mag)
246.784927	-24.302116	14	6	8	17.289±0.055	16.333±0.017	15.664±0.021
246.785004	-24.426464	191	159	54	17.349±0.033	15.587±0.003	14.234±0.002
246.785095	-25.049814	263	263	263	17.147±0.022	16.405±0.034	15.898±0.070
246.785172	-25.105749	263	263	263	16.440±0.003	15.492±0.003	15.127±0.004
246.785202	-25.081661	247	236	133	16.419±0.003	15.520±0.003	15.216±0.004
246.785416	-25.033403	8	2	5	15.927±0.002	15.198±0.002	14.914±0.003
246.785645	-24.882986	239	228	117	16.782±0.005	15.836±0.004	15.435±0.006
246.785797	-25.079819	11	9	8	14.694±0.001	14.031±0.001	13.789±0.001
246.785828	-25.110992	17	6	2	15.851±0.002	15.208±0.002	14.989±0.003
246.786072	-25.054264	262	262	261	17.024±0.008	16.291±0.011	15.743±0.024
246.786163	-24.256680	263	263	263	17.200±0.038	16.331±0.024	15.684±0.032
246.786331	-25.042410	11	11	2	16.313±0.003	15.653±0.003	15.382±0.005
246.786346	-25.149536	64	54	15	14.400±0.001	13.809±0.001	13.610±0.001
246.786453	-24.957067	30	14	4	16.599±0.004	15.726±0.004	15.371±0.005
246.786606	-24.962889	6	5	2	16.648±0.004	15.925±0.004	15.525±0.007
246.786606	-24.835644	263	263	263	17.069±0.007	16.017±0.005	15.531±0.007
246.786743	-24.895596	231	194	236	16.440±0.003	15.380±0.003	14.978±0.003
246.787292	-24.719088	34	30	17	17.441±0.062	16.266±0.008	15.117±0.004
246.787476	-25.029577	48	102	65	14.322±0.001	13.318±0.001	12.942±0.001
246.787537	-25.044146	12	47	48	17.074±0.009	16.311±0.012	15.757±0.024
246.787598	-25.175299	263	263	263	16.923±0.007	16.036±0.006	15.301±0.005
246.787659	-24.930634	263	263	263	14.494±0.001	13.807±0.001	13.538±0.001
246.787750	-24.286547	148	116	43	16.530±0.004	14.970±0.002	14.242±0.002
246.787811	-24.921217	255	256	206	17.118±0.010	16.227±0.009	15.703±0.018
246.787857	-24.200172	121	109	38	12.487±0.001	10.746±0.001	9.857±0.001
246.787888	-25.073311	263	263	263	13.589±0.001	12.704±0.001	12.414±0.001
246.787964	-24.568890	7	4	39	12.650±0.001	10.263±0.001	8.921±0.001
246.788071	-24.919527	111	77	28	15.166±0.001	14.327±0.002	14.042±0.002
246.788193	-24.901449	173	98	24	16.307±0.003	15.540±0.003	15.253±0.004
246.788284	-24.965809	7	7	82	17.137±0.011	16.323±0.012	15.814±0.027
246.788513	-24.233017	263	263	263	17.220±0.053	16.361±0.042	15.746±0.054
246.788635	-25.082127	122	69	23	17.192±0.035	16.387±0.031	15.789±0.060
246.788712	-25.152592	263	263	263	16.240±0.003	15.708±0.004	15.455±0.006
246.788742	-24.249037	71	112	47	17.253±0.020	16.305±0.011	15.657±0.014
246.788834	-24.722067	15	18	18	14.326±0.001	12.201±0.001	11.074±0.001
246.788971	-24.672836	14	4	6	17.192±0.010	13.542±0.001	11.322±0.001
246.788986	-24.220171	257	258	229	16.558±0.004	15.097±0.002	14.503±0.002
246.789001	-25.113501	10	3	2	16.783±0.005	15.859±0.004	15.449±0.006
246.789032	-24.826162	40	18	5	16.865±0.005	15.880±0.004	15.352±0.005
246.789047	-25.176283	3	58	112	16.404±0.003	15.798±0.004	15.496±0.007
246.789062	-25.098370	260	255	206	16.701±0.004	15.785±0.004	15.331±0.005
246.789078	-24.281368	255	257	257	14.150±0.001	12.850±0.001	12.181±0.001
246.789230	-24.621819	262	263	263	16.737±0.006	11.059±0.001	7.051±0.001
246.789322	-24.779991	0	2	8	17.251±0.013	16.101±0.006	15.477±0.006
246.789505	-25.062437	124	144	59	17.217±0.040	16.406±0.035	15.809±0.071

Table 1—Continued

RA (degrees)	Dec (degrees)	N_{Jobs}	N_{Hobs}	N_{Kobs}	J^a (mag)	H^a (mag)	K_s^a (mag)
246.789642	-24.970959	253	262	260	15.856±0.002	15.172±0.002	14.942±0.003
246.789703	-25.173515	256	255	255	16.755±0.005	16.008±0.005	15.605±0.009
246.789719	-24.746996	262	263	261	17.133±0.097	16.450±0.033	15.619±0.029
246.789734	-24.414890	120	76	20	17.415±0.046	16.070±0.005	14.837±0.003
246.789764	-25.119165	263	262	262	16.751±0.004	15.997±0.005	15.600±0.008
246.789795	-25.053850	9	3	5	16.931±0.006	16.204±0.007	15.688±0.015
246.789841	-24.920353	210	257	257	16.153±0.003	15.217±0.002	14.891±0.003
246.789886	-24.194683	246	226	119	17.242±0.080	16.113±0.027	15.405±0.030
246.790070	-25.154381	40	20	5	15.488±0.002	14.893±0.002	14.682±0.003
246.790222	-24.768513	263	263	263	17.284±0.029	16.295±0.011	15.588±0.012
246.790329	-25.034861	258	257	257	17.212±0.037	16.418±0.040	15.780±0.078
246.790482	-24.904238	162	134	46	16.683±0.004	15.821±0.004	15.468±0.006
246.790497	-24.498713	263	263	262	17.346±0.085	16.250±0.007	12.962±0.001
246.790512	-25.066763	250	223	99	16.102±0.003	15.346±0.003	15.067±0.004
246.790619	-24.318192	257	257	231	16.299±0.281	15.160±0.278	14.182±0.048
246.790619	-24.907547	261	262	256	17.198±0.040	16.433±0.042	15.888±0.095
246.790649	-24.927452	172	186	105	17.135±0.017	16.409±0.027	15.760±0.059
246.790741	-25.064871	234	246	188	17.088±0.031	16.305±0.056	15.489±0.091
246.790771	-24.813931	3	15	13	15.780±0.002	14.597±0.001	14.042±0.002
246.790787	-24.896832	260	254	183	17.137±0.011	16.293±0.011	15.720±0.020
246.790833	-24.993759	44	22	7	15.476±0.002	14.497±0.001	14.144±0.002
246.790909	-25.146763	13	8	2	16.599±0.004	15.809±0.004	15.469±0.006
246.790924	-25.107670	117	100	78	16.702±0.004	16.001±0.005	15.595±0.009
246.791092	-24.222483	263	263	263	17.310±0.023	16.155±0.007	15.468±0.007
246.791199	-24.963230	259	256	197	15.764±0.002	15.094±0.002	14.840±0.003
246.791245	-25.078129	255	252	190	17.125±0.015	16.365±0.021	15.911±0.045
246.791245	-25.059940	263	263	263	17.185±0.026	16.341±0.026	15.716±0.056
246.791397	-24.936432	51	64	25	17.127±0.011	16.269±0.010	15.758±0.023
246.791473	-25.152332	5	82	92	17.038±0.012	16.333±0.025	15.792±0.066
246.791473	-24.856319	36	31	10	16.919±0.005	15.884±0.004	15.443±0.006
246.791504	-25.121838	90	59	16	16.971±0.006	16.086±0.006	15.622±0.010
246.791626	-25.037598	258	258	253	16.099±0.002	15.379±0.003	15.113±0.004
246.791824	-24.486958	10	3	1	16.649±0.004	15.116±0.002	14.181±0.002
246.791824	-25.050394	26	27	8	17.180±0.032	16.291±0.035	15.812±0.056
246.791916	-25.151964	137	164	93	17.021±0.022	16.230±0.034	15.758±0.085
246.791916	-24.759487	263	263	263	11.323±0.001	10.681±0.001	10.500±0.001
246.791962	-25.139137	90	257	260	16.930±0.006	16.189±0.007	15.709±0.015
246.792038	-24.980467	27	15	2	17.228±0.027	16.402±0.027	15.804±0.059
246.792236	-25.057810	11	253	263	16.957±0.006	16.175±0.007	15.701±0.014
246.792313	-25.076162	263	263	263	16.973±0.008	16.218±0.010	15.758±0.029
246.792511	-24.794077	6	151	246	17.315±0.048	16.309±0.012	15.563±0.013
246.792587	-25.148754	140	166	88	17.076±0.008	16.189±0.007	15.674±0.013
246.792618	-24.819992	123	151	69	16.238±0.003	14.939±0.002	14.387±0.002
246.792618	-24.881552	231	187	56	16.410±0.004	15.618±0.004	15.278±0.007
246.792648	-24.841051	53	21	4	15.529±0.002	14.449±0.001	14.027±0.002

Table 1—Continued

RA (degrees)	Dec (degrees)	N_{Jobs}	N_{Hobs}	N_{Kobs}	J^a (mag)	H^a (mag)	K_s^a (mag)
246.792862	-24.320118	17	5	1	8.751±0.001	7.538±0.001	6.713±0.001
246.792862	-24.881071	248	196	82	16.696±0.006	15.879±0.005	15.448±0.010
246.792984	-24.321806	263	263	263	11.939±0.001	10.430±0.001	9.654±0.002
246.793137	-24.556253	263	263	263	17.142±0.008	13.836±0.001	11.905±0.001
246.793182	-25.182371	263	263	263	16.203±0.004	15.258±0.004	14.942±0.007
246.793243	-25.094690	258	258	258	17.113±0.011	16.213±0.009	15.702±0.017
246.793411	-24.909166	11	4	1	17.133±0.028	16.405±0.038	15.957±0.123
246.793411	-24.924696	104	89	28	15.401±0.001	14.720±0.002	14.474±0.002
246.793442	-24.591965	70	46	12	17.477±0.133	16.512±0.042	15.244±0.006
246.793503	-25.075905	11	254	263	16.569±0.004	15.806±0.004	15.486±0.007
246.793625	-25.115128	247	251	194	17.116±0.014	16.281±0.014	15.735±0.029
246.793930	-25.156067	262	262	263	16.995±0.006	16.100±0.006	15.618±0.009
246.793945	-24.291870	8	2	1	16.717±0.004	15.280±0.002	14.614±0.002
246.793991	-24.962378	255	243	154	12.920±0.001	12.031±0.001	11.732±0.001
246.794006	-25.098042	257	259	255	17.226±0.027	16.391±0.027	15.719±0.048
246.794098	-24.387581	154	93	25	16.139±0.003	14.059±0.001	12.968±0.001
246.794250	-24.773872	9	6	2	16.816±0.005	15.380±0.003	14.675±0.003
246.794281	-25.144764	263	263	261	17.131±0.010	16.300±0.011	15.780±0.024
246.794296	-25.101547	260	261	261	17.076±0.012	16.345±0.019	15.825±0.044
246.794296	-24.998333	263	263	263	13.877±0.001	12.902±0.001	12.584±0.001
246.794342	-24.948334	263	263	263	14.037±0.001	13.331±0.001	13.095±0.001
246.794495	-24.234505	257	241	135	17.275±0.066	16.379±0.035	15.652±0.033
246.794830	-25.163412	263	263	263	16.616±0.004	15.928±0.005	15.530±0.008
246.795090	-24.863716	256	256	195	17.225±0.032	16.344±0.033	15.765±0.054
246.795105	-24.984177	45	57	27	17.055±0.007	16.161±0.007	15.586±0.009
246.795120	-24.763132	89	74	36	17.402±0.036	16.398±0.014	15.645±0.014
246.795212	-24.271233	263	263	263	15.922±0.002	14.317±0.001	13.624±0.001
246.795578	-24.810232	155	131	53	17.197±0.011	15.987±0.005	15.299±0.005
246.795700	-24.758245	173	227	167	13.011±0.001	11.056±0.001	10.156±0.001
246.795731	-24.922565	124	96	29	13.245±0.001	12.384±0.001	12.114±0.001
246.795837	-25.053904	19	20	5	17.134±0.013	16.371±0.018	15.728±0.024
246.795883	-25.154385	10	14	6	16.705±0.004	16.011±0.005	15.633±0.009
246.795914	-24.857080	58	37	9	17.162±0.025	16.358±0.029	15.753±0.050
246.796234	-24.893217	263	263	263	16.841±0.005	15.992±0.005	15.597±0.008
246.796280	-24.823008	2	11	12	17.264±0.033	16.268±0.012	15.582±0.014
246.796432	-24.329012	15	10	4	17.337±0.023	15.517±0.003	14.281±0.002
246.796432	-24.251944	252	248	201	15.504±0.002	13.994±0.001	13.351±0.001
246.796570	-24.679569	156	128	49	17.082±0.008	13.223±0.001	10.563±0.001
246.796585	-25.043989	263	263	262	16.973±0.006	16.188±0.007	15.650±0.014
246.796661	-24.985331	67	54	17	17.133±0.013	16.246±0.010	15.692±0.019
246.796799	-24.939007	263	263	263	16.659±0.004	15.936±0.004	15.558±0.007
246.796951	-24.849644	216	224	148	15.272±0.001	14.197±0.001	13.792±0.001
246.797134	-25.099350	2	153	259	17.156±0.027	16.493±0.042	15.767±0.105
246.797211	-25.094393	260	255	206	16.665±0.004	15.697±0.004	15.338±0.005
246.797485	-24.279591	17	7	8	17.291±0.017	16.057±0.005	15.337±0.005

Table 1—Continued

RA (degrees)	Dec (degrees)	N_{Jobs}	N_{Hobs}	N_{Kobs}	J^a (mag)	H^a (mag)	K_s^a (mag)
246.797562	-24.770283	251	240	139	14.811±0.001	13.103±0.001	12.312±0.001
246.797607	-24.973959	5	34	183	15.298±0.001	14.600±0.001	14.359±0.002
246.797745	-24.873192	22	23	11	15.498±0.002	14.384±0.001	13.983±0.001
246.797791	-24.373859	178	205	103	17.262±0.081	16.390±0.012	15.081±0.004
246.797897	-24.781466	258	258	258	17.273±0.019	16.115±0.006	15.428±0.006
246.797974	-24.959227	233	212	109	17.118±0.015	16.396±0.022	15.841±0.058
246.798065	-24.840797	257	259	252	16.495±0.003	15.542±0.003	15.123±0.004
246.798111	-25.145130	4	6	2	17.113±0.012	16.331±0.014	15.801±0.032
246.798172	-25.107994	73	79	28	14.111±0.001	13.293±0.001	13.038±0.001
246.798233	-24.890268	263	263	263	15.229±0.001	14.462±0.002	14.169±0.002
246.798386	-24.908932	263	263	263	17.002±0.006	16.229±0.008	15.712±0.015
246.798416	-24.977003	260	260	241	17.103±0.010	16.298±0.011	15.745±0.022
246.798538	-24.863157	14	5	4	17.067±0.007	16.218±0.007	15.699±0.013
246.798538	-24.211119	221	263	262	17.324±0.054	16.370±0.025	15.665±0.028
246.798676	-24.947859	174	149	40	16.267±0.003	15.263±0.002	14.913±0.003
246.798691	-25.030790	217	159	51	16.340±0.003	15.564±0.003	15.286±0.005
246.798706	-24.394924	9	11	1	14.270±0.001	11.612±0.001	10.087±0.001
246.798798	-24.916824	12	4	4	15.185±0.001	14.400±0.001	14.118±0.002
246.798813	-24.782558	12	3	8	17.223±0.015	15.896±0.005	15.141±0.004
246.798828	-24.642199	16	4	6	17.301±0.120	14.970±0.002	11.076±0.001
246.798859	-24.889456	27	18	3	17.091±0.029	16.209±0.016	15.606±0.049
246.798859	-24.202517	143	172	68	16.716±0.005	15.418±0.003	14.800±0.003
246.798874	-25.150564	37	42	21	17.143±0.024	16.363±0.022	15.643±0.023
246.798874	-25.078196	257	254	199	17.145±0.017	16.418±0.025	15.902±0.056
246.798904	-25.122555	6	8	3	17.183±0.028	16.365±0.033	15.852±0.066
246.798920	-24.786337	263	263	263	13.748±0.001	11.962±0.001	11.191±0.001
246.798935	-24.889423	256	247	164	17.094±0.027	16.203±0.015	15.626±0.047
246.798965	-25.148296	263	262	263	16.572±0.004	15.937±0.005	15.564±0.008
246.799103	-24.561150	257	261	258	17.352±0.107	16.552±0.071	15.493±0.030
246.799179	-24.725004	2	3	19	17.511±0.115	16.476±0.018	15.166±0.004
246.799225	-24.969505	172	150	55	17.118±0.032	16.458±0.043	15.873±0.079
246.799377	-24.206388	53	47	14	17.219±0.046	16.328±0.024	15.714±0.035
246.799393	-24.206377	219	171	55	17.219±0.046	16.328±0.024	15.714±0.035
246.799530	-24.854488	254	250	198	17.196±0.025	16.395±0.028	15.903±0.060
246.799606	-24.998066	262	262	260	17.150±0.021	16.436±0.035	15.820±0.085
246.799667	-25.155891	49	113	85	17.073±0.012	16.404±0.020	15.831±0.057
246.799728	-24.975271	243	231	128	17.009±0.007	16.105±0.006	15.577±0.009
246.799805	-24.912670	45	102	56	17.041±0.008	16.268±0.009	15.734±0.021
246.799927	-25.042988	200	177	63	16.513±0.004	15.720±0.004	15.432±0.006
246.799973	-24.958683	260	259	231	15.787±0.002	14.945±0.002	14.681±0.003
246.800079	-25.058285	17	18	5	17.110±0.016	16.338±0.019	15.749±0.042
246.800171	-24.891941	263	263	261	15.253±0.001	14.519±0.001	14.224±0.002
246.800217	-25.096254	255	254	225	14.166±0.001	13.307±0.001	13.046±0.001
246.800354	-25.108286	261	263	262	14.861±0.001	14.199±0.001	13.969±0.002
246.800461	-24.887337	263	263	262	15.275±0.001	14.480±0.001	14.164±0.002

Table 1—Continued

RA (degrees)	Dec (degrees)	N_{Jobs}	N_{Hobs}	N_{Kobs}	J^a (mag)	H^a (mag)	K_s^a (mag)
246.800537	-24.580280	210	238	204	15.738±0.002	13.162±0.001	11.561±0.001
246.800537	-25.055054	263	263	263	15.532±0.002	14.771±0.002	14.504±0.002
246.800705	-24.909903	50	28	7	17.091±0.009	16.342±0.012	15.763±0.026
246.801208	-25.064646	10	11	5	13.868±0.001	13.281±0.001	13.065±0.001
246.801285	-24.239605	7	10	5	16.433±0.004	14.994±0.002	14.318±0.002
246.801361	-25.091143	20	8	2	16.649±0.004	15.788±0.004	15.463±0.006
246.801376	-24.808331	126	68	13	17.335±0.054	16.421±0.035	15.727±0.046
246.801437	-25.157614	262	255	191	16.967±0.006	16.288±0.009	15.755±0.023
246.801773	-24.204544	194	48	11	17.313±0.049	16.396±0.028	15.694±0.033
246.801834	-24.971043	18	35	48	17.103±0.009	16.319±0.011	15.775±0.025
246.801895	-24.789610	23	21	3	17.239±0.049	16.403±0.030	15.770±0.037
246.801895	-25.005840	192	143	51	17.114±0.011	16.348±0.014	15.760±0.034
246.802017	-24.981216	171	258	259	15.426±0.001	14.734±0.002	14.469±0.002
246.802078	-24.989614	146	251	247	15.317±0.001	14.514±0.001	14.248±0.002
246.802078	-25.177418	263	263	263	17.077±0.013	16.407±0.026	15.863±0.050
246.802277	-25.150267	263	262	261	17.033±0.024	16.339±0.068	15.795±99.000
246.802399	-25.027691	257	261	259	16.029±0.002	15.279±0.002	15.024±0.004
246.802521	-24.773069	251	252	191	17.194±0.010	15.644±0.003	14.811±0.003
246.802567	-24.884367	110	54	8	16.420±0.003	15.335±0.003	14.912±0.003
246.802597	-24.907017	245	207	190	14.641±0.001	13.816±0.001	13.528±0.001
246.802612	-25.150316	2	4	7	17.044±0.020	16.307±0.062	15.801±0.133
246.802704	-24.879717	90	149	83	16.797±0.005	15.960±0.005	15.530±0.007
246.802734	-25.048882	24	35	12	17.179±0.035	16.416±0.040	15.865±0.073
246.802750	-24.854778	75	128	69	17.039±0.008	16.258±0.010	15.649±0.018
246.802780	-25.123220	151	163	108	17.043±0.026	16.193±0.020	15.466±0.085
246.802780	-25.001261	263	263	263	17.204±0.017	16.324±0.015	15.721±0.028
246.802872	-24.768259	196	202	107	16.931±0.005	15.253±0.002	14.436±0.002
246.802902	-24.953854	2	4	25	17.185±0.015	16.318±0.013	15.731±0.023
246.803009	-25.145508	13	12	5	16.516±0.004	15.624±0.003	15.326±0.005
246.803055	-25.067175	16	11	2	10.637±0.001	9.761±0.001	9.373±0.001
246.803146	-24.816685	28	32	11	15.874±0.002	14.339±0.002	13.695±0.001
246.803162	-24.962584	239	211	91	16.290±0.003	15.456±0.003	15.163±0.004
246.803238	-24.854868	20	8	2	17.036±0.010	16.257±0.012	15.644±0.021
246.803314	-25.122286	83	112	48	14.011±0.001	13.385±0.001	13.164±0.001
246.803635	-24.937506	183	161	56	16.885±0.005	16.162±0.006	15.663±0.012
246.803665	-24.815514	206	154	45	15.547±0.003	14.179±0.003	13.578±0.002
246.803680	-24.262825	10	260	263	17.239±0.013	15.986±0.005	15.308±0.005
246.803818	-24.915289	44	14	3	16.487±0.003	15.784±0.004	15.452±0.006
246.803818	-24.988056	263	263	263	13.502±0.001	12.697±0.001	12.440±0.001
246.803955	-24.300146	263	263	263	17.363±0.039	16.309±0.008	15.461±0.007
246.803970	-25.041616	262	263	263	17.092±0.011	16.389±0.018	15.803±0.044
246.803986	-24.218559	23	18	5	17.316±0.027	16.272±0.011	15.614±0.013
246.804016	-25.081078	154	103	27	17.161±0.011	16.253±0.009	15.722±0.017
246.804138	-25.057652	239	214	105	17.098±0.012	16.376±0.019	15.809±0.046
246.804245	-25.147676	11	99	240	15.901±0.002	15.000±0.002	14.619±0.002

Table 1—Continued

RA (degrees)	Dec (degrees)	N_{Jobs}	N_{Hobs}	N_{Kobs}	J^a (mag)	H^a (mag)	K_s^a (mag)
246.804276	-24.715944	17	5	7	17.188±0.000	16.566±0.072	15.272±0.008
246.804276	-24.246395	137	107	28	17.253±0.041	16.316±0.020	15.727±0.028
246.804337	-24.868439	263	263	263	16.662±0.004	15.477±0.003	14.976±0.003
246.804413	-24.558487	263	263	263	17.367±0.049	15.816±0.004	14.359±0.002
246.804565	-24.969294	248	261	258	17.129±0.013	16.265±0.012	15.715±0.023
246.804871	-25.119028	7	4	24	17.092±0.009	16.210±0.008	15.682±0.013
246.805038	-25.178495	260	260	260	16.218±0.003	15.627±0.003	15.365±0.005
246.805084	-24.805779	102	130	47	17.284±0.017	16.241±0.008	15.596±0.010
246.805176	-24.396465	76	35	7	17.407±0.104	16.497±0.050	15.365±0.011
246.805267	-24.692636	218	234	158	17.207±0.009	12.396±0.001	9.593±0.001
246.805328	-24.197119	32	14	3	16.026±0.004	14.840±0.003	14.303±0.003
246.805359	-24.994448	263	263	263	17.048±0.007	16.296±0.009	15.742±0.021
246.805374	-24.283649	224	262	262	16.375±0.003	14.625±0.002	13.862±0.001
246.805374	-24.897598	263	263	261	17.177±0.015	16.393±0.019	15.785±0.039
246.805557	-24.370056	263	263	262	17.421±0.132	16.509±0.028	15.215±0.005
246.805801	-25.001766	16	3	2	17.007±0.007	16.259±0.009	15.735±0.017
246.805908	-24.885656	177	130	41	17.128±0.008	16.120±0.006	15.596±0.008
246.805954	-24.232336	54	69	20	16.332±0.003	14.963±0.002	14.321±0.002
246.806122	-25.183313	128	78	18	16.724±0.007	16.075±0.012	15.630±0.047
246.806152	-24.849930	263	263	263	17.151±0.008	16.091±0.005	15.466±0.006
246.806244	-24.205643	263	263	263	16.953±0.006	15.659±0.004	15.079±0.004
246.806290	-24.866417	152	191	160	16.932±0.005	15.988±0.005	15.534±0.007
246.806427	-24.831659	237	244	215	17.200±0.014	16.214±0.008	15.616±0.011
246.806442	-24.904440	257	252	186	16.192±0.003	15.315±0.003	15.005±0.003
246.806702	-24.952847	253	257	214	16.626±0.004	15.923±0.004	15.554±0.008
246.807007	-25.051371	263	263	263	16.809±0.006	16.089±0.008	15.631±0.014
246.807037	-24.907747	12	20	9	16.501±0.003	15.504±0.003	15.156±0.004
246.807037	-24.877993	51	235	247	17.071±0.007	15.981±0.005	15.523±0.007
246.807053	-24.838821	2	192	263	16.035±0.002	14.834±0.002	14.307±0.002
246.807236	-24.304626	238	263	263	12.287±0.001	10.254±0.001	9.240±0.001
246.807388	-25.095842	263	262	263	8.783±0.001	8.513±0.001	8.336±0.001
246.807495	-24.937654	256	257	253	16.729±0.004	15.949±0.005	15.570±0.008
246.807587	-25.125143	260	263	263	14.711±0.001	13.901±0.001	13.659±0.001
246.807602	-24.725399	6	15	11	13.386±0.001	11.304±0.001	10.126±0.001
246.807693	-25.147070	152	263	263	17.114±0.015	16.336±0.026	15.709±0.071
246.807724	-25.029575	255	263	263	16.955±0.005	16.020±0.005	15.539±0.007
246.807755	-24.262215	249	257	250	16.760±0.005	15.065±0.002	14.251±0.002
246.807800	-25.178209	263	263	261	16.191±0.003	15.582±0.003	15.345±0.005
246.807999	-25.160095	263	263	263	16.273±0.003	15.717±0.004	15.457±0.006
246.808044	-24.865767	87	39	9	17.308±0.017	16.324±0.010	15.695±0.014
246.808075	-25.157150	179	262	262	17.131±0.028	16.461±0.056	15.547±0.110
246.808380	-24.207184	118	93	27	17.291±0.032	16.223±0.011	15.542±0.015
246.808533	-24.252649	10	44	45	15.356±0.002	13.899±0.001	13.274±0.001
246.808792	-24.971676	257	242	141	17.234±0.019	16.351±0.018	15.785±0.036
246.808884	-25.046068	0	7	43	16.754±0.004	16.044±0.005	15.619±0.010

Table 1—Continued

RA (degrees)	Dec (degrees)	N_{Jobs}	N_{Hobs}	N_{Kobs}	J^a (mag)	H^a (mag)	K_s^a (mag)
246.808990	-24.939152	12	262	227	17.115±0.008	16.167±0.007	15.638±0.011
246.809128	-24.208330	11	251	252	16.145±0.003	14.813±0.002	14.207±0.002
246.809280	-24.793310	255	260	257	17.275±0.041	16.326±0.019	15.693±0.025
246.809479	-25.077837	4	6	18	17.234±0.017	16.309±0.014	15.797±0.028
246.809509	-24.314283	193	238	238	17.279±0.013	15.143±0.002	13.930±0.001
246.809677	-24.960354	9	10	3	17.158±0.022	16.297±0.026	15.710±0.072
246.809708	-25.173199	259	263	263	17.152±0.021	16.256±0.015	15.431±0.012
246.809769	-24.205948	2	8	4	16.895±0.005	15.665±0.004	15.109±0.004
246.809784	-24.525482	7	34	30	17.350±0.046	16.251±0.008	15.125±0.004
246.809814	-24.922585	13	70	60	16.336±0.003	15.311±0.003	14.907±0.003
246.809814	-25.125526	263	263	263	16.398±0.003	15.728±0.004	15.422±0.006
246.810059	-24.824921	263	263	263	16.903±0.005	15.709±0.004	15.132±0.004
246.810303	-24.582663	8	2	1	17.489±0.165	16.538±0.039	15.331±0.009
246.810333	-25.102367	263	263	263	17.259±0.012	16.343±0.011	15.744±0.017
246.810379	-24.859274	263	263	263	11.460±0.001	10.685±0.001	10.378±0.001
246.810410	-24.223303	6	240	263	17.247±0.015	15.925±0.005	15.163±0.004
246.810440	-24.446070	252	255	236	17.450±0.097	15.241±0.002	12.185±0.001
246.810577	-25.014296	263	263	262	16.827±0.005	15.847±0.004	15.411±0.006
246.810593	-24.895792	8	68	78	17.161±0.032	16.303±0.027	15.770±0.055
246.810974	-24.253883	99	104	100	17.291±0.065	16.312±0.039	15.663±0.050
246.810974	-24.386831	263	263	262	17.429±0.070	16.339±0.011	15.167±0.004
246.811020	-24.897003	232	228	228	17.112±0.018	16.280±0.020	15.677±0.042
246.811050	-24.893694	258	259	258	16.841±0.005	15.942±0.005	15.493±0.009
246.811157	-24.232744	91	253	253	17.211±0.012	15.919±0.005	15.166±0.005
246.811432	-24.960543	5	32	259	16.945±0.006	16.218±0.008	15.697±0.016
246.811478	-24.812683	263	263	263	17.079±0.007	15.826±0.004	15.267±0.005
246.811783	-24.892708	12	80	66	14.278±0.001	13.405±0.001	13.087±0.001
246.811813	-24.884420	27	108	110	16.286±0.003	15.218±0.003	14.797±0.003
246.811813	-24.247814	260	259	259	17.342±0.076	16.410±0.035	15.649±0.035
246.811890	-24.328236	259	258	252	17.362±0.033	15.713±0.004	14.441±0.002
246.811920	-24.767988	259	259	259	17.381±0.035	15.951±0.005	14.885±0.003
246.811951	-24.994469	22	23	10	12.537±0.001	11.725±0.001	11.477±0.001
246.811981	-24.984518	6	27	252	16.540±0.004	15.766±0.004	15.428±0.006
246.812210	-24.980316	29	10	3	17.184±0.012	16.278±0.011	15.724±0.018
246.812241	-24.208109	3	30	162	16.790±0.005	15.565±0.003	14.967±0.004
246.812347	-24.808563	29	93	73	16.190±0.003	15.098±0.002	14.623±0.002
246.812515	-25.034811	61	177	164	17.232±0.026	16.319±0.022	15.784±0.047
246.812668	-25.059814	124	190	131	16.380±0.003	15.421±0.003	15.123±0.004
246.812668	-25.108917	205	256	256	17.167±0.023	16.433±0.040	15.892±0.114
246.812683	-24.879004	8	158	260	17.226±0.028	16.419±0.031	15.776±0.065
246.812714	-25.144245	9	83	94	17.178±0.025	16.416±0.046	15.766±0.110
246.812714	-25.166115	153	181	193	17.150±0.018	16.352±0.034	15.914±0.085
246.812805	-24.889853	253	252	252	16.041±0.002	15.288±0.002	14.990±0.003
246.812851	-25.116571	7	5	223	17.144±0.026	16.620±0.080	15.912±0.128
246.812897	-24.937517	6	27	13	16.356±0.003	15.633±0.003	15.338±0.005

Table 1—Continued

RA (degrees)	Dec (degrees)	N_{Jobs}	N_{Hobs}	N_{Kobs}	J^a (mag)	H^a (mag)	K_s^a (mag)
246.812973	-24.378099	2	39	109	17.454±0.101	16.195±0.006	14.647±0.003
246.813004	-25.025707	4	6	49	17.134±0.021	16.370±0.043	15.760±0.108
246.813034	-24.860764	262	262	263	10.656±0.001	9.808±0.001	9.467±0.001
246.813049	-25.023998	2	34	229	15.047±0.001	14.393±0.001	14.139±0.002
246.813095	-24.793125	263	263	263	17.302±0.026	16.233±0.013	15.653±0.018
246.813187	-24.961121	262	263	262	17.173±0.017	16.286±0.014	15.728±0.025
246.813431	-25.056717	7	75	114	17.180±0.025	16.363±0.034	15.774±0.049
246.813477	-25.011923	6	135	230	17.134±0.011	16.359±0.015	15.787±0.035
246.813568	-25.088156	97	96	31	16.874±0.005	16.059±0.005	15.644±0.010
246.813858	-25.131935	5	5	4	17.043±0.007	16.314±0.011	15.776±0.029
246.813858	-24.264278	118	257	257	13.990±0.001	12.532±0.001	11.865±0.001
246.814087	-24.246506	263	263	263	17.404±0.060	16.333±0.021	15.572±0.021
246.814102	-25.084806	68	78	29	16.012±0.002	15.318±0.003	15.064±0.004
246.814117	-25.078478	2	43	73	15.862±0.002	15.093±0.002	14.828±0.003
246.814194	-24.935553	166	112	35	15.760±0.002	15.079±0.002	14.826±0.003
246.814316	-25.180176	144	112	27	16.590±0.005	15.881±0.006	15.498±0.012
246.814407	-24.296274	8	15	10	17.333±0.026	16.203±0.007	15.368±0.007
246.814423	-24.444342	6	7	2	17.257±0.012	13.281±0.001	10.621±0.001
246.814575	-25.075916	262	262	263	17.124±0.009	16.272±0.009	15.738±0.020
246.814636	-24.802275	4	146	210	17.208±0.024	16.293±0.016	15.664±0.025
246.814636	-24.514885	70	258	257	17.461±0.206	16.208±0.007	12.699±0.001
246.814697	-24.999062	263	263	262	16.973±0.006	16.233±0.008	15.690±0.017
246.814728	-24.950096	5	17	12	17.141±0.029	16.385±0.052	16.027±0.150
246.814804	-24.897142	186	195	92	11.853±0.001	10.872±0.001	10.517±0.001
246.814880	-24.905949	7	12	48	15.510±0.002	15.097±0.002	14.876±0.003
246.814896	-24.872330	263	263	263	14.529±0.001	13.619±0.001	13.248±0.001
246.815063	-24.840246	79	119	63	17.116±0.053	16.270±0.032	15.577±0.044
246.815063	-24.379868	263	263	263	17.129±0.114	16.454±0.018	15.208±0.005
246.815140	-25.000675	110	262	262	17.127±0.010	16.195±0.008	15.684±0.014
246.815201	-25.035276	222	240	228	17.154±0.010	16.284±0.010	15.695±0.016
246.815277	-24.934345	148	217	216	17.125±0.021	16.276±0.033	15.625±0.074
246.815308	-25.114077	263	263	263	15.586±0.002	14.838±0.002	14.596±0.003
246.815582	-24.900146	6	95	263	15.393±0.001	14.542±0.001	14.256±0.002
246.815674	-24.268764	15	14	7	17.328±0.039	16.308±0.015	15.544±0.016
246.815674	-24.645327	73	48	16	14.257±0.002	11.550±0.002	10.074±0.001
246.815765	-25.019819	262	263	263	15.775±0.002	14.962±0.002	14.672±0.003
246.815857	-25.184374	2	2	24	15.997±0.006	15.388±0.011	15.200±0.033
246.815994	-25.011663	1	10	13	17.197±0.024	16.395±0.032	15.849±0.081
246.816025	-25.026098	4	50	61	16.632±0.004	15.779±0.004	15.444±0.006
246.816055	-24.928144	16	13	3	16.130±0.002	15.267±0.003	14.994±0.003
246.816071	-24.645321	10	18	8	14.051±0.002	11.360±0.002	9.918±0.002
246.816101	-25.067938	6	263	262	12.933±0.001	12.027±0.001	11.613±0.001
246.816208	-24.420513	257	262	262	17.343±0.114	15.921±0.005	13.250±0.001
246.816223	-25.122643	4	7	4	14.738±0.001	14.042±0.001	13.817±0.001
246.816315	-24.944738	5	59	47	16.481±0.003	15.679±0.004	15.370±0.005

Table 1—Continued

RA (degrees)	Dec (degrees)	N_{Jobs}	N_{Hobs}	N_{Kobs}	J^a (mag)	H^a (mag)	K_s^a (mag)
246.816406	-24.927629	262	263	262	16.150±0.012	15.288±0.013	15.019±0.016
246.816696	-24.802416	2	263	263	14.353±0.001	13.121±0.001	12.631±0.001
246.816910	-24.857738	9	64	54	17.413±0.033	16.446±0.022	15.812±0.035
246.816925	-24.250999	263	263	263	16.829±0.005	15.461±0.003	14.768±0.003
246.816971	-24.271143	263	263	263	17.056±0.007	15.708±0.004	15.007±0.004
246.817062	-24.285788	48	240	252	15.099±0.001	13.187±0.001	12.283±0.001
246.817078	-24.918362	258	257	257	17.156±0.014	16.360±0.021	15.809±0.047
246.817200	-24.760880	263	263	263	17.310±0.052	16.282±0.007	15.255±0.005
246.817230	-24.849861	2	263	263	17.247±0.025	16.324±0.017	15.719±0.027
246.817245	-24.292763	4	9	263	17.147±0.009	15.410±0.003	14.321±0.002
246.817444	-24.906212	11	253	257	15.120±0.001	14.316±0.001	14.020±0.001
246.817444	-24.368603	54	30	5	17.411±0.159	16.419±0.014	14.863±0.003
246.817688	-24.924608	39	19	4	13.644±0.001	12.956±0.001	12.700±0.001
246.817841	-25.019424	263	263	263	16.673±0.004	15.880±0.004	15.506±0.007
246.817902	-24.821552	11	98	263	17.279±0.045	16.372±0.029	15.792±0.048
246.817963	-24.818445	28	67	51	14.163±0.001	12.917±0.001	12.438±0.001
246.818085	-24.844728	16	4	3	17.297±0.017	16.184±0.007	15.555±0.009
246.818222	-25.058460	2	260	263	16.881±0.006	16.137±0.009	15.670±0.021
246.818344	-24.520683	263	263	263	17.650±99.000	16.712±0.175	15.169±0.005
246.818359	-25.057701	11	263	263	17.014±0.011	16.156±0.013	15.615±0.037
246.818359	-25.002043	263	263	263	17.090±0.007	16.141±0.006	15.647±0.010
246.818390	-24.961386	7	133	263	17.093±0.008	16.317±0.010	15.762±0.024
246.818420	-25.010834	13	215	197	17.036±0.007	16.214±0.007	15.708±0.014
246.818436	-25.097715	263	263	263	16.447±0.003	15.802±0.004	15.493±0.006
246.818481	-25.036804	3	260	262	17.134±0.012	16.267±0.013	15.726±0.027
246.818756	-24.913109	263	263	263	16.911±0.005	16.144±0.006	15.688±0.011
246.818771	-25.040178	2	26	33	14.563±0.001	13.870±0.001	13.649±0.001
246.818848	-25.053625	30	176	171	17.201±0.015	16.324±0.014	15.723±0.027
246.818954	-24.956951	6	36	61	17.077±0.008	16.330±0.012	15.779±0.025
246.818985	-25.017204	263	263	263	16.761±0.004	15.944±0.005	15.547±0.007
246.819183	-24.315990	3	8	4	16.949±0.005	14.472±0.001	13.211±0.001
246.819183	-25.004133	218	167	55	17.115±0.009	16.271±0.009	15.739±0.020
246.819275	-25.116165	96	242	248	17.148±0.011	16.397±0.014	15.846±0.033
246.819321	-24.955347	12	61	37	17.039±0.008	16.227±0.010	15.702±0.020
246.819412	-25.137871	263	263	263	16.900±0.005	16.010±0.005	15.565±0.008
246.819748	-24.892799	230	240	176	14.773±0.001	14.036±0.001	13.757±0.001
246.819778	-24.909964	8	263	263	14.040±0.001	13.406±0.001	13.155±0.001
246.819885	-25.161388	21	86	48	16.939±0.006	16.269±0.009	15.762±0.022
246.819962	-24.622938	211	262	263	8.006±99.000	16.499±0.105	15.330±0.011
246.819977	-25.061438	10	7	5	16.680±0.004	15.779±0.004	15.453±0.006
246.820023	-24.304783	263	263	263	17.438±0.085	16.388±0.016	15.374±0.010
246.820038	-24.976824	263	263	263	14.428±0.001	13.495±0.001	13.201±0.001
246.820129	-24.828171	6	60	61	17.331±0.030	16.339±0.020	15.764±0.036
246.820374	-24.226870	261	261	261	17.309±0.023	16.162±0.007	15.440±0.007
246.820374	-25.058681	263	263	263	16.895±0.005	16.083±0.006	15.626±0.010

Table 1—Continued

RA (degrees)	Dec (degrees)	N_{Jobs}	N_{Hobs}	N_{Kobs}	J^a (mag)	H^a (mag)	K_s^a (mag)
246.820526	-25.128313	262	263	263	17.148±0.026	16.393±0.082	15.868±0.122
246.820755	-24.959143	17	13	3	17.183±0.027	16.454±0.044	15.907±0.090
246.820755	-24.926773	117	151	87	17.049±0.006	16.170±0.006	15.689±0.012
246.820862	-25.048775	8	25	18	17.183±0.015	16.333±0.016	15.733±0.026
246.821045	-25.038465	34	62	111	17.170±0.027	16.410±0.053	15.798±0.084
246.821152	-24.786402	6	16	9	11.841±0.001	10.168±0.001	9.491±0.001
246.821213	-25.123453	26	21	5	17.044±0.007	16.357±0.012	15.780±0.031
246.821259	-24.980469	7	3	9	17.054±0.006	16.072±0.005	15.585±0.008
246.821381	-24.862169	3	4	18	17.134±0.009	16.258±0.009	15.680±0.015
246.821426	-24.964455	4	11	9	16.353±0.003	15.542±0.003	15.244±0.004
246.821518	-25.155359	263	263	263	15.620±0.002	14.931±0.002	14.711±0.003
246.821533	-24.948534	126	263	263	15.976±0.002	15.310±0.003	15.073±0.004
246.821686	-24.586926	20	9	8	17.501±0.113	16.269±0.008	14.663±0.003
246.821686	-24.217978	244	257	258	17.348±0.058	16.102±0.023	15.568±0.034
246.821716	-24.873997	0	6	27	17.018±0.006	16.114±0.006	15.608±0.010
246.821716	-24.304703	263	263	263	17.381±0.037	15.911±0.005	14.799±0.003
246.821854	-25.132893	9	7	9	16.810±0.005	15.973±0.005	15.569±0.008
246.821976	-25.101770	37	52	22	15.152±0.001	14.525±0.001	14.314±0.002
246.821976	-24.374475	245	256	256	17.341±0.124	15.567±0.003	13.418±0.001
246.822113	-24.818075	186	262	262	16.466±0.003	15.287±0.002	14.805±0.003
246.822144	-24.953121	119	241	230	15.638±0.002	14.809±0.002	14.539±0.002
246.822296	-24.884794	261	263	262	15.988±0.002	15.121±0.002	14.771±0.003
246.822327	-24.253325	6	261	262	17.250±0.015	16.171±0.008	15.446±0.009
246.822327	-24.972134	14	65	43	17.095±0.010	16.389±0.017	15.792±0.039
246.822464	-24.275709	83	263	263	17.319±0.041	16.251±0.011	15.506±0.010
246.822464	-24.271452	103	250	252	17.301±0.017	16.166±0.007	15.438±0.007
246.822464	-25.071115	261	262	262	14.797±0.001	14.197±0.001	13.981±0.001
246.822495	-24.837114	79	68	21	17.272±0.014	16.216±0.008	15.616±0.010
246.822617	-25.181715	110	263	263	17.067±0.012	16.348±0.025	15.839±0.088
246.822632	-24.535255	262	262	259	17.326±0.000	16.477±0.068	15.383±0.017
246.822739	-24.218828	9	91	108	15.993±0.002	14.378±0.002	13.707±0.001
246.822998	-25.134197	81	76	24	17.086±0.012	16.311±0.024	15.751±0.053
246.823074	-24.482300	263	263	263	17.397±0.054	14.226±0.002	11.325±0.001
246.823151	-25.093666	29	263	263	17.114±0.010	16.238±0.010	15.738±0.021
246.823288	-24.998472	263	263	263	17.129±0.013	16.348±0.021	15.793±0.054
246.823334	-24.217033	259	257	216	16.319±0.003	14.652±0.002	13.983±0.002
246.823456	-24.964003	0	4	35	17.040±0.007	16.212±0.008	15.673±0.016
246.823547	-24.213146	3	9	21	17.125±0.008	15.853±0.005	15.224±0.005
246.823563	-24.971457	2	3	17	17.062±0.008	16.291±0.011	15.751±0.024
246.823761	-25.001028	211	175	62	14.635±0.001	13.696±0.001	13.398±0.001
246.823822	-24.791279	34	48	22	17.340±0.043	16.378±0.015	15.724±0.018
246.823822	-25.180845	68	74	37	16.654±0.004	16.033±0.006	15.657±0.013
246.823990	-25.140650	119	255	256	16.873±0.005	16.160±0.006	15.679±0.012
246.824524	-24.832378	2	46	58	17.196±0.075	16.361±0.028	15.729±0.037
246.824554	-24.989000	221	263	263	15.963±0.002	15.284±0.002	15.025±0.004

Table 1—Continued

RA (degrees)	Dec (degrees)	N_{Jobs}	N_{Hobs}	N_{Kobs}	J^a (mag)	H^a (mag)	K_s^a (mag)
246.824661	-24.982924	2	254	254	13.391±0.001	12.648±0.001	12.381±0.001
246.824661	-25.084904	141	124	38	16.232±0.003	15.348±0.003	15.083±0.004
246.824677	-25.056828	86	95	37	16.831±0.005	15.963±0.005	15.552±0.007
246.824707	-24.236753	70	227	222	16.111±0.003	14.514±0.001	13.828±0.001
246.824951	-24.888184	263	263	263	14.140±0.001	13.170±0.001	12.688±0.001
246.824966	-25.088102	11	21	19	14.842±0.001	14.212±0.001	14.002±0.002
246.825027	-25.116644	12	263	263	17.124±0.028	16.288±0.048	15.886±0.089
246.825058	-25.151209	10	242	262	16.616±0.004	15.725±0.004	15.363±0.006
246.825256	-24.999552	4	7	3	16.681±0.004	15.925±0.005	15.524±0.007
246.825302	-25.107641	237	248	213	17.118±0.009	16.395±0.012	15.837±0.026
246.825348	-25.098766	25	262	263	17.146±0.025	16.368±0.049	15.685±0.088
246.825394	-24.954557	110	119	64	16.718±0.004	15.804±0.004	15.360±0.005
246.825424	-24.803761	11	262	262	17.366±0.053	16.406±0.035	15.730±0.047
246.825623	-24.210924	7	7	7	17.022±0.006	15.585±0.003	14.955±0.003
246.825623	-24.275944	263	263	263	17.327±0.097	16.371±0.039	15.710±0.048
246.825668	-25.152166	14	99	93	15.732±0.002	15.081±0.003	14.871±0.003
246.825699	-24.214834	2	2	61	17.200±0.076	16.306±0.040	15.766±0.058
246.825714	-24.481264	163	225	170	17.386±0.120	14.667±0.002	10.537±0.001
246.825714	-25.119190	259	258	258	16.613±0.004	15.847±0.004	15.580±0.007
246.825821	-24.853411	12	41	29	14.866±0.001	13.513±0.001	13.010±0.001
246.825897	-25.094269	6	222	262	17.122±0.009	16.284±0.010	15.743±0.018
246.825943	-25.143360	258	258	180	16.763±0.005	16.114±0.006	15.652±0.012
246.825974	-25.099680	2	36	259	16.771±0.004	16.098±0.006	15.653±0.012
246.825989	-25.145239	258	252	203	17.042±0.007	16.236±0.008	15.699±0.019
246.826065	-24.832100	2	34	45	17.174±0.014	16.227±0.010	15.639±0.017
246.826309	-24.853836	7	11	3	13.779±0.001	12.602±0.002	12.118±0.001
246.826492	-24.914923	18	15	5	11.482±0.001	10.566±0.001	9.954±0.001
246.826508	-24.568972	219	185	78	17.505±0.130	16.459±0.015	15.046±0.004
246.826538	-24.385300	74	58	16	8.006±99.000	16.522±0.112	15.334±0.014
246.826584	-24.407238	4	27	20	16.825±0.005	13.222±0.001	11.262±0.001
246.826599	-24.654037	3	8	6	17.570±0.000	15.540±0.003	12.234±0.001
246.826675	-24.244341	189	256	257	17.395±0.034	16.264±0.011	15.542±0.012
246.826767	-24.295275	75	77	38	17.481±0.083	16.396±0.017	15.518±0.013
246.826874	-24.282934	60	42	12	17.312±0.020	16.072±0.006	15.247±0.005
246.827026	-24.484921	0	3	5	14.518±0.001	11.326±0.001	9.511±0.001
246.827057	-24.840117	263	263	263	17.285±0.023	16.324±0.018	15.735±0.030
246.827209	-25.104805	4	140	209	16.222±0.003	15.443±0.003	15.197±0.004
246.827271	-24.874434	263	263	263	16.971±0.005	15.837±0.004	15.277±0.005
246.827286	-24.232441	5	11	107	16.911±0.005	15.446±0.003	14.735±0.003
246.827362	-24.907248	262	262	261	14.950±0.001	14.053±0.001	13.770±0.001
246.827362	-25.034981	263	261	244	17.154±0.013	16.292±0.014	15.748±0.030
246.827393	-24.223770	147	181	121	17.180±0.097	16.339±0.024	15.617±0.026
246.827515	-25.037420	253	262	262	17.091±0.009	16.351±0.013	15.765±0.035
246.827560	-24.974918	235	181	57	17.208±0.031	16.346±0.032	15.642±0.075
246.827652	-25.042166	247	239	244	17.117±0.011	16.348±0.016	15.746±0.032

Table 1—Continued

RA (degrees)	Dec (degrees)	N_{Jobs}	N_{Hobs}	N_{Kobs}	J^a (mag)	H^a (mag)	K_s^a (mag)
246.827774	-24.255419	263	263	263	17.417±0.049	16.328±0.013	15.470±0.011
246.827789	-25.143541	263	263	263	17.079±0.008	16.337±0.012	15.804±0.032
246.828049	-24.958103	263	263	259	12.891±0.001	12.237±0.001	12.008±0.001
246.828064	-25.014517	263	263	263	17.137±0.013	16.390±0.020	15.832±0.047
246.828186	-24.935110	5	26	66	16.183±0.003	15.323±0.003	15.016±0.004
246.828354	-24.814524	263	263	263	16.274±0.003	14.988±0.002	14.484±0.002
246.828629	-24.888716	5	254	263	17.165±0.011	16.295±0.011	15.732±0.022
246.828690	-25.127262	261	263	263	16.522±0.003	15.552±0.003	15.151±0.004
246.828857	-24.964579	230	260	260	16.552±0.004	15.804±0.004	15.470±0.006
246.828949	-25.053549	16	5	5	15.398±0.001	14.516±0.001	14.249±0.002
246.828949	-24.843361	173	257	258	17.253±0.025	16.351±0.019	15.783±0.033
246.828949	-25.004822	263	263	263	16.158±0.002	15.386±0.003	15.124±0.004
246.829025	-25.114702	51	22	3	8.515±0.001	7.496±0.001	7.132±0.001
246.829163	-25.154951	263	263	263	17.188±0.020	16.396±0.029	15.841±0.054
246.829208	-25.030420	198	186	189	13.721±0.001	13.071±0.001	12.852±0.001
246.829285	-24.918404	263	263	263	16.547±0.004	15.786±0.004	15.481±0.006
246.829453	-25.133770	83	99	36	16.581±0.004	15.666±0.003	15.332±0.005
246.829544	-25.089117	2	6	27	17.120±0.013	16.346±0.022	15.857±0.048
246.829895	-24.852825	3	3	64	16.860±0.005	15.568±0.003	15.024±0.004
246.829987	-24.969124	36	39	13	15.210±0.001	14.351±0.001	14.081±0.002
246.830017	-25.050905	256	263	262	17.124±0.012	16.405±0.022	15.809±0.050
246.830154	-24.953032	11	249	250	14.787±0.001	13.930±0.001	13.661±0.001
246.830170	-24.963333	2	20	39	14.918±0.001	14.253±0.001	14.006±0.002
246.830170	-24.995886	3	224	210	16.560±0.004	15.693±0.004	15.380±0.005
246.830170	-24.871124	69	64	32	17.164±0.008	16.091±0.006	15.578±0.008
246.830185	-25.176193	262	257	201	16.541±0.004	15.871±0.004	15.505±0.007
246.830200	-25.163034	256	237	132	14.736±0.001	14.155±0.001	13.965±0.001
246.830231	-25.048679	3	57	137	16.028±0.002	15.126±0.002	14.733±0.003
246.830475	-24.948984	261	262	83	15.222±0.001	14.497±0.001	14.242±0.002
246.830521	-24.585075	4	132	242	17.511±0.177	16.427±0.073	15.398±0.020
246.830582	-24.901579	8	31	74	16.879±0.005	16.063±0.005	15.634±0.009
246.830704	-24.320072	262	259	230	17.363±0.066	16.250±0.008	14.767±0.003
246.830841	-24.941483	259	263	263	16.964±0.006	16.146±0.006	15.676±0.012
246.830887	-24.810902	263	263	263	17.308±0.019	16.238±0.009	15.604±0.011
246.831299	-24.694487	4	16	71	9.397±0.001	8.638±0.001	8.395±0.001
246.831329	-25.076397	4	7	6	16.239±0.003	15.331±0.003	15.043±0.004
246.831390	-24.938969	263	263	263	16.198±0.003	15.297±0.003	15.017±0.004
246.831635	-25.125776	10	7	8	16.973±0.006	16.294±0.009	15.775±0.023
246.831711	-24.696379	247	222	113	15.764±0.005	14.906±0.006	14.371±0.004
246.831726	-25.019041	238	202	72	17.038±0.007	16.268±0.010	15.740±0.023
246.831848	-24.696634	3	2	14	15.785±0.005	14.910±0.006	14.372±0.004
246.831985	-25.167995	9	65	80	16.513±0.003	15.635±0.004	15.339±0.005
246.832260	-25.088472	3	208	263	15.949±0.002	15.271±0.003	15.041±0.004
246.832336	-25.137829	189	261	262	15.799±0.002	14.943±0.002	14.663±0.003
246.832336	-24.979900	244	262	262	17.128±0.017	16.307±0.025	15.757±0.058

Table 1—Continued

RA (degrees)	Dec (degrees)	N_{Jobs}	N_{Hobs}	N_{Kobs}	J^a (mag)	H^a (mag)	K_s^a (mag)
246.832352	-24.845949	2	18	15	15.898±0.002	14.896±0.002	14.465±0.002
246.832474	-24.891180	34	20	6	16.978±0.005	16.040±0.005	15.590±0.008
246.832489	-24.986134	6	22	11	17.069±0.011	16.141±0.009	15.604±0.017
246.832809	-24.985641	97	79	8	17.056±0.014	16.166±0.026	15.667±0.055
246.833023	-25.026093	6	9	11	17.195±0.017	16.291±0.014	15.748±0.027
246.833115	-25.145355	4	10	226	17.212±0.019	16.349±0.021	15.766±0.047
246.833221	-25.115040	175	244	233	14.719±0.001	13.916±0.002	13.661±0.001
246.833221	-24.872257	263	263	263	16.971±0.006	16.033±0.005	15.545±0.008
246.833313	-24.242626	15	12	7	17.470±0.074	16.358±0.022	15.656±0.025
246.833344	-25.073643	47	236	246	13.581±0.001	12.921±0.001	12.702±0.001
246.833557	-25.010609	13	12	3	17.181±0.015	16.297±0.014	15.731±0.029
246.833557	-25.057409	263	263	263	17.222±0.025	16.364±0.025	15.723±0.053
246.833664	-25.013830	34	263	263	17.047±0.007	16.127±0.006	15.638±0.010
246.833679	-25.159058	6	262	263	16.249±0.003	15.529±0.003	15.263±0.004
246.834030	-25.090479	21	29	11	16.394±0.003	15.544±0.003	15.281±0.005
246.834076	-24.949476	100	261	263	17.231±0.036	16.330±0.028	15.762±0.051
246.834106	-24.981091	3	7	5	17.123±0.015	16.315±0.021	15.740±0.049
246.834106	-25.107405	221	217	145	17.181±0.015	16.437±0.022	15.799±0.049
246.834152	-24.206753	263	263	263	14.223±0.001	12.919±0.001	12.301±0.001
246.834274	-24.951828	255	234	136	16.740±0.004	16.034±0.005	15.594±0.009
246.834335	-25.109379	15	42	29	17.184±0.016	16.522±0.027	15.921±0.066
246.834381	-25.140711	259	258	259	17.223±0.026	16.406±0.033	15.717±0.065
246.834488	-24.790178	8	82	82	17.096±0.007	15.756±0.004	15.067±0.004
246.834717	-25.017221	5	15	172	14.149±0.001	13.525±0.001	13.303±0.001
246.834732	-25.052048	106	260	263	15.281±0.001	14.572±0.001	14.341±0.002
246.834747	-24.999832	217	254	255	14.767±0.001	14.013±0.001	13.760±0.001
246.834885	-25.033688	4	2	34	17.087±0.009	16.362±0.015	15.744±0.036
246.834946	-25.120708	263	263	263	17.064±0.007	16.249±0.008	15.750±0.017
246.835098	-25.028231	6	7	134	17.158±0.021	16.368±0.036	15.758±0.080
246.835358	-24.924492	74	75	24	13.817±0.001	12.936±0.001	12.664±0.001
246.835388	-25.131531	2	237	262	17.173±0.028	16.510±0.065	15.793±0.095
246.835663	-24.930628	6	8	8	16.698±0.004	15.954±0.005	15.556±0.008
246.835770	-24.216524	18	16	6	17.038±0.006	15.631±0.003	14.939±0.003
246.835770	-25.155512	49	22	5	17.122±0.010	16.272±0.011	15.733±0.026
246.835861	-24.821684	195	253	244	16.474±0.003	15.345±0.003	14.910±0.003
246.835999	-24.980551	50	23	6	14.770±0.001	14.104±0.001	13.842±0.001
246.836136	-24.378178	263	263	263	17.648±0.151	16.514±0.032	15.287±0.007
246.836426	-24.963886	22	259	263	17.047±0.007	16.204±0.007	15.709±0.015
246.836548	-24.973097	1	11	20	16.408±0.003	15.537±0.003	15.246±0.004
246.836990	-24.960287	9	263	263	17.104±0.009	16.367±0.014	15.780±0.032
246.837051	-25.144472	7	263	263	17.153±0.014	16.310±0.017	15.759±0.037
246.837097	-25.126892	263	263	263	17.106±0.014	16.320±0.025	15.853±0.069
246.837112	-24.811211	8	4	259	16.134±0.002	15.049±0.002	14.601±0.002
246.837143	-24.259565	207	228	196	17.481±0.154	16.482±0.032	15.649±0.031
246.837234	-25.177019	82	235	244	16.764±0.004	15.946±0.005	15.572±0.008

Table 1—Continued

RA (degrees)	Dec (degrees)	N_{Jobs}	N_{Hobs}	N_{Kobs}	J^a (mag)	H^a (mag)	K_s^a (mag)
246.837265	-24.957001	195	258	260	17.072±0.009	16.297±0.012	15.718±0.028
246.837402	-25.094511	1	4	16	17.132±0.009	16.234±0.009	15.687±0.016
246.837524	-25.074385	211	201	202	17.117±0.013	16.418±0.027	15.700±0.074
246.837723	-24.956022	5	53	261	17.129±0.015	16.379±0.024	15.816±0.062
246.837921	-25.140017	9	4	11	17.154±0.030	16.435±0.056	15.788±0.112
246.837997	-24.946886	13	125	127	16.572±0.004	15.693±0.004	15.347±0.005
246.838028	-25.011377	263	263	263	15.856±0.002	15.129±0.002	14.895±0.003
246.838242	-24.910093	263	263	263	16.424±0.003	15.604±0.003	15.309±0.005
246.838257	-25.040476	235	263	263	17.164±0.019	16.383±0.033	15.805±0.080
246.838272	-24.823854	3	29	21	17.222±0.021	16.314±0.016	15.699±0.030
246.838409	-24.918562	170	261	262	17.162±0.016	16.273±0.015	15.781±0.037
246.838425	-25.034660	3	160	259	16.349±0.003	15.751±0.004	15.453±0.006
246.838562	-25.035938	23	262	262	17.096±0.017	16.386±0.036	15.867±0.090
246.838623	-24.211733	2	6	4	17.081±0.007	15.438±0.003	14.503±0.002
246.838684	-24.963684	8	22	13	17.217±0.022	16.473±0.036	15.767±0.065
246.838715	-24.798454	10	6	6	16.932±0.005	15.624±0.003	14.974±0.003
246.838867	-24.970295	7	4	10	16.161±0.003	15.195±0.002	14.890±0.003
246.838928	-24.988056	263	262	263	17.066±0.007	16.125±0.006	15.614±0.010
246.839005	-24.889656	5	8	5	15.505±0.001	14.579±0.001	14.257±0.002
246.839340	-25.043125	2	10	93	14.497±0.001	13.669±0.001	13.434±0.001
246.839355	-24.780283	56	75	31	15.534±0.002	13.750±0.001	12.820±0.001
246.839447	-24.870535	30	67	25	16.029±0.002	14.966±0.002	14.574±0.003
246.839462	-24.695250	221	173	60	15.271±0.001	11.182±0.001	8.435±0.001
246.839523	-25.144169	6	259	263	16.059±0.002	15.211±0.002	14.960±0.003
246.839569	-25.001389	8	115	133	16.625±0.004	15.638±0.003	15.237±0.004
246.839584	-24.836538	159	140	65	17.282±0.034	16.280±0.019	15.742±0.032
246.839966	-25.093983	10	8	10	17.016±0.007	16.277±0.009	15.754±0.021
246.840118	-24.197416	2	125	239	15.634±0.003	14.244±0.002	13.578±0.001
246.840179	-24.942076	8	141	158	16.997±0.006	16.060±0.005	15.615±0.009
246.840347	-24.948963	263	263	263	17.154±0.020	16.310±0.020	15.773±0.047
246.840378	-24.363819	3	263	263	15.616±0.002	12.582±0.001	11.006±0.001
246.840454	-24.288107	24	154	149	17.259±0.012	15.526±0.003	14.491±0.002
246.840546	-24.999432	7	58	72	15.750±0.002	14.792±0.002	14.487±0.002
246.840652	-25.113688	263	263	263	17.130±0.012	16.375±0.018	15.831±0.045
246.840820	-24.870840	4	6	2	17.121±0.012	16.180±0.010	15.633±0.021
246.840836	-24.498091	260	263	263	17.416±0.148	15.007±0.003	10.758±0.001
246.840942	-24.726538	257	257	257	17.237±0.011	13.198±0.001	10.762±0.001
246.840973	-24.457623	35	67	63	17.894±0.000	16.607±0.157	14.399±0.002
246.841003	-24.311779	2	127	205	17.405±0.088	16.163±0.006	14.555±0.002
246.841034	-24.276417	257	258	258	17.307±0.022	15.671±0.004	14.578±0.002
246.841095	-24.995998	8	21	10	15.983±0.002	15.145±0.002	14.902±0.003
246.841400	-24.936111	263	262	262	16.568±0.004	15.863±0.004	15.513±0.007
246.841492	-25.060507	15	30	14	15.867±0.002	15.080±0.002	14.853±0.003
246.841599	-24.494326	263	263	260	17.506±0.142	15.346±0.003	12.838±0.001
246.842010	-24.453028	254	256	256	17.527±0.181	16.364±0.159	15.357±0.017

Table 1—Continued

RA (degrees)	Dec (degrees)	N_{Jobs}	N_{Hobs}	N_{Kobs}	J^a (mag)	H^a (mag)	K_s^a (mag)
246.842010	-25.019814	263	263	258	16.629±0.004	15.942±0.005	15.577±0.008
246.842026	-25.176304	22	54	27	15.711±0.002	15.079±0.002	14.898±0.003
246.842056	-25.109465	3	10	10	16.888±0.005	16.360±0.014	15.794±0.034
246.842102	-24.839359	10	7	9	16.558±0.004	15.436±0.003	15.004±0.003
246.842224	-25.063650	239	50	244	17.176±0.026	16.381±0.050	15.882±0.175
246.842331	-24.217949	244	256	257	17.219±0.010	15.891±0.004	15.189±0.004
246.842422	-24.994144	54	222	221	17.140±0.012	16.343±0.015	15.786±0.035
246.842468	-25.014111	124	58	12	16.751±0.004	15.940±0.005	15.544±0.008
246.842484	-24.952400	229	245	225	13.727±0.001	13.035±0.001	12.786±0.001
246.842499	-25.042917	259	261	260	17.000±0.007	16.241±0.009	15.703±0.021
246.842651	-25.122242	263	263	263	17.196±0.035	16.405±0.050	15.703±0.082
246.842789	-24.823048	4	10	10	15.947±0.002	14.919±0.002	14.462±0.002
246.842834	-25.055759	263	263	263	17.122±0.010	16.359±0.015	15.768±0.034
246.842850	-24.968555	59	263	263	17.143±0.011	16.204±0.009	15.673±0.016
246.842911	-24.876511	2	82	212	15.729±0.002	14.874±0.002	14.563±0.002
246.843002	-24.917770	258	258	258	17.182±0.017	16.400±0.022	15.906±0.068
246.843323	-24.980558	254	262	263	17.211±0.027	16.476±0.045	16.033±99.000
246.843430	-25.017063	13	24	10	16.836±0.005	16.231±0.008	15.742±0.018
246.843597	-25.114965	6	16	9	16.691±0.004	15.778±0.004	15.397±0.006
246.843735	-25.126837	7	34	29	16.826±0.014	15.899±0.023	14.768±0.053
246.843796	-24.809937	248	261	261	14.790±0.001	13.379±0.001	12.805±0.001
246.844116	-25.137478	42	35	13	17.013±0.006	16.249±0.008	15.724±0.017
246.844421	-24.941536	18	134	137	16.524±0.003	15.825±0.004	15.489±0.006
246.844513	-24.227711	54	197	200	16.941±0.005	15.481±0.003	14.758±0.003
246.844559	-24.903578	200	188	190	16.783±0.004	16.012±0.005	15.606±0.009
246.844574	-25.088747	10	2	9	17.148±0.024	16.306±0.025	15.698±0.056
246.844635	-24.221375	5	16	14	17.338±0.037	16.228±0.008	15.422±0.007
246.844894	-25.026644	263	263	263	16.713±0.004	16.003±0.005	15.581±0.009
246.844925	-25.132811	4	10	196	17.174±0.017	16.304±0.016	15.730±0.030
246.844971	-24.776323	2	10	5	17.474±0.147	16.353±0.031	15.587±0.027
246.845016	-25.107878	263	263	263	15.749±0.002	14.835±0.002	14.552±0.002
246.845062	-24.830931	210	187	84	17.247±0.016	16.298±0.012	15.743±0.022
246.845154	-25.077284	62	32	10	17.141±0.031	16.409±0.070	15.708±99.000
246.845184	-25.054090	245	233	135	16.398±0.003	15.473±0.003	15.160±0.004
246.845215	-25.129688	240	235	236	16.336±0.003	15.426±0.003	15.106±0.004
246.845413	-24.857147	169	130	46	17.285±0.035	16.342±0.039	15.866±0.066
246.845459	-24.894798	18	71	58	11.203±0.001	10.522±0.001	10.248±0.001
246.845520	-24.299223	14	8	9	13.310±0.001	10.692±0.001	9.390±0.001
246.845657	-24.899149	263	263	263	16.173±0.002	15.467±0.003	15.194±0.004
246.845718	-24.801941	206	167	52	10.922±0.001	9.832±0.001	9.336±0.001
246.845764	-25.111464	22	29	12	11.767±0.001	10.962±0.001	10.724±0.001
246.845947	-25.158108	263	263	261	17.025±0.008	16.297±0.015	15.651±0.038
246.846069	-25.103779	242	253	229	12.988±0.001	12.396±0.001	12.207±0.001
246.846252	-24.636864	113	98	25	8.006±99.000	16.542±0.071	15.341±0.012
246.846848	-24.844749	258	258	258	17.259±0.025	16.293±0.019	15.705±0.035

Table 1—Continued

RA (degrees)	Dec (degrees)	N_{Jobs}	N_{Hobs}	N_{Kobs}	J^a (mag)	H^a (mag)	K_s^a (mag)
246.846878	-25.087952	144	136	64	16.488±0.004	15.875±0.005	15.550±0.008
246.846909	-24.809896	263	263	263	14.124±0.001	12.613±0.001	11.982±0.001
246.846985	-24.982376	52	127	113	15.747±0.002	15.069±0.002	14.820±0.003
246.847031	-24.284731	253	257	232	17.433±0.045	15.714±0.004	14.283±0.002
246.847076	-24.949142	256	260	255	17.257±0.019	16.314±0.015	15.753±0.030
246.847137	-25.124556	259	253	180	16.707±0.004	16.029±0.005	15.622±0.009
246.847198	-25.138559	52	175	162	15.410±0.001	14.811±0.002	14.621±0.003
246.847214	-25.058886	96	234	235	17.156±0.025	16.424±0.048	16.018±0.156
246.847214	-25.001694	131	97	28	16.360±0.003	15.709±0.004	15.432±0.006
246.847397	-25.163197	14	5	9	16.025±0.002	15.115±0.002	14.838±0.003
246.847534	-25.097773	57	28	4	16.754±0.004	16.100±0.006	15.654±0.012
246.847565	-24.835579	21	30	10	15.524±0.002	14.405±0.001	13.950±0.001
246.847565	-24.952906	261	259	258	17.235±0.037	16.342±0.031	15.706±0.059
246.847610	-24.827932	36	25	5	17.275±0.017	16.315±0.013	15.758±0.022
246.847610	-24.910189	92	34	6	12.585±0.001	11.904±0.001	11.650±0.001
246.847977	-24.625465	255	253	214	17.372±0.148	16.473±0.027	15.342±0.009
246.847992	-25.047968	244	193	68	16.897±0.005	16.179±0.007	15.688±0.014
246.848083	-24.881844	183	99	23	17.169±0.015	16.328±0.016	15.706±0.034
246.848297	-24.207954	217	257	258	12.805±0.001	10.796±0.001	9.851±0.001
246.848846	-24.938471	34	18	4	17.208±0.033	16.365±0.050	15.784±0.092
246.848862	-24.872662	18	7	10	17.105±0.008	16.248±0.009	15.701±0.018
246.848892	-24.929188	207	231	166	15.375±0.001	14.683±0.002	14.439±0.002
246.848969	-24.920094	263	263	263	17.225±0.018	16.312±0.014	15.549±0.012
246.849030	-24.334436	263	263	263	17.400±0.000	16.435±0.018	15.122±0.004
246.849060	-24.888020	240	244	190	16.941±0.005	15.858±0.004	15.368±0.005
246.849289	-24.895975	9	186	263	16.890±0.005	15.857±0.004	15.383±0.005
246.849304	-25.144051	7	4	2	16.217±0.003	15.506±0.003	15.247±0.005
246.849350	-24.992996	219	234	172	17.168±0.032	16.348±0.060	15.652±0.117
246.849411	-24.908739	263	263	263	17.061±0.014	16.203±0.015	15.667±0.035
246.849442	-25.138411	22	145	141	16.986±0.021	16.173±0.023	15.404±0.031
246.849609	-25.071983	226	131	35	17.020±0.009	16.146±0.010	15.567±0.018
246.849609	-25.123215	263	263	263	15.524±0.001	14.854±0.002	14.657±0.003
246.849838	-24.802368	211	131	30	17.303±0.014	16.149±0.006	15.507±0.007
246.849869	-25.099607	123	110	38	16.932±0.005	16.038±0.005	15.601±0.009
246.850021	-25.104734	263	263	263	16.067±0.002	15.112±0.002	14.808±0.003
246.850113	-25.019617	9	7	4	17.108±0.008	16.203±0.008	15.655±0.012
246.850266	-25.092695	263	263	263	17.148±0.023	16.373±0.041	15.728±0.075
246.850281	-24.235538	261	262	261	15.626±0.002	13.192±0.001	12.001±0.001
246.850342	-25.183331	8	10	3	16.813±0.007	16.098±0.011	15.644±0.049
246.850357	-24.981745	263	263	263	16.668±0.004	15.944±0.005	15.551±0.008
246.850525	-24.419603	248	257	231	17.768±0.157	16.470±0.141	15.340±0.016
246.850540	-24.957821	49	21	4	17.023±0.006	16.047±0.005	15.558±0.008
246.850586	-24.821779	49	26	19	17.053±0.007	15.869±0.004	15.319±0.005
246.850861	-24.491453	36	19	7	17.463±0.104	14.946±0.002	12.316±0.001
246.850922	-24.975569	263	263	263	16.951±0.005	16.187±0.007	15.682±0.015

Table 1—Continued

RA (degrees)	Dec (degrees)	N_{Jobs}	N_{Hobs}	N_{Kobs}	J^a (mag)	H^a (mag)	K_s^a (mag)
246.850967	-24.828810	176	166	167	17.358±0.030	16.309±0.014	15.655±0.018
246.851074	-25.163605	6	3	9	17.172±0.019	16.430±0.035	15.833±0.105
246.851242	-24.959164	263	263	263	16.100±0.002	15.533±0.003	15.302±0.005
246.851334	-24.984615	259	258	258	15.681±0.002	14.690±0.002	14.327±0.002
246.851440	-25.073889	121	102	43	17.027±0.008	16.322±0.014	15.715±0.035
246.851471	-24.253382	258	258	258	17.839±99.000	16.529±0.050	15.409±0.019
246.851547	-24.771383	158	122	32	17.324±0.032	15.827±0.004	14.693±0.003
246.851624	-24.893143	5	6	11	16.978±0.006	16.081±0.005	15.607±0.009
246.851669	-24.696526	144	110	29	17.397±0.061	15.026±0.002	12.697±0.001
246.851715	-25.052362	8	3	3	17.108±0.012	16.334±0.019	15.725±0.058
246.851746	-24.945715	6	8	2	16.962±0.006	15.951±0.005	15.512±0.007
246.851868	-24.874552	149	99	23	17.092±0.008	16.280±0.009	15.714±0.019
246.851929	-25.018158	40	17	4	16.966±0.006	16.171±0.007	15.701±0.014
246.852005	-24.780596	121	110	110	17.310±0.071	16.340±0.014	15.481±0.011
246.852142	-25.064922	243	237	237	15.875±0.002	15.086±0.002	14.845±0.003
246.852554	-24.943756	263	263	261	16.562±0.004	15.821±0.004	15.462±0.006
246.852600	-24.318920	9	152	177	17.308±0.018	14.780±0.002	13.240±0.001
246.852676	-24.967419	139	148	60	15.209±0.001	14.246±0.001	13.848±0.001
246.852676	-24.684278	262	253	197	17.456±0.149	16.470±0.094	13.485±0.001
246.852692	-25.056276	263	263	263	16.066±0.002	15.347±0.003	15.111±0.004
246.852722	-24.403076	59	39	12	17.630±0.228	16.452±0.094	15.108±0.004
246.852737	-24.493141	121	89	23	17.416±0.077	14.824±0.002	12.470±0.001
246.852890	-24.799362	228	253	254	17.376±0.028	16.189±0.007	15.408±0.006
246.852936	-24.210127	108	61	18	17.353±0.027	15.958±0.005	15.011±0.004
246.852951	-25.155163	227	225	139	17.106±0.010	16.367±0.015	15.791±0.040
246.853165	-24.998333	4	19	14	15.053±0.001	14.190±0.001	13.939±0.001
246.853165	-24.992508	15	6	9	17.043±0.007	16.275±0.009	15.737±0.021
246.853317	-24.213434	169	193	112	17.559±0.053	15.996±0.005	14.813±0.003
246.853531	-24.880571	198	166	29	16.895±0.005	15.913±0.005	15.501±0.007
246.853729	-24.964790	62	23	5	17.038±0.006	16.170±0.007	15.675±0.013
246.854050	-24.908134	19	10	4	15.459±0.001	14.529±0.001	14.235±0.002
246.854202	-24.847368	35	10	3	17.214±0.023	16.403±0.027	15.771±0.056
246.854202	-25.050755	258	258	258	17.064±0.007	16.199±0.008	15.721±0.017
246.854233	-24.904264	10	3	11	12.160±0.001	11.717±0.001	11.497±0.001
246.854248	-24.860634	24	26	8	17.167±0.011	16.265±0.010	15.690±0.018
246.854431	-25.004349	238	234	149	17.040±0.007	16.316±0.011	15.752±0.024
246.854507	-24.913679	263	263	263	16.967±0.006	16.157±0.006	15.688±0.012
246.854782	-24.775953	16	6	5	15.527±0.001	12.957±0.001	11.683±0.001
246.854797	-24.900816	152	103	35	14.931±0.001	14.172±0.001	13.903±0.001
246.854858	-24.770180	8	3	4	17.182±0.000	16.407±0.018	15.373±0.009
246.854858	-25.157503	263	263	263	16.906±0.005	16.209±0.008	15.727±0.018
246.854950	-25.114880	247	249	244	16.921±0.005	16.163±0.007	15.663±0.014
246.855103	-25.038677	8	36	215	17.135±0.009	16.193±0.008	15.683±0.015
246.855133	-24.941397	8	13	16	15.234±0.001	14.355±0.001	14.086±0.002
246.855164	-24.238661	243	243	231	17.733±99.000	16.428±0.019	15.380±0.009

Table 1—Continued

RA (degrees)	Dec (degrees)	N_{Jobs}	N_{Hobs}	N_{Kobs}	J^a (mag)	H^a (mag)	K_s^a (mag)
246.855164	-24.855272	263	263	263	15.667±0.002	14.512±0.001	14.119±0.002
246.855194	-25.034742	146	133	47	13.414±0.001	12.678±0.001	12.456±0.001
246.855255	-25.025486	263	263	263	15.548±0.002	14.922±0.002	14.725±0.003
246.855377	-25.182871	28	15	4	15.556±0.002	14.918±0.003	14.746±0.009
246.855469	-25.046059	4	20	19	17.138±0.020	16.198±0.012	15.376±0.010
246.855499	-24.209146	6	3	6	17.259±0.012	15.258±0.003	14.131±0.002
246.855515	-24.951509	263	263	263	17.191±0.022	16.314±0.021	15.837±0.041
246.855545	-25.014486	30	5	10	16.888±0.005	16.157±0.006	15.666±0.013
246.855560	-25.105873	59	45	12	15.455±0.002	14.988±0.002	14.825±0.003
246.855606	-25.094454	257	252	200	17.135±0.022	16.438±0.046	15.822±0.087
246.855606	-24.985775	263	263	263	13.120±0.001	12.500±0.001	12.273±0.001
246.855804	-25.042227	15	167	175	17.144±0.014	16.432±0.025	15.812±0.058
246.855865	-24.639664	127	78	20	8.006±99.000	16.547±0.058	15.354±0.012
246.855957	-25.057350	51	21	4	15.530±0.002	14.854±0.002	14.630±0.003
246.856461	-24.915743	263	263	261	16.614±0.004	15.812±0.004	15.459±0.006
246.856827	-25.004416	51	32	6	17.135±0.017	16.362±0.023	15.741±0.061
246.856857	-24.918577	247	244	224	16.834±0.005	16.095±0.006	15.652±0.011
246.856873	-24.624504	34	22	6	17.392±0.039	16.298±0.009	15.265±0.005
246.856918	-25.155945	32	14	4	17.144±0.010	16.234±0.010	15.695±0.019
246.856979	-24.833332	73	86	24	17.279±0.037	16.260±0.017	15.710±0.028
246.857086	-24.769829	263	263	263	17.263±0.101	16.409±0.017	15.449±0.010
246.857193	-24.866022	11	2	5	17.201±0.017	16.185±0.009	15.622±0.015
246.857269	-25.167200	34	50	19	17.071±0.008	16.365±0.013	15.765±0.036
246.857330	-25.057373	262	261	250	16.884±0.006	16.068±0.006	15.579±0.014
246.857422	-24.742287	206	246	209	17.435±0.146	16.531±0.034	15.180±0.005
246.857452	-24.981190	140	169	146	13.128±0.001	12.346±0.001	12.086±0.001
246.857559	-24.806473	223	258	259	17.162±0.009	15.615±0.003	14.849±0.003
246.857651	-25.092489	126	104	19	16.796±0.004	15.985±0.005	15.608±0.009
246.857803	-25.089394	263	263	263	16.743±0.004	16.012±0.005	15.624±0.009
246.857834	-24.823725	263	263	263	17.180±0.025	16.243±0.017	15.601±0.029
246.857849	-24.819990	36	25	7	17.163±0.008	15.924±0.004	15.363±0.005
246.857864	-24.913782	7	5	2	17.202±0.015	16.299±0.013	15.763±0.028
246.857910	-24.217772	134	113	35	17.248±0.161	16.491±0.042	15.562±0.028
246.857910	-25.105707	254	253	248	17.188±0.023	16.364±0.029	15.699±0.056
246.857925	-24.992556	263	263	263	16.879±0.005	16.160±0.007	15.672±0.013
246.857956	-25.053688	263	263	263	15.194±0.001	14.459±0.001	14.243±0.002
246.858414	-24.886251	63	24	6	15.083±0.001	13.990±0.001	13.611±0.001
246.858414	-25.087481	255	253	226	16.732±0.004	15.888±0.004	15.452±0.006
246.858444	-24.787994	259	261	260	16.726±0.004	15.026±0.002	14.191±0.002
246.858780	-25.020296	262	262	247	17.032±0.007	16.217±0.009	15.694±0.019
246.858795	-25.028168	1	6	9	16.381±0.003	15.753±0.004	15.467±0.006
246.858826	-25.084181	262	262	262	15.224±0.001	14.557±0.001	14.349±0.002
246.858932	-25.170238	252	243	149	17.162±0.023	16.516±0.059	15.872±0.124
246.858963	-24.920425	101	98	42	15.991±0.002	15.275±0.003	15.025±0.004
246.859146	-25.124193	239	235	142	16.976±0.006	16.210±0.007	15.722±0.016

Table 1—Continued

RA (degrees)	Dec (degrees)	N_{Jobs}	N_{Hobs}	N_{Kobs}	J^a (mag)	H^a (mag)	K_s^a (mag)
246.859161	-25.141941	77	33	7	17.127±0.012	16.293±0.015	15.769±0.031
246.859329	-24.323023	226	250	230	16.558±0.004	14.331±0.001	12.972±0.001
246.859329	-25.099474	257	252	190	16.795±0.004	15.872±0.004	15.519±0.007
246.859467	-25.131371	263	263	263	16.040±0.002	15.417±0.003	15.198±0.004
246.859543	-25.161518	14	6	6	16.508±0.004	15.899±0.005	15.564±0.008
246.859558	-24.712914	17	7	2	17.433±0.086	15.218±0.002	12.604±0.001
246.859604	-24.986753	22	11	2	14.014±0.001	13.142±0.001	12.885±0.001
246.859833	-25.031816	263	263	263	16.763±0.004	15.820±0.004	15.476±0.006
246.859909	-24.973471	13	12	5	16.881±0.006	15.937±0.005	15.472±0.010
246.859924	-24.878780	73	40	8	17.160±0.014	16.329±0.017	15.726±0.035
246.860001	-24.744164	207	218	143	17.567±0.126	15.517±0.003	13.342±0.001
246.860397	-24.656380	259	260	239	15.631±0.002	12.043±0.001	9.850±0.001
246.860458	-24.886707	3	16	11	17.086±0.019	16.279±0.028	15.683±0.067
246.860550	-24.945471	115	69	13	14.636±0.001	13.732±0.001	13.359±0.001
246.860580	-24.263487	7	9	10	17.239±0.000	16.434±0.017	15.341±0.007
246.860611	-25.017414	35	49	22	17.157±0.017	16.271±0.017	15.711±0.034
246.860611	-24.754229	176	109	31	17.337±0.035	15.061±0.002	13.370±0.001
246.860764	-24.962925	263	263	263	17.131±0.010	16.368±0.015	15.784±0.037
246.860779	-24.431711	262	262	257	13.027±0.001	12.367±0.001	11.896±0.001
246.860779	-24.857788	263	263	263	17.113±0.008	16.196±0.007	15.665±0.012
246.860794	-24.529734	11	5	7	17.651±0.000	16.455±0.018	14.944±0.003
246.860825	-25.122658	263	263	263	17.142±0.026	16.401±0.043	15.719±0.095
246.860840	-24.974094	197	169	56	15.120±0.001	14.261±0.001	13.995±0.002
246.860901	-24.206709	262	256	193	17.413±0.052	16.373±0.014	15.495±0.011
246.860916	-24.679146	16	6	2	17.400±0.063	15.093±0.004	12.623±0.003
246.861160	-25.163675	262	262	262	16.065±0.002	15.495±0.003	15.294±0.005
246.861252	-24.793060	263	263	263	17.413±0.000	16.364±0.031	15.671±0.033
246.861313	-25.026508	260	261	262	17.035±0.007	16.313±0.010	15.796±0.026
246.861328	-24.886789	205	179	190	17.107±0.026	16.249±0.026	15.760±0.063
246.861435	-24.891266	3	5	11	17.267±0.016	16.311±0.013	15.738±0.021
246.861450	-25.032595	259	258	259	17.124±0.010	16.330±0.015	15.748±0.033
246.861496	-24.209957	261	261	256	17.399±0.105	16.357±0.011	15.411±0.007
246.861511	-25.057495	263	263	263	17.120±0.021	16.351±0.040	15.789±0.099
246.861526	-24.874649	85	101	43	17.218±0.026	16.382±0.031	15.836±0.056
246.861633	-24.990892	30	23	6	17.026±0.006	16.225±0.008	15.733±0.018
246.861816	-25.008595	66	47	14	17.056±0.007	16.296±0.010	15.772±0.024
246.862076	-25.086529	157	134	48	17.132±0.021	16.451±0.048	16.051±0.178
246.862244	-24.907288	263	263	263	15.814±0.002	14.925±0.002	14.640±0.002
246.862335	-24.680904	10	6	8	17.375±0.077	13.474±0.002	9.749±0.001
246.862396	-25.173771	17	25	12	16.054±0.002	15.421±0.003	15.189±0.004
246.862457	-24.960445	65	53	16	17.093±0.008	16.206±0.008	15.722±0.015
246.862610	-24.872503	119	163	80	15.750±0.002	14.861±0.002	14.517±0.002
246.862701	-25.082016	50	47	11	17.187±0.034	16.443±0.051	15.583±0.109
246.862717	-24.822046	263	263	261	16.265±0.003	15.012±0.002	14.507±0.002
246.862778	-24.838659	118	103	33	16.499±0.003	15.372±0.003	14.965±0.003

Table 1—Continued

RA (degrees)	Dec (degrees)	N_{Jobs}	N_{Hobs}	N_{Kobs}	J^a (mag)	H^a (mag)	K_s^a (mag)
246.862778	-24.538191	145	116	33	17.371±0.038	14.454±0.001	12.375±0.001
246.862823	-25.022079	257	257	217	15.238±0.001	14.551±0.001	14.341±0.002
246.862854	-25.150562	142	85	18	14.869±0.001	14.081±0.001	13.861±0.001
246.862961	-24.383713	2	21	8	17.460±0.076	16.288±0.008	15.130±0.004
246.863037	-25.069435	65	183	168	14.101±0.001	13.548±0.001	13.370±0.001
246.863037	-24.972597	174	178	89	17.239±0.028	16.380±0.037	15.804±0.094
246.863205	-25.160500	261	257	208	17.174±0.012	16.381±0.015	15.859±0.032
246.863235	-25.132231	43	13	5	14.108±0.001	13.479±0.001	13.274±0.001
246.863235	-24.850195	262	258	238	16.128±0.002	15.201±0.002	14.850±0.003
246.863266	-24.860819	260	254	184	17.115±0.008	16.027±0.005	15.521±0.007
246.863525	-25.176794	263	263	263	15.993±0.002	15.355±0.003	15.157±0.004
246.863907	-25.168009	61	83	30	16.871±0.005	16.187±0.007	15.692±0.018
246.863922	-24.905951	45	39	12	17.125±0.009	16.317±0.012	15.778±0.027
246.864044	-25.096376	259	251	174	17.041±0.007	16.170±0.007	15.701±0.013
246.864105	-24.521235	248	248	170	12.363±0.001	10.368±0.001	9.306±0.001
246.864304	-25.099035	205	205	111	15.180±0.001	14.514±0.001	14.313±0.002
246.864441	-24.360088	27	12	3	17.309±0.040	15.247±0.003	14.025±0.002
246.864456	-24.985218	85	61	15	17.083±0.008	16.215±0.008	15.675±0.016
246.864487	-25.102493	3	74	136	17.202±0.015	16.323±0.016	15.808±0.034
246.864487	-24.784399	19	15	3	17.340±0.031	15.817±0.004	14.724±0.003
246.864594	-25.164925	69	199	179	13.576±0.001	12.782±0.001	12.556±0.001
246.864746	-25.089663	58	263	263	16.472±0.003	15.827±0.004	15.515±0.007
246.864868	-24.869503	260	262	260	17.272±0.021	16.398±0.022	15.823±0.042
246.864929	-25.137539	161	261	263	17.123±0.012	16.368±0.020	15.819±0.053
246.865082	-24.907696	119	249	253	17.227±0.017	16.446±0.021	15.817±0.051
246.865204	-24.359596	17	59	34	17.302±0.058	15.442±0.003	14.211±0.002
246.865463	-24.351675	59	229	231	17.576±0.170	16.527±0.047	15.434±0.018
246.865494	-25.084070	210	202	202	16.684±0.004	15.765±0.004	15.451±0.006
246.865555	-24.927305	152	262	262	16.934±0.005	16.177±0.007	15.685±0.014
246.865646	-24.986620	2	4	263	17.245±0.031	16.339±0.032	15.825±0.062
246.865692	-25.124537	8	117	198	16.963±0.006	16.094±0.006	15.617±0.012
246.865692	-24.950155	253	224	107	17.124±0.023	16.375±0.041	15.713±0.157
246.865738	-24.922380	178	259	262	17.144±0.021	16.389±0.038	15.804±0.122
246.865814	-24.877401	263	263	263	16.000±0.002	14.901±0.002	14.524±0.002
246.865875	-25.157244	257	262	262	17.175±0.027	16.402±0.058	15.961±0.085
246.866028	-25.154570	3	2	61	17.118±0.011	16.405±0.020	15.803±0.043
246.866165	-25.024445	4	6	262	16.852±0.005	16.075±0.005	15.594±0.009
246.866226	-24.355835	32	203	225	17.352±0.139	16.521±0.028	15.486±0.015
246.866257	-24.213516	6	3	96	17.372±0.032	15.739±0.004	14.589±0.002
246.866318	-25.168741	11	9	2	16.458±0.003	15.881±0.005	15.573±0.008
246.866394	-24.999266	68	81	35	17.131±0.033	16.340±0.049	15.705±0.081
246.866394	-24.875408	263	263	263	17.207±0.013	16.182±0.008	15.652±0.014
246.866425	-25.151302	6	21	16	17.101±0.024	16.314±0.046	15.867±0.153
246.866440	-25.054108	83	230	233	16.854±0.005	16.179±0.007	15.718±0.016
246.866531	-25.169928	70	45	12	17.084±0.015	16.327±0.039	15.789±0.081

Table 1—Continued

RA (degrees)	Dec (degrees)	N_{Jobs}	N_{Hobs}	N_{Kobs}	J^a (mag)	H^a (mag)	K_s^a (mag)
246.866638	-24.662069	29	251	262	17.275±0.163	16.442±0.163	15.250±0.009
246.866684	-24.659260	3	263	263	17.285±0.028	13.535±0.002	10.217±0.001
246.866730	-24.924974	15	7	3	16.094±0.002	15.330±0.003	15.096±0.004
246.866760	-25.122454	260	259	259	14.449±0.001	13.571±0.001	13.280±0.001
246.866882	-24.458328	3	8	57	8.006±99.000	15.948±0.061	14.942±0.046
246.866928	-24.608168	36	39	16	17.409±0.033	15.153±0.002	13.525±0.001
246.866928	-24.759716	50	190	180	17.394±0.000	16.467±0.047	15.357±0.012
246.866959	-24.983807	2	249	262	17.057±0.007	16.253±0.008	15.756±0.019
246.867035	-25.062162	2	71	242	15.507±0.001	14.885±0.002	14.701±0.003
246.867310	-24.528580	6	229	257	17.510±0.092	15.988±0.005	13.760±0.001
246.867416	-25.039640	24	67	54	16.709±0.004	15.758±0.004	15.376±0.005
246.867432	-24.893436	6	45	247	16.313±0.003	15.452±0.003	15.146±0.004
246.867462	-25.067192	5	28	28	14.542±0.001	13.947±0.001	13.759±0.001
246.867630	-24.888224	70	38	10	14.213±0.001	13.464±0.001	13.164±0.001
246.867722	-25.126432	1	2	14	15.805±0.002	15.189±0.002	15.014±0.003
246.867798	-24.949869	78	56	15	13.006±0.001	12.051±0.001	11.775±0.001
246.867950	-24.940281	147	255	258	17.191±0.020	16.330±0.024	15.738±0.044
246.868301	-25.124754	11	60	40	17.026±0.033	16.145±0.043	15.640±0.100
246.868332	-24.361423	7	263	263	17.393±0.070	16.273±0.008	15.243±0.005
246.868393	-25.162584	3	18	7	14.982±0.001	14.424±0.001	14.252±0.002
246.868393	-24.275549	263	263	263	17.435±0.083	15.863±0.004	14.220±0.002
246.868454	-25.051800	41	216	222	17.206±0.030	16.346±0.036	15.877±0.080
246.868515	-24.455685	22	96	83	15.658±0.003	12.069±0.003	9.975±0.001
246.868637	-25.103365	263	263	263	17.096±0.010	16.371±0.016	15.765±0.039
246.868744	-24.997038	68	37	9	15.362±0.001	14.536±0.001	14.311±0.002
246.868835	-25.020145	235	216	104	17.145±0.027	16.434±0.067	15.767±0.000
246.868896	-24.947245	9	263	263	16.005±0.002	15.326±0.003	15.098±0.004
246.868927	-24.669441	19	6	3	17.346±0.149	16.574±0.083	15.361±0.012
246.869003	-24.200632	10	5	11	17.326±0.095	16.334±0.012	15.478±0.009
246.869141	-24.921534	30	23	6	17.211±0.016	16.280±0.012	15.546±0.013
246.869141	-24.800817	235	230	230	17.278±0.015	15.958±0.005	15.233±0.004
246.869217	-24.888842	2	58	113	16.912±0.005	15.890±0.005	15.366±0.005
246.869308	-24.856850	10	259	263	17.232±0.019	16.334±0.018	15.775±0.035
246.869308	-24.802727	26	33	13	16.521±0.003	14.756±0.002	13.991±0.002
246.869354	-24.878738	263	263	263	17.105±0.008	16.222±0.008	15.738±0.017
246.869370	-24.968189	10	263	263	17.129±0.012	16.349±0.017	15.776±0.044
246.869370	-25.037422	6	262	263	17.136±0.020	16.339±0.027	15.682±0.060
246.869385	-24.887428	255	259	254	17.154±0.011	16.168±0.008	15.631±0.014
246.869537	-24.903152	2	33	74	16.855±0.005	16.068±0.005	15.647±0.009
246.869705	-24.908840	262	259	231	12.584±0.001	11.988±0.001	11.703±0.001
246.869705	-24.970646	263	263	263	13.926±0.001	13.304±0.001	13.110±0.001
246.869858	-24.285242	253	244	162	17.382±0.064	14.847±0.002	12.884±0.001
246.869904	-24.451868	5	21	13	16.513±0.034	14.642±0.053	13.484±0.054
246.869919	-24.929714	1	31	72	16.402±0.003	15.548±0.003	15.266±0.004
246.869934	-25.166969	18	136	152	16.929±0.007	16.144±0.010	15.643±0.033

Table 1—Continued

RA (degrees)	Dec (degrees)	N_{Jobs}	N_{Hobs}	N_{Kobs}	J^a (mag)	H^a (mag)	K_s^a (mag)
246.870041	-25.004745	2	7	5	16.501±0.003	15.566±0.003	15.176±0.004
246.870071	-25.144436	3	7	4	14.413±0.001	13.853±0.001	13.668±0.001
246.870117	-25.167648	5	193	262	16.383±0.003	15.545±0.004	15.186±0.006
246.870178	-25.156761	2	9	8	17.207±0.032	16.356±0.039	15.853±0.092
246.870300	-24.320404	9	3	3	17.166±0.036	16.239±0.043	15.499±0.055
246.870346	-24.336649	0	3	33	8.006±99.000	16.510±0.082	15.469±0.027
246.870483	-24.987814	195	156	50	17.162±0.011	16.285±0.011	15.735±0.018
246.870529	-24.603134	263	263	263	17.516±0.181	16.533±0.049	15.503±0.024
246.870575	-24.964520	260	263	262	16.944±0.006	16.239±0.008	15.763±0.018
246.870590	-25.077671	1	4	183	15.820±0.002	15.230±0.002	15.024±0.004
246.870590	-25.106920	4	5	4	12.919±0.001	12.369±0.001	12.187±0.001
246.870819	-24.216721	238	233	124	17.450±99.000	16.492±0.032	15.489±0.018
246.870850	-24.451984	4	9	11	16.655±0.030	14.857±0.054	13.734±0.037
246.870880	-25.038754	263	263	263	17.160±0.021	16.458±0.045	15.893±0.122
246.870911	-24.867290	263	262	262	15.124±0.001	14.087±0.001	13.729±0.001
246.871017	-24.274200	263	263	263	17.319±0.155	16.544±0.090	15.384±0.020
246.871063	-24.953115	248	253	254	15.646±0.002	14.829±0.002	14.588±0.002
246.871140	-24.796391	263	262	256	17.319±0.018	16.200±0.007	15.489±0.007
246.871368	-24.890699	5	10	5	15.751±0.002	14.947±0.002	14.641±0.002
246.871368	-25.024389	61	85	38	16.415±0.003	15.510±0.003	15.203±0.004
246.871399	-24.813623	11	11	8	16.568±0.004	15.316±0.003	14.755±0.003
246.871445	-24.967485	6	22	15	16.083±0.002	15.241±0.002	14.967±0.003
246.871521	-24.365564	15	21	8	17.415±0.056	16.265±0.008	15.266±0.005
246.871597	-25.053867	5	5	8	15.788±0.002	15.183±0.002	14.976±0.003
246.871964	-25.114471	258	258	258	17.110±0.030	16.275±0.058	15.763±0.118
246.872086	-24.569023	155	252	254	17.342±0.020	14.653±0.002	12.820±0.001
246.872177	-24.451967	15	22	11	17.138±0.061	15.607±0.020	14.640±0.024
246.872314	-25.020634	109	83	26	16.428±0.003	15.732±0.004	15.441±0.006
246.872498	-25.050228	212	221	137	13.122±0.001	12.335±0.001	12.081±0.001
246.872528	-24.911339	208	175	67	17.212±0.024	16.409±0.035	15.840±0.061
246.872681	-24.654474	261	257	200	16.761±0.006	12.981±0.001	10.156±0.001
246.872787	-24.877350	257	255	204	16.727±0.004	16.107±0.006	15.612±0.010
246.872894	-24.924698	256	256	241	17.050±0.007	16.229±0.008	15.737±0.020
246.872925	-24.985529	4	10	8	17.150±0.021	16.346±0.036	15.986±0.000
246.873260	-24.827129	263	263	261	17.309±0.051	16.355±0.038	15.747±0.066
246.873367	-25.024284	263	262	262	16.889±0.005	16.147±0.007	15.662±0.014
246.873383	-24.490191	262	262	260	17.539±0.151	16.444±0.014	14.464±0.002
246.873657	-24.316839	14	14	3	17.474±0.047	15.429±0.003	13.867±0.001
246.873672	-24.781668	262	262	262	17.460±0.147	16.389±0.037	15.609±0.036
246.873749	-24.930420	23	6	11	17.223±0.021	16.311±0.017	15.712±0.031
246.873947	-24.879484	131	121	122	16.102±0.002	15.099±0.002	14.730±0.003
246.873993	-25.162390	6	6	3	16.381±0.003	15.808±0.004	15.531±0.007
246.874054	-25.020283	184	178	70	16.913±0.005	16.098±0.007	15.636±0.012
246.874191	-25.124998	263	262	261	16.775±0.005	16.008±0.005	15.544±0.009
246.874268	-24.989990	256	232	123	16.973±0.006	16.093±0.006	15.628±0.010

Table 1—Continued

RA (degrees)	Dec (degrees)	N_{Jobs}	N_{Hobs}	N_{Kobs}	J^a (mag)	H^a (mag)	K_s^a (mag)
246.874298	-24.969509	215	166	56	17.168±0.017	16.376±0.027	15.807±0.070
246.874329	-25.137653	258	258	258	17.081±0.008	16.224±0.009	15.660±0.014
246.874359	-25.090769	263	263	263	17.021±0.006	16.285±0.009	15.735±0.021
246.874390	-24.977333	258	258	258	17.088±0.009	16.193±0.009	15.677±0.016
246.874405	-24.800447	198	179	70	17.220±0.012	16.128±0.006	15.470±0.006
246.874649	-24.821753	36	37	14	17.401±0.067	16.347±0.028	15.650±0.042
246.874817	-25.177647	2	108	205	17.129±0.012	16.286±0.013	15.766±0.031
246.874878	-24.560108	263	263	263	17.418±0.100	15.520±0.003	12.420±0.001
246.874924	-24.887274	15	10	4	11.490±0.001	10.800±0.001	10.505±0.001
246.875061	-24.944588	175	188	94	15.756±0.002	15.047±0.002	14.826±0.003
246.875107	-24.360357	187	260	231	17.499±0.134	16.438±0.035	15.622±0.030
246.875259	-25.082378	54	99	48	16.781±0.004	16.073±0.006	15.622±0.012
246.875412	-25.013149	263	263	263	15.977±0.002	15.237±0.002	15.029±0.004
246.875549	-24.992615	257	260	236	16.010±0.002	15.332±0.003	15.116±0.004
246.875565	-25.098337	20	12	2	16.305±0.003	15.632±0.003	15.380±0.005
246.875580	-25.078901	262	262	256	12.539±0.001	11.935±0.001	11.615±0.001
246.875793	-24.462006	8	3	5	15.444±0.001	11.495±0.001	8.981±0.001
246.875870	-25.185534	7	4	4	14.699±0.004	14.097±0.007	13.918±0.011
246.875961	-24.607851	12	9	3	17.532±0.080	16.113±0.006	14.754±0.003
246.876068	-24.941650	259	256	208	15.477±0.001	14.654±0.002	14.428±0.002
246.876083	-24.921795	35	17	4	16.670±0.004	15.959±0.005	15.563±0.008
246.876083	-25.062065	115	57	10	17.085±0.026	16.406±0.060	15.958±99.000
246.876221	-25.145437	261	259	209	14.698±0.001	13.920±0.001	13.705±0.001
246.876251	-24.925430	217	205	97	17.095±0.013	16.203±0.012	15.631±0.023
246.876343	-25.103128	262	261	250	15.936±0.002	15.211±0.002	14.976±0.003
246.876373	-24.926353	178	198	129	17.134±0.025	16.247±0.025	15.767±0.052
246.876495	-24.834927	28	9	2	16.599±0.004	15.516±0.003	15.065±0.004
246.876648	-25.008373	137	74	18	16.378±0.003	15.767±0.004	15.450±0.006
246.876648	-24.347902	263	263	263	17.445±0.130	16.453±0.022	15.374±0.009
246.876862	-24.593222	136	187	92	17.395±0.065	16.241±0.007	14.960±0.003
246.876999	-24.363041	249	255	247	17.493±99.000	16.422±0.032	15.636±0.026
246.877014	-25.174389	108	128	65	16.678±0.004	15.967±0.005	15.603±0.009
246.877228	-24.542961	259	248	164	13.006±0.001	12.430±0.001	12.194±0.001
246.877274	-24.196602	261	260	217	16.189±0.007	14.236±0.002	13.380±0.002
246.877518	-25.095985	52	37	10	17.076±0.015	16.341±0.024	15.769±0.053
246.877579	-25.163483	20	52	35	17.155±0.028	16.413±0.056	15.971±0.122
246.877594	-24.883186	10	57	43	15.654±0.002	14.512±0.001	14.139±0.002
246.877609	-24.888214	69	262	263	16.818±0.005	16.000±0.005	15.558±0.008
246.877640	-24.510548	142	239	242	17.275±0.116	16.596±0.035	15.382±0.011
246.877853	-25.094152	141	257	261	17.071±0.020	16.378±0.046	15.794±0.101
246.877991	-24.924438	30	16	4	15.974±0.002	15.144±0.002	14.882±0.003
246.878098	-25.105009	32	17	4	17.133±0.012	16.257±0.013	15.737±0.018
246.878113	-24.850231	256	241	155	17.052±0.007	16.060±0.006	15.561±0.008
246.878265	-25.008005	233	262	262	17.065±0.008	16.191±0.009	15.633±0.015
246.878326	-25.059849	22	19	6	13.573±0.001	12.948±0.001	12.752±0.001

Table 1—Continued

RA (degrees)	Dec (degrees)	N_{Jobs}	N_{Hobs}	N_{Kobs}	J^a (mag)	H^a (mag)	K_s^a (mag)
246.878342	-24.487194	14	5	10	17.503±0.133	16.555±0.024	14.942±0.003
246.878479	-24.855137	247	253	213	14.270±0.001	13.029±0.001	12.586±0.001
246.878510	-24.790745	31	22	4	12.181±0.001	10.385±0.001	9.474±0.001
246.878571	-24.415533	16	238	255	12.729±0.001	10.998±0.001	10.078±0.001
246.878616	-24.982397	2	6	15	17.076±0.023	16.399±0.074	15.926±0.117
246.878662	-25.009520	257	263	263	16.622±0.004	15.923±0.005	15.571±0.008
246.878784	-24.459188	7	13	7	17.649±0.103	16.708±0.127	15.059±0.005
246.878876	-24.977203	11	54	263	17.197±0.021	16.510±0.035	15.830±0.058
246.878983	-25.005232	7	17	14	13.175±0.001	12.288±0.001	12.028±0.001
246.879013	-24.930347	263	263	263	16.814±0.005	15.822±0.004	15.398±0.005
246.879074	-25.099659	5	151	189	14.477±0.001	14.052±0.001	13.904±0.001
246.879166	-25.065256	46	71	35	17.064±0.010	16.215±0.012	15.636±0.020
246.879181	-25.154293	241	239	245	16.755±0.006	16.097±0.007	15.652±0.019
246.879425	-25.130018	108	111	54	17.035±0.007	16.163±0.007	15.630±0.012
246.879456	-24.567505	168	153	52	13.422±0.001	11.317±0.001	10.327±0.001
246.879471	-25.066801	97	61	8	15.138±0.001	14.396±0.001	14.191±0.002
246.879547	-24.229218	258	258	258	17.553±0.105	16.437±0.019	15.367±0.009
246.879562	-25.048986	263	263	263	17.153±0.023	16.477±0.047	15.957±0.136
246.879715	-25.178942	162	194	124	16.563±0.004	15.896±0.005	15.608±0.009
246.879761	-24.864498	262	262	262	17.283±0.023	16.319±0.015	15.735±0.025
246.879807	-24.800550	171	184	100	17.354±0.056	16.382±0.024	15.749±0.029
246.879822	-25.045582	5	5	7	16.843±0.005	15.870±0.005	15.474±0.006
246.879929	-25.018751	33	16	4	15.798±0.002	15.166±0.002	14.974±0.003
246.880112	-24.992887	60	48	34	17.119±0.019	16.314±0.021	15.728±0.041
246.880127	-24.853968	175	256	261	14.736±0.002	13.728±0.002	13.299±0.001
246.880157	-25.071445	38	24	7	16.247±0.003	15.621±0.004	15.375±0.005
246.880234	-24.897501	262	263	263	16.059±0.002	15.301±0.003	15.044±0.004
246.880508	-24.824379	262	262	261	17.201±0.021	16.133±0.009	15.540±0.013
246.880692	-24.276352	258	257	258	17.470±0.000	16.531±0.059	15.368±0.015
246.880814	-25.040216	180	262	262	17.082±0.009	16.117±0.007	15.348±0.006
246.880844	-25.150623	143	152	151	8.439±0.013	8.168±0.001	8.094±0.055
246.880981	-25.163467	121	262	262	17.174±0.016	16.313±0.020	15.721±0.038
246.881058	-25.119898	246	263	263	15.666±0.002	15.037±0.002	14.825±0.003
246.881226	-24.337467	257	263	263	17.384±0.066	15.716±0.004	14.211±0.002
246.881271	-24.968410	3	263	263	14.983±0.001	14.248±0.001	14.027±0.002
246.881317	-25.084084	255	255	257	14.364±0.001	13.765±0.001	13.574±0.001
246.881348	-24.888725	263	263	262	16.668±0.004	16.149±0.006	15.716±0.013
246.881424	-24.640041	263	263	263	17.546±0.100	16.308±0.010	15.198±0.005
246.881744	-25.076838	259	260	261	16.130±0.003	15.312±0.003	15.091±0.004
246.881821	-24.928511	117	129	146	16.564±0.004	15.755±0.004	15.424±0.007
246.881866	-24.631775	4	4	211	17.381±0.031	15.581±0.004	14.369±0.002
246.881897	-24.326202	4	263	263	17.366±0.085	15.953±0.006	14.441±0.003
246.882034	-24.841801	62	263	263	17.252±0.021	16.239±0.012	15.660±0.019
246.882050	-24.905821	263	263	263	17.196±0.013	16.249±0.010	15.715±0.019
246.882141	-24.970427	263	263	263	17.148±0.024	16.421±0.044	15.784±0.083

2.2.1. Detection and Completeness Limits

For non-variable stars, the photometric measurement uncertainty is characterized by the standard deviation of all photometric measurements in a particular band. P08 showed that this photometric standard deviation as a function of apparent magnitude, for 2MASS photometry, follows the form of two distinct power laws. One power law describes brighter sources, where Poisson statistics dominate the uncertainty, while the second describes the dimmer sources, where the uncertainty is dominated by instrumental noise. The point of intersection between these two power laws, or “break point”, designates the survey completeness limit where source detection drops below 100%. This power law model is used to predict the photometric scatter for a star, and any star that has a dispersion significantly ($> 5\sigma$) above this is identified as a candidate variable. The model, as a function of apparent magnitude m , is given by the following expression:

$$10^{[\sigma_{m,model} \pm \nu_{m,model}(m)]} = b_{m,l} \pm \sigma_{b_{m,l}} + (a_{m,l} \pm \sigma_{a_{m,l}})10^{0.4m} \quad (1)$$

where $a_{m,l}$, $b_{m,l}$, $\sigma_{a_{m,l}}$, and $\sigma_{b_{m,l}}$ represent the slope, intercept and respective errors for each fit in each band over magnitude region l . This model is first applied to our sample of 1678 stars using coefficients derived by P08 from the entire 2MASS Calibration Field data set. These coefficients, however, yield a relatively poor fit to the ρ Oph calibration field. The lower noise in the ρ Oph data is attributed to better average seeing conditions during these observations. As a result, the model is re-fit on the ρ Oph data set alone to derive a new set of coefficients. The new coefficients with errors are listed in Table 2. Fig 1 shows the best-fit model along with the observed photometric scatter in each band.

The model yields completeness limits for this survey of 16.63, 15.75 and 15.10 mag in J , H and K_s , respectively. These are significantly fainter limits than the 2MASS PSC as a whole, which are 15.8, 15.1 and 14.3 mag in J , H and K_s , respectively. The approximate detection limits for this study, found by averaging the apparent magnitudes for the 10 faintest objects meeting our detection criteria, are 17.7, 16.7 and 16.0 mag in J , H and K_s respectively.

3. VARIABILITY ANALYSIS

3.1. Selection Criteria for Variability

Numerous surveys have used time-series analysis on multi-wavelength photometry to characterize young star variability (Mathieu et al. 1997; Carpenter et al. 2001, 2002; Grankin et al. 2007, 2008; Morales-Calderón et al. 2011; Findeisen et al. 2013; Wolk et al. 2013, and

Table 1—Continued

RA (degrees)	Dec (degrees)	N_{Jobs}	N_{Hobs}	N_{Kobs}	J^a (mag)	H^a (mag)	K_s^a (mag)
246.882217	-24.855089	261	262	262	17.247±0.033	16.296±0.020	15.698±0.033
246.882492	-25.014971	150	263	263	16.452±0.004	15.758±0.005	15.445±0.007
246.882492	-24.839403	263	263	263	17.257±0.026	16.262±0.014	15.715±0.023
246.882614	-25.061298	6	262	263	16.243±0.003	15.294±0.003	14.992±0.004
246.882843	-25.177279	263	263	263	16.701±0.006	15.974±0.008	15.536±0.021
246.882919	-24.974188	263	263	263	17.086±0.012	16.335±0.019	15.875±0.045
246.883072	-25.176561	263	258	218	16.815±0.007	16.048±0.009	15.656±0.035
246.883102	-25.091089	263	263	263	16.980±0.011	16.225±0.016	15.728±0.048
246.883133	-24.865528	4	263	263	17.239±0.023	16.334±0.023	15.762±0.043
246.883270	-25.012573	263	263	263	17.130±0.014	16.281±0.017	15.737±0.040
246.883652	-25.091648	3	178	263	16.987±0.011	16.233±0.019	15.708±0.055
246.883667	-24.527349	2	9	173	17.489±99.000	16.577±0.077	15.360±0.019
246.883682	-25.148535	2	263	263	15.429±0.003	14.684±0.002	14.528±0.003

^aUnweighted mean apparent magnitude of Cal-PSWDB photometry

Table 2. Model Fit Parameters for Observed Photometric Scatter^a

Band	Range ^b	$a_{m,l} \pm \sigma_{a_{m,l}}$	$b_{m,l} \pm \sigma_{b_{m,l}}$
J	<16.63	$(3.046 \pm 0.043) \times 10^{-8}$	1.01326±0.00087
J	>16.63	$(1.484 \pm 0.083) \times 10^{-8}$	1.08343±0.00046
H	<15.75	$(6.467 \pm 0.055) \times 10^{-8}$	1.01444±0.00041
H	>15.75	$(4.03 \pm 0.16) \times 10^{-8}$	1.0628±0.0059
K_s	<15.10	$(1.2247 \pm 0.0094) \times 10^{-7}$	1.0134±0.0036
K_s	>15.10	$(4.98 \pm 0.25) \times 10^{-8}$	1.0934±0.0042

^aSee §2.2.1 for explanation of parameters.

^bRange in apparent magnitude; apparent magnitudes of < 6 are excluded from this model.

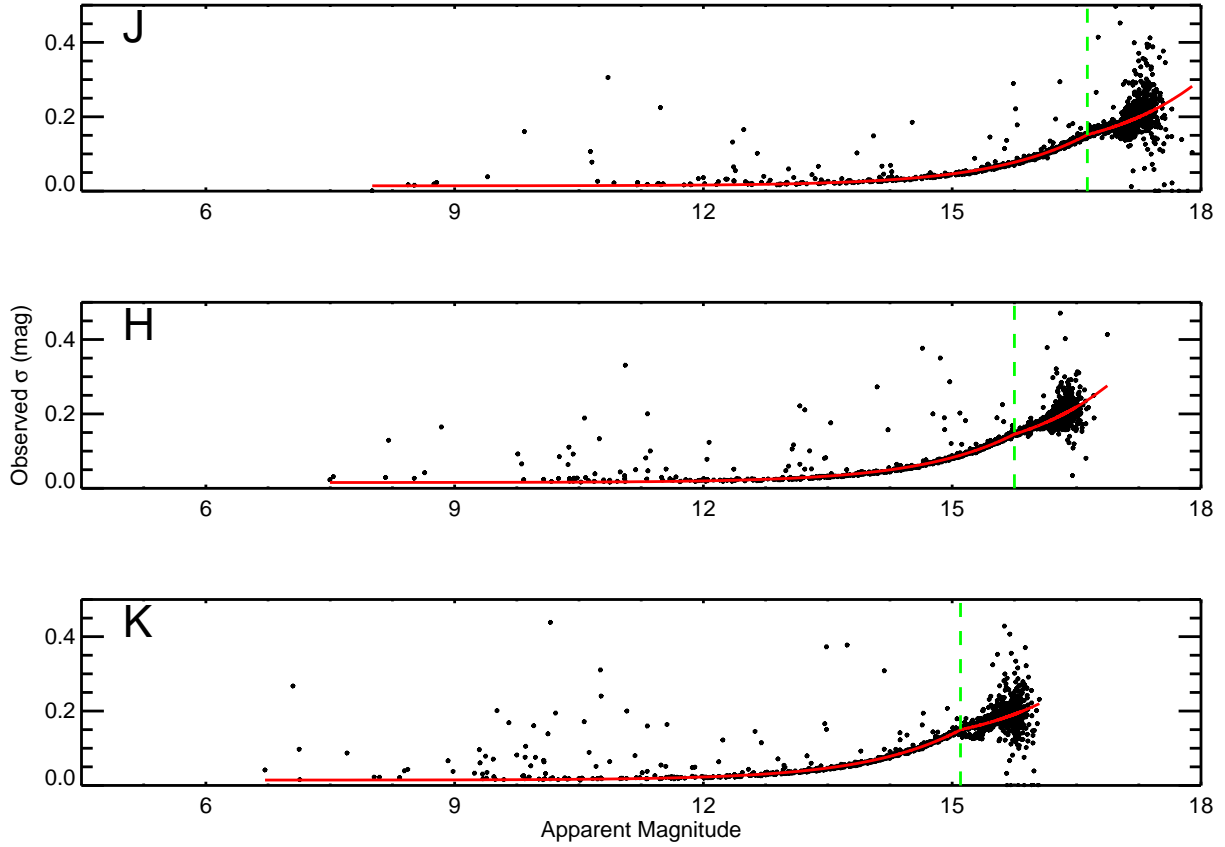


Fig. 1.— Photometric standard deviation versus apparent magnitude derived from up to 1584 observations of each sample star; there are 1678 sample stars in total. The solid red line corresponds to the photometric model fit to this sample. The dashed green line marks the break magnitude, where the detection rate drops below 100%, in each band. The break magnitudes are $J = 16.63$, $H = 15.75$, and $K_s = 15.10$ mag.

references therein). The methods for identifying stellar variability are nearly as numerous as the variability studies themselves. These include, but are not limited to, the Stetson index, excess photometric dispersion, χ^2 statistic, cross-correlation and Fourier analysis (Stetson 1996; Carpenter et al. 2001; Barsony et al. 2005; Alves de Oliveira & Casali 2008).

Variable stars are identified in this work through 3 complementary methods that are sensitive to different types of variability. A full description of these techniques are presented in P08. The same terminology used in P08 is adopted in this work. Here a summary is presented along with specifics regarding this sample. The first and second methods, “flickering” and “excursive”, identify variability in each band individually. The third method uses the Stetson index to identify correlated variability between bands.

3.1.1. Flickering Variability

Flickering variability describes when the star’s photometric scatter significantly differs from the predicted scatter. Flickering variability is sensitive to continuous variability, as consistent, substantial variations are needed to significantly increase the observed photometric dispersion above the expected non-variable value. To identify flickering variables, an observed dispersion is calculated for all scan measurements of a star prior to combining as a scan group. This is then compared to the star’s expected dispersion with associated uncertainty, σ , calculated using the noise model described in § 2.2.1 (Eqn 1 and Fig 1). If the observed dispersion exceeds the expected dispersion by more than 5σ , the star is a candidate variable. This search is done separately for each of the 3 bands (J, H, K_s); a star can thus be flagged as a flickering variable in 1, 2 or all 3 bands. Following this criterion, 17 stars flag in only a single band, 23 flag in two bands and 54 flag in all three bands. If variability is intrinsic to the star, the expectation is the flickering will occur in more than one band. Low signal-to-noise photometry (the number of observations, N_{obs} , is typically less than 500) might likely account for the 9 candidate variables that flicker in the K band only. It might also account for the 11 candidate variables that flicker in both the H and K bands. However there is no obvious explanation for the 17 candidate variable stars that flicker only in the J or H , J and H , or J and K bands. The average dispersions for these variable stars in J , H and K_s are 0.12 ± 0.46 , 0.12 ± 0.43 and 0.11 ± 0.35 mag, respectively. The listed errors are the standard deviation of the average dispersion. These values represent the dispersion intrinsic to the source, or specifically the dispersion after the predicted non-variable measurement dispersion is subtracted in quadrature from the observed dispersion.

3.1.2. *Excursive Variability*

Excursive variability describes when the average magnitude of a individual scan group is significantly deviant from the mean of all the star’s scan groups. Excursive variability is sensitive to short time-scale variations such as a single eclipse event or flare. Excursive candidate variables are identified if the average magnitude for a single scan group exceeds the global mean by more than 5σ , where here σ is the co-added uncertainty in the scan group photometry. As with flickering variability, this search is done separately for each of the 3 bands. From the final variable catalog, 21 stars flag in only a single band, 19 flag in two bands and 41 flag in all three bands. Low signal-to-noise photometry (N_{obs} typically less than 500) might account for the 10 candidate variables that are excursive in the K band only. It might also account for the 12 candidate variables that are excursive in both the H and K bands. However there is no obvious explanation for the 19 candidate variable stars that are excursive only in the J or H , J and H , or J and K bands. The average number of deviant scan groups per star in our variable catalog is 24, 42 and 57 in J , H and K_s bands, respectively.

3.1.3. *Stetson Index*

The Stetson index describes the correlation in a star’s photometric variation between different bands. The Stetson index is sensitive to variability whose amplitude is not significantly different between photometric bands. For example, the Stetson index is not sensitive to a strong increase in the $Br\gamma$ emission line strength that might only affect 1 band. This index has been previously used on other molecular cloud 2MASS variability surveys in Orion A and Chameleon I (Carpenter et al. 2001, 2002). The Stetson index is computed for all 1678 stars; a star is considered a candidate variable if this index is > 0.2 . P08 determined this criterion based on 18 of 23 periodic variables, in that work, having indices above this value. The same index is adopted here since the observing methodology is identical in both works. This index is smaller than those adopted for the Orion A (0.55) and Chameleon I (1.00) surveys. The Orion A survey contained 29 epochs over a 36 day temporal baseline and the Chameleon I survey contained 15 epochs over 5 months. The smaller number of observed epochs in each case causes these surveys to be less sensitive to variability and thus in need of a higher index. A Stetson index of zero indicates random noise or no correlation between the photometry in different bands. A positive index indicates correlation between the photometry in two bands. The higher the index, the greater the correlation between the photometry. Using the Stetson index 57 stars flag as variable.

3.1.4. Excluding Seeing Induced Variables

A common way in which a non-variable star is misidentified as variable is from photometric variations caused by changing atmospheric seeing. Both photometric techniques used here (PSF fitting, fixed sums) are susceptible to this, especially in regions that are crowded or where there is bright nebular emission. Seeing estimates, corresponding to the average FWHM for each calibration scan, are provided for the Cal-PSWDB photometry. The typical seeing values range between 2.5'' to 2.7'' over the entire observing season (Cutri et al. 2006).

The possibility of changes in brightness being correlated with changes in the seeing are first investigated. This is done by computing the Pearson r-correlation statistic for each star, n . The statistic is given by the following:

$$r_n = \frac{\sum_{t=1}^{N_{m,n}} (m_{n,t} - \bar{m}_n)(S_{m,t} - \bar{S}_m)}{\sqrt{\sum_{t=1}^{N_{m,n}} (m_{n,t} - \bar{m}_n)^2} \sqrt{\sum_{t=1}^{N_{m,n}} (S_{m,t} - \bar{S}_m)^2}} \quad (2)$$

where m is the band, $S_{m,t}$ is the m -band seeing FWHM in arcseconds at epoch t and \bar{S} is the average seeing in m -band. The separate quantities are summed over all $N_{m,n}$ m -band observations for star, n . This statistic spans the range from -1 to 1 with negative values indicating inversely correlated variations and positive values corresponding to directly correlated variations. An inverse correlation means as the seeing worsens the star gets brighter. A direct correlation refers to the opposite effect. Since in Eqn 2, the photometry comparison (numerator) is computed in magnitudes and the photometric standard deviation (denominator) is computed first in flux units then converted to magnitudes, this can result in r values slightly outside the -1 to 1 range. A slight trend exists in the sample of 1678 stars toward an inverse seeing correlation in each band. The average r statistics in J , H and K_s are -0.12, -0.11 and -0.05, respectively. Inverse correlation is likely caused by crowded fields where as the seeing worsens, flux from surrounding stars may encroach into the measured star's aperture or spatial profile. While these correlations are not very significant in most cases, it is noted the seeing in one band is slightly correlated with the seeing in another band. This is consistent with multi-band photometry taken simultaneously. To look for correlations between bands, the Pearson index for J and H are plotted in Fig 2. To characterize and flag seeing induced variability, a single seeing test is constructed to provide an estimate of seeing effects on measured photometry. Each correlation statistic (r_J , r_H , r_K) is considered a component of a single "seeing vector". This vector is rotated and transformed from cartesian to cylindrical coordinates so the z -axis corresponds to $r_J = r_H = r_K$. This representation causes the seeing correlation to be axisymmetric about the z -axis, thus reducing the characterization of multi-band seeing correlation by one dimension. A

“seeing ellipse” is described by

$$\frac{z_n^2}{\sigma_z^2} + \frac{\rho_n^2}{\sigma_\rho^2} = 1 \tag{3}$$

where z_n is the component of the seeing vector for star n , with standard deviation σ_z , along the z -axis. ρ_n is the component for star n along the ρ -axis, with the standard deviation σ_ρ . Both σ_z and σ_ρ are determined from the distribution of the ensemble 1678 stars. A candidate variable is flagged as seeing correlated when the seeing vector length is larger than the seeing ellipse for the ensemble. This is the case when the left-hand side of Eqn 3 is greater than unity. This test excludes 19 candidate variables; the variability of these stars is likely solely caused by fluctuations in atmospheric seeing.

3.1.5. Final Variable Catalog

From the target sample of 1678 stars, 101 stars (6%) are identified as variable. These variable stars are referred to as the *variable catalog*. The variable catalog is listed in Table 3. The full set of light curves, color curves and color-color plots for all variables stars is only available on-line. For inclusion into the variable catalog, a star must not exhibit seeing correlated photometry (see § 3.1.4) and must meet 2 of the 7 variability criteria (see §3.1.1 - 3.1.3). In addition, the 2 criteria must be met in different bands or in a single band along with the Stetson criterion. This last condition is imposed in order to prevent identifying variability due to poor quality or spurious photometry that is missed by the previous filters. The amplitudes of variability for stars within the variable catalog span a wide range. The range in ΔK_s spans 0.04 to 2.31 mag and $\Delta(H-K_s)$ varies from 0.01 to 1.62 mag. The variable catalog contains 47 stars with $\Delta K_s > 0.25$ mag and 66 stars with $\Delta(H-K_s) > 0.1$ mag.

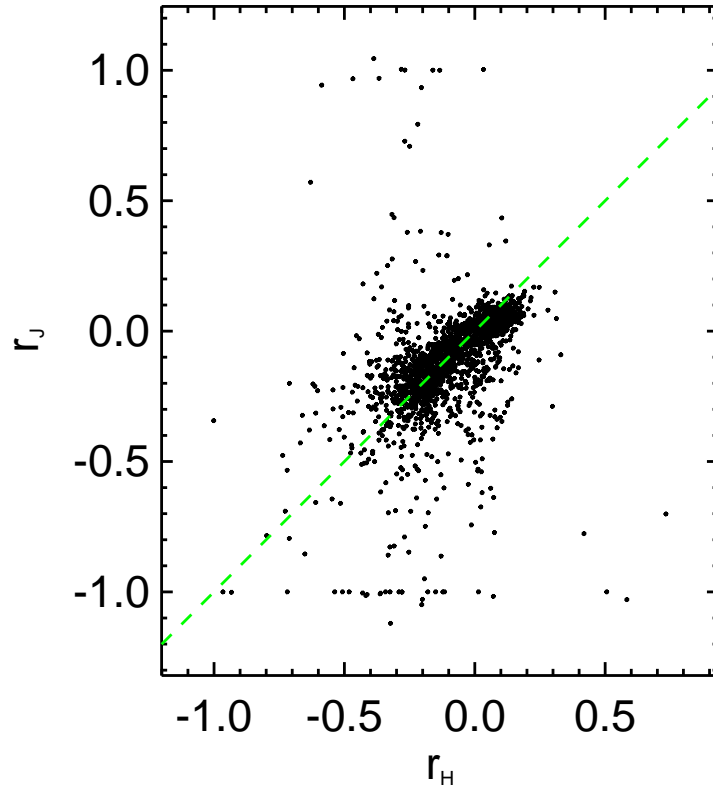


Fig. 2.— Seeing correlation between the J and H bands for the 1678 sample stars. The dashed green line is a 1:1 correlation between the seeing correlation in the J band, r_J , and H band, r_H . The line also corresponds to the projected z -axis as described in the text just prior to Eqn 3

Table 3. Catalog of Variable Stars in ρ Oph

RA (degrees)	Dec (degrees)	Varability Flags ^a	ΔK_s (mag)	$\Delta(J-H)$ (mag)	$\Delta(H-K_s)$ (mag)	Type	YSO Class ^b	'On Cloud'
246.732269	-25.137508	1101010	0.114	0.150	0.123	irregular	—	no
246.736557	-24.230934	1111111	0.476	0.235	0.173	periodic	—	yes
246.737396	-24.922001	1000010	0.167	0.153	0.180	irregular	—	no
246.7388	-24.594057	0010010	0.166	—	—	irregular	II	yes
246.739273	-24.88303	0001010	0.160	0.105	0.139	irregular	—	no
246.73941	-24.880718	1111110	0.854	—	—	irregular	—	no
246.741165	-24.964417	0001100	0.108	0.093	0.124	irregular	—	no
246.743301	-24.358301	1111111	0.292	0.140	0.257	periodic	II	yes
246.743774	-24.76016	1111111	0.500	0.415	0.270	LTV	II	yes
246.744202	-24.76741	0010100	0.131	0.198	0.168	irregular	—	yes
246.744324	-24.309591	1111111	0.294	0.241	0.180	irregular	II	yes
246.746017	-24.599096	1111111	0.218	0.185	0.380	LTV	II	yes
246.746155	-24.787884	1111110	1.109	—	—	irregular	—	yes
246.74649	-24.582909	0000010	0.631	—	—	irregular	I	yes
246.748657	-24.261997	1111100	0.078	0.124	0.073	irregular	—	yes
246.752335	-24.273695	1100000	0.061	0.082	0.066	irregular	—	yes
246.752975	-24.774199	1111101	0.061	0.091	0.084	LTV	—	yes
246.75676	-24.360228	1111111	0.078	0.074	0.180	LTV	III	yes
246.75972	-24.624172	1111100	0.082	0.083	0.176	irregular	—	yes
246.761093	-24.776232	1101001	0.049	0.061	0.122	LTV	—	yes
246.76149	-25.045506	1100000	0.053	0.062	0.083	irregular	—	no
246.761902	-24.31514	0001110	0.060	0.086	0.064	irregular	—	yes
246.764984	-24.33481	1110111	0.894	—	0.707	LTV	II	yes
246.76709	-24.474903	1110111	0.294	0.275	0.523	LTV	II	yes
246.768814	-24.716524	1111111	0.084	0.051	0.065	periodic	III	yes
246.768997	-24.70384	1111111	0.086	0.047	0.050	periodic	III	yes
246.769058	-24.454285	1111111	0.411	0.232	0.329	periodic	II	yes
246.770874	-25.146795	1100000	0.052	0.084	0.077	irregular	—	no
246.771545	-24.335421	1110000	0.049	0.079	0.078	irregular	—	yes
246.773605	-24.670246	0010010	0.337	—	—	periodic	II	yes
246.774628	-24.99383	1100000	0.044	0.078	0.055	irregular	—	no
246.774902	-24.476698	0000110	0.182	—	0.157	irregular	II	yes
246.777481	-24.696856	1111111	0.224	0.128	0.099	periodic	II	yes
246.778244	-24.637451	0110111	1.125	—	1.065	LTV	I	yes
246.784149	-24.707903	1001001	0.069	0.061	0.195	irregular	—	yes
246.787857	-24.200172	1111111	0.508	0.242	0.204	periodic	II	yes
246.787964	-24.56889	1111111	0.330	0.137	0.102	periodic	II	yes
246.788971	-24.672836	0110110	0.195	—	0.119	LTV	II	yes
246.78923	-24.621819	1111111	1.636	—	0.628	periodic	I	yes
246.791824	-24.486958	1111111	0.334	—	0.366	irregular	II	yes
246.792862	-24.320118	1110010	0.198	1.272	0.098	LTV	II	yes
246.7957	-24.758245	1000001	0.056	0.073	0.074	irregular	—	yes
246.79657	-24.679569	1110111	0.984	—	1.123	LTV	II	yes
246.798706	-24.394924	1111001	0.058	0.067	0.122	LTV	III	yes
246.798828	-24.642199	0110111	1.012	—	0.784	LTV	II	yes

Table 3—Continued

RA (degrees)	Dec (degrees)	Varability Flags ^a	ΔK_s (mag)	$\Delta(J-H)$ (mag)	$\Delta(H-K_s)$ (mag)	Type	YSO Class ^b	'On Cloud'
246.79892	-24.786337	1010001	0.069	0.079	0.074	irregular	—	yes
246.800537	-24.58028	1111111	0.729	0.346	0.402	periodic	II	yes
246.803055	-25.067175	1111111	0.339	0.157	0.112	periodic	—	no
246.807236	-24.304626	1111111	0.155	0.085	0.090	irregular	II	yes
246.807388	-25.095842	1110000	0.059	0.065	0.091	irregular	—	no
246.807602	-24.725399	1111111	0.560	0.249	0.133	LTV	II	yes
246.807755	-24.262215	0110000	0.205	—	0.291	irregular	—	yes
246.808533	-24.252649	1110000	0.109	0.200	0.149	irregular	—	yes
246.813034	-24.860764	1111111	0.330	0.213	0.111	periodic	—	no
246.813858	-24.264278	1010000	0.069	0.099	0.088	irregular	—	yes
246.814423	-24.444342	0110111	0.562	—	0.850	LTV	II	yes
246.814636	-24.514885	0010010	0.445	—	—	LTV	II	yes
246.815674	-24.645327	1111111	0.299	0.262	0.297	LTV	II	yes
246.816071	-24.645321	1111111	0.213	0.258	0.305	periodic/LTV	II	yes
246.816208	-24.420513	0110010	0.356	—	—	periodic	II	yes
246.816925	-24.250999	0110000	0.352	—	0.534	irregular	—	yes
246.816971	-24.271143	1010000	0.391	—	0.517	irregular	—	yes
246.821976	-24.374475	0110010	0.163	—	1.137	LTV	0	yes
246.822739	-24.218828	0100000	0.155	0.217	0.315	irregular	—	yes
246.823074	-24.4823	0110111	0.728	—	0.813	LTV	I	yes
246.826492	-24.914923	1111111	0.807	0.354	0.327	periodic	—	no
246.826584	-24.407238	0110111	0.135	—	0.371	periodic/LTV	III	yes
246.826599	-24.654037	1110111	0.528	—	0.009	periodic	I	yes
246.827026	-24.484921	1111111	0.640	0.161	0.186	periodic	II	yes
246.831299	-24.694487	0001111	0.092	0.057	0.071	periodic	III	yes
246.839462	-24.69525	1111111	0.215	0.276	0.158	irregular	II	yes
246.840378	-24.363819	0100000	0.050	0.184	0.069	irregular	III	yes
246.840836	-24.498091	0110111	1.199	—	1.256	LTV	I	yes
246.840942	-24.726538	0010000	0.062	—	0.056	periodic	III	yes
246.843735	-25.126837	1111111	0.700	—	0.751	irregular	—	no
246.84552	-24.299223	1111111	0.130	0.044	0.071	periodic	III	yes
246.845718	-24.801941	1111111	0.134	0.097	0.062	LTV	—	yes
246.846909	-24.809896	1001001	0.074	0.099	0.094	irregular	—	yes
246.848297	-24.207954	1111001	0.052	0.066	0.080	LTV	—	yes
246.852676	-24.684278	0010010	0.749	—	—	LTV	I	yes
246.852737	-24.493141	0010010	0.094	—	0.327	periodic	—	yes
246.854782	-24.775953	0100101	0.065	0.089	0.173	LTV	—	yes
246.85556	-25.105873	1111111	0.402	0.272	0.295	periodic	—	no
246.859329	-24.323023	0111111	0.326	0.432	0.175	irregular	II	yes
246.859558	-24.712914	0010010	0.098	—	0.200	periodic	I	yes
246.860397	-24.65638	1111111	0.318	0.185	0.207	periodic	II	yes
246.860779	-24.431711	1111111	0.211	0.099	0.096	periodic	II	yes
246.862335	-24.680904	0110110	0.393	—	0.927	LTV	I	yes
246.862778	-24.538191	0010010	0.090	—	0.478	periodic	—	yes
246.864105	-24.521235	1111111	0.305	0.121	0.082	periodic	II	yes

Fig 3 contains the co-added calibration field in the direction of ρ Oph; the target sample of 1678 stars and the variable catalog of 101 stars are plotted to show their spatial distribution. It is clear that target stars are not evenly distributed in the field. A demarcation line at $\delta = -24^\circ 51'$ is set as an ad hoc determination of cloud membership. North of this limit is considered “on cloud” while anything south is classified as “off cloud”. This demarcation corresponds roughly to where $A_V = 5$ mag (Cambr esy 1999). Comparing the variability north and south of this demarcation, the “on-cloud” variable fraction increases to 15% while the variable fraction for the “field” drops to a mere 1%. This is consistent with the expectation young stars are more often found spatially close to molecular clouds and are more variable than field stars.

3.2. Known Young Stars in the ρ Oph Field

Clues to the formation and evolution of young stars may be revealed by relating the variability to the stars’ evolutionary states. As originally proposed by Lada (1987), young stars are classified into four evolutionary stages or *classes* (Class 0, Class I, Class II and Class III). Class assignment is typically based on photometry through the infrared slope index in the wavelength range from 2 to 25 μm . Class 0 stars represent cloud cores undergoing the initial stages of protostellar collapse. Class I stars are heavily embedded protostars with in-falling material from a circumstellar envelope forming an accretion disk. Class II stars are fully assembled stars with accretion primarily from the circumstellar disk channeled onto the star along magnetic field lines; classical T Tauri (CTTS) stars are another name for Class II stars. The last stage, Class III, represents stars yet to reach the main-sequence with depleted or no accretion disks due to mass accretion onto the star, photo-evaporation, or planet formation. They may nevertheless retain debris disks or disks with depleted inner holes. These stars are also known as weak-lined T Tauri stars (WTTS).

To identify if any of the 1678 sample stars have a previously assigned evolutionary class, the sample is cross-referenced with the ρ Oph L1688 cloud core mid-IR surveys by Bontemps et al. (2001, hereafter B01) and Gutermuth et al. (2009, hereafter G09). The measurements obtained by B01 were taken with the *ISO* ISOCAM LW2 and LW3 broad band cameras centered on 6.7 μm and 14.7 μm , respectively. The G09 survey obtained measurements in the *Spitzer* IRAC 3.6, 4.5, 5.8 and 8.0 μm bands complemented by *J*, *H* and *K_s* 2MASS data for stars are used when there are no detections in either 5.8 or 8.0 μm . In addition, 24 μm *Spitzer* MIPS data is also used to verify YSO classifications in cases with high SNR ($\sigma < 0.2$ mag) and star luminosity ($[24] < 7$ mag).

The B01 survey provides YSO classifications for 54 of the 1678 target sample stars, while

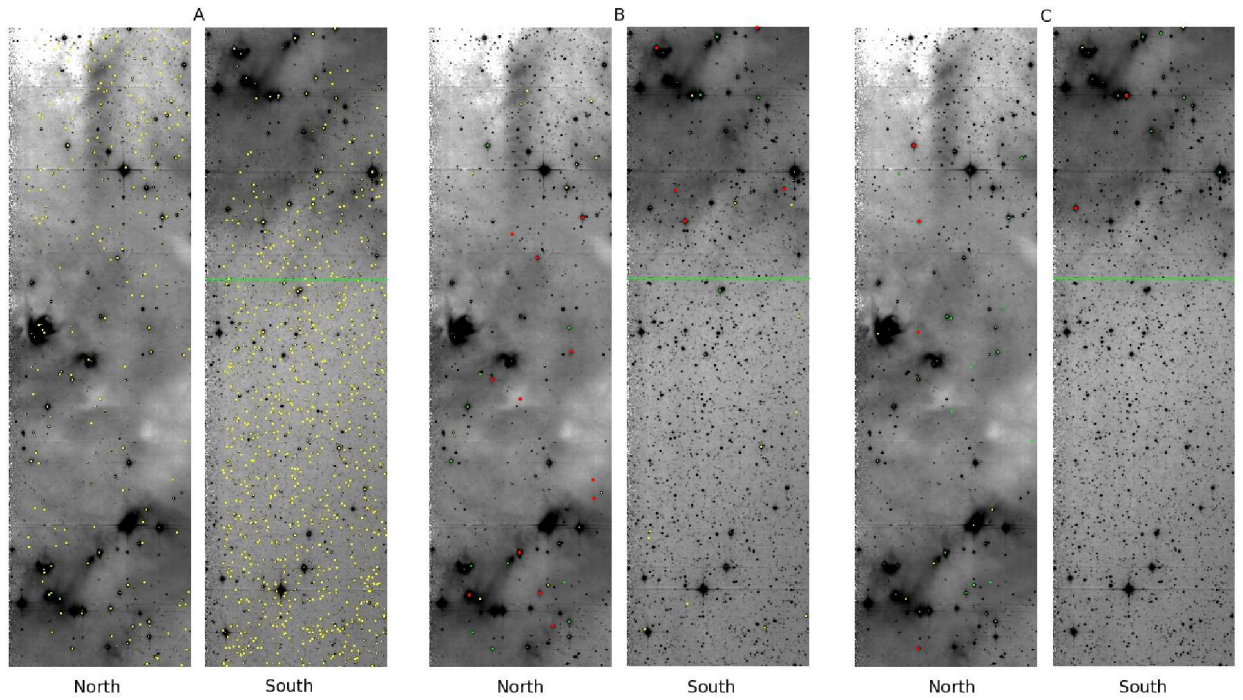


Fig. 3.— ρ Ophiuchus field. *A*: The field is split into “North” and “South” panels. The 1678 source sample is overlaid in yellow. *B*: The same field overlaid with all variable sources. Green - periodic variables (§5.1). Red - time-scale variables (§5.2). Yellow - irregular variables (§5.3). *C*: Same field overlaid with all classified YSO sources (§3.3). Yellow - Class I. Green - Class II. Red - Class III. The green line in all “South” panels represents a demarcation at δ : $-24^\circ 51'$ where $A_V = 5$ mag (Cambr esy 1999). North of this demarcation contains higher visual extinction.

G09 provides classifications for 58 stars. However, overlapping targets between these surveys results in 40 stars classified by both B01 and G09, yielding YSO classifications for only 72 target sample stars. For 5 stars classified by both B01 and G09, the two surveys disagree on the classification. G09 classifies these 5 stars as belonging in an earlier evolutionary stage by one class than B01 (i.e. WL 22 is classified as Class I by G09 and a Class II by B01). In these cases, the classification by G09 is adopted because of the broader wavelength coverage utilized. Assuming the B01 survey identified all the young stellar objects in the ρ Oph region (425 YSOs), this survey contains $\sim 17\%$ of these YSOs. Of the 72 stars with YSO classifications, 79% are identified as variable stars. As a function of YSO class, 92% of both Class I (12 of 13) and Class III (11 of 12) are variable stars. The variable fraction decreases to 72% (34 of 47) for Class II stars. The majority (14 stars) of the non-variable YSOs are Class II while ISO-Oph 99 is Class I. All of these stars are located “on cloud”. As a YSO evolves in time the median brightness and color variability amplitudes decrease. The median peak-to-trough ΔK_s amplitude for Class I, II, and III stars are 0.77, 0.31, and 0.08 mag, respectively. The median peak-to-trough $\Delta(H-K_s)$ color amplitudes are 0.81, 0.21, and 0.07 mag for each class respectively.

3.3. Advantages of High Cadence Variability Studies

In this section, the advantages of high cadence, long temporal baseline observations in variability studies are investigated. The results of this work are compared to the Alves de Oliveira & Casali (2008, hereafter AC08) survey of the ρ Oph central cloud core. The AC08 survey searched for variability in thousands of target stars within a ~ 0.8 deg² field of view. These stars were observed in the H and K_s bands during 14 epochs spanning May, June and July 2005 and 2006. The magnitudes of target stars fell within 11 to 19 mag in H and 10 to 18 mag in K_s .

This survey and AC08 have 464 stars in common. The prescription for identifying variables in AC08 is based on χ^2 fitting and cross-correlations between the H and K_s photometry. Comparing the number of variables detected from the 464 stars, AC08 identifies 32 (7%) variables while this work identifies 82 (18%). The larger fraction of detected variables by this survey could be attributed to the higher sampling over a longer temporal baseline or from different sensitivities in the adopted variability criteria. To determine which explanation is more probable, histograms of the ΔK_s peak-to-trough amplitudes for the variables identified by both this work and AC08 within the joint 464 star sample are computed. Fig 4 contains these histograms as well as the histograms for the $\Delta(H-K_s)$ peak-to-trough color amplitudes. It is clear from Fig 4 the fraction of variables with $\Delta K_s < 0.5$ mag detected by

each survey is nearly identical. The same is true for variables with $\Delta(H-K_s) < 0.55$ mag. Therefore, the higher fraction of variables detected, as compared to AC08, is most likely a consequence of the higher observing cadence. It is worth noting that 7 stars within the joint sample are identified as variable by AC08, but are not in this work. This work identified 5 of these stars as having photometry correlated with seeing. Therefore these stars may have been intrinsically variable within the observing window, however this variability could not be confidently confirmed.

While the detection fraction of low amplitude variables is nearly identical between surveys, the detection fraction of high amplitude variability stars is not. AC08 does not detect variables with $\Delta K_s > 0.7$ mag or $\Delta(H-K_s) > 0.55$ mag. This work finds 5.25% of detected variables have ΔK_s amplitudes greater than these upper limits. In addition, 6% of detected variables have $\Delta(H-K_s)$ color amplitudes greater than these upper limits. Within the 464 star joint sample, 25 stars are identified as variable in both this work and AC08. Strong correlations exist between the difference in amplitudes measured between surveys and the amplitudes measured in this work (see Fig 5). Sparsely sampled photometry will underestimate the amplitude of variability in both magnitude and color.

High cadence, long temporal baseline observations are vital for fully characterizing the variability of young stars. It increases the detection fraction of the survey allowing for more accurate statistics, such as the incidence of variable stars and distribution of variability amplitudes. In addition, this strategy is needed to sample the full amplitude of variability.

3.4. New Candidate ρ Oph Members

As photometric variability is an ubiquitous characteristic of young stars, it is a useful tool for assessing youth and potential membership in the ρ Oph star forming region. However, variability alone is not sufficient evidence for identifying potential members and additional constraints are needed, such as spatial location and location on a color-magnitude diagram. Candidate ρ Oph membership is first determined by cross-referencing the final variable catalog with previous surveys to identify previously known ρ Oph members (Strom et al. 1995; Barsony et al. 1997, 2005; Grosso et al. 2000; Ozawa et al. 2005; Wilking et al. 2005; Pillitteri et al. 2010). These are the same surveys used by AC08 to assign membership to their variable stars. This identifies 62 of the 101 variable stars as confirmed members of ρ Oph, which are plotted on a K_s versus $(H-K_s)$ color-magnitude diagram in Fig 6. For comparison, the 53 variable stars determined as ρ Oph members by AC08 are also plotted. Eleven stars are identified as ρ Oph in both surveys. A dashed line connects the data for these stars as observed by AC08 and this work. The solid black line indicates a 3 Myr

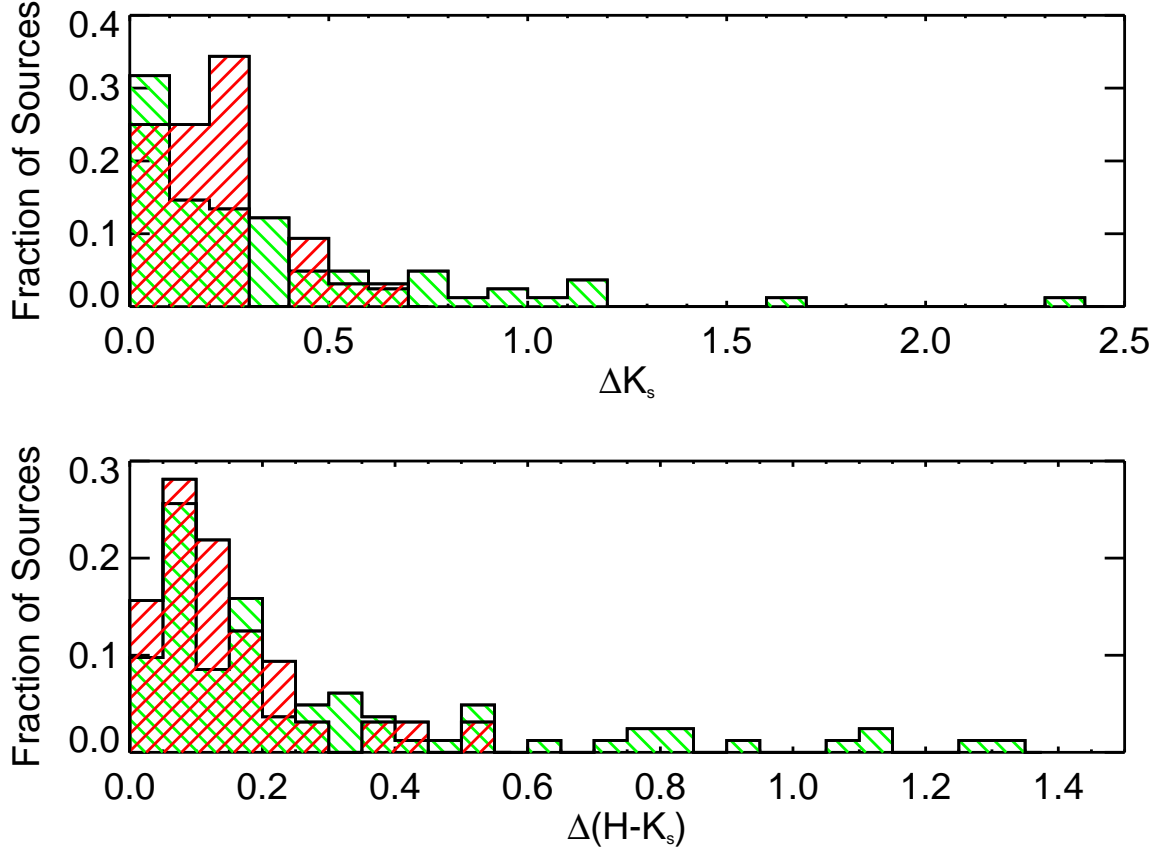


Fig. 4.— *Top*: Histograms of ΔK_s for AC08 (red forward hatching) and this work (green backward hatching). The two distributions are statistically indistinguishable. *Bottom*: Histograms of $\Delta(H-K_s)$ for AC08 and this work. Each survey is represented the same as the top plot. This work detects larger amplitudes in both ΔK_s and $\Delta(H-K_s)$ than AC08.

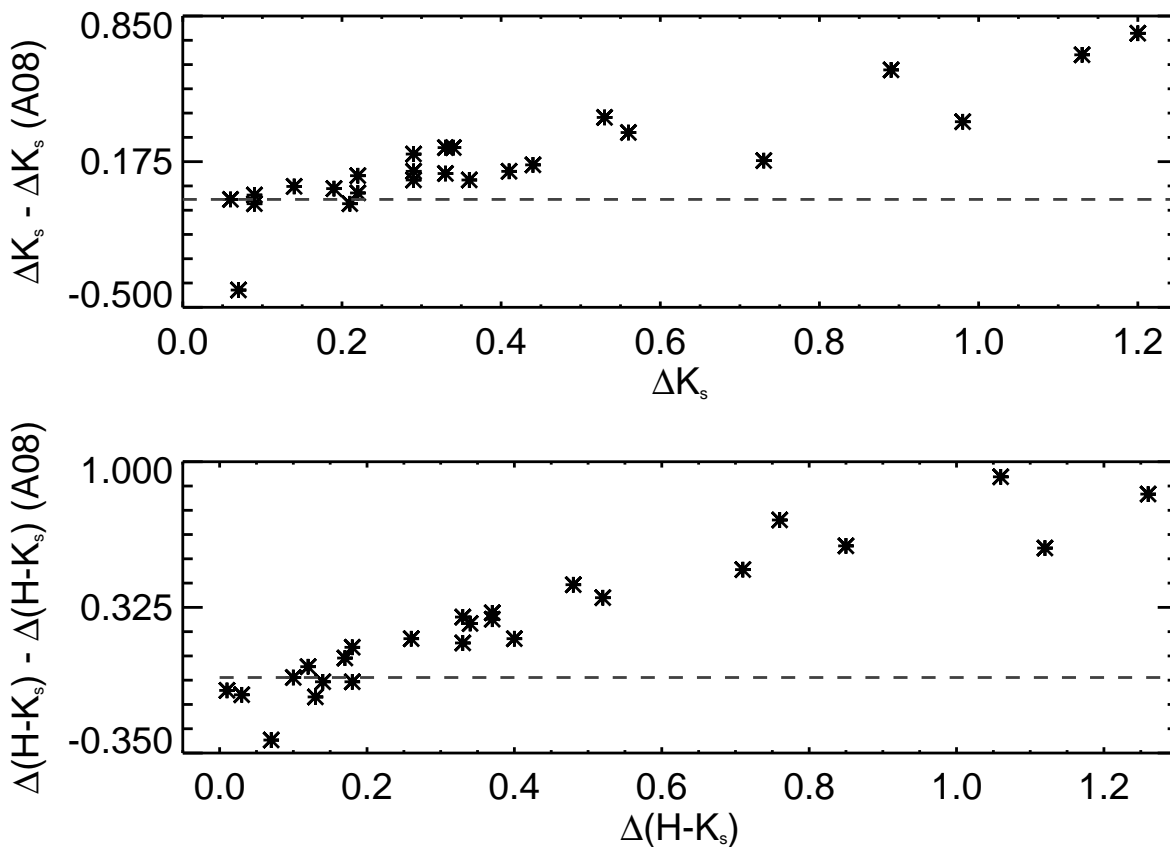


Fig. 5.— The difference between amplitudes measured by AC08 and this work. *Top:* The comparison between measured K_s variability. *Bottom:* The comparison between measured $(H-K_s)$ color variability. In both cases, there is good agreement between the surveys for low amplitude variability. However as the amplitude increases, AC08 underestimates the variability. The dashed line in both plots indicates a difference of zero.

isochrone constructed using NextGen models for masses between 0.02 to 1.4 M_{\odot} at a distance of 129 pc (Baraffe et al. 1998). The distance is the weighted average between previous measurements (Loinard et al. 2008; Mamajek 2008). A star is classified as a new candidate member if it is located “on cloud” (see §3.1.5) and is brighter and redder than the 3 Myr isochrone (see Fig 6). Table 4 contains the 22 stars identified as candidate ρ Oph members from the previously unassociated 39 stars. Candidate member 2MASS J16270597-2428363 is classified as a Class II YSO thereby increasing the likelihood of membership. Follow up spectroscopic observations in the mid-IR for the remaining candidates to determine whether these stars are YSOs will provide additional evidence for membership.

4. TIME-SERIES ANALYSIS

Characterizing the amplitude, time-scale, and form (e.g. periodic vs. aperiodic) of variability provides valuable insights into the underlying physical mechanism(s) causing the brightness variations. Period-searching algorithms have been very helpful in this regard (e.g. (Lomb 1976; Scargle 1982)). In this section, two separate methods for measuring the time-scales of variability are discussed.

4.1. Periodicity Analysis via the Plavchan Algorithm

A novel period-searching algorithm, henceforth called the Plavchan algorithm (PA), is implemented to detect periodicity in identified variable stars. The algorithm described below is a more mature version than the one used in Plavchan et al. (2008). The version of the algorithm is used in the NASA Exoplanet Archive periodogram tool (von Braun et al. 2009; Ramirez et al. 2009). Tens of thousands of test periods are investigated by the PA algorithm with a uniform frequency sampling between 0.1 and 1000 days. For each trial period, P_j , the PA starts by generating a phase-folded light curve from the time-series photometry. A phase is defined as the time (t_i) modulo the test period (P_j). This light curve is smoothed via boxcar smoothing with a phase width, $p = 0.06$. This smoothed light curve is designated as the prior, or reference curve. When the measured photometry for a periodic source is folded to the test period, the photometry is assumed to be approximately continuous and smoothly varying over the phased cycle. The difference between the measured photometry and the prior is computed for every photometric measurement, m_i . This difference is compared to the difference between the measured photometry and a “non-variable” straight line, defined by the photometric mean (see Fig 7). A poor fit results when these two differences are equal or nearly equal to each other. A good fit results when the difference between the data and

Table 3—Continued

RA (degrees)	Dec (degrees)	Variability Flags ^a	ΔK_s (mag)	$\Delta(J-H)$ (mag)	$\Delta(H-K_s)$ (mag)	Type	YSO Class ^b	'On Cloud'
246.866684	-24.65926	0110111	0.784	—	0.549	periodic	I	yes
246.872681	-24.654474	1111111	2.312	—	1.318	LTV	I	yes
246.875793	-24.462006	1111111	0.155	0.110	0.233	LTV	II	yes
246.877228	-24.542961	1100000	0.070	0.075	0.082	irregular	—	yes
246.87851	-24.790745	1110101	0.067	0.057	0.057	periodic	III	yes
246.878571	-24.415533	1111111	0.282	0.106	0.160	LTV	II	yes
246.878784	-24.459188	0010000	0.926	—	—	LTV	I	yes
246.879166	-25.065256	1111110	1.057	—	—	irregular	—	no
246.879456	-24.567505	1111001	0.058	0.054	0.071	periodic	III	yes
246.880157	-25.071445	1111110	0.566	0.386	0.473	irregular	—	no
246.883682	-25.148535	1110000	0.613	0.318	0.679	irregular	—	no

^aFirst three flags correspond to flickering variability. The second three flags correspond to excursive variability. The seventh flag corresponds to the Stetson index. Flag is set to 1 when true; 0 otherwise

^b(Bontemps et al. 2001; Gutermuth et al. 2009)

Table 4. Candidate ρ Ophiuchus Members

RA (degrees)	Dec (degrees)	Catalog ID ^a	J^b (mag)	H^b (mag)	K_s^b (mag)	$(J-H)$ (mag)	$(H-K_s)$ (mag)
246.744202	-24.76741	65861-2446029	15.392±0.001	14.000±0.001	13.364±0.001	1.392	0.636
246.746155	-24.787884	70054-2446444	16.935±0.032	16.255±0.011	15.567±0.012	0.680	0.688
246.748657	-24.261997	65967-2415433	14.229±0.001	12.404±0.001	11.642±0.001	1.825	0.762
246.752335	-24.273695	70055-2416255	13.432±0.001	11.840±0.001	10.997±0.001	1.592	0.842
246.752975	-24.774199	70072-2446272	13.670±0.001	12.002±0.001	11.233±0.001	1.668	0.769
246.761093	-24.776232	70266-2446345	13.348±0.001	11.596±0.001	10.665±0.001	1.752	0.930
246.761902	-24.31514	70285-2418546	13.090±0.001	11.049±0.001	10.096±0.001	2.041	0.953
246.771545	-24.335421	70516-2420077	12.700±0.001	10.440±0.001	9.341±0.001	2.260	1.099
246.774902	-24.476698	70597-2428363	16.905±0.005	14.467±0.001	13.029±0.001	2.438	1.439
246.784149	-24.707903	60819-2442286	15.365±0.001	12.252±0.001	10.723±0.001	3.113	1.529
246.795700	-24.758245	71096-2445298	13.011±0.001	11.056±0.001	10.156±0.001	1.955	0.900
246.807755	-24.262215	71384-2415441	16.760±0.005	15.065±0.002	14.251±0.002	1.696	0.814
246.808533	-24.252649	71404-2415096	15.356±0.002	13.899±0.001	13.274±0.001	1.457	0.625
246.813858	-24.264278	71531-2415515	13.990±0.001	12.532±0.001	11.865±0.001	1.458	0.667
246.816925	-24.250999	71605-2415039	16.829±0.005	15.461±0.003	14.768±0.003	1.368	0.693
246.816971	-24.271143	71604-2416163	17.056±0.007	15.708±0.004	15.007±0.004	1.348	0.701
246.821976	-24.374475	71726-2422283	17.341±0.124	15.567±0.003	13.418±0.001	1.774	2.149
246.822739	-24.218828	71744-2413079	15.993±0.002	14.378±0.002	13.707±0.001	1.614	0.671
246.845718	-24.801941	72297-2448071	10.922±0.001	9.832±0.001	9.336±0.001	1.089	0.496
246.846909	-24.809896	72325-2448357	14.124±0.001	12.613±0.001	11.982±0.001	1.511	0.631
246.848297	-24.207954	72357-2412288	12.805±0.001	10.796±0.001	9.851±0.001	2.009	0.945
246.854782	-24.775953	72514-2446335	15.527±0.001	12.957±0.001	11.683±0.001	2.569	1.275

^aThe catalog ID has been truncated by 2MASS J162 for 2MASS catalog stars

^bUnweighted mean apparent magnitude of Cal-PSWDB photometry

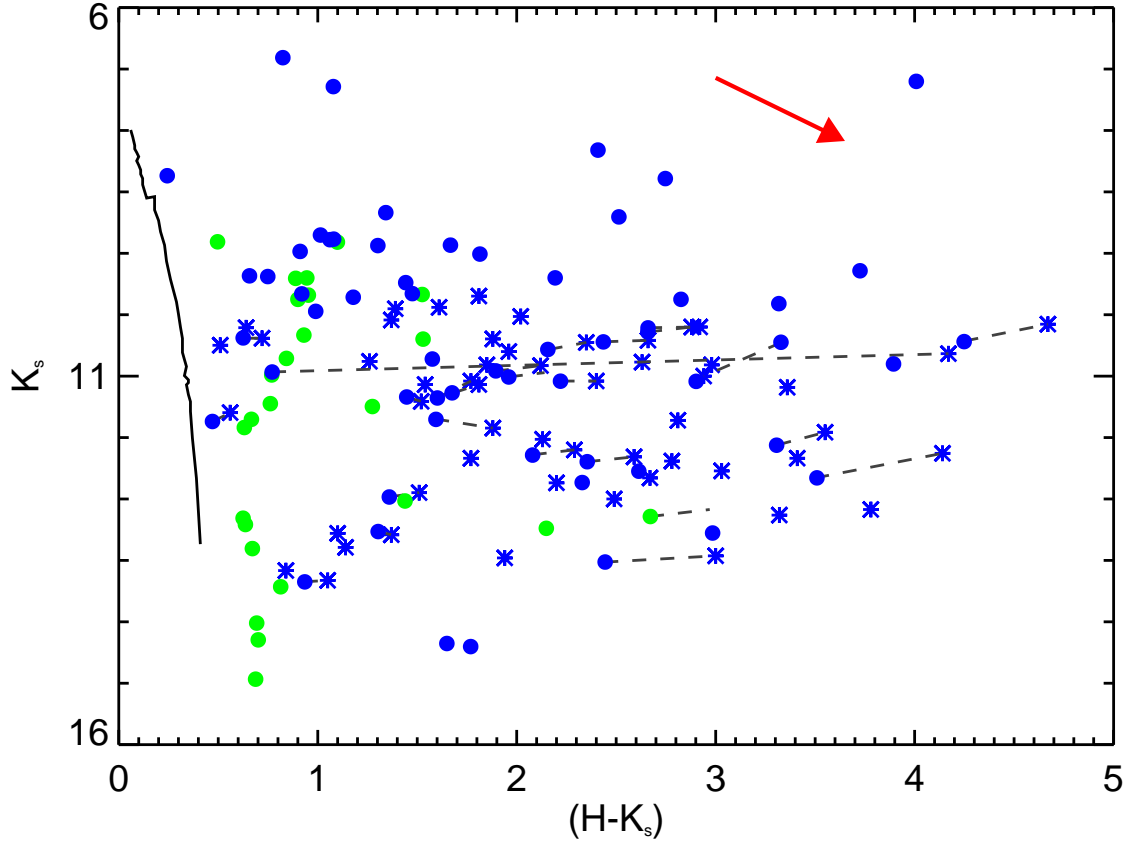


Fig. 6.— Candidate ρ Oph membership. The filled blue circles indicate variables previously identified as ρ Oph members. The green filled circles mark the 22 new candidate ρ Oph members. The blue asterisks indicate the AC08 measured K_s and $(H-K_s)$ for variables previously identified as ρ Oph members. The dashed lines connect the same variable as it is detected in this work. The solid black line is a 3 Myr isochrone constructed using NextGen models for masses between 0.02 and 1.4 M_{\odot} for a distance of 129 pc (Baraffe et al. 1998). The red arrow corresponds to a reddening vector $A_V = 10$ mag.

the smoothed prior is smallest. This normalization removes the dependence on the absolute value and dispersion in m_i . A quality of fit, $\chi_{n_0}^2$, is computed by Eqn 4 only over the 40 data points with the poorest fits ($n_0 = 40$) (i.e. the epochs with the largest difference between the data, m_i , and the prior (average) in the denominator (numerator)):

$$\chi_{n_0}^2 = \frac{\sum_{i=1}^{n_0} (m_i - \bar{m})^2}{\sum_{i=1}^{n_0} (m_i - m_{prior_i})^2} \quad (4)$$

where the prior term, m_{prior_i} , is the mean of m_i if m_i is within the boxcar smoothing window. The summations in the numerator and denominator in Eqn 4 are over independent sets of poorly fit measurements, since the poorest fit measurements by the prior might not be the same as the measurements that deviate the most from the mean. The best-fits periods have the largest $\chi_{n_0}^2$ value. In other words, $\chi_{n_0}^2$ represents the power of the periodic signal. The power indicates, for the PA, the relative improvements of the prior compared to a straight line for a given test period P_j .

To evaluate the statistical significance of the power value for a peak period in the periodogram, or in other words to compute a false-alarm probability (FAP), there are several possible quantitative methodologies to arrive at an appropriate probability distribution. The approaches include - one, an analytic derivation from first principles; two, a monte carlo of periodograms generated by randomly swapping measurement values at each epoch; three, the distributions of power values at other periods in the same (adequately sampled) periodogram; and four, the distribution of maximum power values for all sources in an ensemble (mostly non-variable) survey. The first approach is rarely used in the literature, with the noted exception of the Lomb-Scargle periodogram (Scargle 1982). In the case of the Lomb-Scargle periodogram and typical radial velocity surveys, however, systematic errors in the velocity measurements can invalidate the assumptions in the first approach. The second monte carlo approach is often used as a more reliable method for Lomb-Scargle periodograms (Marcy & Butler 1998), and is equally applicable to the PA periodogram. In this section, the third method to evaluate a period’s statistical significance is discussed. This third method is readily applicable to most time-series and is the method used in this work for computing the FAP for found periods. In the Appendix, the fourth method is discussed. The fourth method is survey dependent, but provides the insight that the PA periodogram is “well-behaved” with respect to changes in data values, number of observations, and algorithm parameters p and n_0 .

The distribution of power values in an adequately sampled PA periodogram for a non-variable source is best described by a log-normal distribution. In this instance, adequately sampled means covering a broad dynamic range of periods and sampling the periodogram

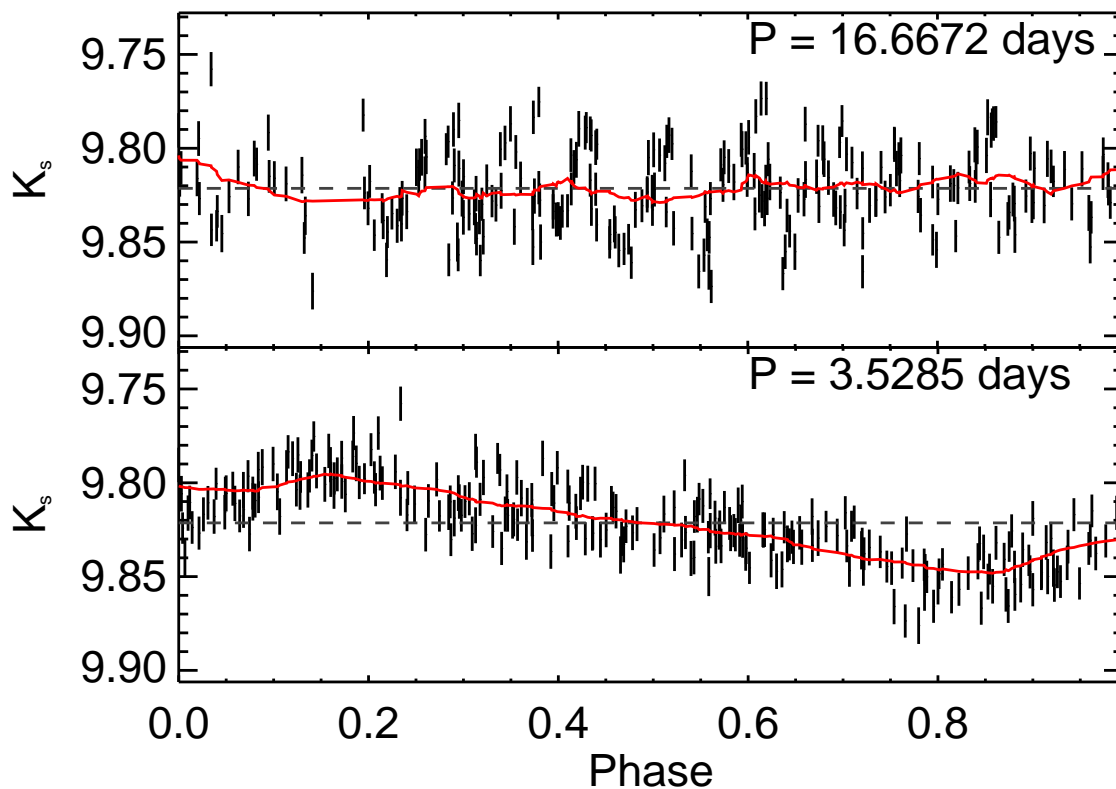


Fig. 7.— Demonstration of Plavchan Algorithm on ISO-Oph 96. *Top*: Light curve phased to a period of 16.6672 days. This period is considered insignificant. *BOTTOM*: phased to a period of 3.5285 days. This is the most significant period from the periodogram. The dotted line indicates the mean magnitude for this star. The red lines in the middle and bottom panels is the prior generated for each period. Computing the χ^2_{40} for the 3.5285 and 16.6672 day periods indicates the power value for the former is $\sim 9\times$ larger, implying a much larger statistical significance.

at a large number of periods representative of the expected frequency resolution dictated by the cadence. Fig 8 contains the periodogram for the non-periodic star 2MASS J16265576-2508150. The power values vary about a mean value, or a “significance floor”. The distribution is slightly asymmetric with a slight bias towards power values greater than the mean, consistent with a normal distribution in log-space. Fig 9 shows this distribution is very similar to the periodogram power value distribution for the boxcar least-squares (BLS) periodogram applied to the same source (Kovács et al. 2002), albeit with a different mean and standard deviation. The BLS periodogram traditionally makes the assumption of a normal distribution for evaluating the statistical significance of a peak period in the distribution of power values from an adequately sampled periodogram. However, again, a log-normal distribution is a more appropriate prescription for the BLS distribution (von Braun et al. 2009; Ramirez et al. 2009). While the assumption of a normal distribution of power values is probably adequate for both algorithms, a normal distribution will ascribe a greater statistical significance (i.e. a smaller FAP) to a peak period than a log-normal distribution. Therefore, the more conservative log-normal distribution is adopted in evaluating the statistical significance of peak periods in both the BLS and PA periodograms.

To determine if a period is statistically significant for a given source in this survey, the log of power values from the PA periodogram are computed, as well as the mean and standard deviation of the log-distribution. Power values that are 5σ outliers in the periodogram are identified as statistically significant periods with low FAP. Each of these significant periods are investigated via visual inspection of the photometry folded to the period in question. Finally the statistical significance of the derived period is confirmed by either the Lomb-Scargle or BLS algorithms, depending on the folded light curve shape. The Lomb-Scargle algorithm is optimized to identify sinusoidal-like periodic variations, while the BLS algorithm is better equipped in identifying eclipse-like periodic variations. Thus, the PA periodogram excels at identifying periodic signatures from both sinusoidal-like and eclipse-like time-series periodic variations (Plavchan et al. 2008). The period error is derived from the 1σ width of a Gaussian fit to the period’s peak in the periodogram. In order to avoid confusion in the fit from other peaks, only periods within $\pm 3\%$ of the most significant peak are fit. An upper bound to confident periods is placed at 200 days. Stars are rejected as truly periodic with larger periods since the star will complete at most 3 cycles within the observing baseline. These “periods” are reported as timescales and described in §5.2.1.

From the 101 variables, 32 stars (32%) are identified to exhibit periodic variability with periods ranging from 0.49 to 92 days. Table 5 contains the list of periodic variables.

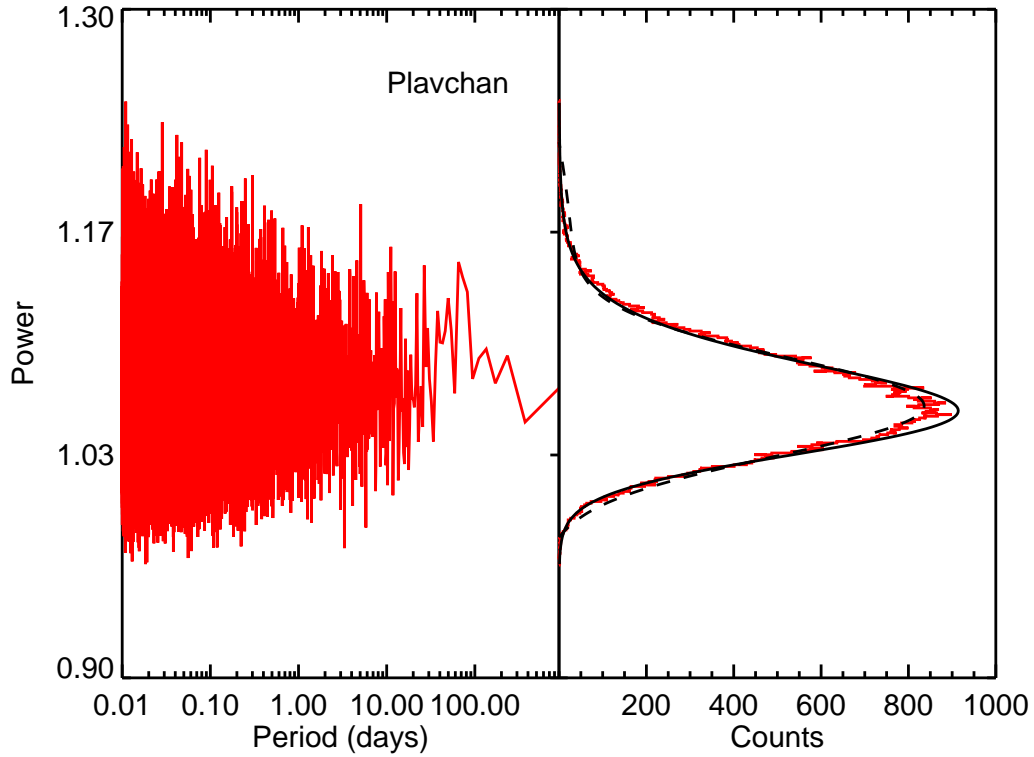


Fig. 8.— *Left*: Periodogram for the irregular variable 2MASS J16265576-2508150 using the PA. *Right*: The histogram of periodogram power values used to determine the significance of calculated periods. The solid line indicates a log-normal distribution fit to the histogram values and the dashed line indicates a normal distribution fit. The log-normal fit is used as it results in a more conservative higher false alarm probability.

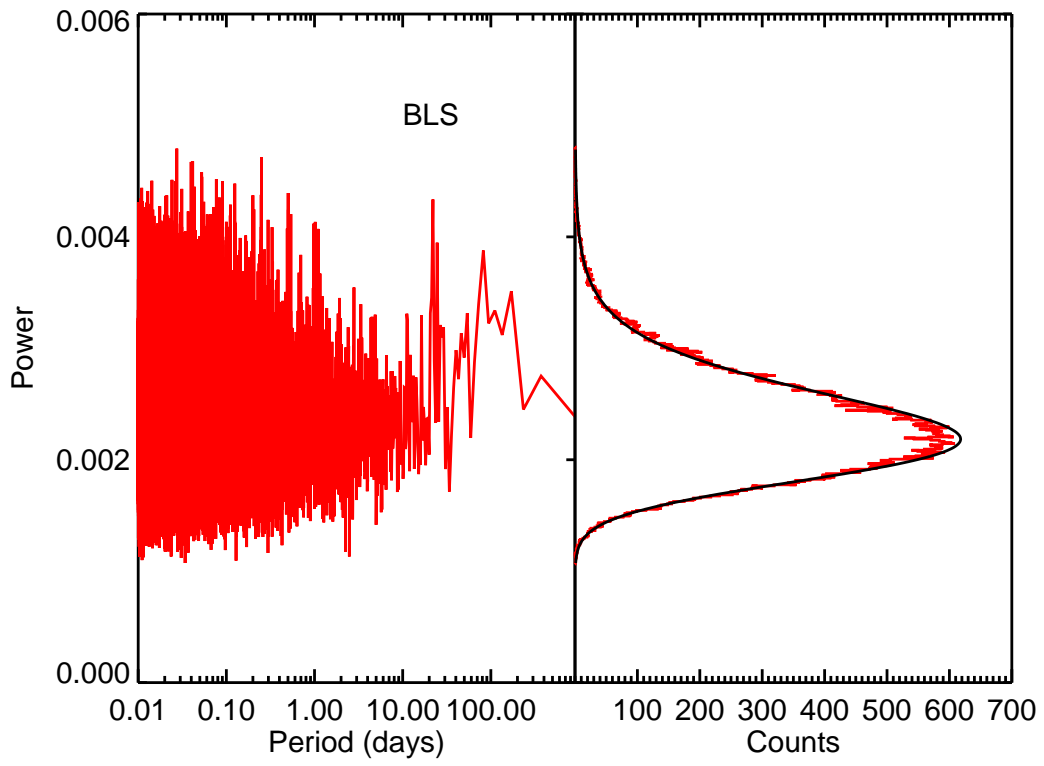


Fig. 9.— Same as Figure 8 however using the BLS algorithm

4.1.1. *Detecting Secondary or Masked Periodic Variability*

The PA found two statistically distinct ($>20\sigma$) periods for YLW 1C. The time-series folded to the shorter period (5.7792 days) exhibits a sinusoidal-like shape. The time-series folded to the longer period (5.9514 day) exhibits an “eclipse-like” shape where the star periodically dims from a near constant continuum flux. This prompted a search for secondary periods in the other 5 stars that exhibit eclipse-like periodic variability. We found 3 stars (YLW 1C, 2MASS J16272658-2425543, YLW 10C) to vary periodically at two distinctly different periods; sinusoidal-like variability at one period and eclipse-like variability at the other. Initially the secondary period is not statistically significant; it is only discovered when the time-series of the eclipse event is removed. The PA is run only on the time-series preceding each eclipse ingress and after each eclipse egress. A small number (~ 10) of sharp drops outside the eclipse events in the time-series for 2MASS J16272658-2425543 and YLW 10C are also omitted from the PA analysis. Errors in the secondary periods are determined in the same manner as the primary periods.

Since multiple variability mechanisms may be common in variable stars (Herbst et al. 1994; Morales-Calderón et al. 2011), we attempted to search for periodic variability in stars where the variability was complex. For 6 variable stars, the stellar brightness fluxuates about a mean level for one or two consecutive years. During the remaining time, a large amplitude variation is observed lasting longer than 50 days. The PA is run on the nearly constant time-series omitting the large amplitude variation event. In 2 stars (WL 20W and ISO-Oph 126), the PA found a significant period in the “whitened” time-series. The time-series folded to the appropriate period results in sinusoidal-like variability with an amplitude $\sim 50\%$ smaller than the large amplitude variation. This larger amplitude variation effectively masked the smaller amplitude periodic signal. For each star, the periodic variability could not be recovered during the large amplitude variation. Fig 10 contains the K_s light curves for WL 20W and ISO-Oph 126, as well as the K_s light curves folded to the identified periods. For WL 20W, 93 out of 262 scan groups were removed before the PA analysis. For ISO-Oph 126, 149 out of 262 scan groups were removed. Fig 11 shows the periodograms for both stars using the full time-series and the whitened time-series.

4.2. **Measuring Long Time-Scale Variability**

The long temporal baseline of the photometric time-series allows for the analysis of variability on month and year time-scales which are time-scales not well explored for young stars. Long time-scale (>50 days) variability differs from periodic or irregular variability in that the mean flux value may not remain nearly constant from season to season. In addition,

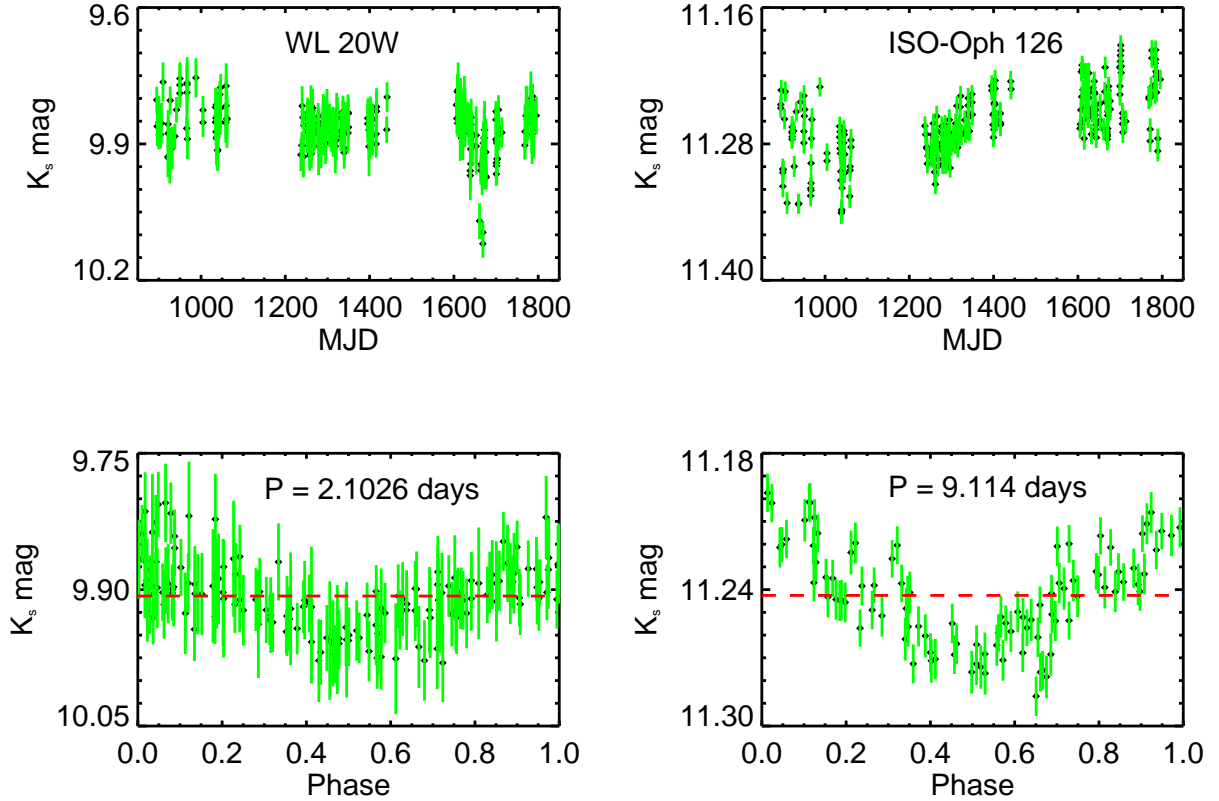


Fig. 10.— *TOP*: The K_s light curves for WL 20W and ISO-Oph 126. Both light curves display a large amplitude long time-scale variation. *BOTTOM*: The folded K_s light curves for WL 20W ($P = 2.1026 \pm 0.0060$ days) and ISO-Oph 126 ($P = 9.114 \pm 0.90$ days). The periods are only detected once the photometry affected by the large amplitude variation is removed. This data is not included in the folded light curves.

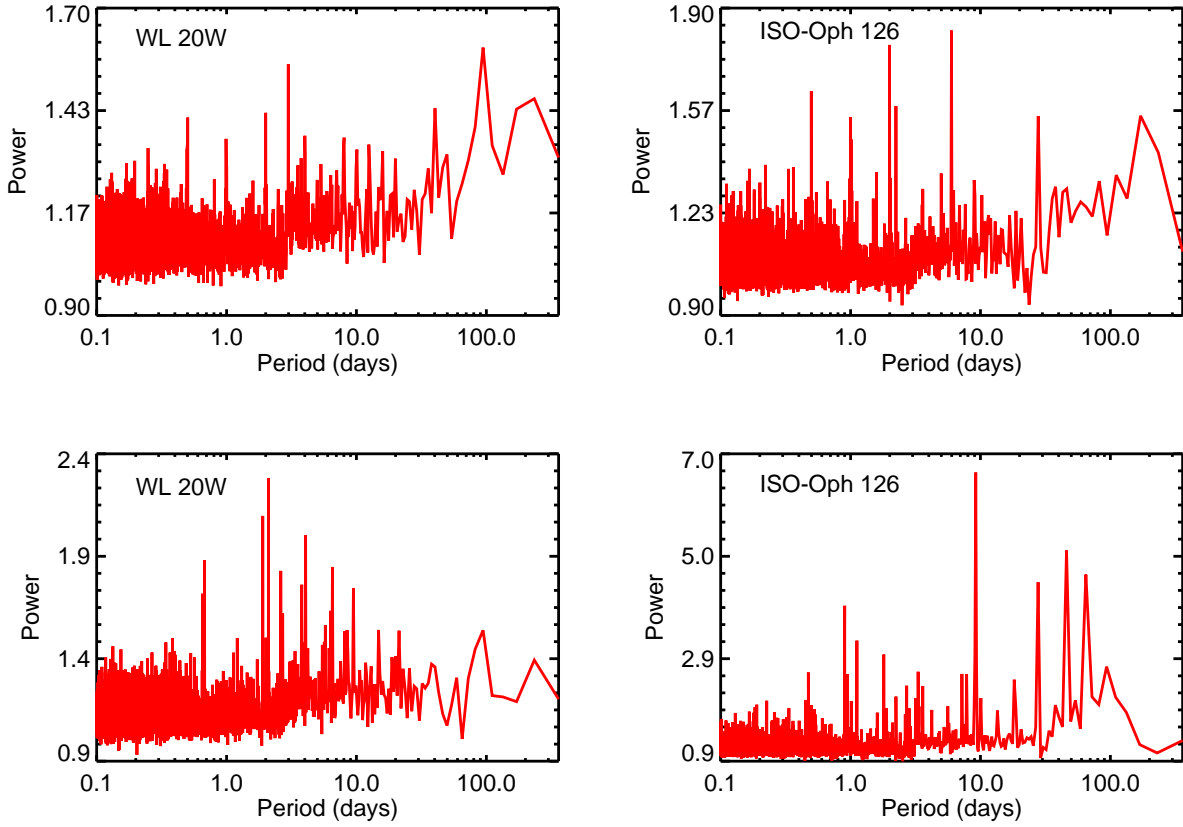


Fig. 11.— Periodograms for WL 20W and ISO-Oph 126 including and excluding the long time-scale event photometry. *TOP*: The periodograms from running the PA on the full data set including the large amplitude long time-scale variation. *BOTTOM*: The periodograms from the PA only on the photometry not affected by the large amplitude variation. The 2.1026 day period is only seen and significant in the lower periodogram for WL 20. The same is true for the 9.114 day period of ISO-Oph 126. Additionally, this period peak power value is nearly 3x more significant than any power value detected using the complete set of photometry.

the photometry in one season may systematically brighten or dim while remaining constant in the other two seasons. Examples of these two phenomenon in the time-series for WL 20W and ISO-Oph 126 are shown in Fig 10. The intention in this section is to measure the time-scale of the single largest amplitude aperiodic or irregular variation.

Two criteria are used to identify stars exhibiting long time-scale variability. The first criteria is the difference between the photometric mean magnitude from one season to either of the remaining two seasons must be greater than 3σ , where σ is the average photometric error of the data over the entire temporal baseline (see Fig 23, WL 6). The second criteria is that the slope in the photometry in at least one season must be greater than $\pm 5^\circ$. The quality of the line fit determining the slope is assessed by visual inspection. The motivation for the second criterion is illustrated by WL 14 (see Fig 21). An obvious decreasing trend in the photometry is seen in the third season, however the sharp flux drop in the second season causes the mean flux between the two seasons to not satisfy the first criterion. Of the 101 variables, 31 stars (31%) satisfy at least one of these criteria and are designated long time-scale variables (LTVs).

A differencing technique is employed to measure the time-scale over which a LTV changes from one extreme in flux to the other. Fig 12 provides a visual demonstration of this method. In the top panel of Fig 12, a gradual dimming over the entire data set is observed. This global trend is seen in the time-series of 68% of the LTVs. Two different types of variability are believed responsible for the global trend and the long time-scale variation. Removal of the global trends provides an unbiased analysis of the shorter time-scale variation in the time-series superimposed on these trends. The global trend is a sustained, but small amplitude effect superimposed over the time-series including the larger amplitude, long time-scale variation. LTVs with these global trends are split evenly with 50% dimming over time and 50% brightening. The amplitude of the global trends range from 7.5 to 330 millimag/year, with a median value of 26 millimag/year. The median value corresponds to a change in the stellar flux of ~ 60 millimag over the temporal baseline.

An accurate time-scale measurement for the largest amplitude variation can be complicated by the presence of small time-scale variability. The middle panel of Fig 12 shows how the light curve is smoothed with a 50 day moving median filter. The length of 50 days is chosen by visual inspection of the smoothed light curves; this timescale suppresses the smaller amplitude, shorter time-scale variability while preserving the shape of the long time-scale variation. The time-scale for the long time-scale variation is set to be the time difference between when the LTV is at one extreme in flux (i.e. brightest state) to the opposite extreme (i.e. dimmest state). This time-scale is determined by subtracting the smoothed magnitude found at time i with the smoothed magnitude found at time j using the following:

$$M_{i,j} = \sum_{i=1}^{N_{obs}} \sum_{j=1}^{N_{obs}} (m_j^* - m_i^*) \quad (5)$$

where $M_{i,j}$ is the Δmag between time j and time i , m_j^* is the magnitude at time j , m_i^* is the magnitude at time i and N_{obs} is the total number of observations. The time between the largest Δmag is recorded as the time-scale. In many cases, the full time-scale of the variation cannot be measured due to the data sampling. The bottom panel of Fig 13 shows the quantity $M_{i,j}$ as a function of times between measurements i and j . The “landscape” shows multiple peaks each corresponding to various time-scales of variability. The highest peak is only considered as only the time-scale associated with the greatest change in magnitude (i.e. largest $M_{i,j}$) is sought. Either extreme flux state may fall within a gap in the photometry or outside the date range of observations. Therefore these time-scales should be treated as lower bounds. The variability time-scales range from 64 to 790 days. Not all LTVs display only one discrete long time-scale variation. ISO-Oph 119 clearly shows two distinct long time-scale variations. For ISO-Oph 119 and similar cases, only the time-scale for the largest amplitude variation is measured. Figs 27 to 30 contain the K_s light curves for these LTVs.

Despite observations spanning ~ 2.5 years, in most cases it is not possible to conclude whether or not long time-scale variability is periodic. However, 6 LTVs have photometry suggestive of periodic behavior based on visual inspection of the stars’ folded light curves corresponding to periods ranging from 207 to 589 days. The light curves are folded to the most significant period found by the PA. These candidate periodic stars are identified in the first column of Table 6. These sources are not included with the periodic variables as the found periods are greater than the 200 day confidence limit (see §4.1).

5. DISCUSSION

The observational goal of this study is to measure the amplitudes and timescales of stellar variability, particularly in young stars. This information, in turn, places constraints on the physical mechanisms responsible for the variability. Empirical methods based on correlations between observed magnitudes and color have been employed to characterize stellar variability of young stars (Carpenter et al. 2001, 2002; Alves de Oliveira & Casali 2008). These methods consider variability due to rotational modulation of hot or cool starspots, variable extinction, variable mass accretion and structure changes in the circumstellar environment. Cool starspots are believed to be caused by localized magnetic inhibition of convection energy transport. Hot starspots, on the other hand, result from either surface flaring or heating by mass accretion onto the surface along magnetic field lines. Extinction

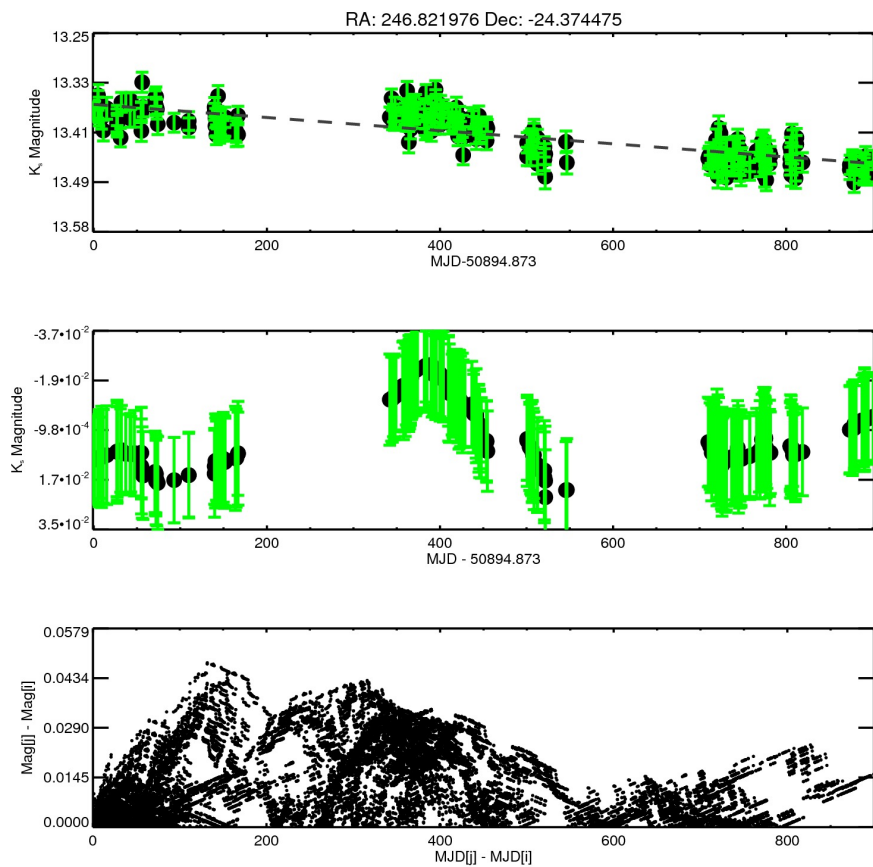


Fig. 12.— A demonstration of the method used to estimate the variability time-scale of LTVs. *Top:* The K_s light curves for 2MASS J16271726-2422283. The gray dashed line is a linear least-squares fit to the data. *Middle:* The same light curve after the data are smoothed and the linear fit is removed. The smoothing is done using a moving median filter with a 50 day width. *Bottom:* This shows the Δmag as a function of the time between individual photometric measurements, m_j^* and m_i^* . The recorded 132 day time-scale corresponds to highest peak, or largest Δmag occurring in the middle plot. This time-scale describes the star flux decrease from ~ 400 to ~ 525 2MASS MJD.

may occur from asymmetries in an accretion disk or even from isolated dense regions of the parent molecular cloud passing through the line of sight. Variable mass accretion rates can cause the star brightness to vary through the clearing of the inner circumstellar disk. In addition, variability may be caused by energy released as material in an accretion disk moves toward a star by viscous processes. Finally, these mechanisms are not mutually exclusive and are often seen to exist simultaneously (Herbst et al. 1994).

Each of the above variability mechanisms can be distinguished based on the temporal nature of the variability and correlations between color variability to stellar brightness.¹ The following set of qualitative observables are developed to classify the observed variability and to connect these variations to physical mechanisms.

- Long-lived cool starspots result in periodic variability with periods consistent with the rotational periods of young stars ($\lesssim 14$ days) (Rebull 2001). This variability is often sinusoidal in shape. At the temperature range of most YSOs, the near-IR wavelength regime samples the Rayleigh-Jeans tail of the stellar energy distribution where the contrast between the starspot and surrounding photosphere is small (e.g. Vrba et al. (1985)). Therefore, the $(J-H)$ and $(H-K_s)$ colors should remain constant (within photometric errors) as the brightness varies.
- Variability by hot starspots can either result in periodic or irregular variability. Long-lived hot starspots caused by accretion onto the stellar surface may result in periodic variability. However it should be noted that accretion induced hot spots may display aperiodic behavior due to a stochastic accretion rate. Variability caused by flares will be aperiodic and will have time-scales on the order of hours to days. As with cool starspots, the period of variability will be consistent with the rotational periods of young stars. In both cases the affected photosphere should be hotter than the surrounding surface resulting in the star becoming bluer as the star brightens (Rodonò & Cutispoto 1988; Panagi & Andrews 1995; Yu & Gan 2006).
- Variable extinction can result in either periodic or long time-scale variability. Variability caused by asymmetries in the inner circumstellar disk, if present, may be periodic with periods from days to weeks. Unlike variability caused by starspots, periodic variable extinction need not appear sinusoidal but present more likely as eclipse-like features. These eclipse-like features are sharp drops or “dips” in the stellar flux with a regularity dependent on the observing cadence. Variability caused by asymmetries in

¹The correlations between stellar color and brightness are based on models in Carpenter et al. (2001, and references herein).

the outer circumstellar disk (> 1 AU) will not be periodic within the temporal baseline of this study due to long period of revolution around the host star. This variability and variable extinction from inter-cloud material can occur on long time-scales, however as the time-scale depends on the system geometry, there is no expectation as to its duration. Variable extinction causes the star to redden as the star dims.

- Variability caused by a variable accretion rate within the circumstellar disk is not expected to be periodic. The time-scale of variability does place constraints on the physics causing this rate change (e.g. disk viscosity, time variable magnetic field) (Armitage 1995; Mahdavi & Kenyon 1998; Lai 1999; Terquem & Papaloizou 2000; Carpenter et al. 2001). During times of lower accretion rates, the inner disk cools and the inner hole becomes larger. This, in turn, decreases the contribution of dust reradiation, particularly in the K_s band, to the overall energy budget of the star and circumstellar disk system. Therefore while the total system flux drops, a larger percentage of emitted radiation is from the star causing the system to become bluer as the system dims. However, if the inner circumstellar disk edge is dominated by the dust sublimation temperature, a observationally similar effect will result. In this case, an increased accretion rate raises the star’s effective temperature in turn increasing both the distance to the circumstellar disk inner rim and disk vertical height. The result would be that the system would become brighter as it reddens. Both physical scenarios produce a qualitatively identical result to the observed correlation between brightness and color.

In an attempt to identify the dominant variability mechanism, stars in the variable catalog are placed into subclasses based on the observed shape and time-scale of variability. These subclasses are: periodic, long time-scale and irregular. These classifications along with the above criterion identified the likely dominant variability mechanism for 53 of the 101 stars in the variable catalog. The type of variability associated with each star is listed in Table 3 and each sub-class is described in the following subsections. The periodic sub-class accounts for 32% of the variable catalog with the majority (88%) lying “on cloud”. Long time-scale variables make up 31% of the variable catalog. All LTVs reside “on cloud”. The irregular subclass contains the most members comprising 40% of the variable catalog. Only 68% of irregular variables lie “on cloud”. These subclasses are rough descriptions and are by no means mutually exclusive. For instance, WL 20W and ISO-Oph 126 are placed into both the periodic and long time-scale subclasses.

These criteria do not always allow for the dominant variability mechanism to be identified. The main reasons preventing an estimate of the mechanism are: the time-scale/period or color correlation is contrary to the above diagnostics, no dominant amplitude variability is clearly evident, or the photometry in J and H is below the completeness limits in each

band resulting in no useful color information. Mechanisms appended with a question mark in Table 3 either possess a marginal color correlation via visual inspection, or the diagnostics did not definitively differentiate between proposed mechanisms.

5.1. Periodic Variables

The PA identifies 32 of 101 stars (32%) within the variable catalog as periodic with periods ranging from 0.49 to 92.28 days. Table 4 contains the list of periodic variables. The light curves for certain subsets of periodic variables are very similar in form when phased to the identified period. This allows for periodic variables to be separated into two sub-categories: sinusoidal-like and eclipse-like. Assignment to a particular sub-category is based upon visual inspection of the folded light curve in the band with the highest signal-to-noise.

5.1.1. Sinusoidal-like Periodic Variables

Figs 13 to 16 contain the K_s light curves for sinusoidal-like periodic variables. This sub-category of sinusoidal-like periodic variables includes the most periodic variables (25 stars) with periods ranging from 0.49 to 25.55 days. The peak-to-trough ΔK_s amplitudes range from 0.06 to 1.64 mag, with a median value of 0.29 mag. The peak-to-trough $\Delta(H-K_s)$ color amplitudes range from 0.01 to 0.63 mag, with a median value of 0.19 mag. Typically, the light curve folded to the most significant period shows only one sinusoidal cycle. However, four stars (ISO-Oph 100, WL 10, WL 13, YLW 13A) show what could be interpreted as a second cycle at half the frequency (i.e. double the period).

Probable variability mechanisms are identified for these stars by applying the criteria discussed in §5. Correlations are qualitatively examined between the ensemble K_s photometry and stellar colors when folded to the star’s period. Fig 17 illustrates examples of these interpretations for both cool and hot starspots. For 18 of the sinusoidal-like periodic variables (72%), the variability in the $(J-H)$ and $(H-K_s)$ colors does not correlate with the K_s variability. This favors rotational modulation by cool starspots as the dominant variability mechanism. For 3 sinusoidal-like periodic variables (12%), the $(J-H)$ and $(H-K_s)$ colors become bluer as the star brightens. This is consistent with the behavior expected from rotational modulation by an accretion induced hot starspot. The $(J-H)$ and $(H-K_s)$ colors become redder as the star dims for 1 (4%) sinusoidal-like periodic variable. This favors variable extinction as the dominant variability mechanism. Finally for the remaining 3 sinusoidal-like periodic variables (12%), no dominant variability mechanism could be

Table 5. Periodic Variables

Catalog ID ^a	Period ^b (days)	ΔK_s (mag)	$\Delta(J-H)$ (mag)	$\Delta(H-K_s)$ (mag)	YSO Class	Sub-Category	Var. Mech. ^c
ISO-Oph 83	25.554±0.071	0.476	0.235	0.173	—	Sinusoidal	Extinction
YLW 1C	5.7753±0.0085	0.292	0.140	0.257	II	Sinusoidal	Hot Starspot(s)
	5.9514±0.0014	0.29	—	—		Eclipse	Extinction
ISO-Oph 96	3.5285±0.0032	0.084	0.051	0.065	III	Sinusoidal	Cool Starspot(s)
ISO-Oph 97	14.520±0.088	0.086	0.047	0.050	III	Sinusoidal	Cool Starspot(s)
ISO-Oph 98	5.9301±0.0092	0.411	0.232	0.329	II	Sinusoidal	Cool Starspot(s)
ISO-Oph 100	3.682±0.002	0.337	—	—	II	Sinusoidal	Unknown
ISO-Oph 102	3.02173±0.00044	0.224	0.128	0.099	II	Eclipse	Cool Starspot(s)?
ISO-Oph 106	3.4370±0.0012	0.508	0.242	0.204	II	Eclipse	Extinction
WL 10	2.4149±0.0027	0.330	0.137	0.102	II	Sinusoidal	Cool Starspot(s)?
WL 15	19.412±0.085	1.636	—	0.628	I	Sinusoidal	Unknown
WL 11	3.0437±0.0038	0.729	0.346	0.402	II	Sinusoidal	Hot Starspot(s)?
65744-2504017	0.83141±0.00030	0.339	0.157	0.112	—	Sinusoidal	Hot Starspot(s)?
71513-2451388	8.004±0.046	0.330	0.213	0.111	—	Eclipse	Extinction
WL 20W	2.1026±0.0060	0.213	0.258	0.305	II	Sinusoidal	Cool Starspot(s)
YLW 10C	2.9468±0.0029	0.356	—	—	II	Eclipse	Extinction?
	3.0779±0.0025	0.28	—	—		Sinusoidal	Cool Starspot(s)?
71836-2454537	2.7917±0.0017	0.807	0.354	0.327	—	Sinusoidal	Hot Starspot(s)?
ISO-Oph 126	9.114±0.090	0.135	—	0.371	III	Sinusoidal	Cool Starspot(s)
ISO-Oph 127	6.365±0.014	0.528	—	0.009	I	Sinusoidal	Cool Starspot(s)
WL 4	65.61±0.40	0.640	0.161	0.186	II	Inverse Eclipse	Circumbinary Disk
YLW 13A	7.0270±0.0056	0.092	0.057	0.071	III	Sinusoidal	Cool Starspot(s)
ISO-Oph 133	6.354±0.011	0.062	—	0.056	III	Sinusoidal	Cool Starspot(s)
ISO-Oph 135	5.536±0.019	0.130	0.044	0.071	III	Sinusoidal	Cool Starspot(s)
72463-2429353	6.581±0.012	0.094	—	0.327	0	Sinusoidal	Cool Starspot(s)
72533-2506211	0.485143±0.000050	0.402	0.272	0.295	—	Sinusoidal	Unknown
ISO-Oph 139	3.7202±0.0041	0.098	—	0.200	I	Sinusoidal	Cool Starspot(s)
YLW 16C	1.14182±0.00043	0.318	0.185	0.207	II	Sinusoidal	Cool Starspot(s)
72658-2425543	2.9602±0.0013	0.211	0.099	0.096	II	Eclipse	Extinction
	1.52921±0.00065	0.17	—	—		Sinusoidal	Cool Starspot(s)
72706-2432175	18.779±0.099	0.090	—	0.478	—	Sinusoidal	Cool Starspot(s)
WL 13	23.476±0.077	0.305	0.121	0.082	II	Sinusoidal	Cool Starspot(s)
YLW 16A	92.28±0.84	0.784	—	0.549	I	Inverse Eclipse	Circumbinary Disk
ISO-Oph 149	1.24505±0.00039	0.067	0.057	0.057	III	Sinusoidal	Cool Starspot(s)
ISO-Oph 148	3.5548±0.0039	0.058	0.054	0.071	III	Sinusoidal	Cool Starspot(s)

^aThe catalog ID has been truncated by 2MASS J162 for 2MASS catalog stars

^bThe FAP for all periods are <1%

^cA question mark denotes variability mechanisms that are uncertain due to insufficient color information

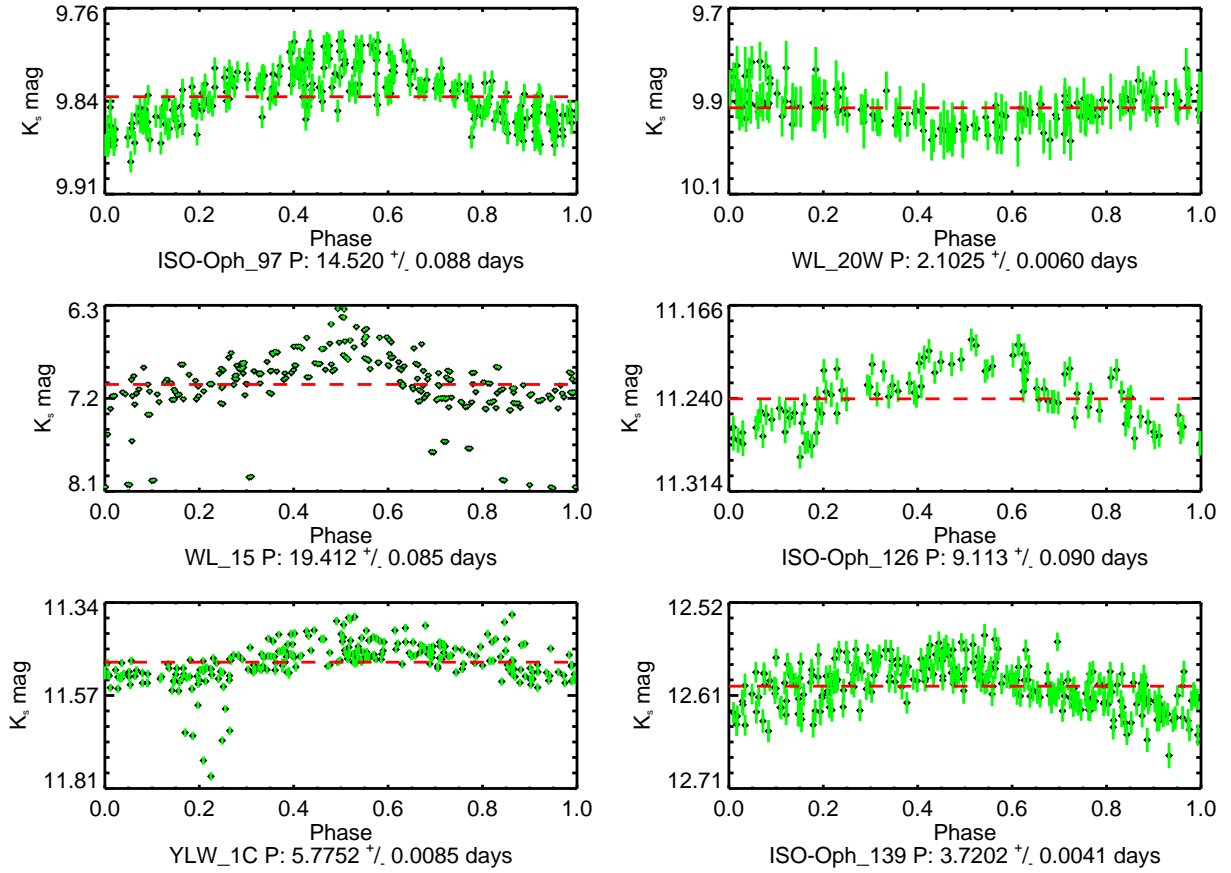


Fig. 13.— The folded K_s light curves for 6 sinusoidal-like periodic variables. The red line indicates the star's mean magnitude.

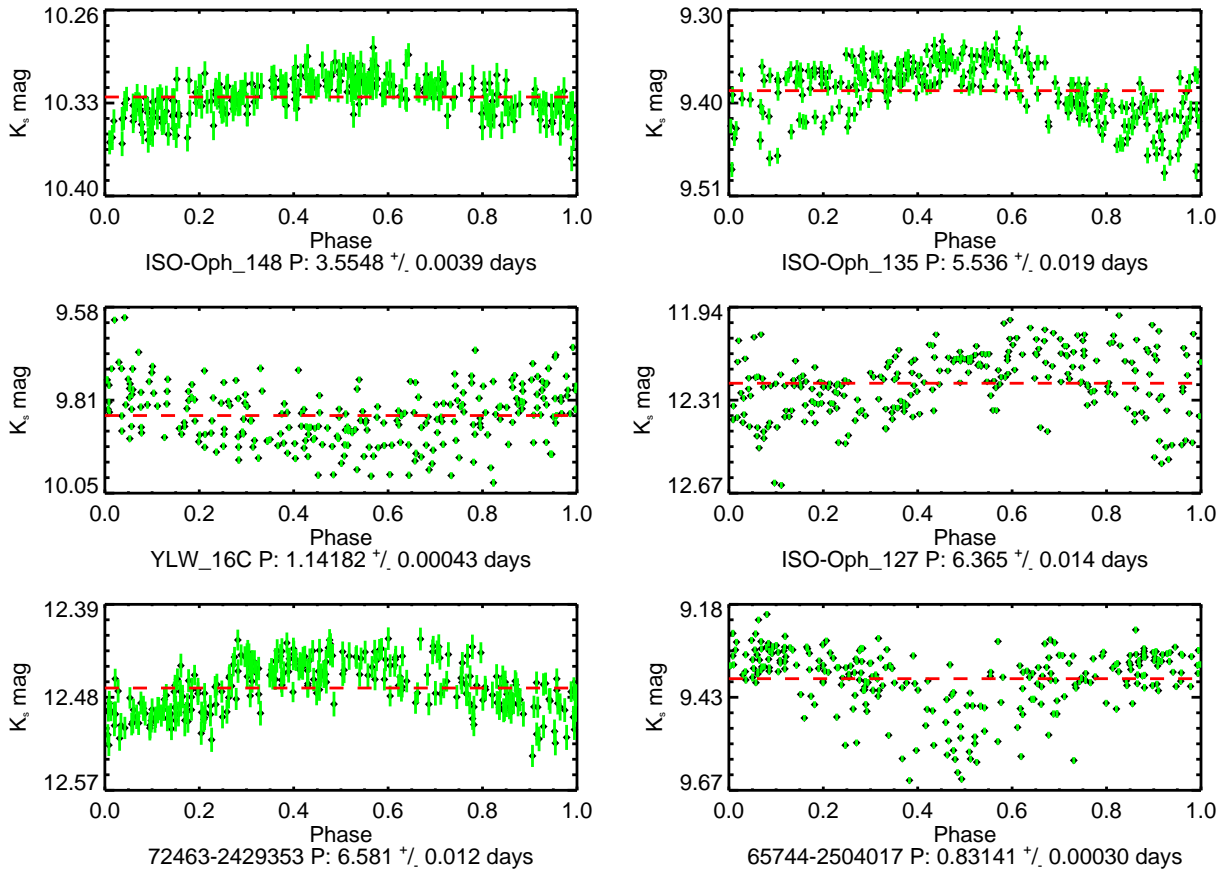


Fig. 14.— The folded K_s light curves for 6 sinusoidal-like periodic variables. The catalog name for stars labeled with a 2MASS designation have been truncated by 2MASS J162. The red line indicates the star’s mean magnitude.

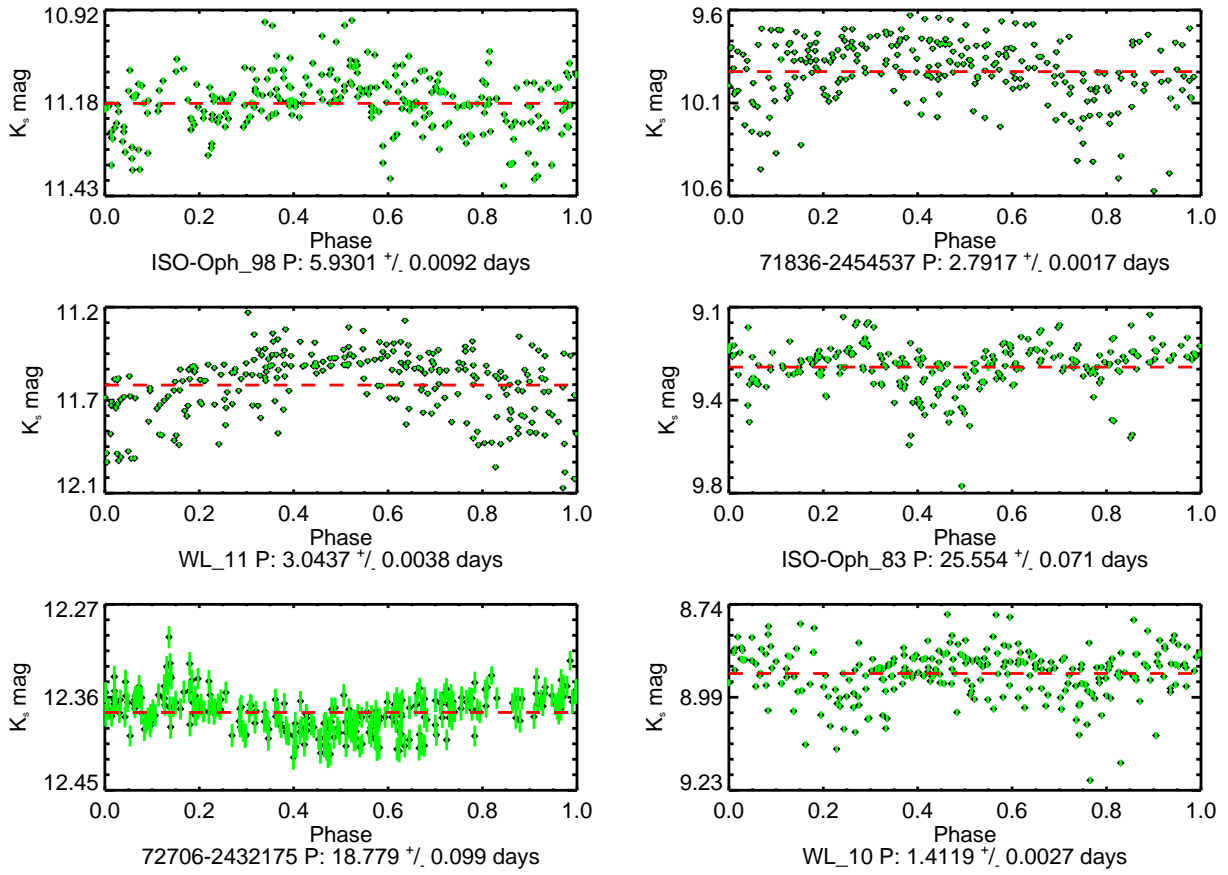


Fig. 15.— The folded K_s light curves for 6 sinusoidal-like periodic variables. The catalog name for stars labeled with a 2MASS designation have been truncated by 2MASS J162. The red line indicates the star's mean magnitude.

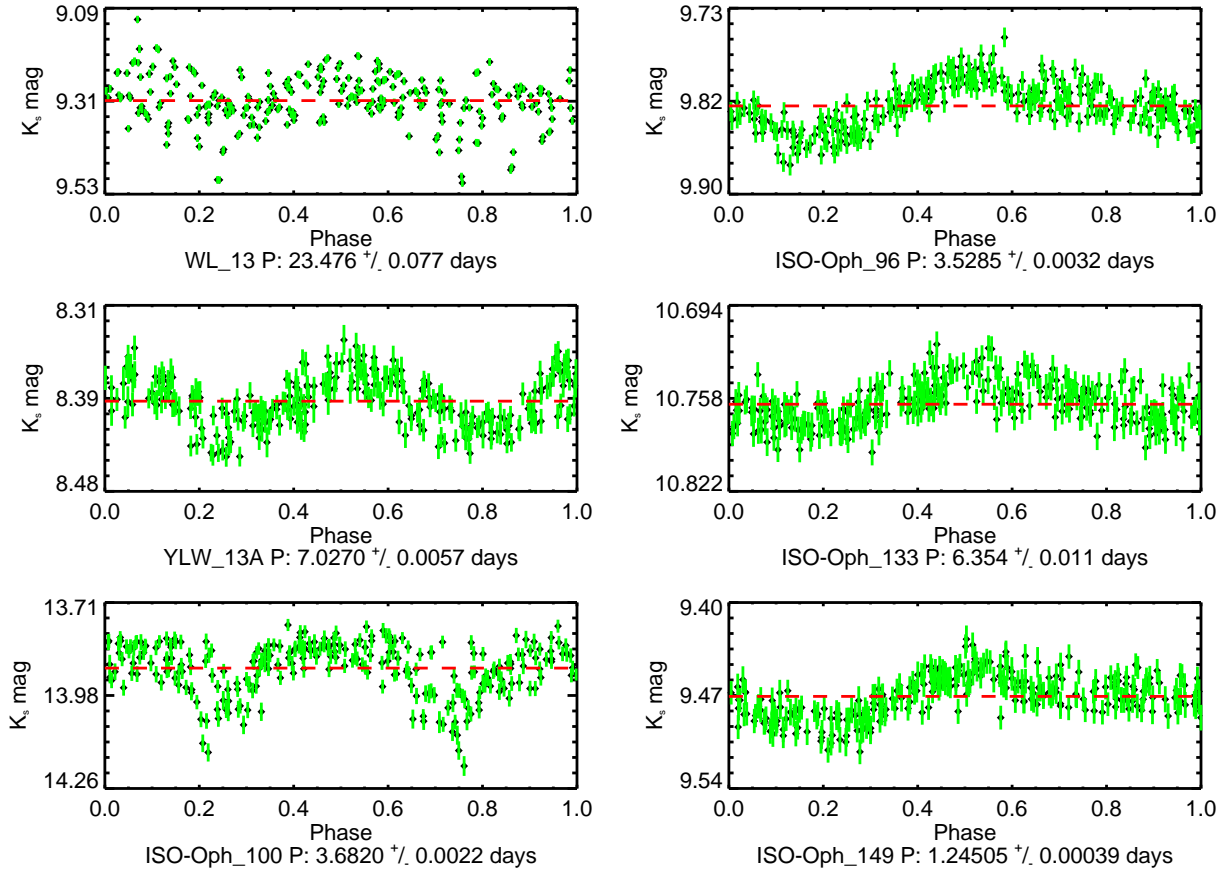


Fig. 16.— The folded K_s light curves for 6 sinusoidal-like periodic variables. The red line indicates the star's mean magnitude.

assigned using the adopted criteria.

All sinusoidal-like periodic variables except 3 (2MASS J1625744-2504017, 2MASS J16271836-2454537 and 2MASS J16272533-2506211) are located “on cloud”. This sub-category contains 19 stars with a YSO classification: 3 Class I (25%), 8 Class II (24%) and 8 Class III (73%).² The variability mechanism for 2 of the Class I stars is cool starspots, while the mechanism could not be identified for the third. Of the Class II stars, 5 vary due to cool starspots, 1 from an accretion-induced hot starspot and 1 is unknown. The variability of all Class III stars is caused by cool starspots.

Two key points can be made by analyzing the 18 sinusoidal-like periodic variables where cool starspots is the believed variability mechanism. First, cool starspots on young stars persist on preferential longitudes on year timescales. This is evidenced by a lack of phase drift in the folded light curves. This phenomenon of preferential or *active* longitudes have been associated with a number of chromospherically active stars (e.g. RS CVns, FK Com) (Strassmeier et al. 1988; Zeilik et al. 1988; Henry et al. 1995; Jetsu 1996). Second the variability amplitude due to cool starspots changes on much shorter timescales as evidenced by the significant scatter within the folded light curves. This amplitude variability is likely caused by an evolving starspot covering factor and/or starspot temperature. The covering factor is defined as the area of the observed stellar disk covered by the starspot(s).

ISO-Oph 96, ISO-Oph 133, ISO-Oph 149 and 2MASS J16272533-2506211 differ from the remaining sinusoidal-like periodic variables as the light curves for these 4 stars are asymmetric (i.e. they have a sharp increase in flux then decrease more slowly). The $(J-H)$ and $(H-K_s)$ color variability are not correlated to the K_s variability for the first three asymmetric sinusoidal-like periodic variables. This favors a dominant variability mechanism of rotational modulation by cool starspots. Asymmetric light curves have been observed for both WTTS and chromospherically active dwarf stars (Cutispoto et al. 2001, 2003; Grankin et al. 2008; Frasca et al. 2009). In both cases, the variability is believed to be caused by magnetically generated cool starspots. “Reverse” asymmetric light curves with a slow rise in source flux followed by a steep drop are also observed. Frasca et al. (2009) is able to closely model the *RIJH* asymmetric light curves of the WTTS V1529 Ori by rotating a stellar surface with two cool starspots of unequal areas separated by $\sim 130^\circ$ in longitude. The size of the leading cool starspot determines if a “forward” or “reverse” asymmetric light curve is seen.

2MASS J16272533-2506211, hereafter designated ‘J211’, is peculiar due to its unique and difficult to interpret brightness and color variations. Fig 18 contains K_s , $(J-H)$ and

²The percentages indicate the percentage of variable stars in each class that are sinusoidal-like periodic variables.

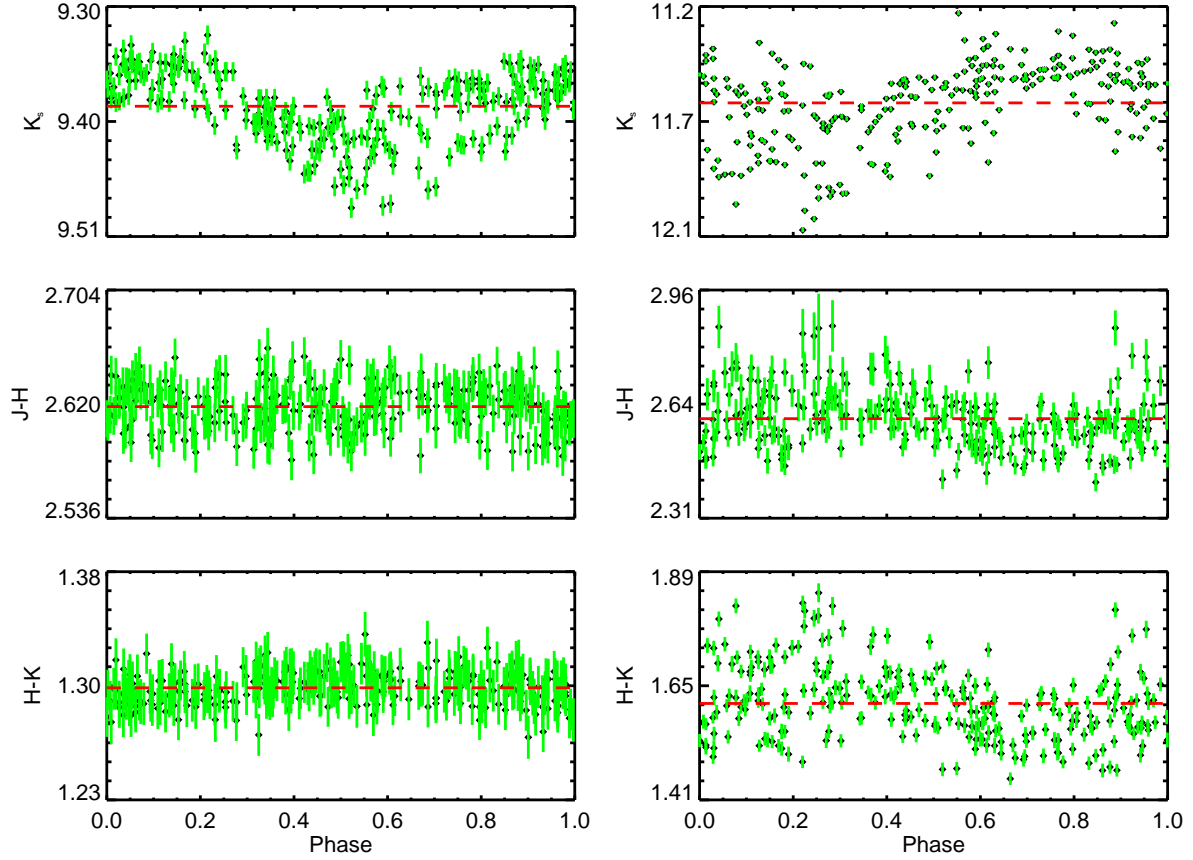


Fig. 17.— *Left*: The folded K_s and color curves for the sinusoidal-like periodic variable ISO-Oph 135. The lack of near-IR color changes with brightness changes favors cool starspots as the variability mechanism. *Right*: The folded K_s and color curves for the sinusoidal-like periodic variable WL 11. The stellar color becomes bluer as the K_s photometry becomes brighter. This favors rotational modulation of accretion induced hot starspots as the dominant mechanism. The red line in each plot indicates the mean value.

$(H-K_s)$ photometry for J211 folded to $P = 0.485143 \pm 0.000050$ days. This is the shortest period star among the periodic variables. The peak-to-trough K_s amplitude is 0.40 mag and the $\Delta(H-K_s)$ color amplitude is 0.30 mag. The $(J-H)$ color for J211 clearly becomes bluer for a phase duration of ~ 0.3 (~ 3.5 hrs) centered approximately on the times of maximum brightness. Somewhat surprisingly, however, no similar variation is seen in the $(H-K_s)$ color during the same period. The data is deemed reliable as the J and H photometry are significantly brighter than the survey completeness limits. The variability mechanism is not identified for J211 as this K_s -color behavior is inconsistent with any criteria discussed in §5. The shape of the light curve coupled with the short period suggests J211 might be a RR Lyrae variable. However the peculiar color behavior is not expected in these stars.

5.1.2. Eclipse- and Inverse Eclipse-like Periodic Variables

Eclipse-like periodic variables possess photometry containing sharp periodic drops in source flux. The duration of these drops, or possibly “eclipses”, is in all cases less than a phase of 0.3 when the photometry is folded to the most significant period. Fig 19 contains the folded light curves for the 6 eclipse-like periodic variables. These eclipse-like periodic variables are assigned to this subclass by visual inspection; it is not possible to confidently state that these sharp changes in photometry are *bona fide* occultations of star light (i.e. true eclipses).

The periods for the eclipse-like periodic variables range from 2.95 to 8.00 days. The durations of these eclipses range from 5.8 to 12.7 hours. The ΔK_s amplitudes range from 0.21 to 0.51, with a median value of 0.31 mag. The $\Delta(H-K_s)$ color amplitude range from 0.10 to 0.25 mag, with a median value of 0.11 mag. These amplitudes in both magnitude and color represent the total change in stellar flux and they do not necessarily represent eclipse depths since there is considerable scatter in the out-of-eclipse photometry. The eclipse depths and how they are determined are described below. The variability mechanism for the eclipse is determined in the same manner as with the sinusoidal-like periodic variables. Correlations between the K_s photometry and stellar colors $(J-H)$ and $(H-K_s)$ for the eclipse event are assessed visually and compared with the criteria discussed in §5. For 4 (66%) eclipse-like periodic variables, the $(J-H)$ and $(H-K_s)$ colors become redder as the star dims. The color correlation coupled with the short, periodic behavior favor extinction, possibly by the inner region of a circumstellar disk, as the dominant variability mechanism causing the eclipse. The variability in the colors during the eclipse for ISO-Oph 102 are not correlated with the K_s photometry consistent with variability caused by rotational modulation of cool starspots. Unfortunately, both the J and H photometry for YLW 10C are dimmer than the survey

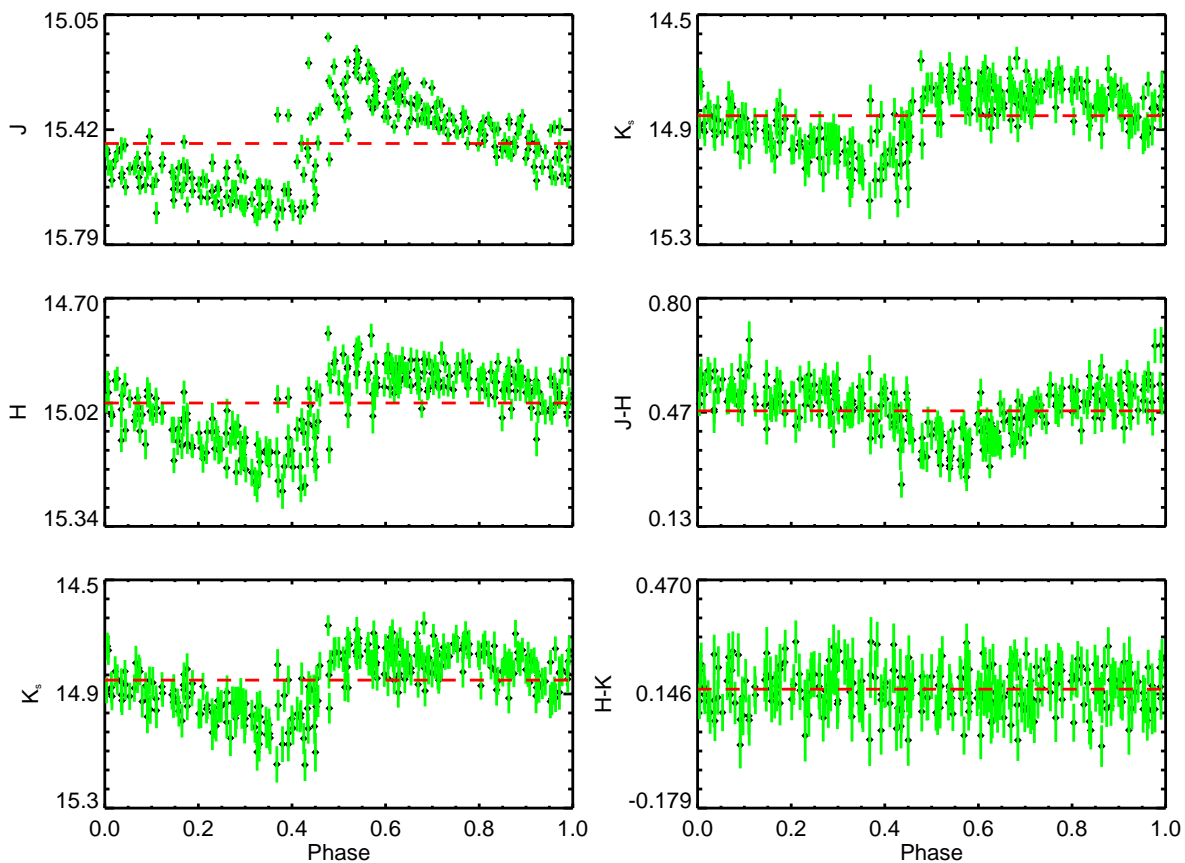


Fig. 18.— *Left*: The J , H and K_s light curves of 2MASS J16272533-2506211 folded to a period of 0.485143 ± 0.000050 days. *Right*: The K_s , $(J-H)$ and $(H-K_s)$ light and color curves folded to the above period. The significant difference in form of the J folded light curve to the other two suggests the cause for the variability in the $(J-H)$ color arises mainly from the J band. The red line in each plot indicates the mean value in each case.

completeness limits and the lack of color information prevents confident identification of a variability mechanism. All 6 eclipse-like periodic variables are classified as YSO Class II (15%)³. All stars in this sub-category are located “on cloud” except 2MASS J16271513-2451388.

Morales-Calderón et al. (2011, YSOVAR) qualitatively identified a number of similar eclipse-like variables in their mid-IR variability survey of YSOs within the Orion Nebula Cluster. The survey found 38 stars exhibiting brief, sharp drops in stellar flux. These stars are identified as AA Tau or “dipper” variables. The variability mechanism is believed to be due to high latitude warps in the inner accretion disk periodically occulting the star (Bertout 2000; Bouvier et al. 2003). The 4 eclipse-like variables that show evidence of extinction could be considered AA Tau variables, and possibly all 6 eclipse-like systems.

Under the assumption all 6 eclipse-like periodic variables are AA Tau variables, constraints on the spatial location within the circumstellar disk and size of the hypothetical occulter are investigated. Marsh et al. (2010) performed a deep mid-IR imaging survey of the ρ Oph 2MASS Calibration field used in this work. They computed the T_{eff} , A_V and mass for 5 of the 6 eclipse-like periodic variables. This was done by fitting model spectra to observed SEDs. The SEDs were computed from photometry in the J , H , K , [3.5] and [4.5] bands. The model spectra were obtained using the COND, DUSTY and NextGen models. T_{eff} and A_V are found by minimizing the following equation:

$$\phi(T_{eff}, \alpha, A_V) = \sum_{\lambda=1}^5 \frac{1}{\sigma_{\lambda}^2} [f_{\lambda}^{obs} - \alpha 10^{-0.4r_{\lambda}A_V} f_{\lambda}^{mod}(T_{eff})]^2 - A_V \beta \quad (6)$$

where α is a flux scaling factor, f_{λ}^{obs} and $f_{\lambda}^{mod}(T_{eff})$ are the respective observed and model fluxes at wavelength λ , σ_{λ} is the flux uncertainty, r_{λ} is the absorption at wavelength λ relative to A_V and β is a constant penalty parameter. In the Rayleigh-Jeans regime a degeneracy exists between T_{eff} and A_V such that a high temperature star seen through low extinction will have a SED similar to that of a low temperature star seen through high extinction. The parameter β is used to break this degeneracy by penalizing solutions with low values of A_V . This parameter was optimized by using the published photometry of a large sample of spectroscopically confirmed brown dwarfs. Values of A_V have errors between 1 to 2.7 while T_{eff} is accurate to within 860 K. The COND and DUSTY models then yield a model-unique mass for each star. They used a mass-temperature relationship to derive the mass for hotter stars fit by the NextGen models. They conclude an accuracy in the mass estimate to within

³The percentage indicates the percentage of variable Class II stars that are eclipse-like periodic variables

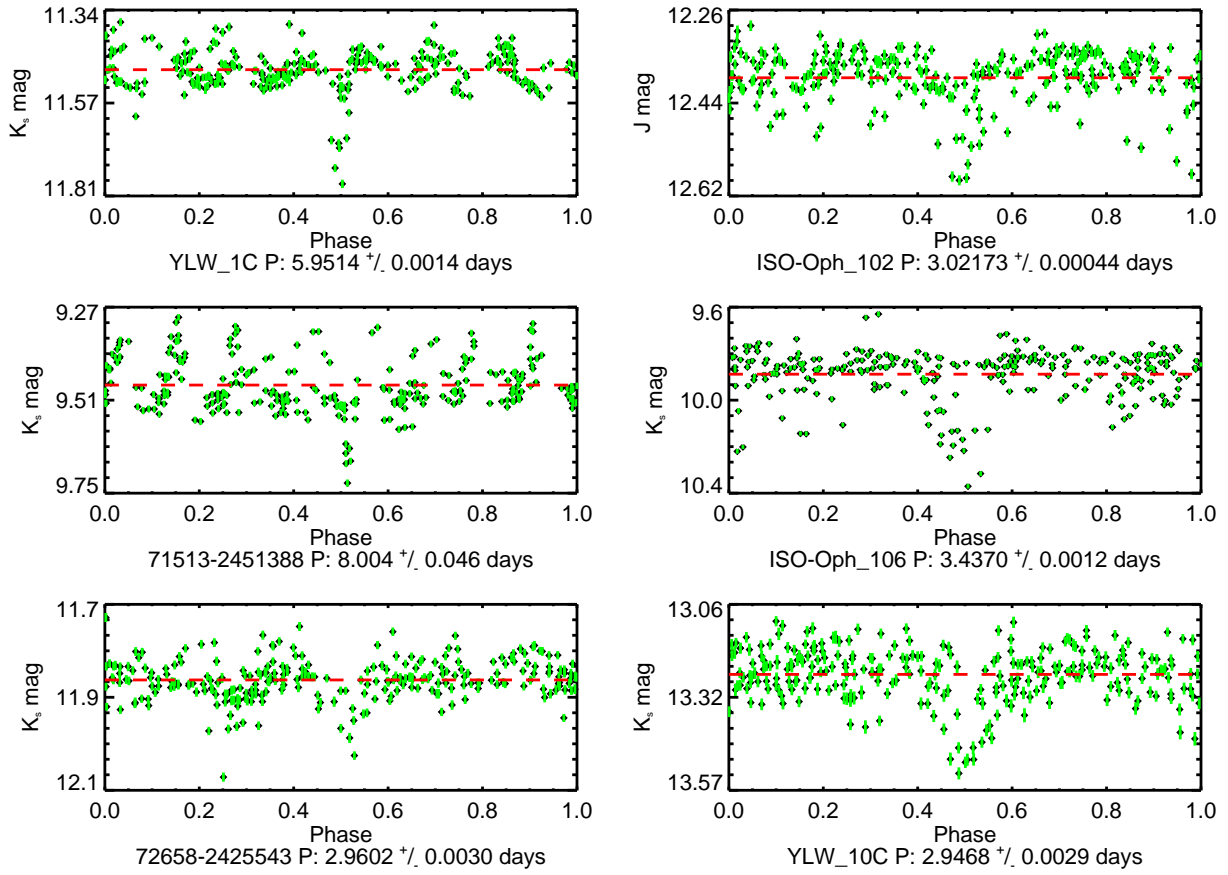


Fig. 19.— The folded J and K_s light curves for 6 eclipse-like periodic variables. The catalog name for stars labeled with a 2MASS designation have been truncated by 2MASS J162. The red line indicates the star’s mean magnitude

a factor of ~ 2 -3.

For the case of ISO-Oph 106, a 1 Myr isochrone from Siess et al. (2000) is used to determine the T_{eff} and radius for ISO-Oph 106 by assuming a mass of $0.5 M_{\odot}$. The stellar radius for the remaining eclipse-like periodic variables is computed by $R_{\star} = (\frac{L_{\star}}{T_{eff}^4})^{\frac{1}{2}}$, where each quantity is in solar units. The stellar luminosity, L_{\star} , is computed using the prescription outlined in Natta et al. (2006) except in the case of YLW 10C. The prescription relates the stellar luminosity as a function of J magnitude and extinction A_J . The extinction is computed using the $(J-H)$ and $(H-K)$ colors corrected into the CIT system using the ρ Oph extinction law by Kenyon et al. (1998) and the CTTS locus defined by Meyer et al. (1997). The J band photometry for YLW 10C is below the survey completeness limit. The luminosity for this star is found using the 1 Myr isochrone mentioned above and the mass determined by Marsh et al. (2010). The estimated mass, T_{eff} , A_V , and R_{\odot} are in Table 5.

Assuming the occulter has negligible mass and orbits under Keplerian rotation, the occulter’s distance from the host star can be computed for each eclipse-like periodic variable. The diameter of the occulter is computed from the duration of the eclipse event and its location in the circumstellar disk. Strictly speaking, the computed diameters are along the orbital path. No assumption concerning the occulter geometry (i.e. spherical, ellipsoid) is made. This diameter is considered a strict lower bound as the disk geometry, occulter impact parameter and occulter opacity are unknown. The eclipse depth, however, is determined by first removing the eclipse-event photometry from the time-series data (see §4.1). The eclipse depth is then determined to be the difference between the maximum magnitude in the eclipse feature relative to a median non-eclipse mean magnitude. This calculation results in occulter distances that range between 1.83 to 7.21 R_{\star} , with a median value of 3.20 R_{\star} . The occulter size ranges from 0.58 to 5.07 R_{\star} , with a median value of 2.05 R_{\star} . The range in ΔK_s eclipse depth is 0.12 to 0.51 mag, with a median value of 0.27 mag. Table 5 summarizes the results of this investigation.

Table 6. Summary of Eclipse-Like Periodic Variable Characteristics

Star	L (L_{\odot})	M (M_{\odot})	T_{eff} (K)	R_{\star} (R_{\odot})	a (R_{\star})	D (R_{\star})	ΔK_s (mag)
YLW 1c	1.81	1.16	4738	2.01	7.21	2.04	0.29
2MASS J16271513-2451388	0.52	0.11	3033	2.63	3.09	0.58	0.26
2MASS J16272658-2425543	0.062	0.043	2783	1.07	2.84	2.05	0.17
ISO-Oph 102	0.22	0.059	2888	1.88	1.82	1.37	0.12
ISO-Oph 106	0.88	0.50	3769	2.06	3.69	3.48	0.51
YLW 10c	0.746	0.35	3901	1.90	3.21	3.63	0.28

Inverse eclipse-like periodic variables are similar to eclipse-like periodic variables, but the “eclipse” is an increase in source flux rather than a decrease. Fig 20 contains the folded K_s and color curves for WL 4 and YLW 16A, the 2 inverse eclipse-like periodic variables in the variable catalog. WL 4 is a Class II YSO whose period of variability is 65.61 ± 0.40 days. The peak-to-trough ΔK_s amplitude is 0.67 mag and the peak-to-trough $\Delta(H-K_s)$ color amplitude is 0.19 mag. The $(J-H)$ color for WL 4 becomes redder as the star brightens during the inverse eclipse event. However, the $(J-H)$ color change starts just prior and ends just after the inverse eclipse event. The difference in each case is ~ 0.1 in phase or ~ 6.6 days. The $(H-K_s)$ color is not correlated with the K_s variability.

The period of variability for YLW 16A is longer than WL 4 at 92.28 ± 0.84 days. The amplitudes of variability for YLW 16A, a Class I YSO, are also larger with peak-to-trough ΔK_s and $\Delta(H-K_s)$ amplitudes of 0.95 and 0.34 mag, respectively. As the J band photometry is dimmer than the survey completeness limits, no reliable $(J-H)$ color information is available. The $(H-K_s)$ color variability is sinusoidal-like, but is not aligned with the K_s variability. Both stars reside “on cloud”.

The variability mechanism for both WL 4 and YLW 16A is believed to be related, and similar to the interpretations proposed in separate letters (Plavchan et al. 2008, 2013). Here the proposed variability mechanism is summarized. Both systems contain a visual binary companion detected through high resolution direct imaging (Ratzka et al. 2005; Plavchan et al. 2013). The two visible components for WL 4 are separated by $0.176''$ and separated by $0.3''$ in the case of YLW 16A. This corresponds to a projected linear separations of 23 AU and 39 AU, respectively, given a mean distance of 129 pc (see §3.4). In each system, the large amplitude variability is believed to be intrinsic to one of the visible pair. This component is, in turn, hypothesized to be a close binary surrounded by a circumbinary disk; this system is thus a triple system. The influence of the wide companion has caused the plane of the circumbinary disk to be inclined to the orbital plane of the inner binary. The variability results when each component of the inner binary is periodically obscured by the circumbinary disk as the binary orbits around the barycenter. Kusakabe et al. (2005) proposed a similar model to explain the variability for KH-15D.

5.2. Long Time-Scale Variables

The largest amplitude variability in long time-scale variables is not observed to be periodic, but show consistent trends, unlike irregular variables. The K_s light curves are shown in Fig 21 to 25; all 31 LTVs (31% of the variable catalog) are listed in Table 7.

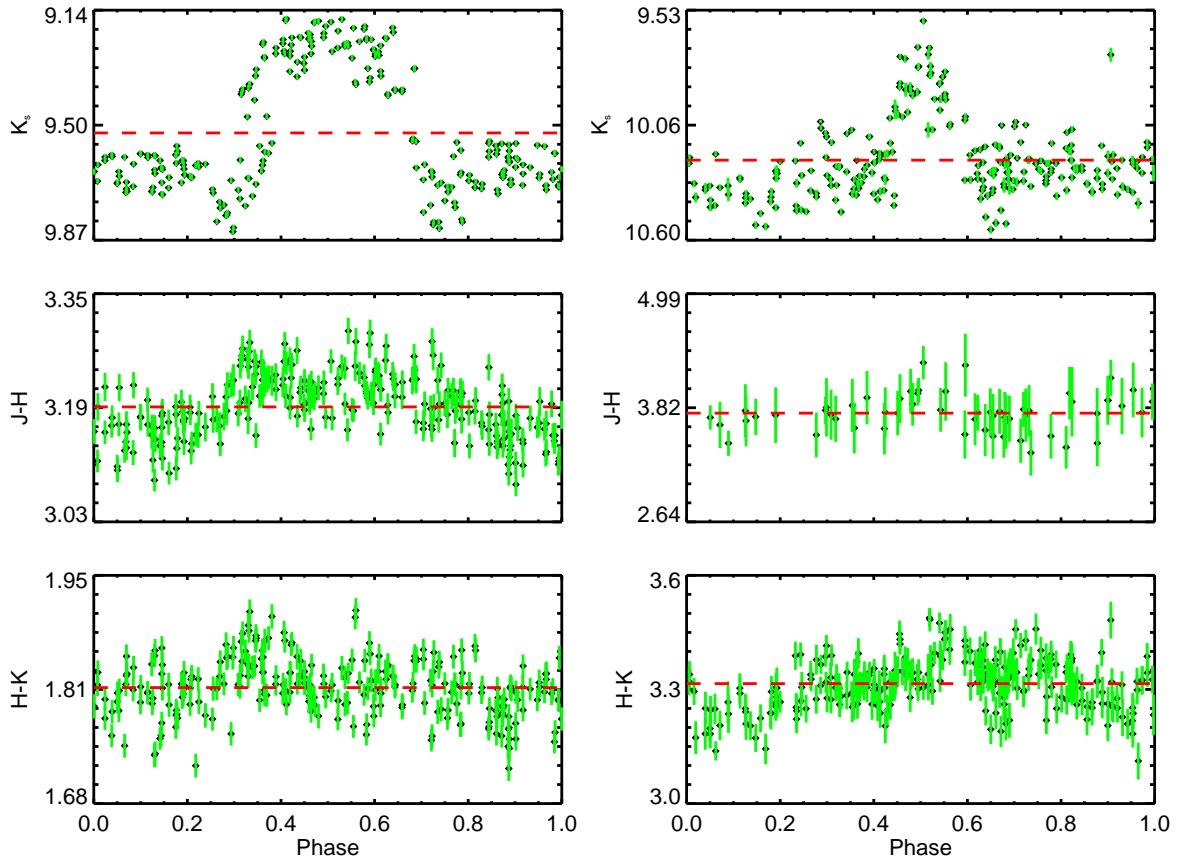


Fig. 20.— The folded K_s and color curves for the inverse eclipse-like periodic variables WL 4 ($P = 65.6$ days) and YLW 16A ($P = 92.3$ days). The red line in each plot indicates the mean value in each case.

Table 7. Time-Scale Variables

Catalog ID ^a	Time-Scale (days)	ΔK_s (mag)	$\Delta(J-H)$ (mag)	$\Delta(H-K_s)$ (mag)	YSO Class	Var. Mech.
ISO-Oph 88	310	0.500	0.415	0.270	II	Extinction
WL 14	384	0.218	0.185	0.380	II	Extinction
70072-2446272	543	0.061	0.091	0.084	—	Extinction
ISO-Oph 91	143	0.078	0.074	0.180	III	Extinction
70266-2446345	313	0.049	0.061	0.122	—	Extinction
ISO-Oph 94	64	0.894	—	0.707	II	Extinction
WL 1 ^b	226	0.294	0.275	0.523	II	Accretion?
WL 17 ^b	578	1.125	—	1.065	I	Unknown
ISO-Oph 107	355	0.195	—	0.119	II	Accretion
YLW 8A	355	0.198	1.272	0.098	II	Accretion
ISO-Oph 112 ^b	207	0.984	—	1.123	II	Extinction
ISO-Oph 113	120	0.058	0.067	0.122	III	Unknown
WL 19 ^b	589	1.012	—	0.784	II	Accretion?
ISO-Oph 117	530	0.560	0.249	0.133	II	Accretion
YLW 10B ^b	578	0.562	—	0.850	II	Unknown
ISO-Oph 119	76	0.445	—	—	II	Unknown
WL 20E	81	0.299	0.262	0.297	II	Accretion
WL 20W	122	0.213	0.258	0.305	II	Extinction
71726-2422283	132	0.163	—	1.137	—	Unknown
YLW 12A	92	0.728	—	0.813	I	Accretion
ISO-Oph 126	349	0.135	—	0.371	III	Extinction
WL 6	172	1.199	—	1.256	I	Accretion?
72297-2448071	327	0.134	0.097	0.062	—	Accretion?
72357-2412288	354	0.052	0.066	0.080	—	Extinction
ISO-Oph 137	89	0.749	—	—	I	Unknown
72514-2446335	750	0.065	0.089	0.173	—	Unknown
YLW 15A	478	0.393	—	0.927	I	Extinction
YLW 16B	140	2.312	—	1.318	I	Extinction
YLW 17B ^b	516	0.155	0.110	0.233	II	Accretion
ISO-Oph 151	398	0.282	0.106	0.160	II	Accretion
ISO-Oph 150	239	0.926	—	—	I	Unknown

^aThe catalog ID has been truncated by 2MASS J162 for 2MASS catalog stars

^bCandidate sinusoidal-like periodic LTV

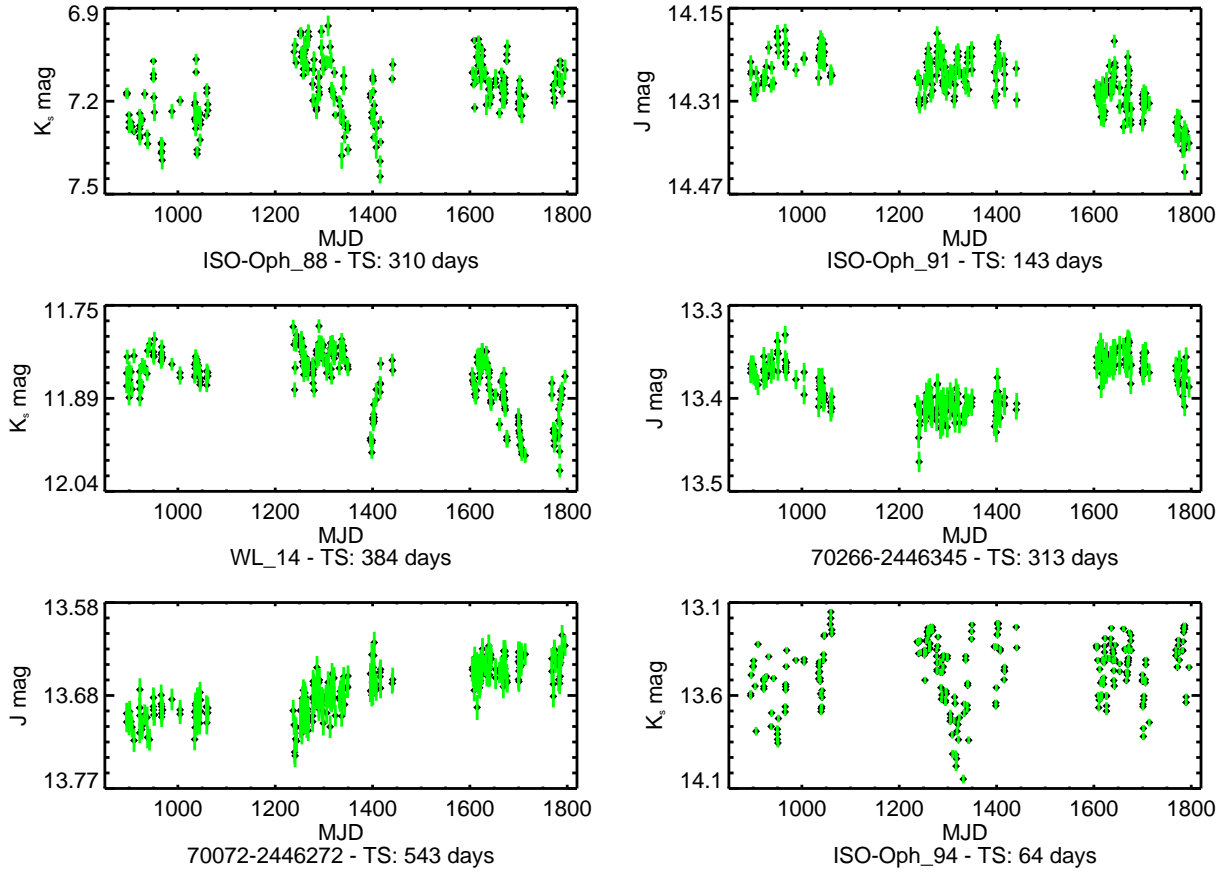


Fig. 21.— The J or K_s light curves for 6 long time-scale variables. The the highest signal-to-noise light curve of these 2 is illustrated.

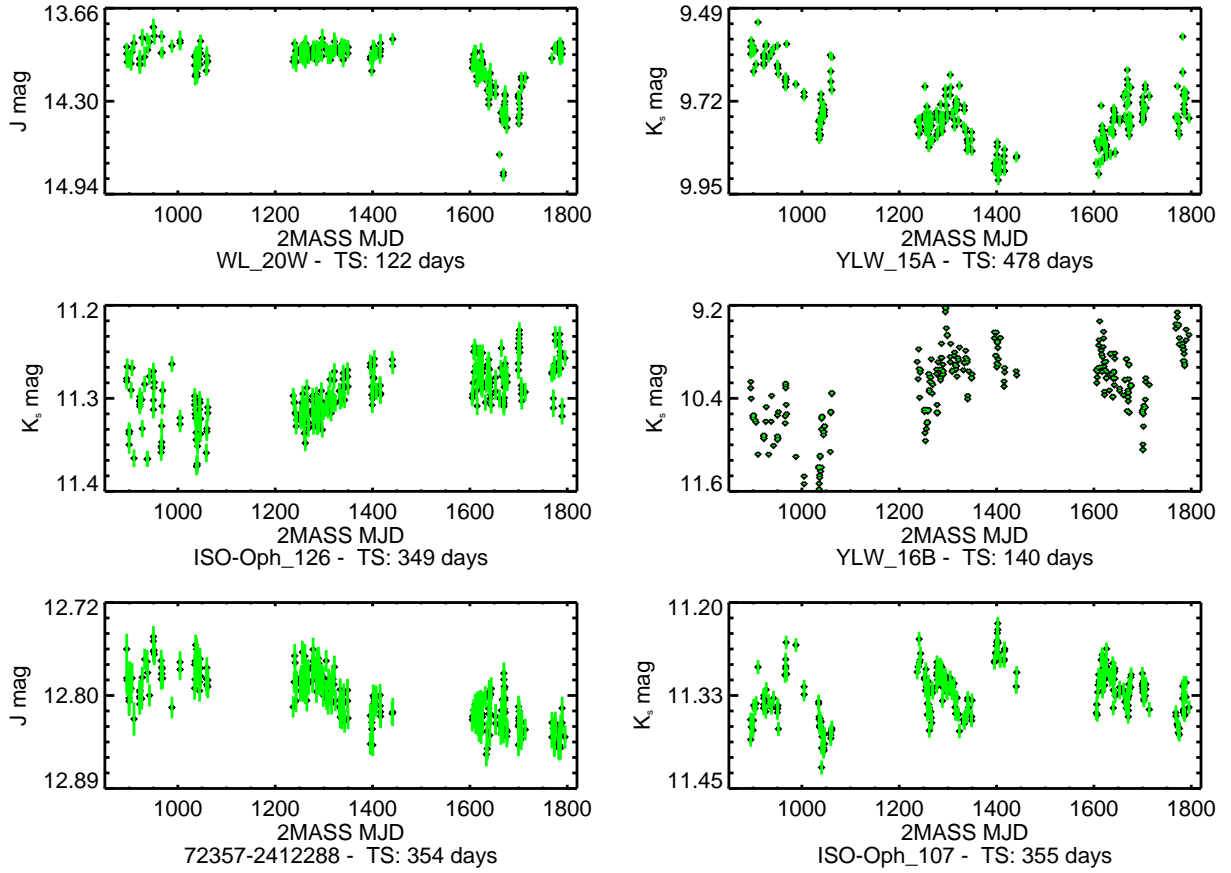


Fig. 22.— The J or K_s light curves for 6 long time-scale variables. The the highest signal-to-noise light curve of these 2 is illustrated.

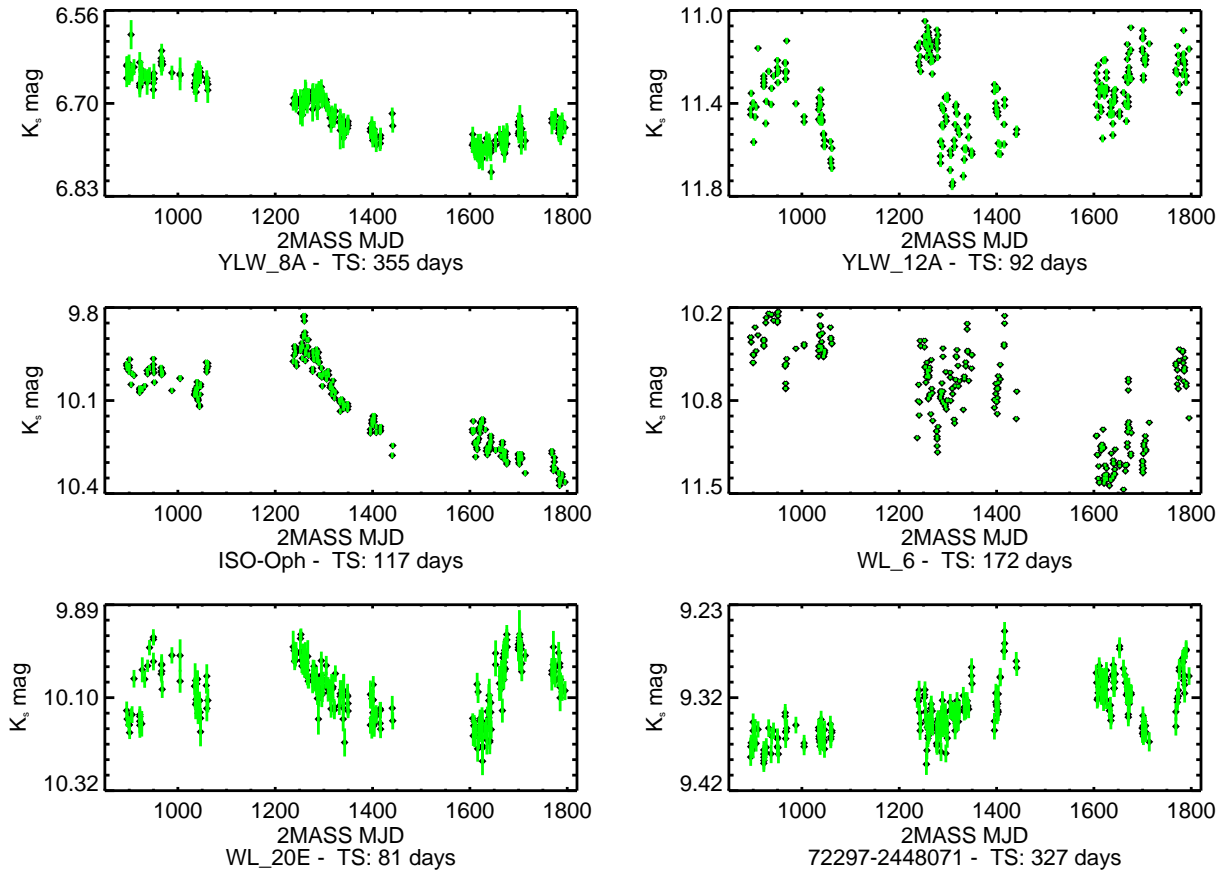


Fig. 23.— The K_s light curves for 6 long time-scale variables.

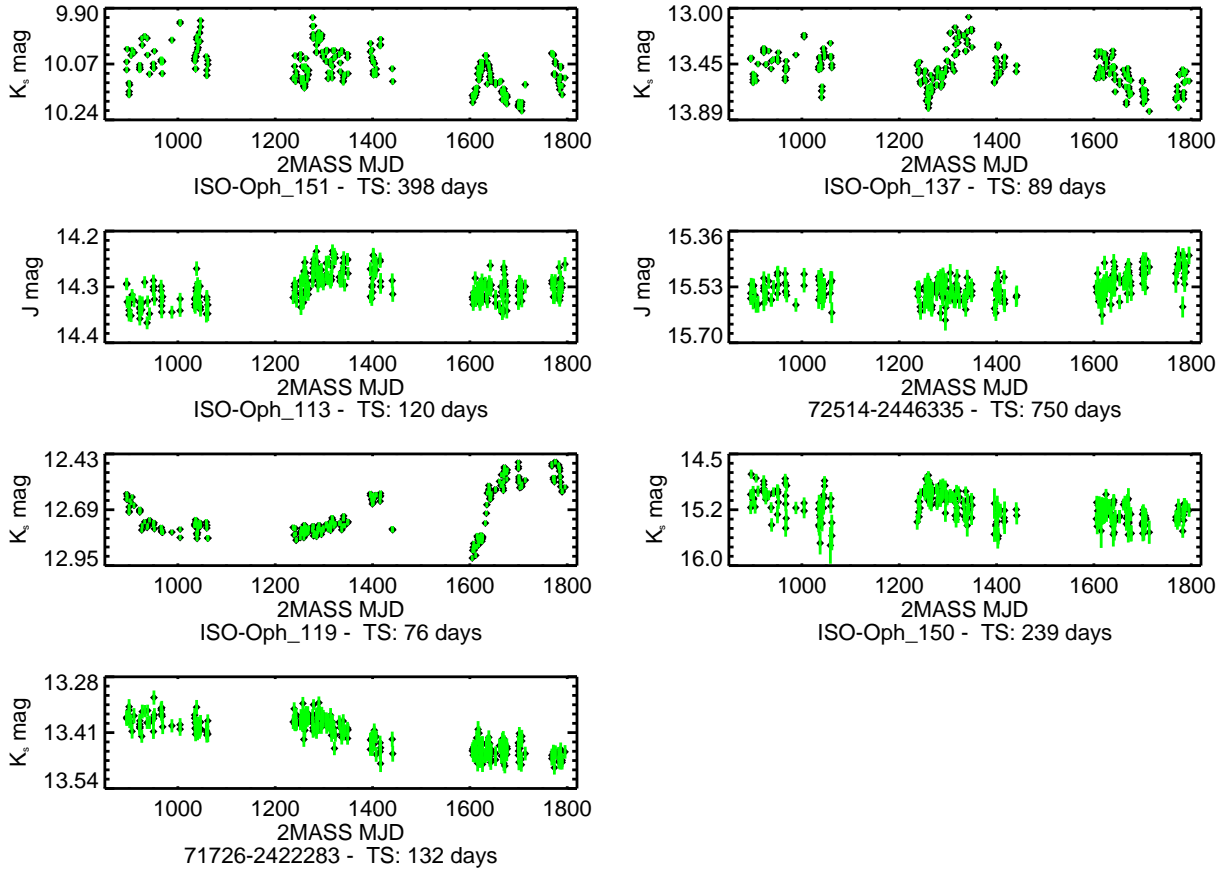


Fig. 24.— The J or K_s light curves for 7 long time-scale variables. The the highest signal-to-noise light curve of these 2 is illustrated.

In §4.2, a method for quantifying the time-scale of the extended brightness variations is detailed. These time-scales range from 64 to 790 days, the latter being near the full duration of the observing campaign. The peak-to-trough ΔK_s amplitudes for all LTVs range from 0.05 to 2.31 mag, with a median value of 0.29 mag. The peak-to-trough $\Delta(H-K_s)$ color amplitudes range from 0.06 to 1.32 mag, with a median value of 0.23 mag. The two most probable mechanisms for these aperiodic variations with time-scales much longer than typical stellar rotation periods are variable extinction and variable mass accretion rates. Fig 25 shows two examples of the change in K_s brightness and stellar color caused by these two mechanisms. Extinction causes the star to become redder as the star dims. Changes in the mass accretion rate cause stars to become bluer as the star dims. For 12 LTVs (39%), the $(J-H)$ and $(H-K_s)$ colors become redder as the star dims favoring variable extinction as the dominant variability mechanism. The $(J-H)$ and $(H-K_s)$ colors become bluer as the star dims in 11 LTVs (34%) favoring variable mass accretion rates as the dominant variability mechanism. The remaining 7 LTVs (23%), either do not have useful color information because the J or H (or both) photometry is below the survey completeness limits, or the brightness-color correlation does not agree with any of the 4 listed variability criteria. No dominant variability mechanism is assigned to these stars.

One intriguing scenario to explain why LTVs do not seem to favor one variability mechanism over another is the viewing angle. For LTVs where variable accretion is the favored mechanism, the system could be more face-on providing a clearer view of the inner disk hole. Variable extinction due to circumstellar disk asymmetries is more easily seen at higher disk inclinations where the “puffed up” outer disk attenuates the light from the inner disk. As these two mechanisms have opposing brightness-color correlations, systems with no measured correlations may represent intermediate viewing angles. In this case, the measured effects from variable accretion will “cancel” out or confuse the measured effects from variable extinction.

All LTVs are located “on cloud” and 25 stars of the 31 LTVs are classified as a YSO: 7 Class I (58%), 15 Class II (44%) and 3 Class III (27%).⁴ The favored variability mechanism in the Class I LTVs is variable extinction for 2 stars, variable mass accretion for 2 stars and unidentified for 3 stars. The variability in the Class II LTVs is consistent with variable extinction in 5 stars, variable mass accretion in 8 stars and is not identified for 2 stars. The K_s -color correlation in 2 Class III LTVs favors variable extinction as the dominant variability mechanism while the mechanism for variability in the third Class III LTV is not identified.

⁴The percentages indicate the percentage of variable stars in each class that are sinusoidal-like periodic variables.

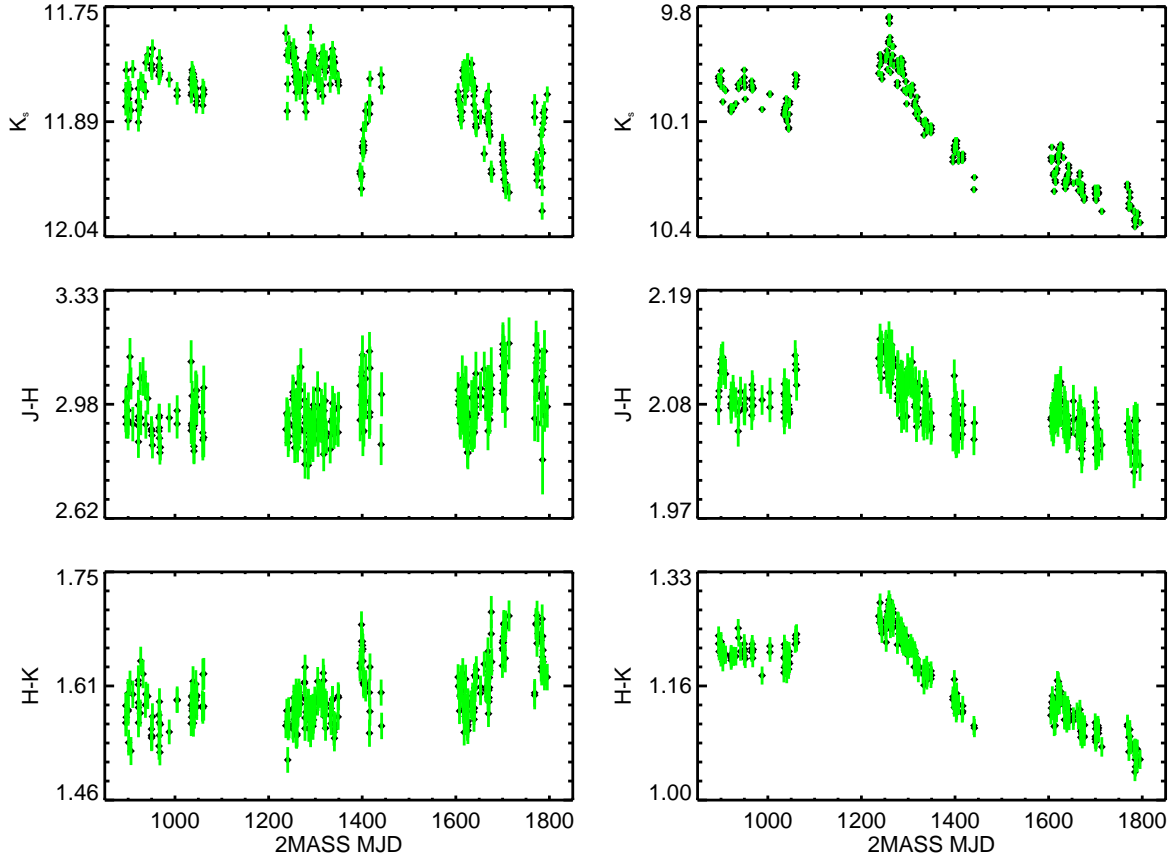


Fig. 25.— *Left*: The K_s light, $(J-H)$ color curve, and $(H-K_s)$ color curve for the long time-scale variable WL 14. This is an example of variability caused by extinction. As the K_s magnitude drops the colors become redder. *Right*: The same light and color curves for the long time-scale variable ISO-Oph 117. This is an example of variability caused by variable mass accretion. As the K_s magnitude drops the colors become bluer.

Based upon visual inspection of folded light curves, 6 LTVs are considered candidate periodic variables. These candidate periodic LTVs are denoted in Table 6 and Fig 26 contains their folded K_s light curves. The variability time-scales, ranging from 207 to 589 days, for the candidate periodic LTVs are measured using the Lomb-Scargle algorithm. The PA does not find the time-scales found by Lomb-Scargle to be significant. The stars, on average, have higher flux and color amplitude variability than the LTVs taken as a whole. The peak-to-trough ΔK_s amplitude for these candidate periodic variables range from 0.16 to 1.13 mag, with a median value of 0.77 mag. The peak-to-trough color amplitude range from 0.23 to 1.12 mag, with a median value of 0.82 mag. For 3 candidate periodic LTVs, the $(J-H)$ and $(H-K_s)$ colors become bluer as the star dims favoring a variable mass accretion rate as the dominant variability mechanism. The $(H-K_s)$ color of ISO-Oph 112 reddens as the star dims. This is consistent with variable extinction as the dominant variability mechanism. A combination of J band photometry below the survey completeness limits and the K_s - $(H-K_s)$ color correlation not matching any of the 4 criteria precludes the identification of the dominant variability mechanism for 2 candidate periodic LTVs. All the candidate periodic LTVs are classified as a YSO: 1 Class I star and 5 Class II stars.

5.3. Irregular Variables

The variable catalog contains 40 stars (40%) that are clearly variable, but the largest amplitude variability is not periodic or coherent on long time-scales. The K_s light curves are located in Figs 27 to 31. Table 8 contains the list of irregular variables.

The ΔK_s amplitude range from 0.04 to 1.11 mag, with a median value of 0.14 mag. The $\Delta(H-K_s)$ color amplitude range from 0.05 to 0.75 mag with a median value of 0.14 mag. Using the variability criteria, discussed in §5, the primary variability mechanism is only identified for 4 irregular variables (2MASSJ16265861-2446029, ISO-Oph 116, YLW 13B, ISO-Oph 87). The first three exhibit a long time-scale variation in at least one observing season where the star becomes bluer as it dims. This is indicative of variable mass accretion as the variability mechanism. These stars are not considered LTVs as this variability is not the largest amplitude variability in the time-series. The variable accretion for YLW 13B is identified to occur for ~ 115 days in the second year with a $\Delta K_s \sim 0.15$ mag and $\Delta(H-K_s)$ 0.11 mag (see Fig 30). ISO-Oph 116 varies via variable accretion at least twice (see Fig 28). The first time occurs for ~ 170 days in the first year with ΔK_s 0.14 mag and $\Delta(H-K_s)$ 0.07 mag. The second time occurs for ~ 70 days in the third year with $\Delta K_s \sim 0.11$ mag and $\Delta(H-K_s)$ 0.07 mag. The average error in both K_s and $(H-K_s)$ is 0.01 mag for both YLW 13B and ISO-Oph 116. In the case of 2MASSJ16265861-2446029, only the $(J-H)$ color becomes

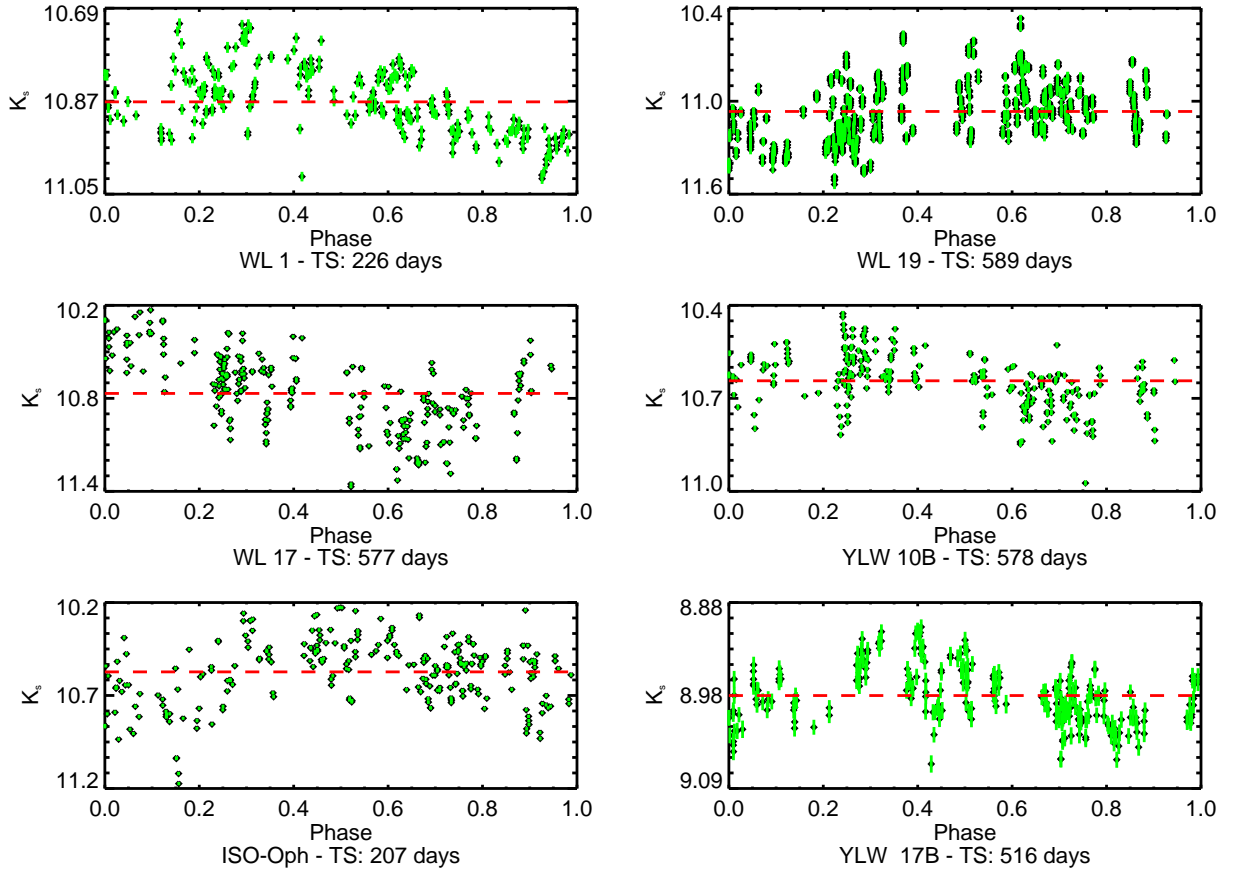


Fig. 26.— The K_s folded light curves for 6 candidate periodic long time-scale variables. The red line indicates the star's mean magnitude

Table 8. Irregular Variables

Catalog ID ^a	ΔK_s (mag)	$\Delta(J-H)$ ^b (mag)	$\Delta(H-K_s)$ ^c (mag)	YSO Class	Var Mech
65576-2508150	0.114	0.150	0.123	—	Unknown
65699-2455192	0.167	0.153	0.180	—	Unknown
WL 21	0.166	—	—	II	Unknown
65744-2452589	0.160	0.105	0.139	—	Unknown
65789-2452371	0.854	—	—	—	Unknown
65789-2457518	0.108	0.093	0.124	—	Unknown
65861-2446029	0.131	0.198	0.168	—	Accretion?
ISO-Oph 87	0.294	0.241	0.180	II	2 “flare” events
70054-2446444	1.109	—	—	—	Unknown
WL 22	0.631	—	—	I	Unknown
65967-2415433	0.078	0.124	0.073	—	Unknown
70055-2416255	0.061	0.082	0.066	—	Unknown
WL 16	0.082	0.083	0.176	—	Unknown
70276-2502437	0.053	0.062	0.083	—	Unknown
70285-2418546	0.060	0.086	0.064	—	Unknown
70501-2508484	0.052	0.084	0.077	—	Unknown
70516-2420077	0.049	0.079	0.078	—	Unknown
70591-2459376	0.044	0.078	0.055	—	Unknown
70597-2428363	0.182	—	0.157	II	Unknown
60819-2442286	0.069	0.061	0.195	—	Unknown
71003-2429133	0.334	—	0.366	II	Unknown
71096-2445298	0.056	0.073	0.074	—	Unknown
71173-2447109	0.069	0.079	0.074	—	Unknown
ISO-Oph 116	0.155	0.085	0.090	II	Accretion
71377-2505450	0.059	0.065	0.091	—	Unknown
71384-2415441	0.205	—	0.291	—	Unknown
71404-2415096	0.109	0.200	0.149	—	Unknown
71531-2415515	0.069	0.099	0.088	—	Unknown
71605-2415039	0.352	—	0.534	—	Unknown
71604-2416163	0.391	—	0.517	—	Unknown
71744-2413079	0.155	0.217	0.315	—	Unknown
YLW 13B	0.215	0.276	0.158	II	Accretion
ISO-Oph 131	0.050	0.184	0.069	III	Unknown
72330-2507282	0.700	—	0.751	—	Unknown
72325-2448357	0.074	0.099	0.094	—	Unknown
ISO-Oph 138	0.326	0.432	0.175	II	Unknown
73052-2432347	0.070	0.075	0.082	—	Unknown
73107-2504004	1.057	—	—	—	Unknown
73122-2504172	0.566	0.386	0.473	—	Unknown
73208-2508545	0.613	0.318	0.679	—	Unknown

^aThe catalog ID has been truncated by 2MASS J162 for 2MASS catalog stars.

^bEntries with — mark stars with photometry below the survey J band completeness limit.

^cEntries with — mark stars with photometry below the survey H band completeness limit.

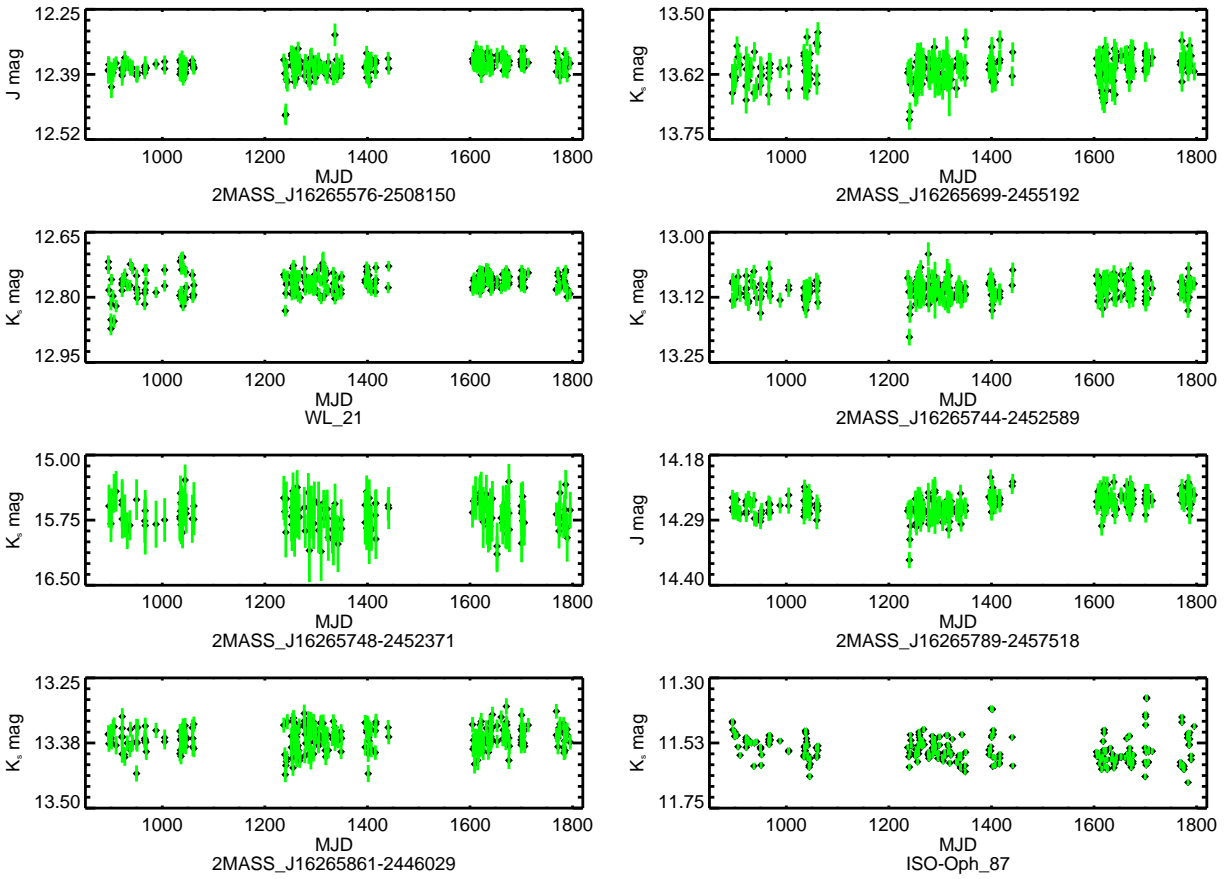


Fig. 27.— The J or K_s light curves for 8 irregular variables.

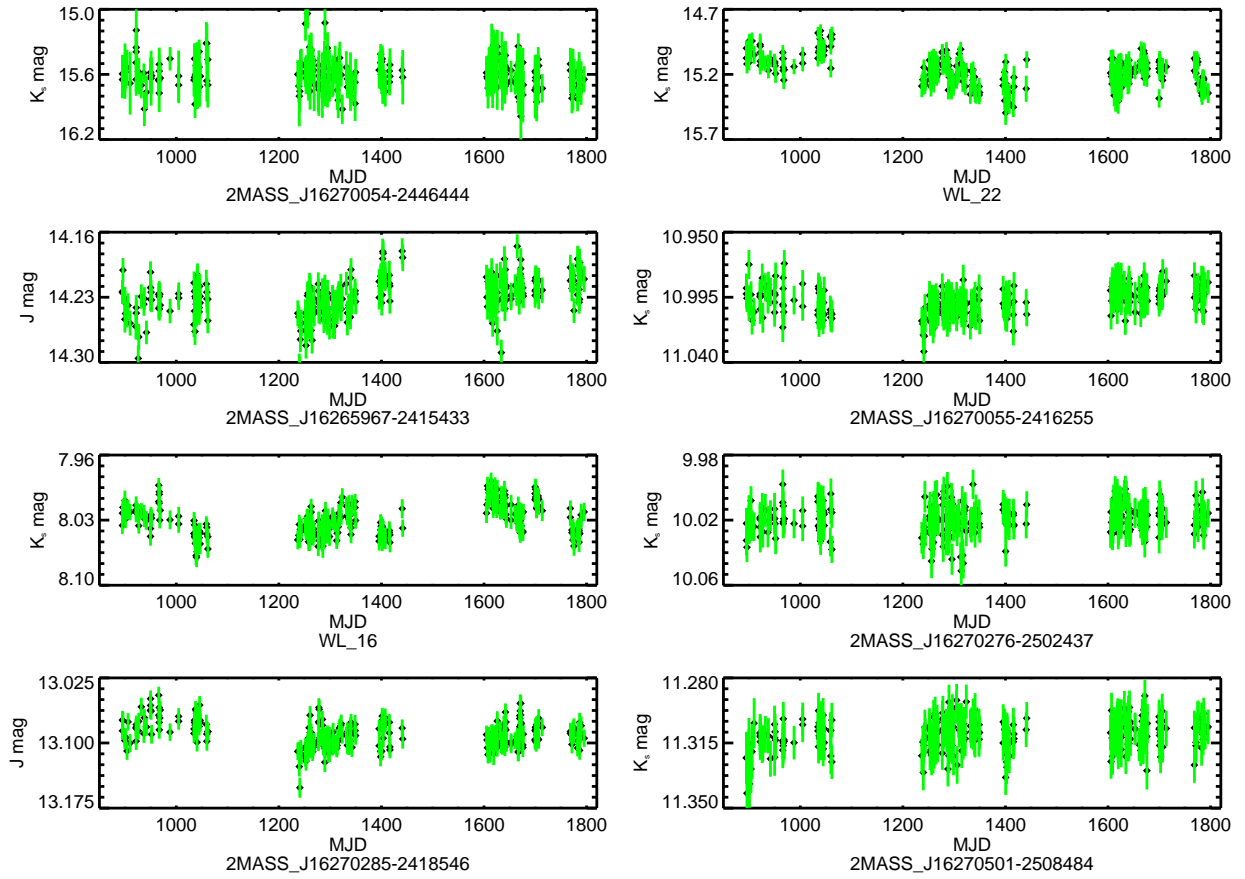


Fig. 28.— The J or K_s light curves for 8 irregular variables.

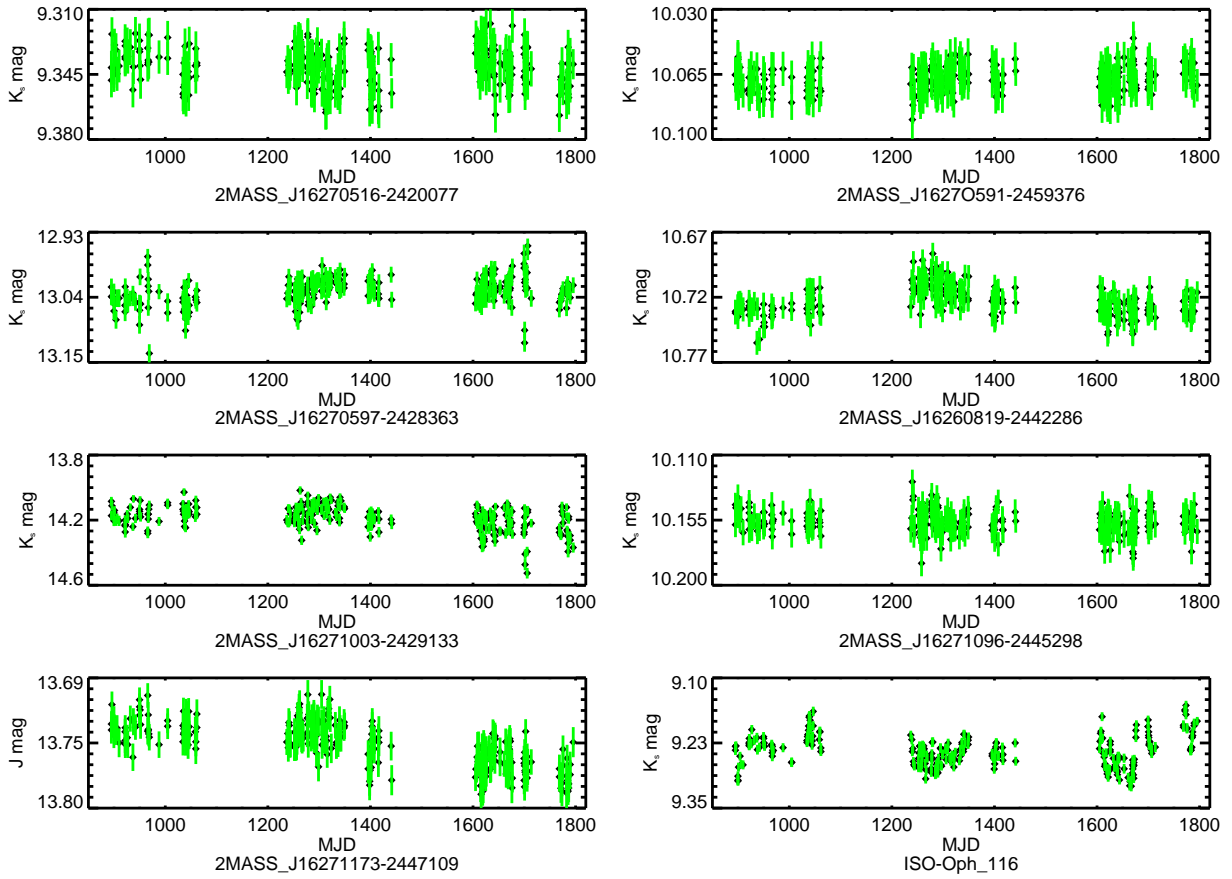


Fig. 29.— The J or K_s light curves for 8 irregular variables.

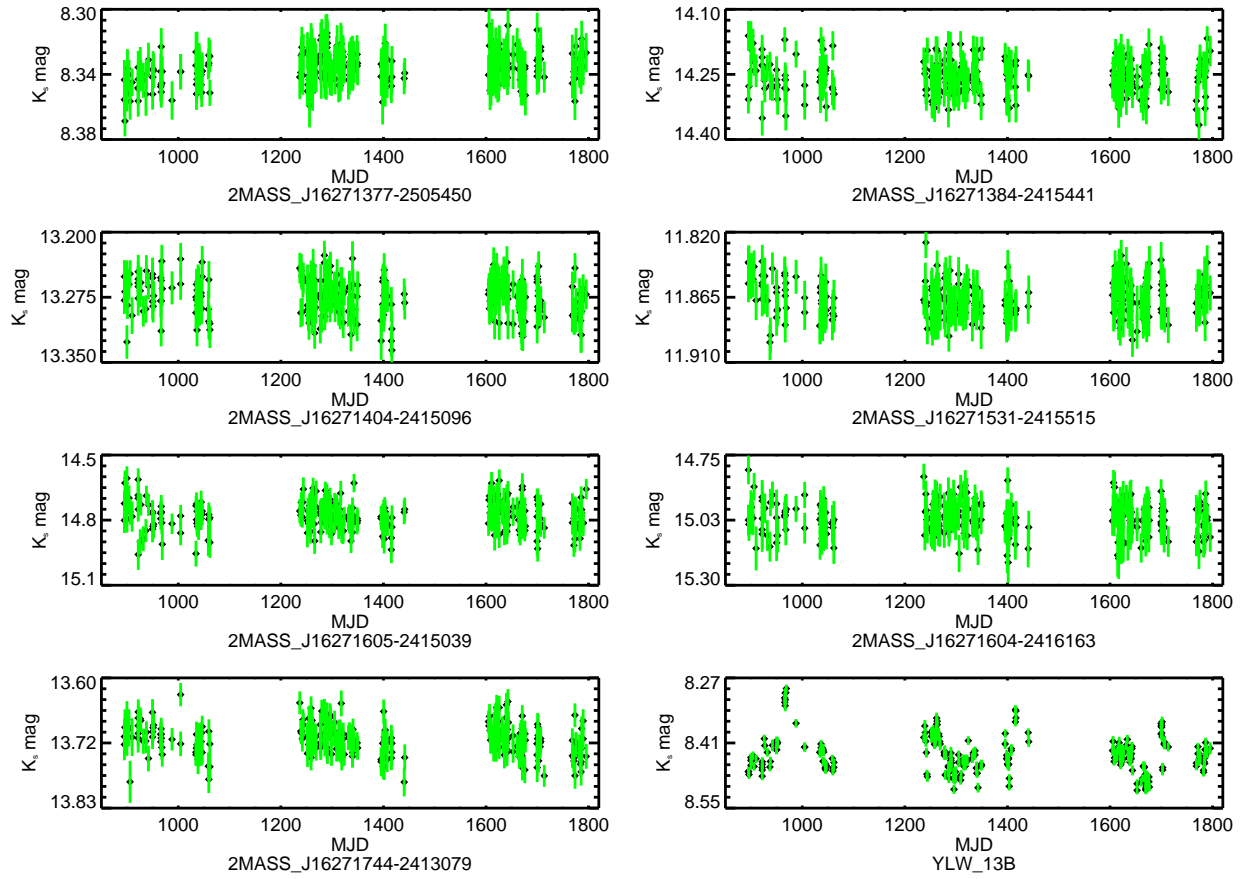


Fig. 30.— The K_s light curves for 8 irregular variables.

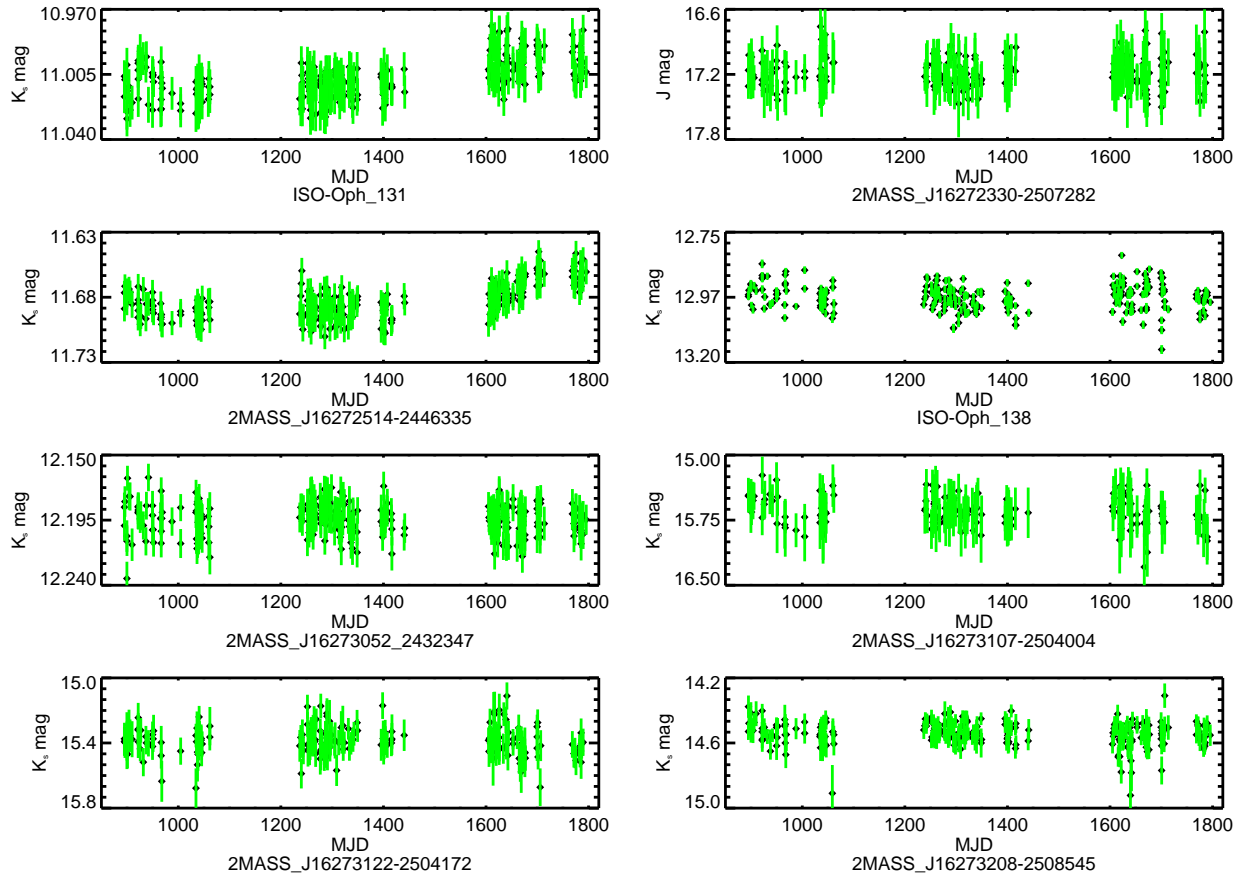


Fig. 31.— The J or K_s light curves for the 8 irregular variables.

bluer making the mechanism identification tentative. The YSO classification for this star is unknown. The J band photometry is too dim in 11 irregular variables to identify the variability mechanism. Of these 11 variables, the H band is also too dim in 5 stars.

The variability in ISO-Oph 87 is peculiar due to two flare-like events that occur in the K_s photometry on approximately 1400 and 1700 2MASS MJD.. Fig 32 contains the K_s , $(J-H)$ and $(H-K_s)$ photometry for this Class II YSO. If the events are truly related to an increase in stellar activity, the star is expected to become bluer in both $(J-H)$ and $(H-K_s)$. However, no change is seen in the $(J-H)$ color and the star reddens in $(H-K_s)$. The first event lasts for ~ 10 days with ΔK_s 0.20 mag and $\Delta(H-K_s)$ 0.13 mag. The second event occurs for ~ 6 days and ΔK_s 0.18 mag and $\Delta(H-K_s)$ 0.16 mag. Two additional, lower amplitude spikes in the K_s photometry between 1600 and 1700 2MASS MJD might also be similar flare-like events.

Irregular variables have the smallest percentage (68%) of stars located “on cloud”. Only 9 stars in this sub-category are classified as a YSO: 1 Class I (8%), 7 Class II (21%) and 1 Class III (9%).⁵ Most (16 stars) of the 22 candidate ρ Oph members are irregular variables. If these candidate members are YSOs then the fraction of YSO irregular variables is comparable to the fraction of periodic and LTV YSOs.

5.4. Examples of Multiple Variability Mechanisms

As discussed in the Introduction, variability studies indicate young stars sometimes exhibit complex photometric behavior believed to result from multiple variability mechanisms acting concurrently. For most stars in this survey, only the highest amplitude variability can be confidently characterized. However, a lower amplitude, second type of variability is definitely seen in 7 variable stars. Four of these seven stars (YLV 1C, 2MASS J16272658-2425543, YLV 10C, WL 4) show evidence for two separate, yet statistically distinct periodic variations. The remaining three stars (WL 20W, ISO-Oph 126, WL 15) are periodically variable underneath a higher amplitude, long time-scale variation. The methods used to identify both the primary and secondary variabilities in these stars is discussed in §4.1. The following subsections contain detailed discussions for each of these stars except WL 4 which is described in Plavchan et al. (2008).

- YLV 1C (ISO-Oph 86): This CTTS exhibits both sinusoidal-like and eclipse-like periodic variability at 2 distinct periods; the periods are distinct from each other to a 20σ confidence level. Fig 33 contains the K_s , $(J-H)$ and $(H-K_s)$ photometry folded

⁵The percentages indicate the percentage of variable stars in each class that are irregular variables.

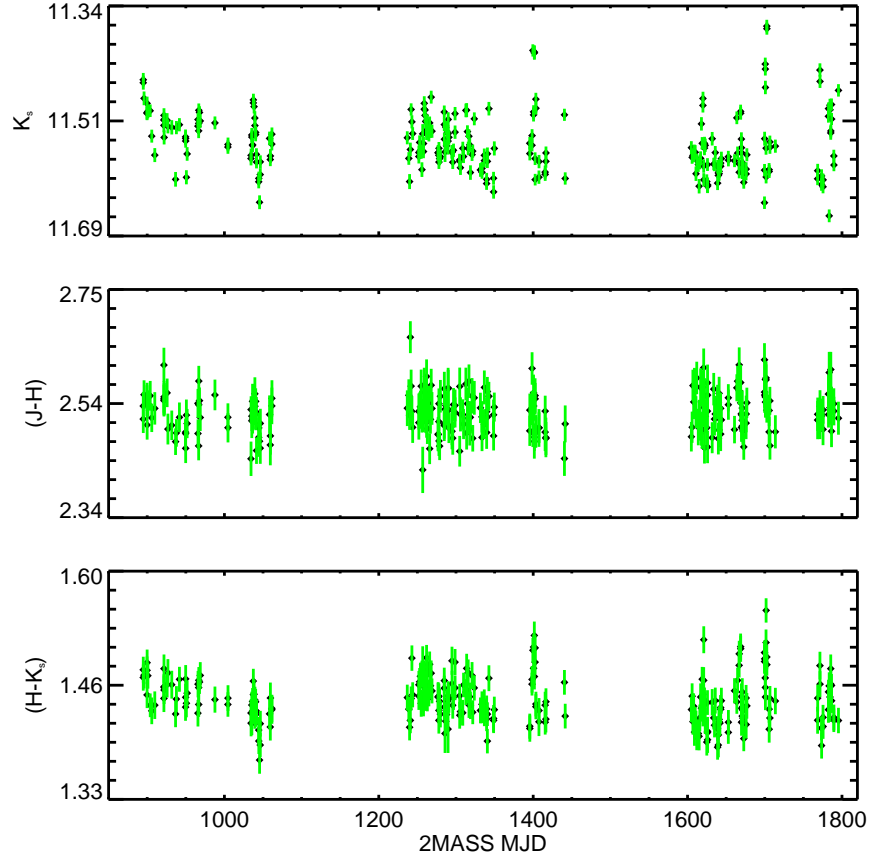


Fig. 32.— The K_s , $(J-H)$ and $(H-K_s)$ photometry for ISO-Oph 87. The photometry contains at least two “flare” events, where the star brightens sharply in K_s , occurring at 1400 and 1700 2MASS MJD. Two other possible “flare” events occur between 1600 and 1700 2MASS MJD. The events become redder as the star brightens rather than becoming bluer as expected for stellar flares.

to the sinusoidal-like period, $P = 5.7792 \pm 0.0085$ days. The peak-to-trough ΔK_s amplitude for this variability is 0.14 mag. The variability in both the $(J-H)$ color and $(H-K_s)$ color is not correlated with the K_s variability. This favors variability caused by rotational modulation of a cool starspot(s). Fig 34 contains the K_s , $(J-H)$ and $(H-K_s)$ photometry folded to the eclipse-like period, $P = 5.9514 \pm 0.0014$ days. The ΔK_s eclipse depth is 0.29 mag. The $(H-K_s)$ color reddens during the eclipse event consistent with variability caused by extinction. This behavior is not seen in the $(J-H)$ color. Since the J band photometry is near the survey completeness limits, the absence of a clear reddening trend may be due to low signal-to-noise in the color curve.

The two periods for YLW 1C is consistent with the interpretation that these events are true occultation events, as proposed for AA Tau (see §5.1.2). The short period, arising from a stellar surface feature(s), traces the stellar rotation rate. The longer period suggests the occultation of the star by an obscuration located just beyond the circumstellar disk co-rotation radius. Following the analysis described in §5.1.2, the occulter of YLW 1C is located $7.2 R_\star$ from the host star and the duration of the occultation is ~ 6.4 hours corresponding to a minimum occulter diameter of $\sim 2.0 R_\star$. The reader is reminded this diameter represents the extent within the orbital path and makes no claim on any preferential occulter shape. The eclipse depth is $\Delta K_s = 0.29$ mag.

The large occulter diameter argues against the direct detection of a hot protoplanet. However recent imaging results suggest that gas giant planets maybe considerably extended in the mass accretion phase (Quanz et al. 2013; Kraus & Ireland 2012). If true in this case, this would demonstrate the existance of a hot protoplanet with a period of 6 days very near the peak in the period distribution for exoplanets (Wright et al. 2012). Alternatively, the event could be caused by an occultation of a warped portion of a circumstellar disk. This scenario has been proposed to explain the near- to mid-IR variability in LRL 31 (Flaherty & Muzerolle 2010; Flaherty et al. 2012). While most YSO disk models invoke axisymmetry, objects such as YLW 1C are prompting the creation of more complex models.

- 2MASS J16272658-2425543: This CTTS, designated 'J543' hereafter, is another star exhibiting both sinusoidal-like and eclipse-like variability with two distinctly different periods. Fig 35 contains the K_s , $(J-H)$ and $(H-K_s)$ photometry folded to the sinusoidal-like period, $P = 1.52921 \pm 0.00065$ days. The peak-to-trough ΔK_s amplitude for this variability is 0.20 mag. The variability in the $(J-H)$ and $(H-K_s)$ colors are not correlated with the K_s photometry, which favors variability caused by rotational modulation of a cool starspot. Fig 36 contains the K_s , $(J-H)$ and $(H-K_s)$ photometry folded to the eclipse-like period, $P = 2.9602 \pm 0.0013$ days. The ΔK_s eclipse depth

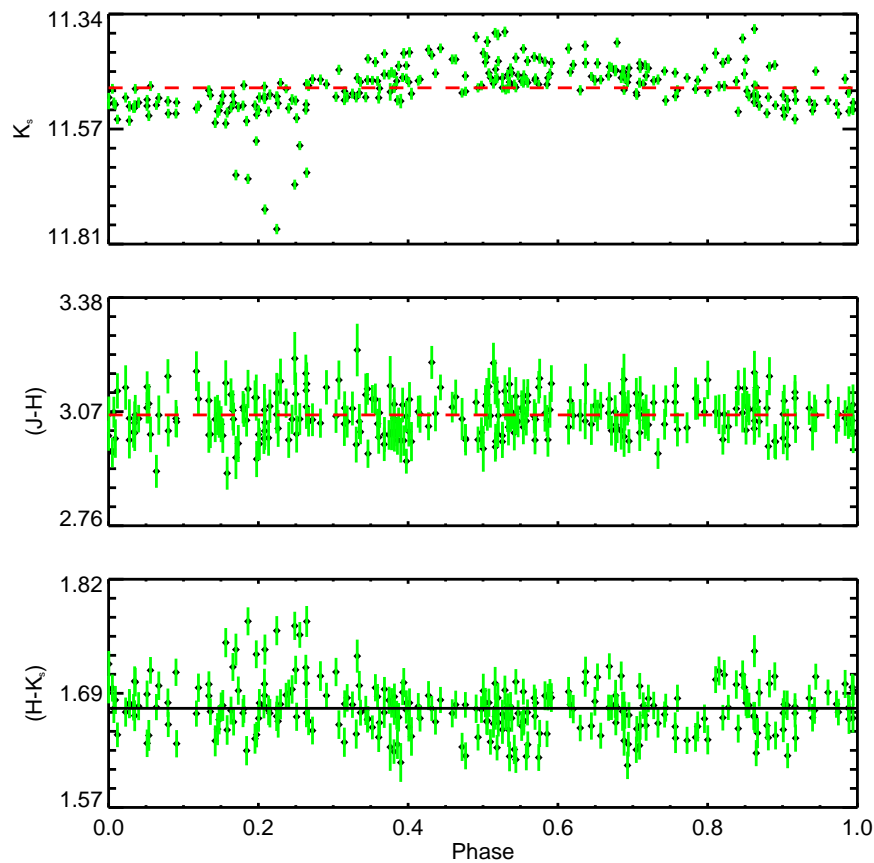


Fig. 33.— The K_s , $(J-H)$ and $(H-K_s)$ photometry for YLW 1C phased to the 5.7752 ± 0.0085 day sinusoidal-like period. The red line indicates the mean value in each panel. The lack of color correlation with ΔK_s points to rotational modulation of cool starspots as the variability mechanism.

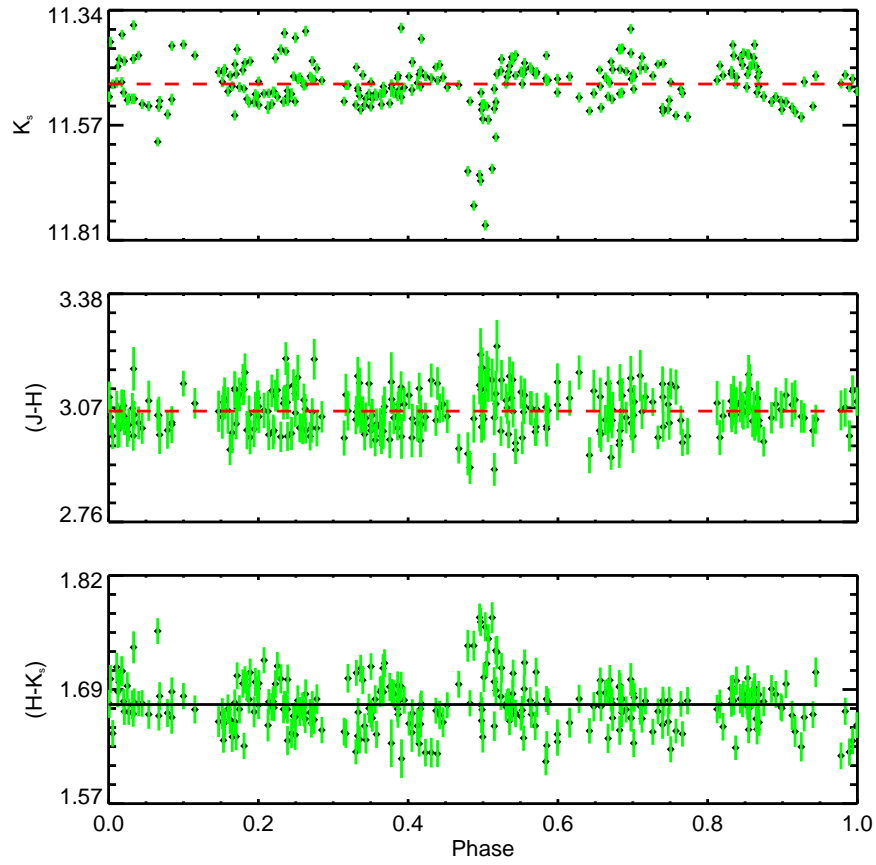


Fig. 34.— The K_s , $(J-H)$ and $(H-K_s)$ photometry for YLW 1C phased to the 5.9514 ± 0.0014 day eclipse-like period. The red line indicates the mean value in each panel. Both colors become redder as K_s dims indicating variable extinction as the likely variability mechanism.

is 0.17 mag. Both the $(J-H)$ and $(H-K_s)$ colors redden during in the eclipse event consistent with variable extinction.

The physical interpretation for the observed variability is identical to that of YLW 1C. The 1.6 day period corresponds to the stellar rotation rate and the 3.0 day period arises from a periodic occultation by an asymmetry in the inner circumstellar disk. The occulter size and distance are $2.8 R_\star$ and $\sim 3.0 R_\star$. Differing from YLW 1C, the occulter for J543 is located approximately a stellar radius beyond the co-rotation radius.

- YLW 10C (ISO-Oph 122): YLW 10C is the third CTTS where two distinct periods are identified. Fig 37 contains the K_s , $(J-H)$ and $(H-K_s)$ photometry folded to the sinusoidal-like period, $P = 3.0779 \pm 0.0025$ days. The peak-to-trough ΔK_s amplitude for this variability is 0.25 mag. Fig 38 contains the K_s , $(J-H)$ and $(H-K_s)$ photometry folded to the eclipse-like period, $P = 2.9468 \pm 0.0029$ days. The ΔK_s eclipse depth is 0.28 mag. Unfortunately, both the J and H photometry are below the survey completeness limits preventing the identification of either variability mechanism.

Given the sinusoidal-like and eclipse-like variability is very similar to both YLW 1C and J543, the same physical interpretation is proposed for this star. However, unlike YLW 1C, the sinusoidal-like variability, presumed to trace the stellar rotation rate, has a longer period by 3.1 hours than the periodic occultations. This places the hypothetical occulter *within* the co-rotation radius. The size and distance to the occulter are $3.31 R_\star$ and $3.75 R_\star$. The occulter is located within the dust sublimation radius as computed using the formulism of Jura & Turner (1998). This formulism is only an approximation as it does not take into account dust evaporation and condensation rates, grain size, or grain composition.

- WL 20W (YLW 11B, ISO-Oph 126): This CTTS is both periodically variable and variable over a long time-scale. As such, WL 20W is designated both a periodic variable and a LTV. Fig 39 contains the K_s , $(J-H)$ and $(H-K_s)$ photometry for this star. The long time-scale variability begins on ~ 1600 2MASS MJD and has a timescale of 122 days. The ΔK_s depth is 0.26 mag. Both the $(J-H)$ and $(H-K_s)$ colors become redder during the long time-scale variation, consistent with variable extinction. The periodic signal is not significant unless the time-series affected by the long time-scale variability is omitted from analysis by the PA (see Fig 11). Fig 40 contains the K_s , $(J-H)$ and $(H-K_s)$ photometry folded to the sinusoidal-like period, $P = 2.1026 \pm 0.0060$ days. The peak-to-trough ΔK_s amplitude for the sinusoidal-like variability is 0.19 mag. Neither the $(J-H)$ nor the $(H-K_s)$ color is correlated to the K_s variability. This favors rotational modulation by cool starspots as the variability mechanism.

The variability of AA Tau has been cited as an explanation for the periodic eclipsing

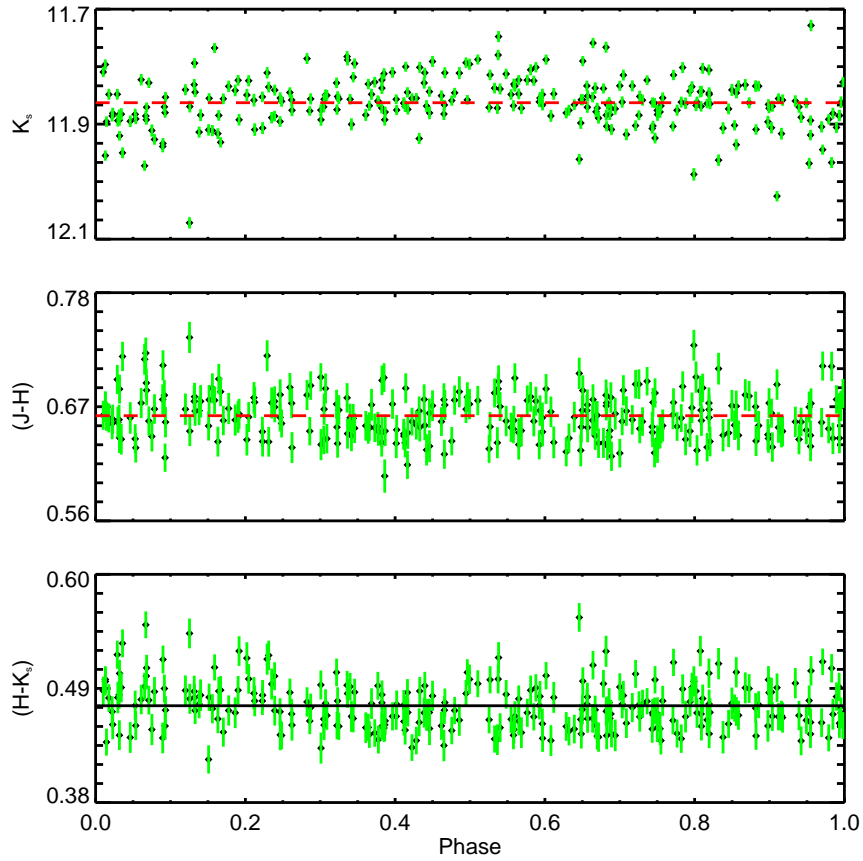


Fig. 35.— The K_s , $(J-H)$ and $(H-K_s)$ photometry for J543 phased to the 1.52921 ± 0.00065 day sinusoidal-like period. The red line indicates the mean value in each panel. The lack of color correlation with ΔK_s points to rotational modulation of cool starspots as the variability mechanism.

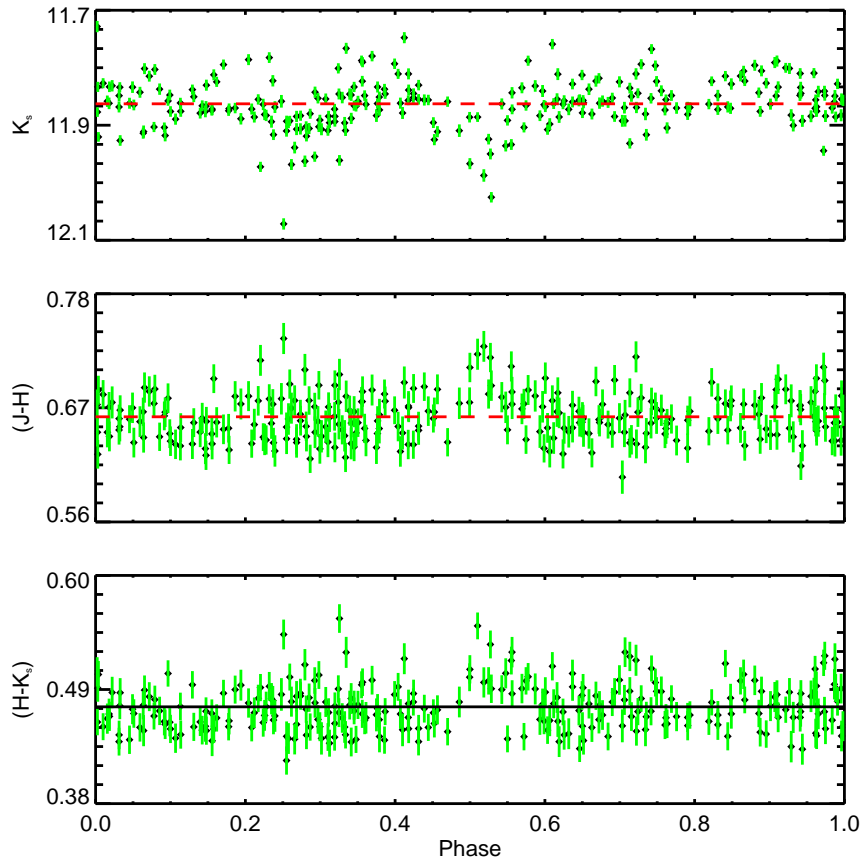


Fig. 36.— The K_s , $(J-H)$ and $(H-K_s)$ photometry for J543 phased to the 2.9602 ± 0.0013 day eclipse-like period. The red line indicates the mean value in each panel. Both colors become redder as K_s dims indicating variable extinction as the likely variability mechanism.

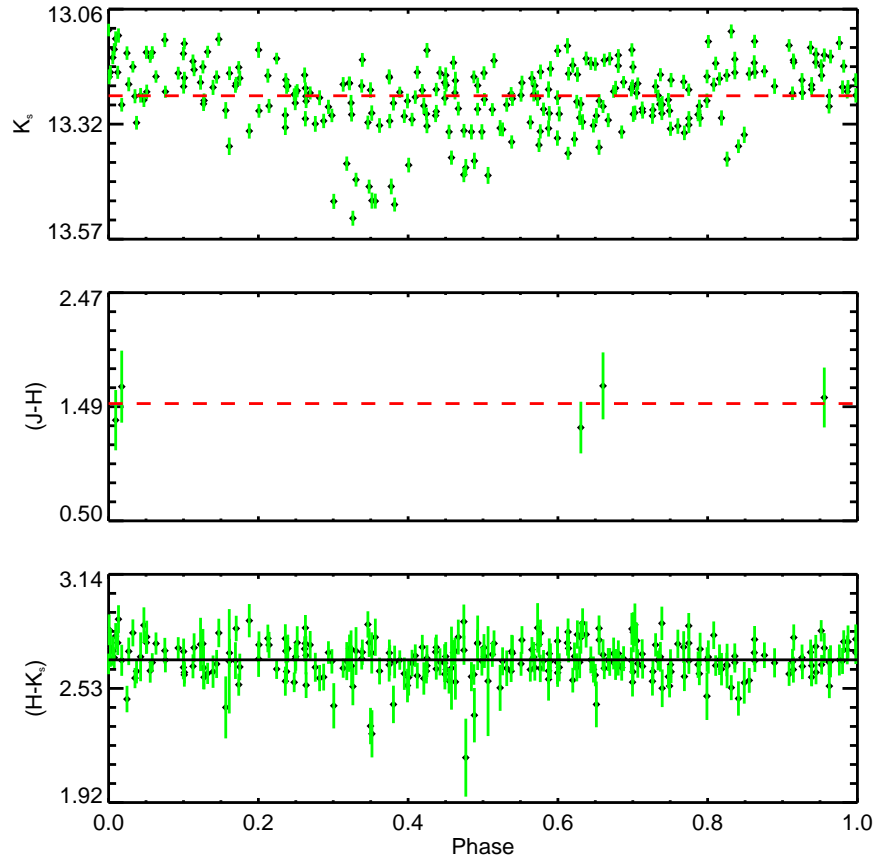


Fig. 37.— The K_s , $(J-H)$ and $(H-K_s)$ photometry for YLW 10C phased to the 3.0779 ± 0.0025 day sinusoidal-like period. The red line indicates the mean value in each panel. The lack of reliable J and H photometry prohibits a confident estimate of the variability mechanism.

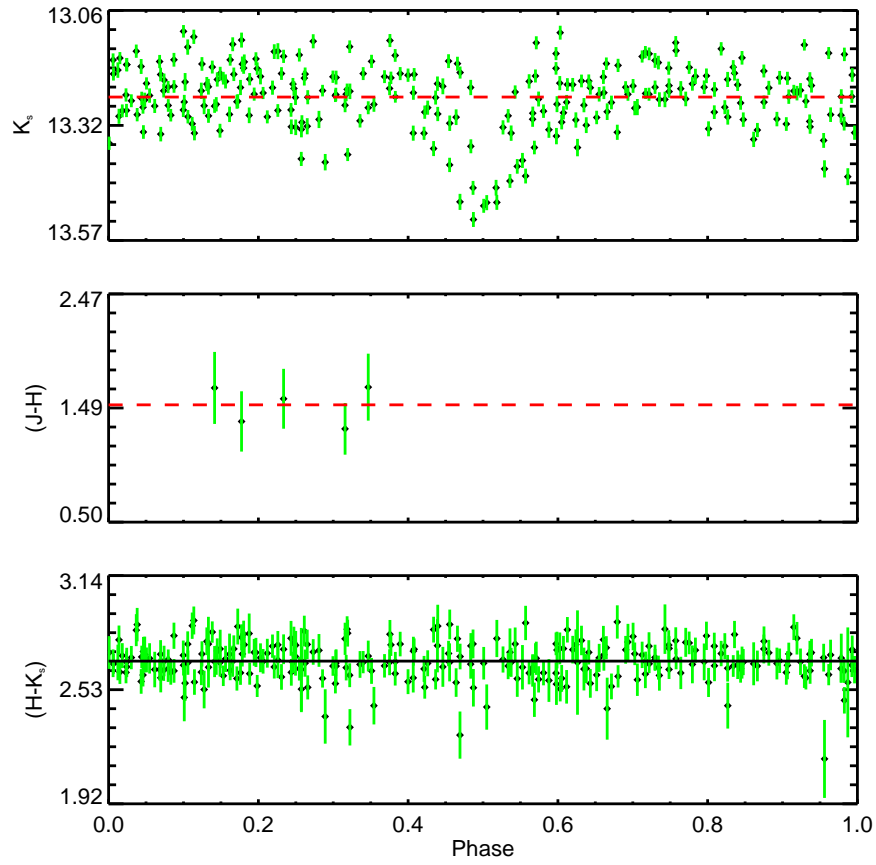


Fig. 38.— The K_s , $(J-H)$ and $(H-K_s)$ photometry for YLW 10C phased to the 2.9468 ± 0.0029 day eclipse-like period. The red line indicates the mean value in each panel.

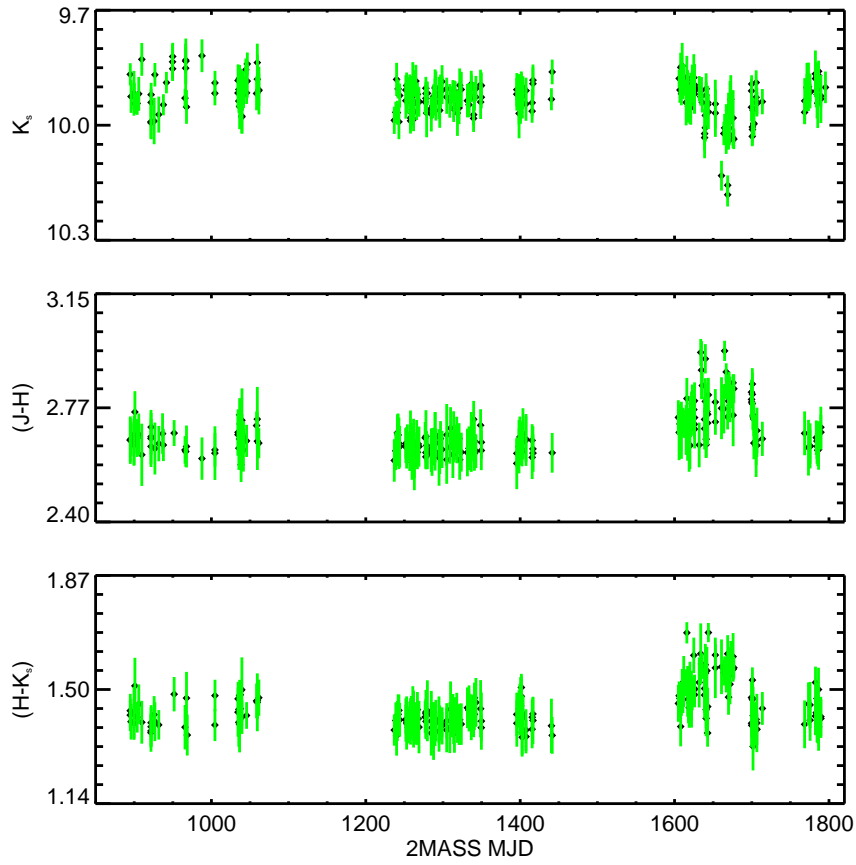


Fig. 39.— The K_s , $(J-H)$ and $(H-K_s)$ photometry for WL 20W. The long time-scale variation is easily seen beginning at ~ 1600 2MASS MJD. Both the $(J-H)$ and $(H-K_s)$ become redder as K_s dims indicating variable extinction as the likely variability mechanism.

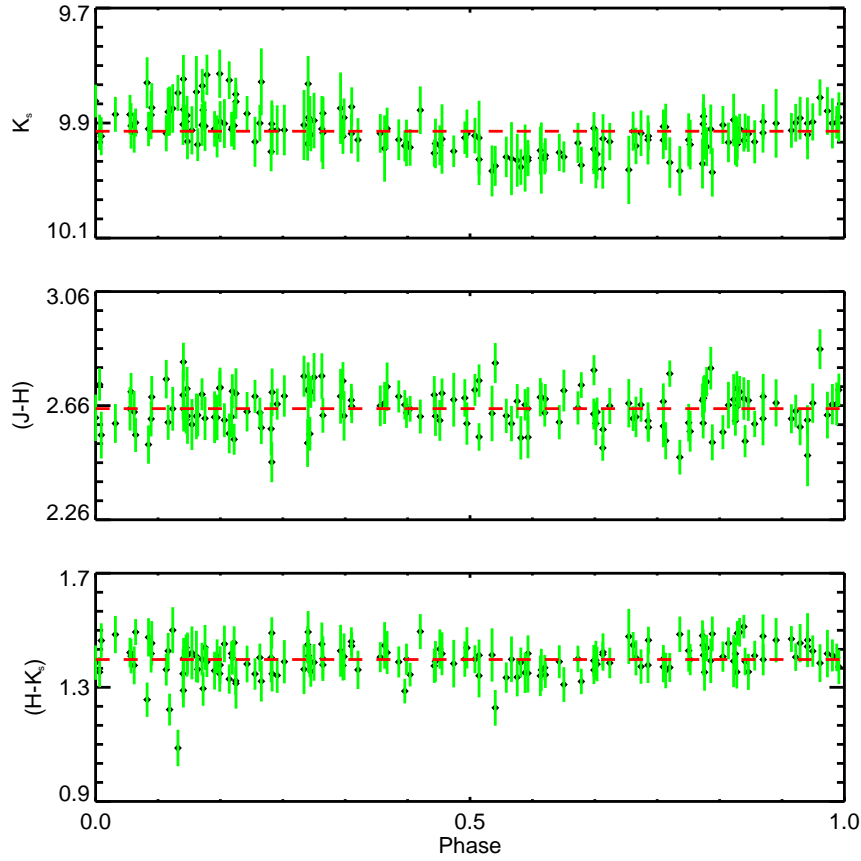


Fig. 40.— The K_s , $(J-H)$ and $(H-K_s)$ photometry for WL 20W folded to the period 2.1026 days. The red line indicates the mean value in each panel. No correlation between ΔK_s and the change in colors points to rotational modulation of cool starspots as the likely variability mechanism. Only the photometry before the time-scale variation is plotted.

variables in this survey. However recently it has been discovered that AA Tau is exhibiting a long time-scale dimming on the order of 2-3 mag in the V band (Bouvier et al. 2013). This long time-scale variation is superimposed on top of the periodic variability. Additionally the system appears to become bluer in this dim state; a phenomenon seen in UX Ori-type variables (Grinin et al. 1991; Herbst et al. 1994). The physical interpretation for UX Ori-type variability is that the star dims due to an asymmetric optically thick occulter beyond the inner circumstellar disk. The bluer color represents a larger contribution of scattered starlight off the occulting material.

This scenario is an alternative explanation than variable mass accretion for the long time-scale variation observed in WL 20W. The eclipse depth corresponds to a 2.9 mag dimming when converted to the V band by using the extinction coefficients given in Cohen et al. (1981); this is consistent with the AA Tau long time-scale variation. The $(J-H)$ and $(H-K_s)$ colors do become bluer during the long time-scale variation also consistent with the observations of AA Tau. Our overall interpretation for the variability in WL 20W is a central star rotating with a 2 day period that is occulted by a pocket of optically thick material located beyond the inner circumstellar disk.

It is worth noting this star belongs to a triple system that is spatially resolved in the mid-IR. Ressler & Barsony (2001) show the most variable member is, in fact, WL 20S. They classify this source as Class I through SED fitting of mid-IR photometry. They show that WL 20E and WL 20W are nearly constant on decadal timescales whereas the flux of WL 20W increased sixfold in 15 years. As the largest separation between these components is $3.66''$, the large aperture size in our work ($4''$) includes all three stars and thus cannot rule out the possibility that the measured variability arises from this southern component.

- ISO-Oph 126: This WTTS is similar to WL 20W in that it exhibits both periodic variability and a long time-scale variation. ISO-Oph 126 is also designated both a periodic variable and a LTV. Fig 41 contains the K_s , $(J-H)$ and $(H-K_s)$ photometry for this star. The J band photometry is below the survey completeness limits. Therefore the $(J-H)$ color is deemed unreliable for analysis. The long time-scale variation dominates the photometry prior to 1400 2MASS MJD with a time-scale of 349 days. The ΔK_s depth of this variation from the continuum brightness is 0.10 mag. The $(H-K_s)$ color becomes redder during the long time-scale variation as the star dims. This is consistent with extinction as the variability mechanism. The PA identifies a significant periodic signal when only the portion of the time-series after 1400 2MASS MJD is analyzed (see Fig 11). Fig 42 contains the K_s , $(J-H)$ and $(H-K_s)$ photometry folded to the sinusoidal-like period, $P = 9.114 \pm 0.090$ days. The peak-to-trough ΔK_s amplitude for the sinusoidal-like variability is 0.06 mag. The $(H-K_s)$ color becomes

bluer as K_s brightens favoring a variability mechanism of rotational modulation by accretion-induced hot starspots.

While the origin of the periodic variability can be attributed to stellar surface features, the favored interpretation of extinction in this case potentially challenges the class identification as a diskless WTTS. While Barsony et al. (2005) could not provide a YSO classification for ISO-Oph 126, the authors could place an upper limit to the spectral index at ≤ -0.88 . This allows for the possibility this star is Class II and surrounded by an optically thick accretion disk.

One intriguing option is the occultation by a disk surrounding an orbital companion. This scenario is invoked to explain long time-scale variability in evolved star systems ϵ Aur (Guinan & Dewarf 2002; Kloppenborg et al. 2010; Stencel et al. 2011), EE Cep (Mikolajewski & Graczyk 1999; Graczyk et al. 2003; Mikolajewski et al. 2005; Gałan et al. 2010) and most recently in the young star system 1SWASP J140747.93-394542.6 (‘J1407’) (Mamajek et al. 2012). Photometric variations within the long time-scale variations are believed to arise from structure within the occulting disk. This structure may represent new planets (EE Cep (Gałan et al. 2010)), or it may represent planetary moons (J1407 (Mamajek et al. 2012)). It is noted that there is significant scatter in the K_s time-series during the first half of the long time-scale variation in comparison to the second half of this variation (see Fig 43). High resolution imaging or radial velocity monitoring may help to confirm the existence of a companion to ISO-Oph 126.

- WL 15 (YLW 7A, ISO-Oph 108): This star is one of the brightest at K_s ($\overline{K_s} = 7.05$ mag) and the reddest ($\overline{(H - K_s)} = 4.01$ mag) in the variable catalog. WL 15 is a Class I YSO. Similar to WL 20W and ISO-Oph 126, this star exhibits a large amplitude, long time-scale variation over-top of a smaller amplitude periodic variability. Unlike WL 20W and ISO-Oph 126, the photometry during the long time-scale variation is too sparse to confidently identify a time-scale. Therefore WL 15 is only designated a periodic variable. Fig 44 contains the K_s , $(J-H)$ and $(H-K_s)$ photometry for WL 15. The J band photometry is below the survey completeness limit and is deemed unreliable for analysis. The long time-scale variation is observed between 1396 and 1443 2MASS MJD with a ΔK_s amplitude of ~ 1 mag. The mean $(H-K_s)$ color does not change as the star dims during this event. Even including the long time-scale variation, the PA found a significant periodic signal. Fig 45 contains the K_s , $(J-H)$ and $(H-K_s)$ photometry for WL 15 folded to the sinusoidal-like period, $P = 19.412 \pm 0.085$ days. This variability has a peak-to-trough ΔK_s amplitude of 0.90 mag. The $(H-K_s)$ color is not correlated to the K_s photometry.

While the colorless periodic variability favors rotational modulation by cool starspots, the amplitude of variability does not. The highest amplitude variability confirmed

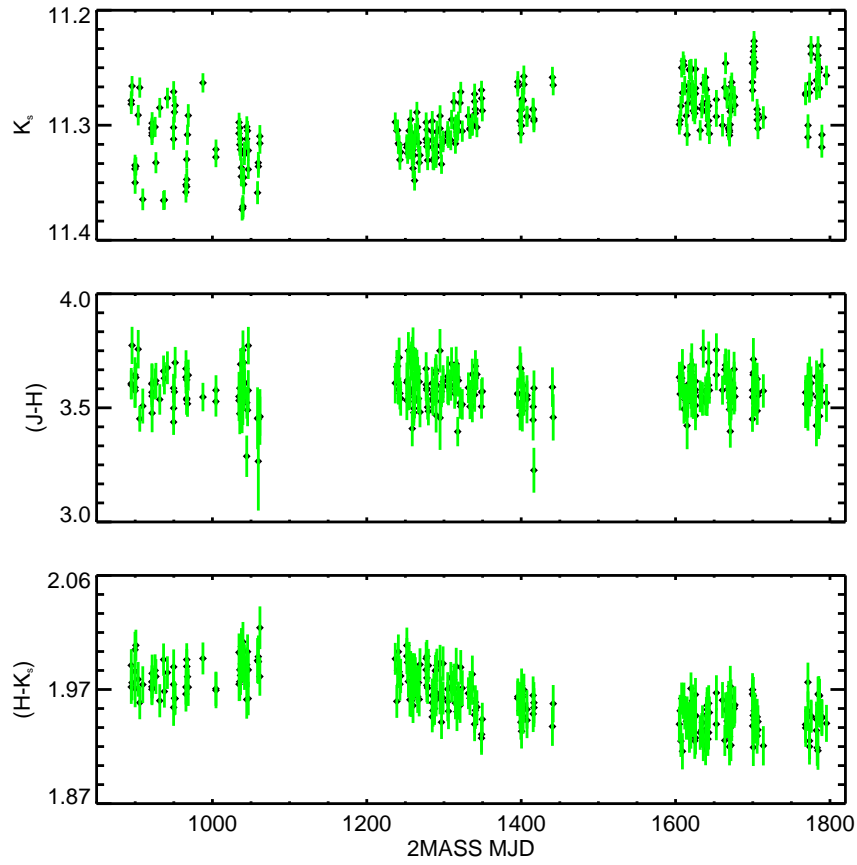


Fig. 41.— The K_s , $(J-H)$ and $(H-K_s)$ photometry for ISO-Oph 126. The long time-scale variation is easily seen prior to ~ 1400 2MASS MJD. Both the $(J-H)$ and $(H-K_s)$ become redder as K_s dims indicating variable extinction as the likely variability mechanism.

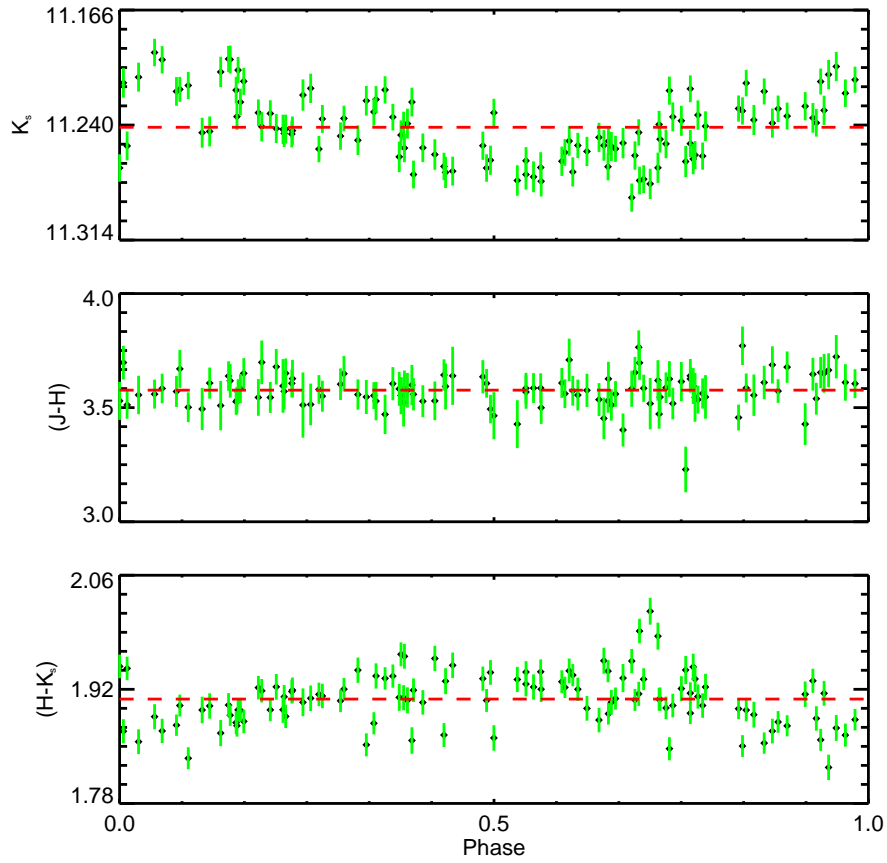


Fig. 42.— The K_s , $(J-H)$ and $(H-K_s)$ photometry for ISO-Oph 126 folded to the period 9.114 days. The red line indicates the mean value in each panel. The $(H-K_s)$ color becomes bluer as K_s brightens favoring a variability mechanism of rotational modulation by accretion-induced hot starspots.



Fig. 43.— The K_s and $(H-K_s)$ photometry for the long time-scale variation in ISO-Oph 126. The K_s shows considerable structure during ingress, but is nearly stable during the “eclipse” egress. The red line indicates the mean magnitude of the continuum photometry.

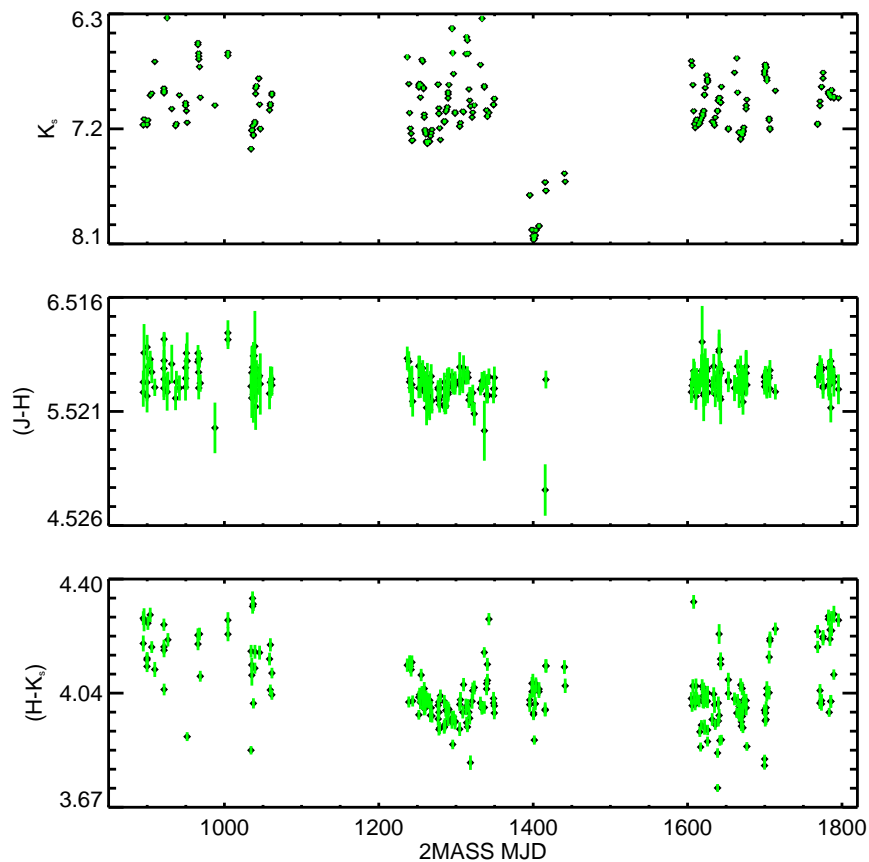


Fig. 44.— The K_s , $(J-H)$ and $(H-K_s)$ photometry for WL 15. The ~ 19 day period is clearly evident and appears to continue even through a ~ 1 mag drop in K_s band flux. The photometry during the larger amplitude flux decrease is too sparse to confidently determine a time-scale. A lack of a trend in the $(H-K_s)$ color during this event highly suggests against extinction except by an opaque occulter.

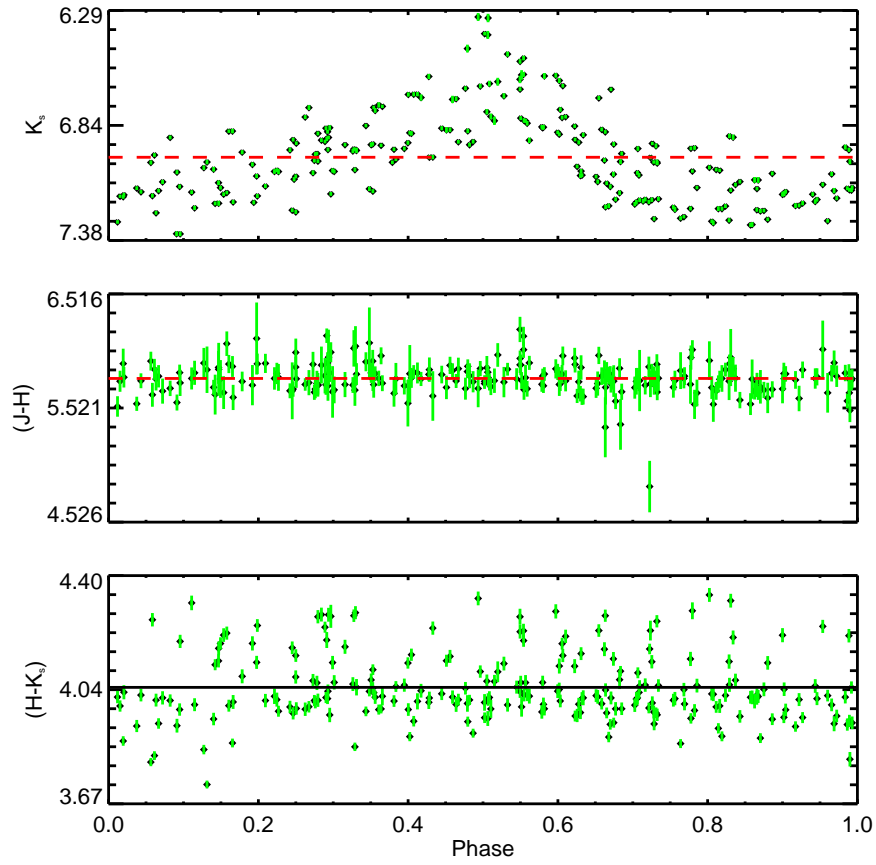


Fig. 45.— The K_s , $(J-H)$ and $(H-K_s)$ photometry for WL 15 folded to the period 19.412 days. The red line indicates the mean value in each panel.

to as caused by cool starspots, to date, is $\Delta V = 0.63$ mag (Strassmeier et al. 1997). This amplitude is nearly 0.3 mag lower than that observed for WL 15. In addition, the contrast between the starspot and surrounding photosphere increases toward bluer wavelengths. Therefore the amplitude will be even larger in the optical. The origin behind the long time-scale variation is equally peculiar. As the $(H-K_s)$ color does not become redder as the star dims, this seems to eliminate extinction as variability mechanism. However, variability by rotational modulation of surface features seems implausible given the timescale and amplitude of the variation.

6. SUMMARY

High precision, high cadence J , H , K_s photometry is obtained for 7815 stars in the direction of the ρ Oph molecular cloud with a temporal baseline of ~ 2.5 yrs. Spurious detections, partially resolved doubles or galactic contamination are eliminated from the photometry. The target sample meeting the specifications for time-series variability analysis includes 1678 stars. A seven point variability test is used to identify 101 variable stars, which is 6% of the parent sample. These tests are sensitive to variability on a variety of different time-scales and forms (e.g. sinusoidal, 'eclipse-like', etc.).

Of the 101 stars in the variable catalog, 15% are located “on cloud” while only 1% lie within the “field”. Location “on cloud”, variability and $(H-K_s)$ colors redder than a 3 Myr isochrone are used to estimate membership in the ρ Oph star forming region. This method has identified 22 stars as previously unknown candidate ρ Oph members.

The effects of observing strategy on variability detection and measured amplitudes is investigated by comparing this work to the ρ Oph variability study performed by Alves de Oliveira & Casali (2008). These two studies have 464 stars in common; AC08 identified 7% as variable stars and this work identifies 18%. The increase in detection fraction is not caused by different sensitivities in the separate variability criteria used in each survey. This work also found both a higher K_s and $(H-K_s)$ color amplitude in 25 stars identified as variable in both surveys than measured by AC08. Therefore a high cadence observational strategy will discover more variables within a given set of stars and it will more accurately characterize intrinsically higher amplitude variability.

The K_s variability and stellar color behaviors are used to estimate the physical mechanism responsible for the variability. Rotational modulation by long-lived cool starspots is expected to produce colorless, periodic variability. Rotational modulation of long-lived hot starspots (e.g. accretion) is, also, expected to be periodic, while short-lived starspots (e.g.

flares) is not. The star becomes bluer as it brightens in both cases. Extinction induced variability is either periodic or exists on long time-scales based on the geometry of the occulter relative to the star. Changes in the mass accretion rate onto the star is not expected to be periodic, but occur on time-scales ranging from days to years. As this rate changes, the star becomes bluer as the star dims.

Identifying periodic variability within the variable catalog is done via a newly improved period-searching algorithm, the Plavchan algorithm. The algorithm tests tens of thousands of periods with uniform frequency sampling between 0.1 to 1000 days. This is done by comparing the observed light curve to a dynamically generated prior. The statistical significance of individual periods is computed via two methods: the distribution of power values at other periods in the same periodogram and the distribution of maximum power values for all sources in an ensemble survey. The Plavchan algorithm finds periodic variability in 32% of the variable catalog with periods ranging from 0.49 to 92 days.

The periodic variables are split into two sub-categories: sinusoidal-like and eclipse/inverse eclipse-like. Sinusoidal-like periodic variability describes a sinusoidal-like change in the observed flux when the time-series is folded to the most significant period. Rotational modulation by cool starspots is believed to be the common variability mechanism in this sub-category. Sinusoidal-like periodic variables are found in each YSO class (3 Class I, 8 Class II, 8 Class III). Eclipse-like periodic variability results in discrete drops, or “dips”, in the observed flux when the time-series is folded to the most significant period. Periods range from 2 to 8 days with the duration of these dips lasting less than 30% of one periodic epoch. This sub-category contains 6 stars with a median peak-to-trough ΔK_s and $\Delta(H-K_s)$ color amplitudes of 0.31 and 0.11 mag, respectively. Variable extinction is the likely mechanism for the eclipse-like variations. All stars in this sub-category are Class II YSOs. The inverse eclipse-like variables, WL 4 and YLW 16A have periods of 65.61 and 92.3 days, respectively. The variability mechanism proposed in both cases is the periodic obscuration of one component in a close binary by a warped circumbinary disk.

In half of the eclipse-like variables (YLW 1C, 2MASS J16272658-2425543, YLW 10C) an additional statistically significant period is identified. This sinusoidal-like periodic variability coupled with the presence of “dips” suggests a rapidly rotating spotted star occulted by a clump of optically thick material in the inner accretion disk. These stars strengthen the interpolation posed to explain the variability of other YSO AA Tau-like variables (Morales-Calderón et al. 2011). The periods corresponding to periodic occultations in YLW 1C and YLW 10C are located near their respective co-rotation radii. The mechanism driving these occultations could arise from a warped inner circumstellar disk caused by an inclined magnetic dipole, or could be the pre-natal cloud of a forming hot Jupiter.

Long time-scale variables is a variability subclass, containing 31 stars, where the measured flux increases or decreases consistently over months or years. The variability time-scale is measured using a differencing technique and approximates the time between maximum and minimum brightness. The measured time-scales range from 64 to 790 days. The peak-to-trough ΔK_s amplitudes range from 0.05 to 2.31 mag and the peak-to-trough $\Delta(H-K_s)$ color amplitudes range from 0.06 to 1.32 mag. Variable extinction and variable accretion rates are both equally likely to cause long time-scale variability. This subclass contains 25 known YSOs with 7 Class I, 15 Class II and 3 Class III stars.

The time-series of irregular variables are aperiodic and do not vary over any discernible time-scale. This subclass contains more members (40) than either the periodic or long time-scale subclasses. The peak-to-trough ΔK_s amplitudes range from 0.04 to 1.11 mag and peak-to-trough $\Delta(H-K_s)$ color amplitudes range from 0.05 to 0.75 mag. No single dominant variability mechanism explains irregular variability. Only 9 known YSOs (1 Class I, 7 Class II, 1 Class III) are irregular variables.

The CTTS WL 20W and the WTTS ISO-Oph 126 are similar in both have a long time-scale variation superimposed onto a periodic signal. In both cases, the physical mechanisms for the variability is consistent with an occultation of a rapidly rotating spotted star by optically thick material outside the inner accretion disk. For WL 20W, the sinusoidal-like variability has a period of 2.1026 days and a peak-to-trough ΔK_s amplitude of 0.19 mag. The long time-scale variability has a duration of 122 days with a ΔK_s eclipse depth of 0.26 mag. For ISO-Oph 126, the sinusoidal-like variability has a period of 9.114 days and a peak-to-trough ΔK_s amplitude of 0.06 mag. The long time-scale variability has a duration of 349 days with a ΔK_s eclipse depth of 0.10 mag.

The very high amplitude periodic variability measured in the Class I star WL 15 is not consistent with any proposed mechanism. The observed 47 day colorless decrease in K_s band brightness of ~ 1 mag is also not easily estimated.

From cross-referencing the target sample with two previous surveys, 72 stars have been assigned a YSO classification (13 Class I, 47 Class II, 12 Class III). The variability fraction of these YSOs is 79%. The variability fraction differs according to YSO class with 92% of Class I and Class III stars identified as variable; this fraction drops to 72% for Class II stars. The amplitude of both brightness and color variability are decreasing functions of YSO class. The median peak-to-trough ΔK_s amplitude for Class I, II and III stars are 0.77, 0.31 and 0.08 mag, respectively. In addition, the median peak-to-trough $\Delta(H-K_s)$ color amplitudes are 0.81, 0.21 and 0.07 mag for each class respectively.

We will now express our thanks to our anonymous referee for their conversation and

comments. We would also like to express our thanks to Mary Barsony for her many insightful questions and suggestions. This publication makes use of data products from the Two Micron All Sky Survey, which is a joint project of the University of Massachusetts and the Infrared Processing and Analysis Center/California Institute of Technology, funded by the National Aeronautics and Space Administration and the National Science Foundation. This research has made use of the NASA Exoplanet Archive, which is operated by the California Institute of Technology, under contract with the National Aeronautics and Space Administration under the Exoplanet Exploration Program. The authors would like to acknowledge the Infrared Processing and Analysis Center’s Visiting Graduate Student program for providing the opportunity and funding for this publication.

APPENDIX. Empirical Determination of $\chi_{n_0}^2$ Dependence on Parameters

In this Appendix an analysis of the dependence of the PA periodogram $\chi_{n_0}^2$ power values on the number of observations and periodogram parameters n_0 and p is presented. The ensemble survey of mostly non-variable stars is used to carry out this analysis and to present an alternative approach to evaluate the statistical significance of periodogram power values.

First, a random subset of 180 stars is chosen from the survey collection of 1678 stars. These stars are evenly distributed in N_{obs} and K_s magnitude. For a given set of parameters p and n_0 , the maximum $\chi_{n_0}^2$ periodogram power value is computed for the 180 stars. Since other algorithms exist that specialize in finding periodic sources with low numbers of detection (Dworetzky 1983, $N_{obs} \sim 20$), test cases are limited to $0.04 < p$ and ≤ 0.5 and $12 < n_0 \leq 250$. Fig A-1 shows the dependence of $\chi_{n_0}^2$ on N_{obs} for the 180 stars with a particular set of p and n_0 . This dependence is somewhat expected – a smaller number of observations can result in an increase in the likelihood for false-positive periodogram peaks.

The distribution of $\chi_{n_0}^2$ values as a function of N_{obs} is well-described by the functional form:

$$F(N_{obs}) = \left(\frac{a}{N_{obs} - b}\right)^{1.5} + c \tag{A-1}$$

where a , b and c represent real numbers that differ for a given p and n_0 . As the power law index decreases below 1.5 for $p < 0.04$ and/or $n_0 < 12$, these ranges are excluded from the analysis. Eqn A-1 is found via trial and error to minimize the residuals when compared to a variety of functional forms tested, rather than from an analytic derivation based upon first principles.

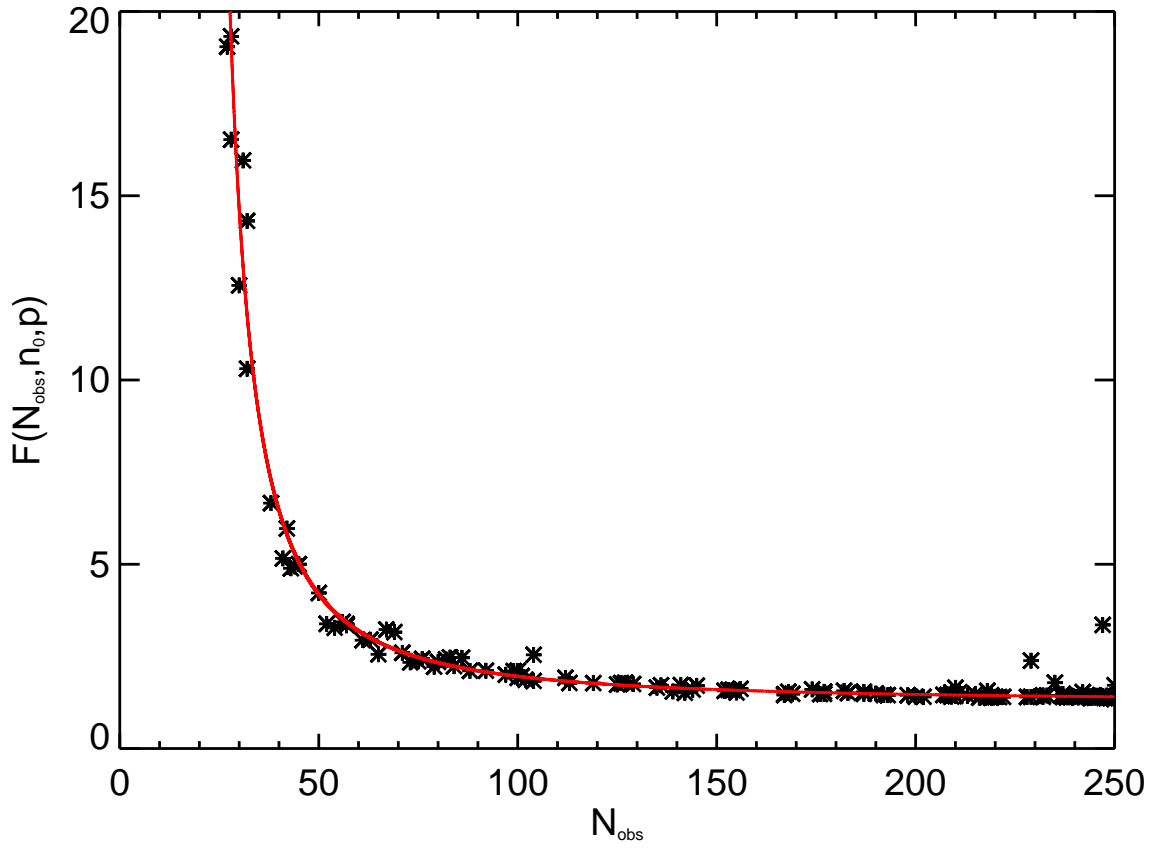


Fig. A-1.— Graph of the $\chi_{n_0}^2$ value as a function of detection size, N_{obs} , for the test case with the parameters: $n_0 = 25$ and $p = 0.06$. The red line represents the functional fit of Eqn A-1 with values of $(a,b,c) = (62.5495,18.4963,1.2523)$ where the residuals are minimized.

The next step is to determine how the constants a , b and c vary as functions of the parameters p and n_0 . Fixing n_0 , the maximum $\chi_{n_0}^2$ as a function of N_{obs} is empirically fit to 10 chosen p values resulting in 10 different values of a , b and c . The same process is repeated except p is fixed and n_0 is varied. Fig A-2 displays the dependence of a on the parameters p and n_0 . Six fits to the dependence of a , b and c on parameters p and n_0 are determined empirically through trial and error to be:

$$f_a(n_0) = -0.3491(n_0 - 17.0796)e^{-0.0451n_0} + 63.4573 \quad (\text{A-2a})$$

$$f_b(n_0) = 1.3023\left(1 - \frac{23.3762}{n_0}\right)e^{-0.0283n_0} + 18.4347 \quad (\text{A-2b})$$

$$f_c(n_0) = 0.2796e^{-0.0381n_0} + 1.1467 \quad (\text{A-2c})$$

$$f_a(p) = 82.6288e^{-12.1989p} + 25.4356 \quad (\text{A-3a})$$

$$f_b(p) = 3.0791p^{-0.6377} \quad (\text{A-3b})$$

$$f_cp = (p - 0.0305)^{-0.0395} + 0.0905 \quad (\text{A-3c})$$

The particular functional forms of A-2 and A-3 are again not analytically motivated, but instead minimize the residuals from a variety of functional forms tested.

These six functions of one parameter are combined into three functions of both parameters p and n_0 . This is accomplished by replacing the constant term in the n_0 function by the entire corresponding p function. The constant term from $f_c(p)$ function is also dropped. Thus, the following functions are found to adequately describe the dependence of a , b and c on parameters p and n_0 for this survey:

$$f_a(n_0, p) = -0.3491(n_0 - 17.0796)e^{-0.0451n_0} + 82.6288e^{-12.1989p} + 25.4356 \quad (\text{A-4a})$$

$$f_b(n_0, p) = 1.3023\left(1 - \frac{23.3762}{n_0}\right)e^{-0.0283n_0} + 3.0791p^{-0.6377} \quad (\text{A-4b})$$

$$f_c(n_0, p) = 0.2796e^{-0.0381n_0} + (p - 0.0305)^{-0.0395} \quad (\text{A-4c})$$

and therefore Eqn A-1 can be rewritten as:

$$F(N_{obs}, n_0, p) = \left(\frac{f_a(n_0, p)}{N_{obs} - f_b(n_0, p)}\right)^{1.5} + f_c(n_0, p) \quad (\text{A-5})$$

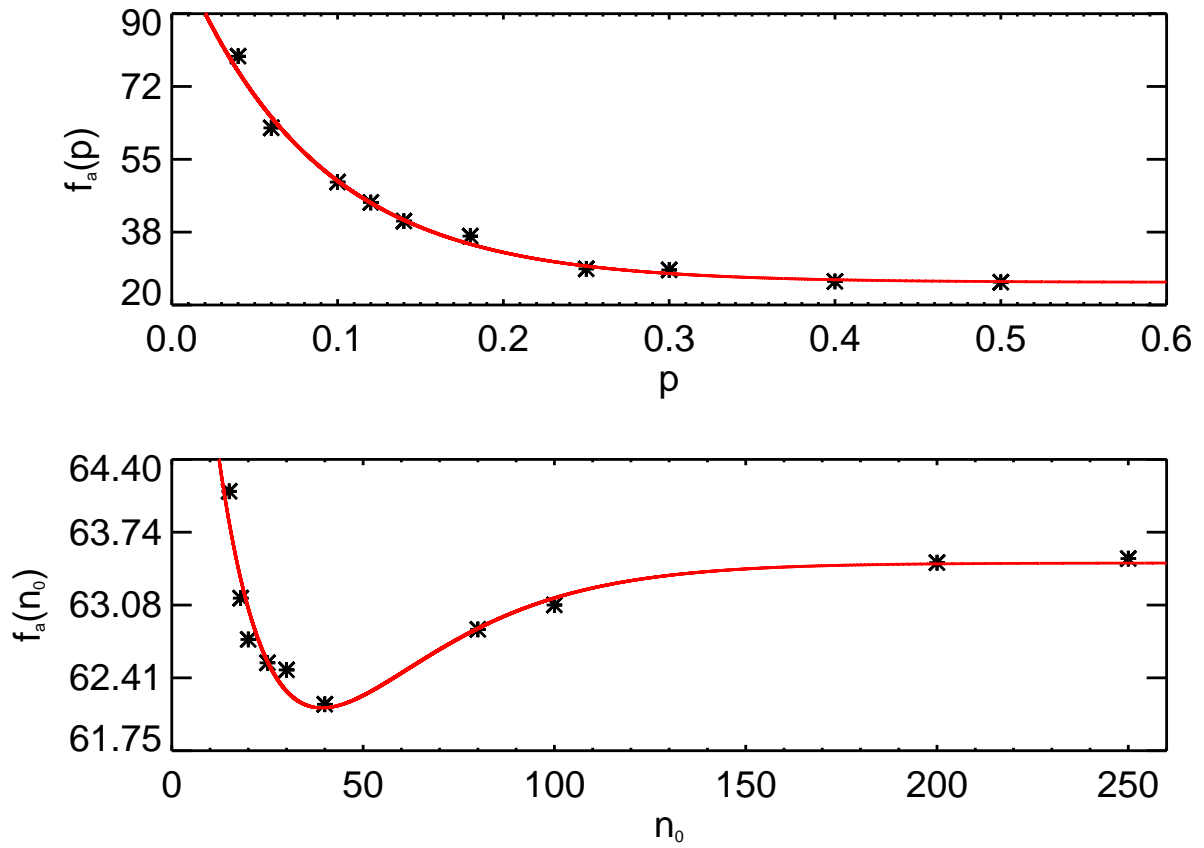


Fig. A-2.— *Top*: Graph of the constant a as a function of parameter p (see Eqn A-3a). *Bottom*: Graph of the constant a as a function of parameter n_0 (see Eqn A-2a).

The values p and $n_0 = 40$ – used throughout this paper to identify periodic variables – are an optimal choice of parameters for this survey. They yield the smallest residuals when the 180 test cases are fit in Eqn A-5. Thus, for this survey the maximum peak power in the periodogram for a non-variable star is approximately given by the expression:

$$F(N_{obs}, 40, 0.06) = \left(\frac{63.8629}{N_{obs} - 18.6927} \right)^{1.5} + 1.2100 \quad (\text{A-6})$$

The validity of the numerical fits (Eqns A-4(a-c)) is verified using an additional 18 test cases with randomly selected values of p and n_0 . The $\chi_{n_0}^2$ versus N_{obs} distributions are again fit using Eqn A-1, yielding 18 “observed” a , b and c values for each pair of p and n_0 . Predicted values for a , b and c are found by using Eqns A-4(a-c) and compared to the “observed” values. The mean percent errors between the observed and predicted values for the 18 test cases are $-1.1 \pm 3.4\%$ for f_a , $1.1 \pm 3.5\%$ for f_b and $-0.1 \pm 1.8\%$ for f_c . Table A-1 contains the percent errors for each of the individual 18 test cases. Eqns A-4(a-c) therefore adequately predict the values a , b and c in Eqn A-1 for any set of parameters p and n_0 within the parameter space explored in this survey. Thus, this demonstrates the PA algorithm is reasonably “well-behaved.” Eqn A-5 could be applied to different surveys and cadences. However, the particular numerical values in Eqns A-4 and A-6 for a , b and c likely depend on the specific cadence of a survey.

To evaluate the statistical significance of a peak period power value in a periodogram, it does not suffice to identify the expected value for the ensemble survey. The scatter about the expected value is also necessary. This scatter, or standard deviation (σ), of the peak period power values about the expected value depends on N_{obs} in a predictable fashion for this survey (Fig A-3). To characterize this scatter, the scatter for each survey star is grouped into bins as a function of N_{obs} , with a bin size of 25. An average σ is computed for each bin and an empirical fit to this distribution is made, given by Eqn A-7:

$$\sigma(N_{obs}) = \frac{2.3790}{N_{obs} - 21.6449} + 0.0105 \quad (\text{A-7})$$

Putting it all together, now an affirmative periodicity condition can be defined. The statistical significance of a measured period for a star in this survey is simply a function of the number of observations. Based on visual inspection of star light curves, this condition is defined by the following:

$$\frac{\chi_{n_0,i}^2}{F(N_{obs_i}, n_0, p)} - 1 > 6\sigma(N_{obs_i}) \quad (\text{A-8})$$

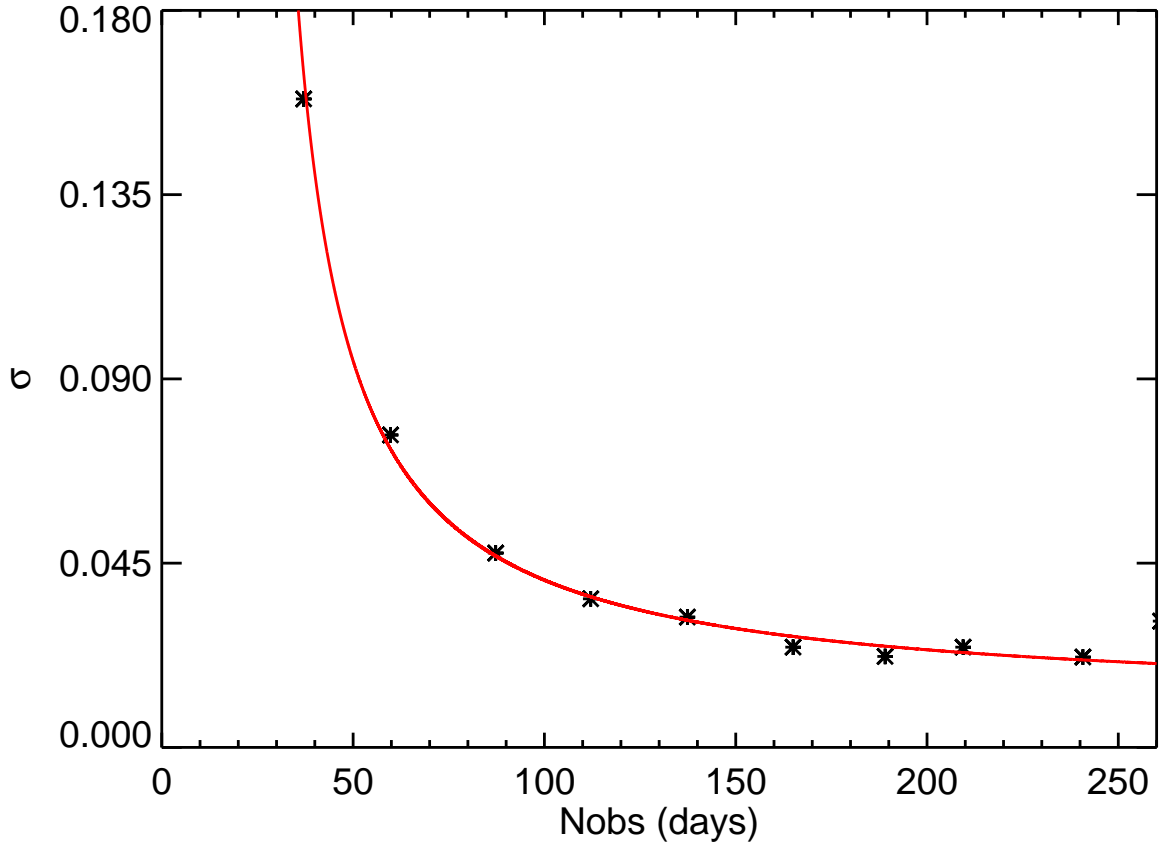


Fig. A-3.— The maximum PA periodogram power value for a star in this survey is found to be well-described by Eqn A-5 (Fig A-1). The scatter about the value predicted by Eqn A-5, σ , is also found to be dependent on N_{obs} as shown in this figure.

Periods where this condition is met can be considered statistically significant for the star investigated. Periods found using this criteria are generally also found to be statistically significant using the methods outlined in §4.1.

REFERENCES

- Alves de Oliveira, C., & Casali, M. 2008, *A&A*, 485, 155
- Armitage, P. J. 1995, *MNRAS*, 274, 1242
- Baraffe, I., Chabrier, G., Allard, F., & Hauschildt, P. H. 1998, *A&A*, 337, 403
- Barsony, M., Kenyon, S. J., Lada, E. A., & Teuben, P. J. 1997, *ApJS*, 112, 109
- Barsony, M., Ressler, M. E., & Marsh, K. A. 2005, *ApJ*, 630, 381
- Bertout, C. 2000, *A&A*, 363, 984
- Bok, B. J. 1956, *AJ*, 61, 309
- Bontemps, S., et al. 2001, *A&A*, 372, 173
- Bouvier, J., Grankin, K., Ellerbroek, L., Bouy, H., & Barrado, D. 2013, *ArXiv e-prints*
- Bouvier, J., et al. 2003, *A&A*, 409, 169
- Cambrésy, L. 1999, *A&A*, 345, 965
- Carpenter, J. M., Hillenbrand, L. A., & Skrutskie, M. F. 2001, *AJ*, 121, 3160
- Carpenter, J. M., Hillenbrand, L. A., Skrutskie, M. F., & Meyer, M. R. 2002, *AJ*, 124, 1001
- Cohen, J. G., Persson, S. E., Elias, J. H., & Frogel, J. A. 1981, *ApJ*, 249, 481
- Cutispoto, G., Messina, S., & Rodonò, M. 2001, *A&A*, 367, 910
- . 2003, *A&A*, 400, 659
- Cutri, R. M., et al. 2006, Explanatory Supplement to the 2MASS All Sky Data Release and Extended Mission Products, <http://www.ipac.caltech.edu/2mass/release/allsky/doc/explsup.html>
- Dullemond, C. P., & Monnier, J. D. 2010, *ARA&A*, 48, 205

- Dworetzky, M. M. 1983, MNRAS, 203, 917
- Findeisen, K., Hillenbrand, L., Ofek, E., Levitan, D., Sesar, B., Laher, R., & Surace, J. 2013, ArXiv e-prints
- Flaherty, K., Muzerolle, J., Rieke, G., Gutermuth, R., Balog, Z., Herbst, W., Megeath, S. T., & Kun, M. 2012, ArXiv e-prints
- Flaherty, K. M., & Muzerolle, J. 2010, ApJ, 719, 1733
- Frasca, A., Covino, E., Spezzi, L., Alcalá, J. M., Marilli, E., Fűrész, G., & Gandolfi, D. 2009, A&A, 508, 1313
- Gałań, C., et al. 2010, in Astronomical Society of the Pacific Conference Series, Vol. 435, Binaries - Key to Comprehension of the Universe, ed. A. Prša & M. Zejda, 423
- Graczyk, D., Mikołajewski, M., Tomov, T., Kolev, D., & Iliev, I. 2003, A&A, 403, 1089
- Grankin, K. N., Bouvier, J., Herbst, W., & Melnikov, S. Y. 2008, A&A, 479, 827
- Grankin, K. N., Melnikov, S. Y., Bouvier, J., Herbst, W., & Shevchenko, V. S. 2007, A&A, 461, 183
- Greene, T. P., & Young, E. T. 1992, ApJ, 395, 516
- Grinin, V. P., Kiselev, N. N., Chernova, G. P., Minikulov, N. K., & Voshchinnikov, N. V. 1991, Ap&SS, 186, 283
- Grosso, N., Montmerle, T., Bontemps, S., André, P., & Feigelson, E. D. 2000, A&A, 359, 113
- Guinan, E. F., & Dwarf, L. E. 2002, in Astronomical Society of the Pacific Conference Series, Vol. 279, Exotic Stars as Challenges to Evolution, ed. C. A. Tout & W. van Hamme, 121
- Gutermuth, R. A., Megeath, S. T., Myers, P. C., Allen, L. E., Pipher, J. L., & Fazio, G. G. 2009, ApJS, 184, 18
- Haisch, Jr., K. E., Lada, E. A., & Lada, C. J. 2001, ApJ, 553, L153
- Henry, G. W., Fekel, F. C., & Hall, D. S. 1995, AJ, 110, 2926
- Herbst, W., Herbst, D. K., Grossman, E. J., & Weinstein, D. 1994, AJ, 108, 1906
- Jetsu, L. 1996, A&A, 314, 153

- Jura, M., & Turner, J. 1998, *Nature*, 395, 144
- Kenyon, S. J., Lada, E. A., & Barsony, M. 1998, *AJ*, 115, 252
- Kloppenborg, B., et al. 2010, *Nature*, 464, 870
- Kovács, G., Zucker, S., & Mazeh, T. 2002, *A&A*, 391, 369
- Kraus, A. L., & Ireland, M. J. 2012, *ApJ*, 745, 5
- Kusakabe, N., et al. 2005, *ApJ*, 632, L139
- Lada, C. J. 1987, in *IAU Symposium*, Vol. 115, *Star Forming Regions*, ed. M. Peimbert & J. Jugaku, 1–17
- Lai, D. 1999, *ApJ*, 524, 1030
- Loinard, L., Torres, R. M., Mioduszewski, A. J., & Rodríguez, L. F. 2008, *ApJ*, 675, L29
- Lomb, N. R. 1976, *Ap&SS*, 39, 447
- Mahdavi, A., & Kenyon, S. J. 1998, *ApJ*, 497, 342
- Mamajek, E. E. 2008, *Astronomische Nachrichten*, 329, 10
- Mamajek, E. E., Quillen, A. C., Pecaute, M., Moolekamp, F., Scott, E. L., Kenworthy, M. A., Collier Cameron, A., & Parley, N. 2012, in *American Astronomical Society Meeting Abstracts*, Vol. 219, *American Astronomical Society Meeting Abstracts*, 404.04
- Marcy, G. W., & Butler, R. P. 1998, *ARA&A*, 36, 57
- Marsh, K. A., Plavchan, P., Kirkpatrick, J. D., Lowrance, P. J., Cutri, R. M., & Velusamy, T. 2010, *ApJ*, 719, 550
- Mathieu, R. D., Stassun, K., Basri, G., Jensen, E. L. N., Johns-Krull, C. M., Valenti, J. A., & Hartmann, L. W. 1997, *AJ*, 113, 1841
- Meyer, M. R., Calvet, N., & Hillenbrand, L. A. 1997, *AJ*, 114, 288
- Mikolajewski, M., & Graczyk, D. 1999, *MNRAS*, 303, 521
- Mikolajewski, M., et al. 2005, *Ap&SS*, 296, 445
- Morales-Calderón, M., et al. 2011, *ApJ*, 733, 50
- Natta, A., Testi, L., & Randich, S. 2006, *A&A*, 452, 245

- Ozawa, H., Grosso, N., & Montmerle, T. 2005, *A&A*, 438, 661
- Panagi, P. M., & Andrews, A. D. 1995, *MNRAS*, 277, 423
- Pillitteri, I., et al. 2010, *A&A*, 519, A34+
- Plavchan, P., Gueth, T., Laohakunakorn, N., & Parks, J. R. 2013, ArXiv e-prints
- Plavchan, P., Jura, M., Kirkpatrick, J. D., Cutri, R. M., & Gallagher, S. C. 2008, *ApJS*, 175, 191
- Quanz, S. P., Amara, A., Meyer, M. R., Kenworthy, M. A., Kasper, M., & Girard, J. H. 2013, *ApJ*, 766, L1
- Ramirez, S., et al. 2009, in *IAU Symposium*, Vol. 253, *IAU Symposium*, 474–477
- Ratzka, T., Köhler, R., & Leinert, C. 2005, *A&A*, 437, 611
- Rebull, L. M. 2001, *AJ*, 121, 1676
- Ressler, M. E., & Barsony, M. 2001, *AJ*, 121, 1098
- Rodonò, M., & Cutispoto, G. 1988, in *Astrophysics and Space Science Library*, Vol. 143, *Activity in Cool Star Envelopes*, ed. O. Havnes, J. E. Solheim, B. R. Pettersen, & J. H. M. M. Schmitt, 163–166
- Scargle, J. D. 1982, *ApJ*, 263, 835
- Siess, L., Dufour, E., & Forestini, M. 2000, *A&A*, 358, 593
- Skrutskie, M. F., et al. 2006, *AJ*, 131, 1163
- Stencel, R. E., et al. 2011, *AJ*, 142, 174
- Stetson, P. B. 1996, *PASP*, 108, 851
- Strassmeier, K. G., Bartus, J., Cutispoto, G., & Rodono, M. 1997, *A&AS*, 125, 11
- Strassmeier, K. G., et al. 1988, *A&A*, 192, 135
- Strom, K. M., Kepner, J., & Strom, S. E. 1995, *ApJ*, 438, 813
- Terquem, C., & Papaloizou, J. C. B. 2000, *A&A*, 360, 1031
- von Braun, K., et al. 2009, in *IAU Symposium*, Vol. 253, *IAU Symposium*, 478–481

- Vrba, F. J., Rydgren, A. E., Zak, D. S., & Schmelz, J. T. 1985, *AJ*, 90, 326
- Wiling, B. A., Meyer, M. R., Robinson, J. G., & Greene, T. P. 2005, *AJ*, 130, 1733
- Wolk, S. J., Rice, T. S., & Aspin, C. A. 2013, *AJ*, 145, 113
- Wright, J. T., Marcy, G. W., Howard, A. W., Johnson, J. A., Morton, T. D., & Fischer, D. A. 2012, *ApJ*, 753, 160
- Yu, X.-X., & Gan, W.-Q. 2006, *Chinese Astron. Astrophys.*, 30, 294
- Zacharias, N., McCallon, H. L., Kopan, E., & Cutri, R. M. 2005, *Highlights of Astronomy*, 13, 603
- Zeilik, M., de Blasi, C., Rhodes, M., & Budding, E. 1988, *ApJ*, 332, 293

Table A-9. Monte Carlo Simulation: Testing Significance Function

n_0	p	Obs. Param. A	Pred. Param. A	% Error ^a	Obs. Param. B	Pred. Param. B	% Error ^a	Obs. Param. C	Pred. Param. C	% Error ^a
12	0.25	31.338	30.382	-3.054	6.796	6.574	-3.259	1.205	1.239	2.815
13	0.04	80.893	76.952	-4.872	22.235	23.263	4.622	1.393	1.372	-1.500
15	0.06	64.109	65.547	2.243	17.776	18.042	1.500	1.308	1.307	-0.042
18	0.05	69.756	70.192	0.625	19.958	20.568	3.054	1.310	1.309	-0.054
18	0.06	63.138	65.036	3.006	18.173	18.284	0.610	1.287	1.290	0.208
25	0.06	62.550	64.284	2.772	18.496	18.560	0.343	1.253	1.257	0.337
25	0.40	25.656	25.169	-1.898	5.833	5.565	-4.602	1.135	1.148	1.136
25	0.10	49.530	48.938	-1.194	13.192	13.411	1.662	1.200	1.219	1.602
25	0.04	79.775	75.265	-5.653	22.927	24.024	4.784	1.290	1.310	1.534
40	0.06	62.172	63.863	2.719	18.604	18.693	0.479	1.208	1.210	0.194
60	0.24	29.562	28.859	-2.378	8.219	7.796	-5.145	1.128	1.092	-3.168
75	0.055	68.359	66.993	-1.998	18.500	19.682	6.390	1.157	1.174	1.423
125	0.30	28.994	27.429	-5.397	6.329	6.666	5.334	1.080	1.055	-2.269
140	0.45	24.910	25.700	3.171	5.127	5.144	0.335	1.067	1.036	-2.884
175	0.14	43.597	40.392	-7.351	10.569	10.796	2.143	1.090	1.092	0.145
180	0.05	71.813	70.318	-2.082	20.056	20.808	3.751	1.147	1.168	1.867
200	0.06	63.461	65.170	2.694	18.439	18.522	0.451	1.145	1.149	0.385
240	0.40	26.132	26.062	-0.268	5.800	5.525	-4.742	1.070	1.040	-2.794

^aNegative % errors indicates the significance function underestimates the actual value.